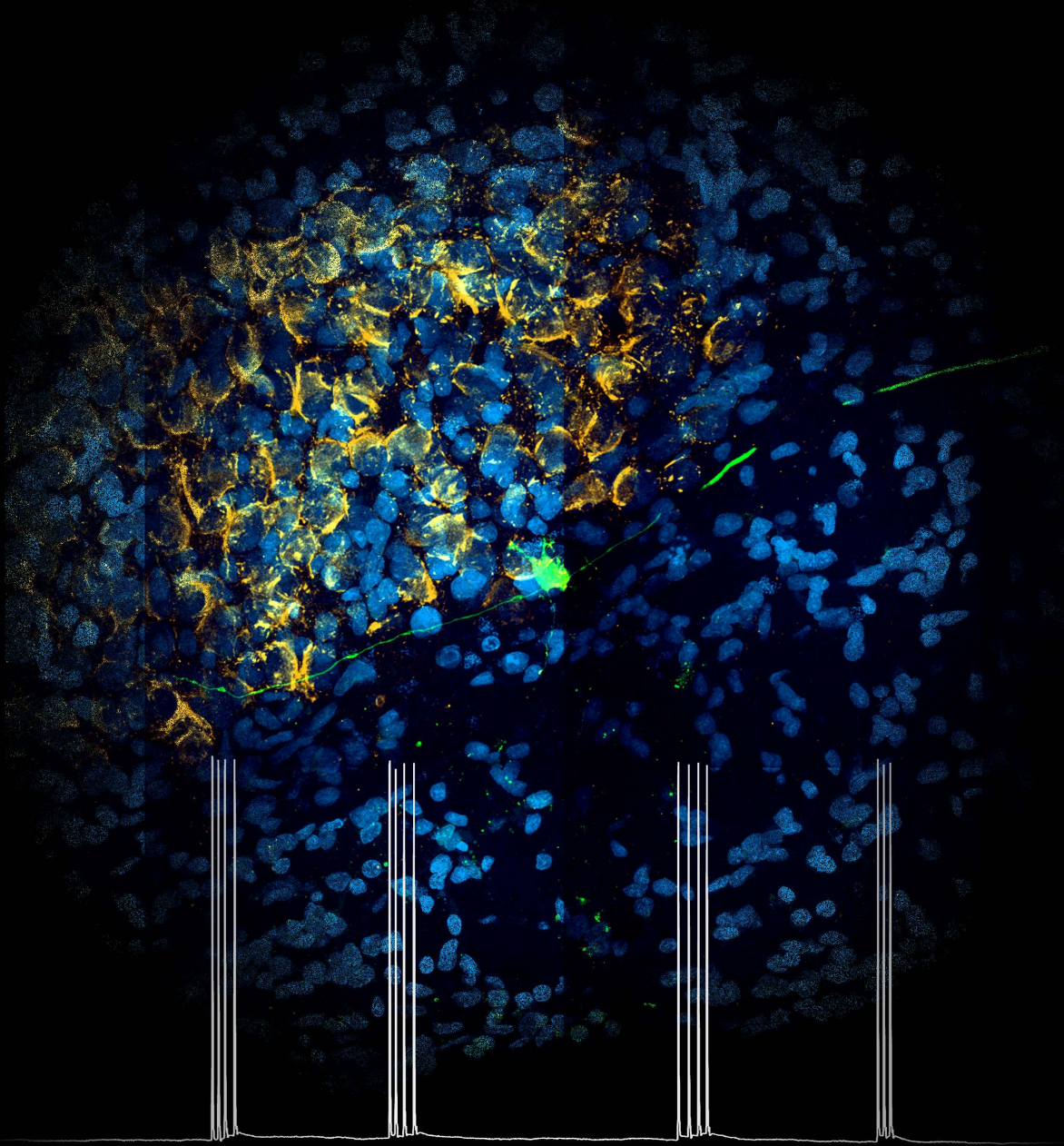


NEURAL ACTIVITY DURING THE FORMATION OF A
GIANT AUDITORY SYNAPSE



Martijn C. Sierksma

Neural Activity During The Formation Of A Giant Auditory Synapse

Martijn C. Sierksma

The research presented in this thesis was conducted at the Neuroscience department of the Erasmus Medical Center of the Erasmus University Rotterdam, Rotterdam, The Netherlands, and was financially supported by the Netherlands Organisation for Earth and Life Science (NWO), grant ‘Development of a giant synapse’ (#823.02.006) given to prof. J. Gerard G. Borst.

Cover design and layout: MC Sierksma & EM Sierksma

Book design and layout: MC Sierksma

Printing: Ridderpint B.V. Ridderkerk

ISBN: 978-94-6299-954-1

© MC Sierksma, 2018

All rights reserved. No part of the material protected by this copyright notice may be reproduced or utilized in any form or by any electronic, mechanical, or other means, now known, or hereafter invented, including photocopying and recording, or in any information storage and retrieval system without prior written permission of the author or, when appropriate, of the publishers of the publications.

**Neural Activity During
The Formation Of A Giant Auditory Synapse**

Neurale activiteit tijdens
de vorming van een auditieve reuzensynaps

Proefschrift

ter verkrijging van de graad van doctor aan de
Erasmus Universiteit Rotterdam
op gezag van de rector magnificus

Prof.dr. H. A. P. Pols

en volgens besluit van het College van Promoties.

De openbare verdediging zal plaatsvinden op
woensdag 23 mei 2018 om 15.30 uur

Martijn Christiaan Sierksma

geboren te Gorinchem.

Erasmus University Rotterdam



Promotiecommissie

Promotor:

Prof.dr. J. G. G. Borst

Overige leden:

Prof.dr. M. H. P. Kole

Prof.dr. C. Lohmann

Dr. M. Schonewille (secretaris)

Co-promotor:

Dr. M. van der Heijden

Table of Contents

1. General Introduction	1
<i>A short history of the synapse</i>	2
<i>The calyx of Held – a special synapse</i>	5
<i>Embryonic development of the auditory brainstem</i>	7
<i>Tonotopical development in the auditory brainstem nuclei</i>	9
<i>The role of neural activity in circuitry development</i>	11
<i>The calyx of Held – a model for synapse development</i>	15
<i>The scope of the thesis</i>	16
2. Resistance to action potential depression in a rat axon terminal <i>in vivo</i>	19
<i>Abstract & Significance</i>	20
<i>Introduction</i>	21
<i>Results</i>	22
<i>Discussion</i>	31
<i>Materials & Methods</i>	34
<i>Supplementary Information</i>	36
3. <i>In vivo</i> matching of postsynaptic excitability with spontaneous synaptic inputs during formation of the rat calyx of Held synapse	51
<i>Abstract</i>	52
<i>Introduction</i>	52
<i>Materials & Methods</i>	54
<i>Results</i>	63
<i>Discussion</i>	86
4. <i>In vivo</i> development of multi-innervation of principal cells of the rat medial nucleus of the trapezoid body	93
<i>Abstract</i>	94
<i>Introduction</i>	94
<i>Materials & Methods</i>	97
<i>Results</i>	103
<i>Discussion</i>	111
5. General Discussion	121
<i>Technical considerations</i>	123
<i>Propagation of neural activity</i>	129
<i>Neural activity in development</i>	137
<i>More ‘a team effort’ than competition?</i>	145
<i>Future directions</i>	146
<i>Conclusions</i>	148
6. Summary / Samenvatting	151
7. List of references	159
8. Addendum	
<i>PhD portfolio, Curriculum Vitae, Dankwoord</i>	

... and I am well aware of the faults that remain; but the measure of my debt is not the shortfall from what might be but the distance traveled from the beginnings.

—*John Bordley Rawls in A Theory of Justice.*

Voor mijn ouders.

General Introduction

Martijn C. Sierksma

One of the main enigmas of the twenty-first century is how the brain is formed, thereby endowing a human being with a wide variety of skills and traits. Among many neuroscientists it is believed that the brain is the body part that defines human's individuality, with the brain as locus of character, personality, emotion, rational thinking, memory, language, motor skills, etc. Notwithstanding these claims, our understanding of the brain is still in its infancy. A focus on how the brain develops might shed light on the exquisite, advanced connectivity of the brain and how developmental brain processes enable an infant to learn its very basic functions. This thesis centers on the developmental changes that occur in a specific part of the auditory brainstem and aims to describe how connectivity is established and adjusted in the developing brain. In this introduction I will describe our recent understanding of the development of the auditory system and the main hypotheses that explain the intricate brain connectivity that exemplifies the auditory system. I will end this introduction with an overview of the topics that will be addressed in this thesis. But first, I will highlight some major advances in brain research of the last century and introduce central neurobiological concepts.

A short history of the synapse

A major change in how we view the brain occurred around the turn of the nineteenth to the twentieth century. At that time it was thought that the brain was a single, continuous structure where signals were transmitted via a fluid or a flow of particles [1-3]. But due to new histological methods in this period, it became clear by the work of famous histologists Golgi – who opposed the new view – and His, Forel, Kölliker, Cajal and others, that the brain was composed of multiple contiguous units which they called neurones or neurons [1, 2, 4, 5]. These neurons usually have a functional polarization in their extensions with extensions that are contacted by other neurons, called dendrites, and an extension that contacts other neurons, called the axon (for an in-depth review, see ref. [6]). These contact points of the axon on the dendrites are so close that it at the time appeared continuous, but by for instance experimentally degenerating the neuron that is contacted, Cajal showed that the axonal side of the contact points was left intact [3, 4]. It took another 60 years for the arrival of electron microscopy to enable researchers to visualize the gap between the axon

and the target membrane, and this observation finally put the old reticular view to rest [1, 5]. This major insight that the brain is composed of discrete neurons paved the way for our understanding of the electrical and chemical properties of the brain.

As a consequence of this neuron doctrine there was a need to understand how neurons could influence each other without physical continuity. The work of sir Sherrington focused on reflexes with the contact points between neurons as the interaction points for the sensory-motor integration, and he introduced the term 'synapse' to mark the 'process of contact' [7]. It was known that electrical impulses could be transmitted along the nerve processes, but how the electrical activity could jump 'through' a synapse was still a question. It was Sherrington's mentor Langley that found that nerve stimulation could release a chemical compound, particularly that autonomic nerve stimulation released a compound that was also found in the suprarenal extracts [3, 8]. Subsequent work of Dale and Loewi (1904-1936) identified a chemical compound that mimicked the effect of vagal nerve stimulation, arguing that nerve endings might release such a compound upon activation [9-11]. Over time, more evidence consolidated that neurons influence their target structures or each other via chemical compounds that became known as neurotransmitters [2, 11]. These findings together laid the foundation for the theory of electrical-chemical neurotransmission between neurons. An electrical impulse runs to the synapse, and subsequently a synapse releases neurotransmitters that cause an electrical impulse in the target neuron. This impulse then can run to the next synapse, and so on.

The next major insights came with the fundamental description of the electrical impulse, the action potential (AP) which travels along the nerves, and a better understanding of how the release of neurotransmitters is caused by an AP. The membrane potential is the difference in potential across the cell membrane. The AP is a stereotypical change in the membrane potential of an excitable cell. The work of Hodgkin and Huxley on squid nerves gave a simple, fundamental description of the AP based on temporal changes in ion channel opening and the movement of the ions through those channels which cause changes in the membrane potential [12]. They suggested that the AP could be described by two currents, a voltage-dependent sodium current (I_{Na}) and

a voltage-dependent potassium current (I_K). The stereotypical nature of the AP is a direct consequence of the intrinsic biophysical properties of sodium and potassium channels. The sequence is initiated by (1) a depolarization-induced opening of the voltage-gated sodium channels resulting in a membrane depolarization due to inflow of sodium ions positively feeding back to the opening of the sodium channels, (2) the opening of potassium channels that allow potassium ions to leave the neuron and counteract the sodium current, (3) the inactivation of sodium channels that terminates the sodium current, (4) the hyperpolarization of the membrane potential by the potassium currents which causes the potassium channel to close and terminates the action potential. Ion pumps are responsible for the maintenance of cellular ion gradients.

Following our understanding of the contribution of ion channels to electrical activity, it became clear how the AP was linked to neurotransmitter release, namely via calcium channels. The work of Katz and Miledi (1965-1967) indicated that when the AP spreads through the terminal voltage-gated calcium channels open and calcium enters the terminal [13-15]. Calcium ions then trigger the release of neurotransmitters, via a chemical cascade that lead to the fusion of small membrane vesicles filled with neurotransmitters with the synaptic membrane. The neurotransmitters are released into the space between the cells, called the synaptic cleft. In the synaptic cleft they diffuse and bind to their appropriate receptors. These receptors can be postsynaptic ion channels that change their conductance upon binding of neurotransmitter, thereby causing an electrical impulse at the postsynaptic structure: this impulse might then trigger the start of a new action potential at the target neuron. This chemical-electrical link has become the fundamental theory of synaptic neurotransmission.

The synapse is a key structure for neurotransmission and brain function. An important property of synapses is that their strength is not fixed, but that the impact of a synapse on its postsynaptic target can be modified. These changes in synaptic strength are called synaptic plasticity. The modification in synaptic strength can remain for minutes to days or even years, and these changes are now generally thought to underlie memory. Neurons typically receive many different synaptic inputs. Generally, many synapses have to be active at the same time to trigger an AP. The integration of these different inputs allows a neuron

to associate different stimuli carried by these inputs. By making long-term adjustments in synaptic strength, specific associations can be ‘stored’ within the network. Therefore, the synapse is a fundamental structure of the brain. However, the size of a typical synapse is the order of a micron and this makes the investigation of a single synapse daunting. An accessible research model was needed to understand the biophysical properties of a synapse.

The calyx of Held – a special synapse

The calyx of Held is a unique axon terminal that is located in the central auditory system (Figure 1.1) [17]. The calyx of Held synapse spans 10-20 μm making it arguably the largest mammalian synapse [18]. This giant nerve ending was first described by the anatomist Hans Held [1, 17]. He called the endings ‘Fasernkörben’ [transl. fiber baskets] (Held 1893, p219 [17]) which later histologists dubbed the calyx of Held [18]. The name derives from its budded-flower appearance in young animals. The calyx covers a large part of postsynaptic soma. Because of its unique shape and size, the calyx of Held caught the interest of both Held (1891) and Cajal (1896; Figure 1.1B), and the work of Held and contemporaries provided important evidence for the neuron view of

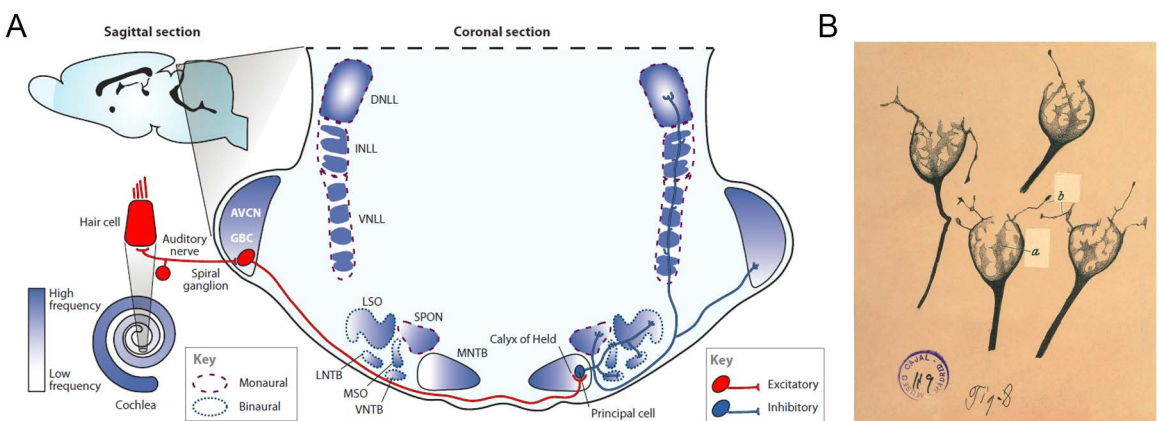


Figure 1.1 The calyx of Held-synapse in the rodent auditory brainstem.

(A) The calyx of Held-synapse is located in the ventral part of the auditory brainstem, is composed of a single postsynaptic neuron of the medial nucleus of the trapezoid body (MNTB), and an axon terminal originating from a globular bushy cell located in the contralateral anteroventral cochlear nucleus (AVCN). The auditory nuclei are tonotopically organized (blue to white gradients). A is reproduced from ref. [16]. (B) A reproduction of the original drawing of Golgi stainings of kitten calyces done by Ramón y Cajal. Courtesy of the Cajal Institute, Cajal Legacy, National Spanish Research Council (CSIC), Madrid, Spain.

Cajal, although, ironically, Held himself was a proponent of the reticular view [4]. A renewed interest in the calyx of Held arose when the first electrophysiological measurements were made by Forsythe (1994)[19] and the first simultaneous recording of the calyx of Held and its postsynaptic target by Borst et al. (1995)[20]. Its size made the calyx one of the few axon terminals that can be targeted for whole-cell electrophysiology, a method where via a glass pipette an electrical connection is obtained with the target structure which enables the measurements of currents and potentials. Different aspects of the work of Katz and Miledi were subsequently confirmed for mammalian synapses in the central nervous system [20, 21] and the calyx of Held became one of the main mammalian models for synaptic neurotransmission [16, 22].

Apart from the use of the calyx of Held as a research model for synapses, it does have a physiological function in the living animal. Its main function is to reliably relay presynaptic activity to the postsynaptic neuron, and the activation of its target neuron will inhibit its targets in the superior olivary complex [22, 23]. The postsynaptic target of the calyx of Held is located within the medial nucleus of the trapezoid body (MNTB). While the MNTB is a monaural nucleus [24], most of its target nuclei respond to both cochleae and play a central role in sound localization in the horizontal plane [23]. Sound localization is achieved by a precisely-timed comparison of synaptic activity originating from both ears [25], and accordingly, the calyx of Held is specialized for precisely-timed neurotransmission [16]. The other synapses found between the cochlea and the calyx of Held, the ribbon synapse of the inner hair cell to the spiral ganglion neuron and the modified endbulb of Held of the calycigenic globular bushy cells in the cochlear nucleus, are also specialized for rapid and precisely-timed transmission of sound-related neural activity [26].

Notwithstanding this wealth of information on the calyx of Held that has been accumulated by over a century of inspiring research, the processes that govern the target-finding at the MNTB of the calycigenic axon and the formation of the calyx of Held are still to be identified to a large extent. What do we know about the development of the auditory system, globally and specifically for the calyx of Held and the MNTB?

Embryonic development of the auditory brainstem

One way of understanding brain development is to know the origins of the cell and to follow the lineages of cell division all the way back to the first cell. The development of an embryo starts with the fertilization of an oocyte with a sperm cell, followed by rounds of mitotic division to create a dense cluster of cells. For mammals the cell cluster will transform into the blastocyst, a structure with an outer layer called the trophoblast giving rise to the placenta and encompassing a fluid-filled cavity, and an inner cell mass giving rise to the embryo [27]. The inner cell mass will undergo a process called gastrulation, in which an invagination is formed through the inner cell mass, subdividing the inner cell mass into the three germ layers: (1) the endoderm which is the origin for the gastrointestinal tract and partly its associated glands, the respiratory system, urinary tracts and the cells aligning the auditory tube; (2) the mesoderm which forms the cardiovascular system including the kidneys, the genitourinary system and the musculoskeletal system; and (3) the ectoderm forming the skin including hair and nails, the non-sensory part of our eyes and teeth, the adrenal medulla, and the nervous system [28, 29]. The following paragraph will discuss the development stages of the ectoderm, focusing on the central auditory system.

While the differentiation of the ectoderm continues, the ectoderm folds inwards and forms a tube, the neural tube [30]. This process is called neurulation; in humans it starts in the third week of pregnancy and is finished after four weeks (abstract for symposium, O’Rahilly and Müller 1994). The anterior part of the neural tube is the origin of the three main parts of the brain: proencephalon, mesencephalon and rhombencephalon [31, 32]. The rhombencephalon can be subdivided into rhombomeres 1-8 which are embryonic areas that harbor the progenitors for the different parts and nuclei of the hindbrain [33, 34]. During this period, a small invagination forms within the rhombencephalon. Upon closure it forms the otic vesicle. The otic vesicle is the origin of the vestibular and cochlear sensory structures including the auditory nerve cells, called spiral ganglion neurons (SGNs) [35-37]. Whether a cell from the otic vesicle develops into a sensory or a non-sensory cell, and into a vestibular or cochlear cell, can partly be explained by genetic factors [38-43]. An extensive review on the development of SGNs has been written by Rubel and

Fritzsch [44].

For rodents, the neural tube closes 9-10 days after fertilization (E9-10) [45-47]. Cells aligning the neural tube continue to divide with one of the daughter cells migrating away and differentiating into a neuron. For the auditory brainstem neurons this happens between E12-17, with distinct cell birth peaks for every nucleus [48, 49]. Most neurons for the cochlear nucleus, the target of the auditory nerve, are born during the same period; however, neuronal division might continue even after birth [48]. The different nuclei of the cochlear complex derive from different origins with rhombomere 5 and 3 contributing to the dorsal nucleus (DCN), anterior ventral nucleus (AVCN) and the posterior ventral nucleus (PVCN), while r2 contributes only to AVCN [33, 45, 49, 50].

Even before the auditory nuclei have fully developed, their neurons already extend their axons to their appropriate targets. While SGNs are born between E9-E13.5 in mice [35], their axonal projections are already present in the cochlear nuclei at E11-12 [35, 51-53], and at the same time SGNs extend neurites to the sensory epithelium of the developing cochlea [35, 44, 54]. In rats, the axons of cochlear neurons enter the superior olivary complex around E13-14 [55, 56]; these neurons extensively branch around E18 [55]. The branching is suggestive for synaptic connectivity, but the inner hair cells still lack the ability to generate action potentials [57] as well as neurotransmitter release until E17 [58]. At E15, in a slice preparation, cochlear neurons already respond to stimulation of the auditory nerve, indicating that functional synapses are nonetheless present within the cochlear nucleus at this stage [59]. Stimulation of the cochlear neurons could elicit responses in the principal neurons of the MNTB at E17 [59, 60]. While the general connectivity is already established at this stage, the circuitry at every nucleus is immature and will undergo phases of refinement and pruning before it will be able to meet the demands of the mature sound-related neurotransmission [44, 61]. In summary, these observations of the embryonic development of the auditory brainstem have given us a time schedule of its development. They do not tell us how all these processes are instructed and what cues are present to guide the development. The next section will look at some major hypotheses that could explain specificity in the connections between auditory areas.

Tonotopical development in the auditory brainstem nuclei

An important characteristic of auditory projections is the tone frequency to which they are most sensitive, the so-called characteristic frequency. An important organizational principle within the auditory nuclei is that they are organized along a *tonotopical* axis, which means that neurons with similar characteristic frequencies lie together (Figure 1.1A). A major developmental question is what establishes the tonotopy across the different auditory nuclei. Multiple hypotheses have been proposed and here I will expand on four of them. These four hypotheses are not mutually exclusive, and multiple, if not all, strategies may be exploited to ensure proper and robust connectivity.

A first hypothesis involves the presence of a temporal separation in development (maturational gradient) throughout the different areas. It proposes that early-born neurons exclusively connect to each other, and similarly for late-born neurons. The mechanism would be that early-born neurons, as they mature earlier, would be the first to arrive at the target nuclei and the first to connect to neurons. Subsequent projections would then connect to neighboring neurons, thereby establishing a topological arrangement. This hypothesis has been tested for the visual system in developing *Xenopus laevis* by retarding the normally pioneering projections of the dorsal retina to an extent that the sequence of tectal invasion was effectively reversed [62]. The normal retinotopical map was still formed, suggesting that the timing of invasion did not determine the map formation, making the timing hypothesis less likely [63]. Still, there might be a role for temporal maturation in the auditory system, but without a clear molecular mechanism, it will be hard to test this for the auditory nuclei.

A second hypothesis presupposes that neurons, when they leave the mitotic cycle, have a specific set of genes encoding for membrane proteins that establish their identity within the auditory system [64]. These membrane proteins would be present during axon invasion, and every axon would probe for a specific membrane code that corresponds to its source identity. This hypothesis is called the chemoaffinity hypothesis, and was first proposed by Roger Sperry (1963) [65]. For *Drosophila* olfaction, partnering between olfaction receptors and the projection neurons, and also for the neuromuscular synapse, is likely established by homophilic interactions of a transmembrane protein family called teneurins

[66, 67]. In contrast, in fish, when either the retina or the tectum is halved by ablation, the remaining structure will reorganize with its projections to connect to the entire target structure (half retina across whole tectum, and whole retina across half tectum), challenging the idea that there is a membrane-anchored code on the neuron independent from its surroundings [63]. Another open question is how tonotopical segregation of the neurons is established, as this hypothesis only explains proper input-target matching. Neuronal migration to their appropriate tonotopical location would be additionally needed.

A third hypothesis proposes that every neuron is differentially sensitive to an environmental factor that has a concentration gradient along the tonotopical axis. Two candidates are brain-derived neurotrophic factor (BDNF) and neurotrophin factor 3 (NT₃). Both factors are synthesized by the sensory epithelium in the otic vesicles, and are expressed in opposing gradients within the cochlea [68, 69]. The genes of their cognate receptors *trkB* and *trkC* are expressed by SGNs [44, 70]. Specific deletions of the genes encoding these proteins showed that these factors are essential for neuronal survival [44]. Interestingly, the cochlear base seemed more affected in *Nt3*-null and *trkC*-null mutants, while the cochlear apex was more affected in *Bdnf*-null *trkB*-null mice [44]. In mice in which the *Nt3* expression was replaced by *Bdnf*, SGN survival was rescued, and on a coarse level it seemed to rescue the innervation [71]. However, abnormal, radially-running fibers were observed which did not form recognizable synapses, consistent with the invasion of the foreign axons by ectopic BDNF [71]. This suggested that additional molecular cues – intrinsic or input-target pairing cues – were needed to form synapses between inner hair cells and SGNs. Notably, these neurotrophins might affect the growth direction of the axon in a way that will depend on other environmental and axon-autonomous cues [72], and putatively on its surrounding electrical activity [73]. Koundakjian *et al.* [52] proposed that the differential presence of Eph receptors could be a second candidate to establish tonotopy in the cochlea. Together, these findings emphasize that the growth factors are promising candidates for establishing tonotopy, and future research needs to show whether their involvement is instructive or permissive for tonotopic development.

A fourth hypothesis presupposes that early connectivity is very broad and neural tonotopical identity is established later in development by a cue that propagates from the cochlea to the higher-order areas via a refinement of connections. Here, the mechanism would encompass that the neurons do not necessarily show a specific identity until connectivity is established. A possible candidate that instructs connectivity might be the neural activity that originates in the cochlea and propagates through the auditory system early in development [74, 75]. Generally, it proposes a strengthening of inputs that contribute to postsynaptic activity, and a weakening of inputs that do not. If the postsynaptic neuron's excitability decreases during development, it would progressively bias the correlative activity to the strongest inputs, and could result in the observed sharpening in the tonotopical organization. Still, this process can only lead to a tonotopical arrangement if this arrangement is already coarsely present.

These four hypotheses can be contrasted by how tonotopical cellular identity is established: is it cell-autonomous (hypothesis 2 and 3) or is it defined by the inputs (hypothesis 1 and 4)? These options are not mutually exclusive and multiple methods might be employed during development. Another way to contrast them could be their temporal sequence: the general developmental strategy might be that a coarse-grained tonotopical arrangement is achieved first (hypothesis 1 and 3), followed by a period of refinement and sharpening of the circuitry (hypothesis 2 and 4). It remains an open question what the actual merit is of each hypothesis for auditory system development. The next section will review the advances made in the last 50 years.

The role of neural activity in circuitry development

The idea that neural activity can adjust neural circuitry has been around for some time. Pioneering work of Nobel laureates Hubel and Wiesel (1960-1970) demonstrated that during an early period in development clusters of visual cortical neurons called ocular dominance columns become predominantly activated by either eye [76, 77]. Although ocular dominance columns are formed before eye opening, sensory deprivation of one eye (by enucleation, eye lid suturing or retinal silencing) results in a redistribution of the active cortical inputs and shrinkage of the sensory-deprived ocular dominance columns [76-

79]. This process only occurred within a brief developmental period after eye opening. Based on their work, a general theory for development was proposed that neural circuitry becomes shaped by sensory experience but only within a transient period, called the sensitive period. Although it has become clear that the opening and closure of the sensitive period can be more plastic than previously presumed [80, 81], the general idea remains valid and has been identified in other sensory modalities as well [81, 82].

Inspired by these successes, researchers focused on the experience-related sensitive periods in the auditory system by investigating the changes in circuitry before and after hearing onset. Early connectivity in the primary auditory nuclei revealed a precise tonotopic organization, few aberrant connections, and the physiological responses demonstrated adult-like tonotopy shortly after hearing onset, precluding a role for sound-induced refinements [44, 61]. Before hearing onset the superior olivary nuclei already demonstrate a level of tonotopic arrangement. The lateral and medial superior olive do go through a major refinement that sharpens their tonotopic map [61, 83-85]. This sharpening was suggested to be dependent on binaural hearing in a sensitive period during development [86]. The fact that tonotopical refinement is experience-dependent in these two nuclei, might reflect the need of binaurally matched tonotopy as these nuclei integrate binaural sound, while other auditory brainstem nuclei are only responsive to one ear [61, 87]. Prior to hearing onset, the monaural circuitry do undergo major refinement that sharpen the tonotopy [52, 55, 61, 88]. One form of refinement occurs by pruning of the axonal branches, the synapses, or even the postsynaptic dendrites, and this sharpens the circuitry in the cochlea [52], in the cochlear nucleus [88], and in the MNTB ([55, 89-91], but see [92] on calyceal pruning). Nonetheless, sensory experience does promote the synaptic maturation of the endbulb and calyx of Held [22, 91, 93-95], enabling high-fidelity transmission at high firing frequencies [16, 26]. Together, these results indicate that the tonotopic organization in the auditory nuclei is mostly established prior to sensory experience.

A second form of refinement exists where synapse strength and postsynaptic excitability concertedly bias the neuron to the stronger synapses. This second form does not need to be reflected in anatomical changes, and might be

particularly important for the specialized synapses in the auditory system, the endbulb of Held [96], the modified endbulb of Held [44, 96], and the calyx of Held [60, 97, 98]. The size of these synapses is enormous ($\sim 5\text{-}20\ \mu\text{m}$), and they harbor many neurotransmitter release sites, enabling the presynaptic terminal to singlehandedly drive the target neuron to AP threshold [26, 99-101]. The immature postsynaptic neuron has a high intrinsic excitability that makes it sensitive to small synapses; it subsequently down-tunes its excitability [26, 60, 96, 97], making it progressively more difficult for weaker synapses to influence the target neuron. This would increasingly bias the neuron to respond to its strongest input. This type of plasticity where synaptic strength and postsynaptic excitability are balanced to maintain a more-or-less constant level of postsynaptic AP firing, is called homeostatic plasticity and may be found for other synapses as well [102]. It is still unclear how proper tonotopy is established for the calyx of Held-synapse: whether it involves giant synapse formation at the appropriate tonotopic location in concert with homeostatic plasticity, or axonal pruning of tonotopically-misplaced branches and calyces, or a combination of the two.

Sensory experience generates neural activity that may change neural circuitry, not only in the periphery, but upon propagation also more centrally. It is therefore interesting that the cochlea of a prehearing mammal is spontaneously active, causing waves of activity that propagate through the developing auditory system [74, 75]. Supporting cells of the cochlea from Kölliker's organ release ATP, which eventually causes a calcium plateau in nearby inner hair cells that triggers glutamate release, thus triggering burst activity in the SGN [75, 103]. In addition, inner hair cells might be intrinsically active before hearing onset [57, 104]. Their activity is also shaped by cholinergic synapses [85, 105-107]. This early spontaneous activity might be an evolutionary solution to substitute acoustically-driven activity to ensure the representation of the entire cochlea in the auditory system. If auditory experience would instruct the development, it would bias the system to those tone frequencies that are present in the environment. As higher frequencies are attenuated in the womb, this component might become underrepresented in the auditory system. This might not be a problem for species with a brief gestation period where this part

of development occurs after birth, such as rats and mice, but for some mammals this developmental period occurs during gestation, and only the part of the auditory system related to the lower tone frequencies would be presented with sound-related neural activity. On a side note, for rats and mice it is not due to the lack of functional central synapses [59, 108] or the lack of mechanotransduction [109, 110] that the pre-hearing auditory brainstem is unresponsive to sound, but mainly due to the occlusion of the middle ear canal and the inefficient mechanics of both the middle ear and the cochlea until the second postnatal week [110, 111]. Therefore, the spontaneous activity of the cochlea may be the cue that informs neural circuitry refinement.

To understand the impact of cochlea-driven activity, researchers perturbed the cochlear function or the propagation of neural activity in prehearing animals, but the interpretation of their results has been limited by the following aspects. Most of these studies might not have altered the pre-hearing activity-dependent development: their manipulation was performed after a period of unperturbed development [98, 112-114]; congenital deafness might not have altered the first stages of development [94, 95, 115-120]. Secondly, the impact of the perturbation is typically assessed after hearing onset, thus involving both prehearing and posthearing activity-dependent development [94, 95, 98, 111-114, 116, 117, 119-121]. Thirdly, genetic perturbations might not limit their effects to the cochlea and its neural activity, but might alter activity-independent development of the auditory brainstem as well [122-126]. Fourthly, and most profoundly, neural activity has a trophic effect and therefore perturbations can lead to large-scale apoptosis, obscuring the activity-dependent development of the circuitry [44, 94, 113, 114, 119, 121, 123, 127, 128]. This trophic effect is mainly restricted to early development [113, 129], a genuine sensitive period of the auditory system. Lastly, compensatory mechanisms might cause a new locus of spontaneous activity in the cochlear nucleus [93], hyperexcitability in other auditory neurons [94, 95, 118], and altered neurotransmission favoring postsynaptic firing throughout the auditory brainstem [94, 117, 122-125, 130], making it hard to untangle the underlying developmental mechanisms at play. These findings do strongly suggest an important role for activity in the development of the auditory system, but a role for neural activity in circuitry refinement is much less clear.

A few studies have reported on perturbations of the giant calyx of Held synapse. Unilateral removal of the middle ear ossicles results in increased number of swellings per calyx in both MNTBs [98]. After hearing onset, a broadening of the calyceal AP was found in a mouse line missing neurotransmitter release in the cochlea ($Ca_v1.3^{-/-}$ -mice) [122]. The synaptic response mediated via NMDA receptors was increased and the presence of NR2B-subunits persisted after hearing onset [122]. In a mouse model for deafness with inner hair cell degeneration, principal neurons have abnormal levels of sodium channels, leading to an increase in sodium currents [118]. In addition, the tonotopic gradient in neuronal properties did not develop within the MNTB [95]. Others did not observe these changes in their mouse models [85, 93, 116]. These changes seem largely consistent with compensatory responses to reduced activity, but the phenotypic changes are apparently very diverse. More detailed experiments are needed to uncover activity-dependent refinement for giant synapses.

The calyx of Held – a model for synapse development

The size of the calyx of Held provides a technical advantage over other axon terminals for electrophysiological recordings [19, 20], capacitance measurements [131] and imaging [132], and gave the opportunity to assess neurotransmission *in vivo* [133, 134]. The target neuron of the calyx of Held, the principal neuron of the medial nucleus of the trapezoid body (MNTB), can be easily identified based on its eccentric nucleus and location close to the ventral midline of the brainstem [22, 135]. The target neuron is functionally and morphologically of a single type. In general, the adult neuron will receive a single calyx. The location of the MNTB at the ventral midline of the brainstem makes it hard to reach from a dorsal approach as you have to traverse the dorsally located brain structures. However, with a ventral approach the MNTB is easily accessible *in vivo* for both electrophysiology and imaging [90]. These properties make the calyx of Held a very attractive model synapse to study synapse development.

The structural development of the calyx has been extensively described. In general, the development proceeds through three stages: (1) a growth cone enters the MNTB and contacts postsynaptic targets; (2) a swelling from the axon forms a cup that covers the postsynaptic soma, and additionally has many collaterals,

(3) the axonal covering becomes fenestrated and the collaterals are eliminated [18, 55, 92, 136]. These structural changes also change functional connectivity. Globular bushy cells initially form synaptic contacts with many principal cells [92, 136], but in the adult a single globular bushy cell gives rise to 1-3 calyces of Held [17, 18, 89, 92]. Similarly, the postsynaptic neuron loses many of its synaptic inputs during development [60, 137] leading to circuitry refinement. An electron microscopy study estimated that more than half of the principal cells will have been contacted by more than one calyx [136, 137], suggesting that during giant synapse formation some form of competition is ongoing for the principal cell's soma [138]. Some of these calyces might arise from the same globular bushy cell as two branches of the axon can converge onto the same cell [92]. In the adult, it has been estimated that in about 10% of the principal cells multiple calyces persist on single neurons [60, 136-138], but this stands in contrast to other landmark papers [17, 18, 20, 89, 133] who have not observed this. Therefore, the presence of both pruning and competition between large calyces are still open questions.

The scope of the thesis

This thesis centers on the neural activity during the development of a giant synapse, the calyx of Held synapse, which is part of the mammalian auditory brainstem. In order to record its activity, I take a unique approach, first performed by dr. Rodríguez-Contreras [90], in which I perform surgery in anesthetized neonatal rats to expose the ventral brainstem, while keeping all synaptic connections between the MNTB and the cochlea intact. This approach allows me to investigate the neural activity of the developing calyx of Held synapse in the first postnatal week of rats. How is the activity at the MNTB organized and how does the activity and the innervation in the MNTB change during this period?

In CHAPTER 2 I focus on the neural activity recorded from the calyx of Held. What are the developmental changes that occur within this period? Can the calyx of Held already fire at the high frequencies that are typical for the auditory brainstem? What are the mechanisms that contribute to the ability of firing at these frequencies?

In CHAPTER 3 I switch to the postsynaptic neuron. Our approach gives the opportunity to record the neural activity during the formation of the calyx of Held. What are the developmental changes in synaptic activity, intrinsic properties and postsynaptic activity at the single-cell level? Are these developmental changes tightly linked? How do the changes in the intrinsic properties of the principal cell change how synaptic activity elicit postsynaptic APs?

In CHAPTER 4 I focus on the multi-innervation of the principal cell. Can we identify the different synaptic inputs of a single neuron? How does the strength of these synapses change during development? How does synaptic strength relate to synaptic morphology? Are there multiple, competing, giant synapses at a single neuron? And what do these changes tell us about synaptic competition?

In CHAPTER 5 the main findings of the previous chapters are recapitulated and discussed. How does the use of anesthesia impact the findings and are the findings reliable given the limitations of electrophysiology when applied *in vivo*? Can we generalize our findings of the developing calyx of Held to other axon terminals? How do the developmental changes in neural activity in the auditory brainstem relate to other developing, topologically-organized brain circuitries? What outstanding questions remain regarding the formation of the calyx of Held synapse?

Resistance to action potential depression
in a rat axon terminal *in vivo*

Martijn C. Sierksma, J. Gerard G. Borst

Proceedings of the National Academy of Sciences of the USA (2017)

Abstract

2

The shape of the presynaptic action potential (AP) has a strong impact on neurotransmitter release. Because of the small size of most terminals in the central nervous system, little is known about the regulation of their AP shape during natural firing patterns *in vivo*. The calyx of Held is a giant axosomatic terminal in the auditory brainstem, whose biophysical properties have been well studied in slices. Here, we made whole-cell recordings from calyceal terminals in newborn rat pups. The calyx showed a characteristic burst firing pattern, which has previously been shown to originate from the cochlea. Surprisingly, even for frequencies over 200 Hz, the AP showed little or no depression. Current injections showed that the rate of rise of the AP depended strongly on its onset potential, and that the membrane potential after the action potential (V_{after}) was close to the value at which no depression would occur during high-frequency activity. Immunolabeling revealed that $\text{Na}_v1.6$ is already present at the calyx shortly after its formation, which was in line with the fast recovery from AP depression we observed in slice recordings. Our findings thus indicate that fast recovery from depression and an inter-AP membrane potential that minimizes changes on the next AP *in vivo*, together enable high timing precision of the calyx of Held already shortly after its formation.

Significance

During high-frequency firing the shape of a presynaptic action potential (AP) can alter, thereby changing neurotransmitter release. In this paper we describe how a giant terminal in the brainstem of newborn rats called the calyx of Held can fire *in vivo* at high frequencies without substantial AP depression. The underlying mechanism was found to be the presence of sodium channels that can recover rapidly from depression in combination with a close match between the potential that is attained following an AP with the potential that maximizes AP stability. Surprisingly, this match was already there shortly after formation of the calyx of Held. We speculate that these mechanisms help synapses to maximize timing precision during high-frequency firing.

Introduction

Action potentials (APs) are followed by a period of decreased excitability called the refractory period. High-frequency firing thus requires special adaptations to minimize this refractory period and maintain AP stability. The changes in the AP waveform that occur at high firing frequencies are especially relevant in presynaptic terminals, where the shape of the AP critically controls calcium influx via voltage-dependent calcium channels, and thus transmitter release [139, 140]. Following the AP, the membrane potential during the recovery period has a large influence on the speed of the recovery from inactivation of voltage-dependent sodium channels and deactivation of voltage-dependent potassium channels, which are two major determinants of the refractory period [140]. In some terminals the AP is followed by a depolarizing after-potential (DAP; [20, 141-146]), whereas in others a hyperpolarizing after-potential (HAP) has been observed [147-151]. The sign of this after-potential depends on the resting potential [143, 144, 152], suggesting that the membrane potential following the AP (V_{after}) might be more important than the sign of the after-potential.

The calyx of Held is a glutamatergic axosomatic terminal whose biophysical properties have been well studied [16]. Its many release sites enables it to act as an inverting relay synapse within the auditory brainstem that reliably drives its postsynaptic partner, a principal neuron in the medial nucleus of the trapezoid body (MNTB), even at firing frequencies >200 Hz [133]. Shortly after its formation, around postnatal day 2 in rodents [55, 92, 137], it already fires in characteristic high frequency bursts *in vivo* [111, 153]. In slice studies, a large DAP has been observed [20], to which resurgent sodium currents [154] make a prominent contribution, and which may promote high-frequency firing [152]. With the exception of cerebellar mossy fiber terminals [141, 145], studies on the biophysical properties of mammalian presynaptic terminals have been performed *ex vivo*, and the functional significance of after-potentials, including their role during natural firing patterns, is currently largely unknown. Here, we make *in vivo* juxtacellular and whole-cell recordings from the calyx of Held in rat pups, and study how the after-potentials contribute to the stability of presynaptic action potentials during natural firing patterns.

Neural Activity During the Formation of a Giant Auditory Synapse

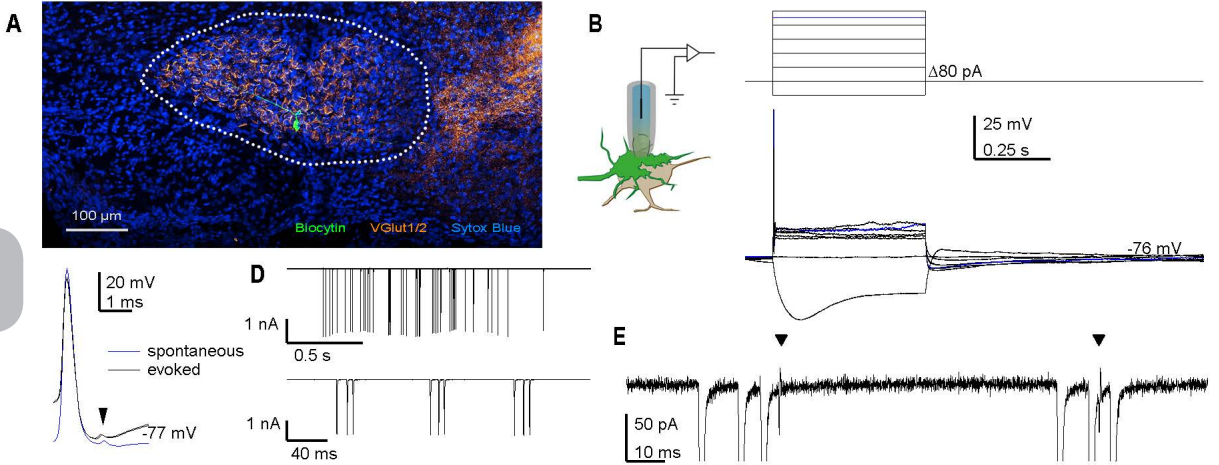
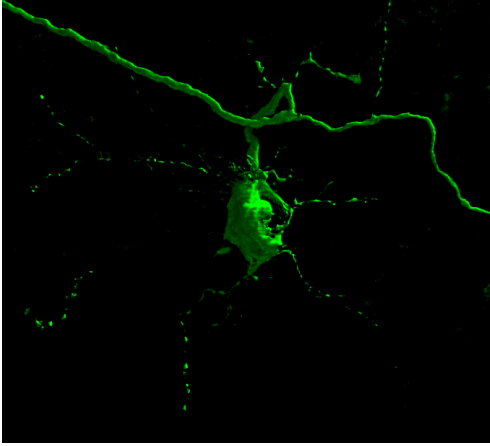


Figure 2.1 Establishing *in vivo* recordings from calyx of Held. (A) Section of the P6 rat ventral brainstem containing the MNTB (outlined) labelled with anti-biocytin (green), anti-vesicular glutamate transporter 1 and 2 (orange), and the nucleotide stain Sytox Blue. The midline is located to the left, and the ventral side to the bottom. (B) *In vivo* whole-cell recording from a calyx (left); upon constant-current injections (top) the terminal showed a depolarizing sag, strong outward rectification and a single action potential (bottom). Blue trace indicates the current threshold for eliciting an AP. Series resistance was compensated off-line. (C) In some recordings, evoked and spontaneous APs were followed by a postspike (arrow head), indicating a postsynaptic AP analogous to the prespike that can be recorded in postsynaptic recordings [19]. (D) In voltage-clamp recordings, periods of spontaneous activity could be recorded (top), which were composed of minibursts (bottom). The ~ 2 Hz-oscillation in the current amplitudes in the top recordings was induced by breathing. (E) Expansion of D illustrates two postspikes (arrow heads), and a lack of synaptic currents. For D-E, command potential was -80 mV; series resistance (36 M Ω) remained uncompensated.

Results

Identification of *in vivo* calyces

To study the contribution of AP depression during physiological firing, we made blind juxtacellular and whole-cell recordings from the calyx of Held in 2-8 days old rat pups. Several converging lines of evidence indicated that we indeed recorded from the calyx of Held, a giant terminal in the auditory brainstem. Firstly, the identity of several calyces was confirmed by biocytin filling and subsequent histological processing (Figure 2.1A; $n = 6$), revealing the typical cup shape of the calyx (Movie 1) and an axon that could often be traced back to the midline and to other auditory nuclei ipsilateral of the MNTB. Secondly, in agreement with previous calyceal recordings in slices [19, 20], terminals



Movie 1. Three-dimensional reconstruction of a calyx recorded in a six-day-old rat pup. Biocytin, which was added to the intra-pipette solution and diffused into the calyx during the whole-cell recording, was detected by immunofluorescence with confocal microscopy. QR links to the movie on the PNAS-website.

responded to constant-current injections with a single, brief and overshooting action potential at the start of the current injection, strong outward rectification and a hyperpolarization-activated, depolarizing voltage sag (Figure 2.1B and Figure 2.5). Thirdly, in some recordings the calyceal AP was followed by a small deflection that likely reflects the postsynaptic AP (arrow in Figure 2.1C). Fourthly, the terminals showed a characteristic firing pattern, consisting of minibursts with high firing frequencies (Figure 2.1D; [74, 153, 155]). Its interval distribution resembled auditory nerve activity at this age (Figure 2.6), which is in agreement with its generation by the cochlea [74]. In contrast to *in vivo* postsynaptic recordings [153], no fast synaptic transients were observed in voltage-clamp mode (Figure 2.1E), which is consistent with the absence of axo-axonal inputs. Therefore, the structures that we recorded from are highly likely to be calyces.

In the first neonatal days, the terminal assumes a cup shape [18, 55, 137]. Accompanying this structural development a number of developmental changes in its biophysical properties occur [156, 157], including a developmental decrease in resting membrane resistance and a substantial increase in the outward rectification, a developmental trend for an increase in the maximal rate of rise, an increase in the rate of repolarization, and a clear shortening of the AP half width (Figure 2.5). APs elicited by brief current injections showed similar

developmental changes. These developmental changes accelerated the terminal's AP, allowing firing at shorter intervals. Surprisingly, even P2-3 calyces fired spontaneously over 150 Hz without apparent failures ($n = 3, 4$ calyces in whole-cell and juxtacellular mode, respectively), indicating that its ability to fire at high frequencies is already present shortly after its formation.

2

Resistance to depression in vivo

During high-frequency firing the shape of the presynaptic action potential remained remarkably constant in both whole-cell and juxtacellular recordings (Figure 2.2A-B). Figure 2.2C shows the maximal rate of rise of the AP as a function of the inter-AP interval in a representative whole-cell recording. While the postsynaptic somatic AP typically depresses $>40\%$ at the shortest intervals *in vivo* [134, 153, 155], the calyceal AP depressed on average only 4% for intervals <5 ms in whole-cell recordings (0.96 ± 0.03 , mean \pm SEM, $n = 9$ calyces; Figure 2.2C-D). Similar values were obtained for juxtacellular recordings (0.977 ± 0.004 , mean \pm SEM, $n = 18$ calyces; Figure 2.2D), suggesting that this finding was not a consequence of washout, nor the result of R_s -related capacitive filtering. Moreover, within a miniburst the maximal rate of rise of the third AP was similar to the first AP (time interval: 21 ± 2 ms, ratio AP_3/AP_1 : 1.02 ± 0.01 , mean \pm SEM, $n = 9$ calyces), showing remarkable stability considering the high firing frequencies and the young age of the animals. In addition, following high-frequency bursting, the half width, defined as the AP width at -35 mV, increased by only $4 \pm 1\%$ (mean \pm SEM, $n = 9$; Figure 2.2D and Figure 2.7). In juxtacellular recordings, the AP half width is best represented by the delay between the positive and negative peak (see Fig. 3F in [134]), and, similarly, in juxtacellular mode this delay increased by $4.0 \pm 0.7\%$ (mean \pm SEM, $n = 18$; Figure 2.2D). The change in half width correlated with the AP depression ($r = -0.55$, $n = 27$; Figure 2.7). We conclude that the shape of the presynaptic AP hardly changed during high-frequency activity.

We next investigated which mechanisms were responsible for the remarkable stability of the presynaptic AP shape. At short intervals, the membrane potential following the AP, V_{after} , will determine the onset potential of the next AP. To see how V_{after} affected the rate of rise of the next AP, we compared consecutive AP pairs during long depolarizing or hyperpolarizing current injections.

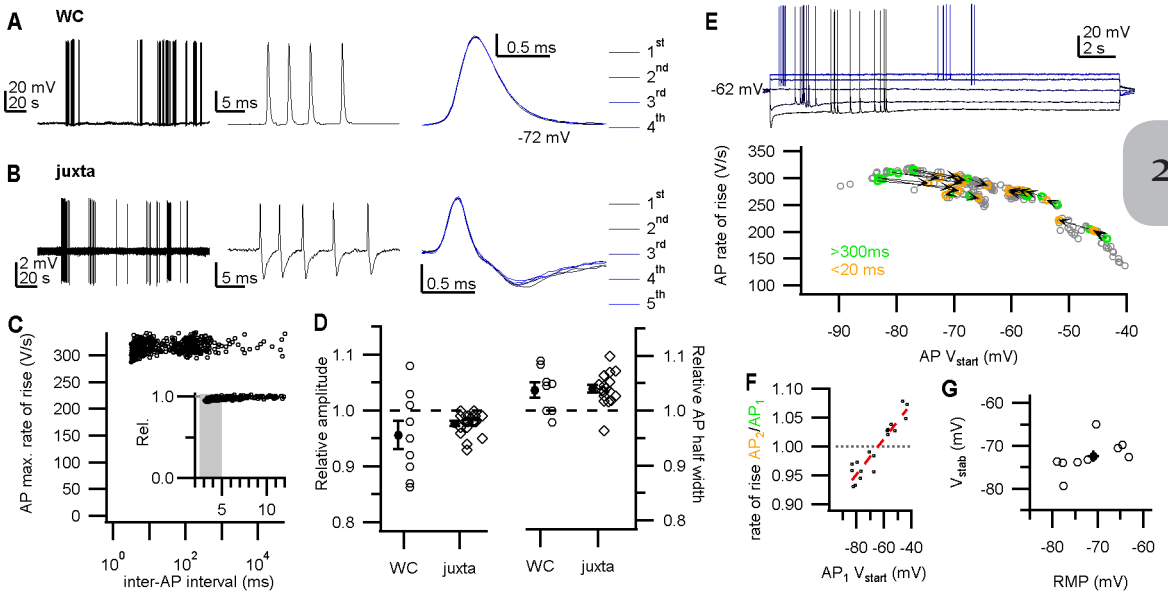


Figure 2.2 Little AP depression during *in vivo* firing. (A) Left, *In vivo* whole-cell recording (WC) shows periods of calyceal bursting activity. Middle, high-frequency miniburst. Right, overlay of the four APs. (B) *In vivo* juxtacellular recording (juxta) shows similar activity as in A, and an overlay of the five eAPs is shown (right). (C) The maximal rate of rise against the inter-AP interval from a single whole-cell recording. (Inset) The maximal rate of rise relative to the preceding AP against the inter-AP interval shows a small but clear depression at short intervals. An average was calculated for the intervals within the grey area to compare between recordings. (D) Left, The relative amplitude at intervals below 5 ms shows a small depression. For WC the relative change in AP rate of rise is shown; for juxta the relative change in eAP amplitude. Right, Changes in AP half width for intervals <5 ms. (E) Top, 20 seconds of constant-current injection with spontaneous burst firing. Constant-current injection started at -120 pA (lowest trace), incrementing 60 pA (indicated in blue shades). Bottom, AP maximal rate of rise against the onset potential. Orange-green connected circle pairs correspond to a pair of APs of which the first AP (AP_1) was not preceded by an AP within 300 ms (green) and the second AP (AP_2) followed AP_1 within 20 ms (orange). (F) The relative rate of rise of AP_2 in E against the onset potential of AP_1 . Red broken line shows linear fit. Intersection with the black broken line where AP_2/AP_1 equals 1 was at -64.9 mV. (G) The stability potential (V_{stab}) vs. the resting membrane potential (RMP). The linear correlation was not significant ($r = 0.5$, $F_{1,7} = 2.8$, $p = 0.14$). Circles in C and E indicate APs. Open circles in D and G indicate recorded calyces; closed circles correspond to averages. Circles in F indicate AP pairs. Bars indicate SEM.

Interestingly, if the calyceal membrane potential was hyperpolarized, the second AP would start at a more depolarized potential than the first and be relatively depressed; conversely, if the first AP started at a depolarized potential, the second AP would start at a more hyperpolarized potential and be potentiated compared to the first AP (Figure 2.2E). To find the potential at which the depression reversed to potentiation, the relative change in the rate of rise of the second AP was plotted against the onset potential of the first AP (Figure 2.2F). The potential at which the AP size was stable was obtained by linear regression. This stability potential V_{stab} was close to the resting membrane potential (RMP; Figure 2.2G), indicating that when V_{after} is close to the RMP, the AP shows minimal change in its rate of rise during high-frequency firing. We could not determine a V_{stab} for the AP half width, as the half width modulation did not change linearly with the onset potential, possibly due to inactivation of other voltage-dependent ion channels. Nevertheless, the half width modulation fell within a limited range (0.95 – 1.05). We therefore conclude from our *in vivo* measurements that if the membrane potential between APs is close to the RMP, the AP waveform remains stable during high-frequency firing.

In slice studies the calyceal AP is typically followed by a 3-12 mV depolarizing after-potential (DAP; [20, 152]), yet *in vivo* we observed in seven out of seventeen recordings a hyperpolarizing after-potential (Figure 2.3A, inset). The after-potential did not change during development ($r = -0.1$, $n = 17$ calyces); it did depend on the RMP, with the direction of the after-potential reversing at -71.3 ± 0.8 mV ($r = -0.88$; $n = 17$ calyces; Figure 2.3A). To analyze how V_{after} changes when the AP started at different membrane potentials, we again looked at the long constant-current injections. V_{after} , measured 1.8 ms after the AP peak, seemed to be largely independent of the onset potential of the AP in all recordings in which the AP started from -75 mV or more negative potentials (Figure 2.3A), whereas at potentials more positive than -70 mV, V_{after} depolarized with a $+0.58 \pm 0.03$ mV per mV change in the AP onset potential (mean \pm SEM, $n = 5$ calyces; Figure 2.8). Instead of focusing on the difference between the membrane potential before and after the AP [20, 152], we will focus on the absolute value of the membrane potential after the AP (V_{after}), which is more important for the impact on the next AP.

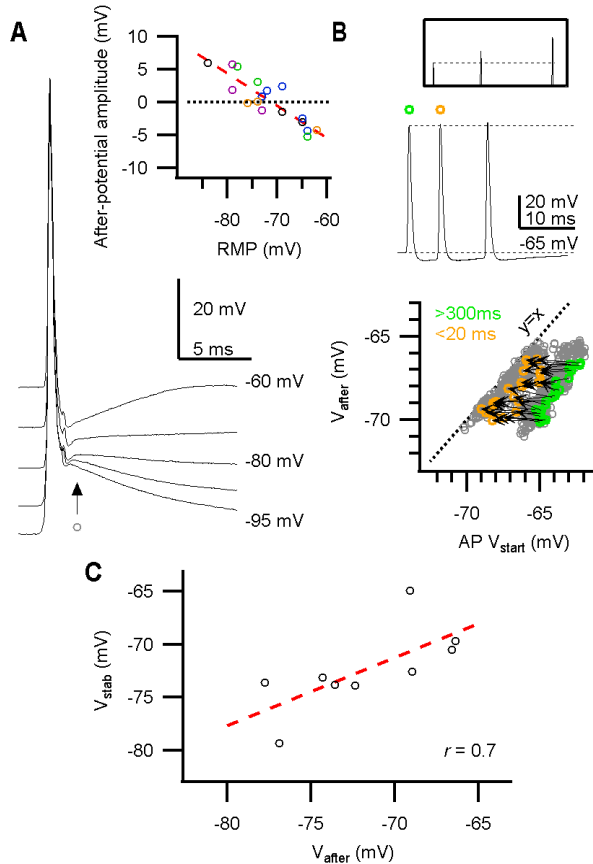


Figure 2.3 During *in vivo* high-frequency firing the membrane potential between APs is close to the potential at which APs are stable. (A) Five spontaneous, peak-aligned APs with different onset potentials due to constant-current injection. The after-potential was measured at 1.8 ms (arrow) after the AP peak. Inset, The after-potential amplitude against the resting membrane potential (RMP). Circle color indicates pup age; black, blue, green, magenta, orange are <P4, P4, P5, P6, >P6, respectively. (B) Top, a high-frequency burst that showed a hyperpolarizing after-potential, and a potentiated AP amplitude (inset). Bottom, the after-potential against the AP onset potential. Grey circle is an AP; green-orange paired circles correspond to a pair of consecutive APs of which the first AP was not preceded by an AP within 300 ms (green) which was followed by a second AP within 20 ms (orange). The arrow represents the change in the after-potential and onset membrane potential for each pair. (C) V_{stab} against the after-potential. For A and C: each circle corresponds to a calyx.

During burst activity, V_{after} becomes the onset potential of the next AP, which may thus keep onset potentials during a burst stable [144]. Indeed, at high firing frequencies the onset potential of an AP overlapped with V_{after} of its predecessor (Figure 2.3B), and when the after-potential was hyperpolarizing, the next AP

could be potentiated (Figure 2.3B). Furthermore, V_{after} was close to V_{stab} (Figure 2.3C). During a period of increased activity, V_{after} became more depolarized, and the after-potential could switch from hyperpolarizing to depolarizing (Figure 2.8). On average, the after-potential depolarized with 1.7 ± 0.2 mV during an active period (mean \pm SEM, $n = 9$ calyces; paired t -test AP_1 vs AP_{15} : $t_8 = 8.5$, $p < 0.01$), and although this change was statistically significant, such a small depolarization of the onset potential would only minimally change the AP properties (cf. Figure 2.2E). Considering the small size of the changes in the after-potential during an active period, we conclude that V_{after} provides a stable AP onset potential at a value that keeps the AP waveform invariant.

Resistance to depression in slices

Two limitations of our *in vivo* recordings were the low-pass filtering related to the high series resistance and the inability to systematically test different afferent activity patterns. We therefore also made calyceal recordings in acute brainstem slices. Afferent fibers were stimulated via a bipolar stimulation electrode placed at the midline. With this approach we tested whether depression would be more extensive at frequencies exceeding the frequencies observed *in vivo* (>400 Hz). At physiological temperatures the calyx was able to fire at these frequencies [101], and the AP rate of rise depressed to 0.88 ± 0.02 at 2-3 ms intervals (mean \pm SEM, $n = 17$, age P4-9). In 16 out of 17 terminals, we could determine both V_{stab} (-70 ± 1 mV, mean \pm SEM) and V_{after} (-71 ± 1 mV, mean \pm SEM). The two were again matched closely ($r = 0.9$; Figure 2.9). V_{after} did not change in 2 mM calcium ($n = 6$; $\Delta V = 0.3 \pm 0.8$, $t_5 = 0.9$, $p = 0.8$; Figure 2.10), suggesting a limited role for calcium channels or calcium-activated channels in setting V_{after} [158]. In addition, no effect of XE991 (10 μ M) on the after-potential was found ($n = 5$; $\Delta V = -0.6 \pm 0.7$, $t_5 = 0.1$, $p = 0.5$; Figure 2.10), suggesting that K_v7 -channels did not significantly contribute to the first milliseconds of the after-potential [158]. Lastly, we quantified the stability of the AP shape during AP trains with different inter-AP intervals (2 ms to 100 ms). The waveform of the first AP differed from the other APs in the train (Figure 2.11). The first AP was sensitive to the current injections ($r = -0.95$), while the second to fifth AP did not change (range of $r = -0.4$ to 0.2 ; Figure 2.11), again indicating that the after-potential stabilizes the calyceal AP shape.

During burst activity the after-potential affects AP depression by the time-dependency of recovery from inactivation and the steady-state channel availability for the next AP. In order to disentangle the two effects we modeled the AP depression (“Supplementary Information”). First, we measured the steady-state depression as a function of the onset potentials by means of current injections. These recordings indicated that the AP is slightly depressed at RMP (V_{half} : -54.8 ± 2.6 mV; k : 7.0 ± 0.9 mV, $n = 14$, mean \pm SEM). Then, we used the steady-state depression to predict the depression induced by a stimulation train that was composed of multiple intervals representing *in vivo*-like activity with additional 2-3 ms intervals (Figure 2.12A). The steady-state values did not capture the depression at the shortest intervals (1 free parameter, explained variance: $60 \pm 5\%$, $n = 14$, mean \pm SEM; Figure 2.12B). Adding recovery from depression, which included a voltage-dependent time constant as described in ref. [159], improved the prediction (2 free parameters, explained variance: $86 \pm 2\%$, $n = 14$, mean \pm SEM; Figure 2.12D), suggesting that steady-state recovery was not attained at the briefest interspike intervals. To reach 96% and 98% recovery from depression to the steady state associated with the onset potential of the next AP took 2.8 ± 0.2 ms and 3.5 ± 0.2 ms respectively (mean \pm SEM, $n = 14$; Figure 2.12C), indicating that most intervals observed *in vivo* are sufficiently long for recovery to reach a steady state. Lastly, we tested to what extent the model with the average values could predict the depression *in vivo* by using the intervals and onset potentials observed in each experiment. The predicted depression matched the observed depression well for animals $>P_4$ ($n = 6$, $r = 0.9$), while for P_3 -4 the model underestimated the *in vivo* depression (-0.16 ± 0.2 , $n = 3$, mean \pm SEM; Figure 2.12H). Together, these findings indicate that at P_5 the rapid recovery from depression allows the calyx to fire at high frequencies with little or no AP depression.

Presence of $\text{Na}_v1.6$ in calyx terminals

The ability of the neonatal calyx of Held to fire at high frequencies with little depression suggests that it expresses sodium channel 1.6 ($\text{Na}_v1.6$) already shortly after its formation [159, 160]. Brainstem sections of different postnatal ages were immunolabeled with a $\text{Na}_v1.6$ antibody. Already at P_2 -3, weak expression was observed throughout the ventral auditory brainstem. The immunolabeling

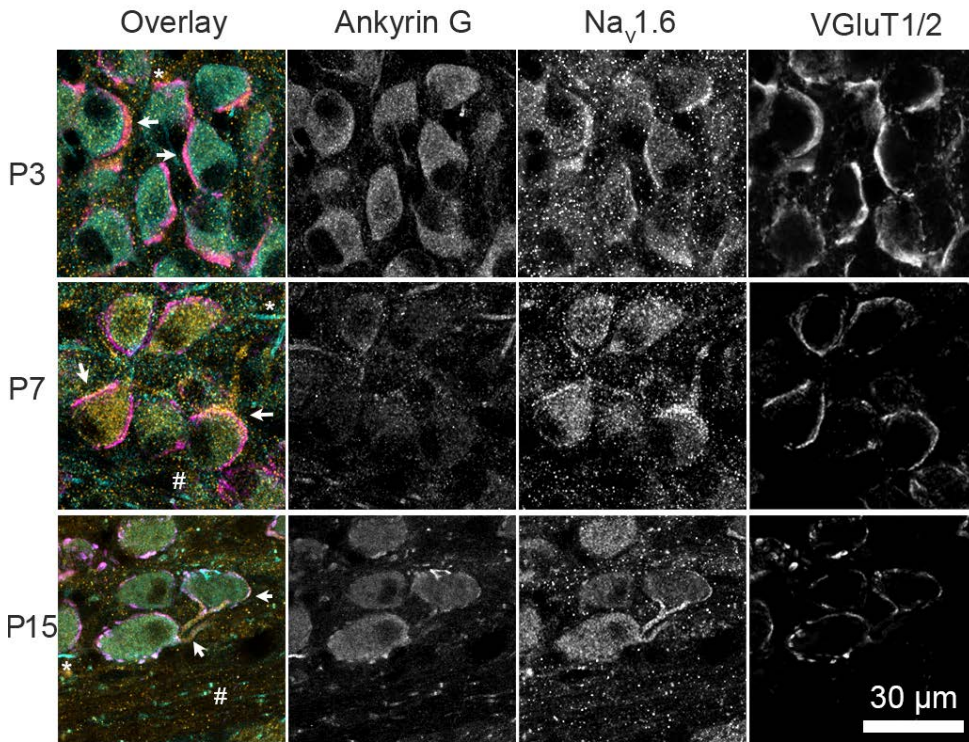


Figure 2.4 Presynaptic labeling of sodium channel 1.6 during postnatal development. Confocal images of the MNTB (P3, P7 and P15 rat) that were immunolabeled for Ankyrin G, sodium channel 1.6 ($\text{Na}_v1.6$) and vesicular glutamate transporter 1/2 (VGluT1/2) reveal co-localization of the strongest $\text{Na}_v1.6$ -staining with presynaptic VGluT1/2. Confocal images were pseudo-colored in ImageJ and contrasted in Adobe Photoshop 11.0.

showed overlap with labeling for the vesicular glutamate transporter 1/2, but not with Ankyrin G (Figure 2.4). No evidence for the presence of heminodes was obtained at this developmental stage. To confirm the presynaptic presence of $\text{Na}_v1.6$, we electroporated *in vivo* the calyceal axons with a fluorescent dye to label the axon that gives rise to the terminal, and again stained those terminals for $\text{Na}_v1.6$ and Ankyrin G. $\text{Na}_v1.6$ signal co-localized with the electroporated axons; no heminodes were observed (Figure 2.13). Surprisingly, $\text{Na}_v1.6$ intensity was highest in the terminal itself, in contrast to a previous report [159], which might be related to the early developmental stage, at which no heminode has yet been formed [161, 162]. We conclude that $\text{Na}_v1.6$ is already present at the calyx of Held shortly after its formation.

Discussion

Here, we report on *in vivo* whole-cell and juxtacellular recordings from the calyx of Held, a terminal whose accessibility for slice recordings has made it a popular subject for studying the biophysics of transmitter release. In developing rodents the calyx of Held fired in a burst manner at >200 Hz with no sign of failures, remarkably little depression or broadening of the AP, and rapid recovery from AP depression. We defined the stability potential V_{stab} as the membrane potential following the AP at which the next AP would not change shape, and found it to be close to the resting membrane potential. Moreover, the membrane potential following the AP (V_{after}) was close to V_{stab} , which means that during high-frequency firing, when V_{after} determined the onset potential of the next AP, AP stability was maximized. Immunolabeling indicated that the sodium channel $Na_v1.6$ was already present in newly formed calyces, providing a molecular basis for the observed lack of AP depression both in slices and *in vivo*. These results thus demonstrate important mechanisms underlying fast signaling during natural firing of the calyx of Held.

Mechanisms limiting AP depression during natural activity

We observed that the shape of the calyceal AP was remarkably invariant during *in vivo* firing. Even though instantaneous firing frequencies of 200 Hz were observed already at P2-3 when the calyx forms, there was little AP depression. Two factors appeared to be crucially important for the lack of a change in the AP's shape: fast recovery from AP depression and a membrane potential between APs that minimized AP waveform changes.

The AP depression obtained in slice recordings was largely independent from the interval between APs. Only at the 2-4 ms intervals a time-dependent component in the recovery was observed. The combination of a steady-state depression with a time-dependent recovery adequately described the observed AP depression, suggesting that the fast recovery of calyceal sodium channels from inactivation [159] provided a reasonable description of the recovery from AP depression. Immunolabeling evidence was obtained for the early presence of $Na_v1.6$, which is known for its swift kinetics and resistance to inactivation during high-frequency firing [163]; the presence of $Na_v1.6$ is in agreement with studies at the calyx of Held at later developmental stages [159, 161, 162]. No evidence

was found for the presence of heminodes, which do not form until the second postnatal week, presumably triggered by myelination [152, 161, 162, 164]. An increase in glial coverage and the replacement of the cup shape by the calyceal fingers precluded an investigation of the properties of the mature calyx *in vivo*. The mature calyx has even briefer APs after hearing onset [156], to which an exclusion of sodium channels from the calyx may contribute [159].

2

A second contributing factor to the resistance to spike depression *in vivo* was that V_{after} was close to V_{stab} , the potential at which the shape of the AP became invariant. The *in vivo* RMP, which was also close to V_{after} , was within the same range as previous slice reports, although in most cases a more negative RMP and a larger DAP were reported [19, 20, 156, 165-167]. Assuming that the larger DAP is due to the more negative RMP, a difference in temperature might explain the difference with many of the earlier slice experiments, since the RMP of the calyx tends to be more depolarized at physiological temperatures [168], and many of the earlier slice experiments were done at room temperature. As the RMP at the calyx of Held is set by the potassium channel subunit $K_{v7.5}$ [165], I_h [169], the Na^+/K^+ -ATPase [170] and a persistent sodium channel [166], subtle differences in any of these four conductances (or driving forces) may be responsible for the observed small difference in RMP compared to some previous slice studies. Apart from $K_{v7.5}$, for which blocking showed little effect on V_{after} , these conductances are also likely to contribute to setting V_{after} , with an additional prominent role for K_v1 channels [167, 171] and resurgent sodium channels [152].

Resurgent sodium currents not only make an important contribution to the after-potential of the calyx of Held, they also promote faster APs and higher frequency signaling [152]. Most likely, the resurgent sodium currents reflect the unblocking of a pore blocking particle from the auxiliary $\text{Na}_v\beta_4$ channel subunit, which can rapidly block $\text{Na}_v1.6$ upon opening [154]. The blocking particle allows for brief APs, and it limits sodium channel inactivation. At very short intervals, facilitation of K-channels may also contribute to keeping the APs brief [172]. Rapid closure of axonal sodium channels is expected to increase the energetic efficiency of the AP [173]. The transient opening of the sodium channel due to the unblocking of this particle at negative potentials has been viewed as a byproduct, but we suggest that the resurgent current serves to set V_{after} close to

V_{stab} , thereby sustaining invariant AP firing. Together, these adaptations thus allow remarkably stable APs, even at high firing frequencies.

Functional implications

In general, the after-potential controls the availability of voltage-dependent ion channels during high-frequency signaling and sets the onset potential of the next AP. More specific functions have been proposed for the after-potential in terminals. The DAP may be responsible for increased excitability following an AP in hippocampal Schaffer collaterals [174], but a large DAP may lead to sodium channel inactivation and spike failures [152]. A decrease in presynaptic AP amplitude might contribute to short-term depression [139], although these changes might be counteracted by a broadening of the AP [175]. By controlling the deactivation of Ca^{2+} channels, the after-potential may directly control transmitter release, but a recent study at the calyx of Held found the total calcium influx to be largely independent of the value of the after-potential [176]. At hippocampal mossy fiber terminals, the DAP may contribute to cumulative inactivation of K_v1 channels, resulting in spike broadening [142], and thereby contributing to the strong synaptic facilitation during high frequency bursts [142, 177]. The transmission characteristics of this synapse differ substantially from the relay function of the calyx of Held synapse [16] or the cerebellar mossy fiber synapse [141], and this difference might partially be a consequence of V_{after} being more depolarized than V_{stab} . For *en passant* boutons, the impedance mismatch imposed by their geometrical shape makes the axon vulnerable for frequency-dependent propagation failures [139]. The use of voltage indicators [144, 149, 150] might allow to test whether the mechanisms identified here may also help to stabilize AP speed and secure AP propagation in boutons.

We propose that, in agreement with data obtained in the crayfish neuromuscular junction [144], an important function of the after-potential is to preserve the shape of the presynaptic AP. The close correspondence of resting membrane potential, V_{stab} and V_{after} makes not only the onset potential of action potential remarkably independent of firing frequency, but also results in a remarkably stable AP shape. For a relay synapse such as the calyx of Held, which excels in being precise and reliable over a wide range of firing frequencies [16], this has obvious advantages. Changes in AP shape due to a change in sodium

channel availability will not only affect the opening of calcium channels, the timing and amplitude of Ca^{2+} -influx, and neurotransmitter release, but will also affect axonal propagation speed, resulting in a loss of timing precision [140]. We conclude that our *in vivo* recordings of the calyx of Held provide new insights into the mechanisms that keep APs stable. Future experiments may clarify how the relation between V_{after} and V_{stab} is controlled, and whether their relation can be dynamically adjusted at the calyx of Held and other presynaptic terminals.

2

Materials & Methods

All experiments complied with institutional and European guidelines, and were approved by the animal ethical committee of the Erasmus MC. Briefly, timed-pregnancy Wistar dams were purchased from Envigo (Horst, The Netherlands) or Charles River (Sulzfeld, Germany) and were housed within the animal facility of the Erasmus MC. The day of birth was taken as postnatal day (P)0. Neonate pups were anesthetized with isoflurane, intubated and mechanically ventilated, and underwent a ventral approach to expose the right ventral brainstem [90, 153]. Prior to the recordings, anesthesia was reduced to 1 % isoflurane which kept the animal areflexive. The *in vivo* electroporation with Alexa Fluor 594 dextran (Molecular Probes) was described in ref. [90]. The *in vivo* electrophysiological methods are detailed in ref. [153]. Junction potential of the K-gluconate based intrapipette solution (-11 mV) was corrected. Gigaseal formation was obtained by gentle suction followed by pipette capacitance (C_p) compensation in voltage-clamp mode of the Axopatch 200B (Molecular Devices Co.). Brief suction was applied to establish the whole-cell configuration, and the RMP was measured immediately after break-in. Voltage recordings were made in CC-fast mode. The recordings were low-pass filtered (4-pole Bessel, 10 kHz) and digitized at 25 kHz. Series resistances (R_s) were measured (Figure 2.5), but the voltage drop across R_s was corrected off-line.

Acute brainstem slices were made as reported in ref. [20]. R_s was fully compensated. C_p was either compensated in voltage-clamp or in current-clamp mode. Recordings were low-pass filtered (4-pole Bessel, 10 kHz) and digitized at 25 or 50 kHz. Custom-written analyses were made in the Igor Pro environment (Wavemetrics). For the depression model we only included the recordings for

which >70% of the total variance was explained (n = 14 of 17 calyces).

The biocytin fluorescent labeling procedure has been described elsewhere [153]. For the immunolabeling of sodium channel 1.6, brainstem sections (40 μm) underwent antigen retrieval by 3h incubation at 80°C in 10 mM sodium citrate; they subsequently followed the same immunolabeling procedure as detailed in refs. [153, 178] with Tris-buffered solutions (pH 7.6). More details can be found in the Supplementary Information.

Acknowledgments: The research was funded by the Nederlandse Organisatie voor Wetenschappelijk Onderzoek – Aard- en Levenswetenschappen ('Development of a giant synapse', #823.02006). The confocal scanning microscope was accessed through the Optical Imaging Center at Erasmus MC. We thank Kees Donkersloot for technical support, and Elize Haasdijk and Erika Goedknecht for support with histology, Fereshta Zakeri for performing control immunolabelings, and Maarten Kole for helpful comments.

Supplementary Information

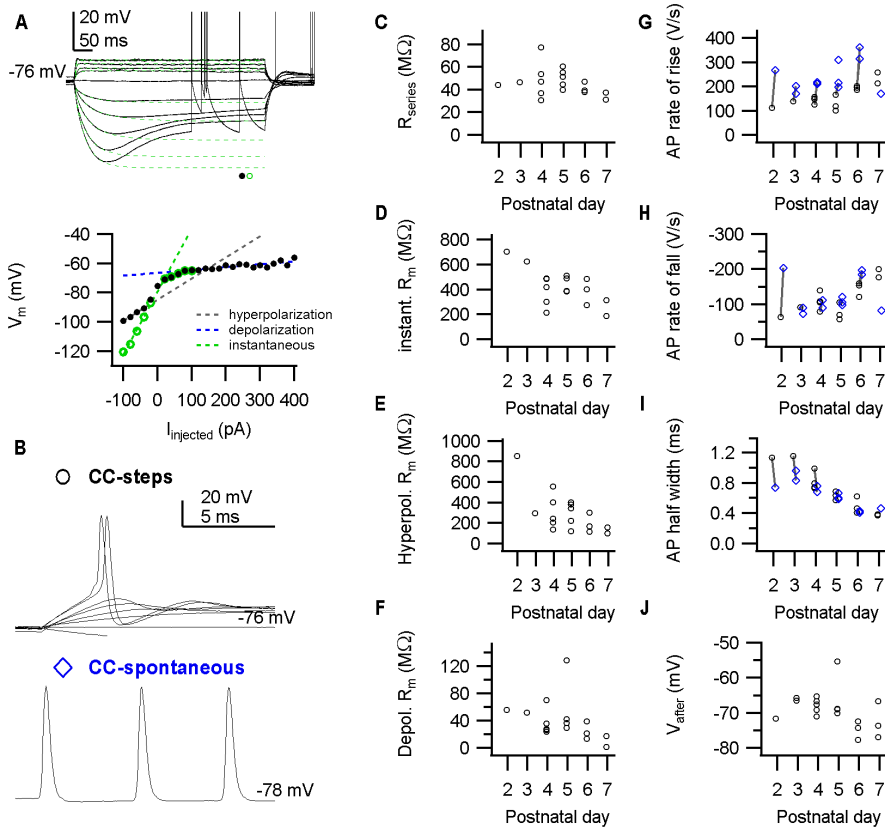


Figure 2.5 Developmental changes in active and passive properties of calyces during whole-cell *in vivo* recordings. (A) Top, example traces of constant-current injections depict a voltage-sag and outward rectification. Traces were fitted with a double-exponential function (green dotted lines). Bottom, steady-state values of the fit (green circles) or the recording (black circles) were obtained at the end of the current injections, and are plotted against the current amplitude. Slope resistances (broken lines) were obtained from line fits. (B) Examples of spontaneous APs (bottom) and APs elicited by constant-current injections (top). (C) Series resistance against pup age. Series resistance was calculated from VC recordings (not shown) as described in ref. [153]. (D) Instantaneous slope resistance (green broken line in A) against pup age. (E) Slope resistance calculated from hyperpolarizing current injections (black broken line in A) against pup age. (F) Slope resistances calculated from depolarizing current injections (blue broken line in A) against pup age. The outward rectification extensively lowers the slope resistance. (G) AP maximal rate of rise of evoked (black circles) and spontaneous APs (blue diamonds) against pup age (labels in B). (H) AP maximal repolarization/rate of fall of evoked (black circles) and spontaneous APs (blue diamonds) against pup age. (I) AP half width of evoked (black circles) and spontaneous APs (blue diamonds) against pup age. (J) V_{after} of spontaneous APs against pup age. Data points indicate calyces. The lines in G-I connect spontaneous APs (blue diamonds) with evoked APs (black circles) recorded from the same calyx.

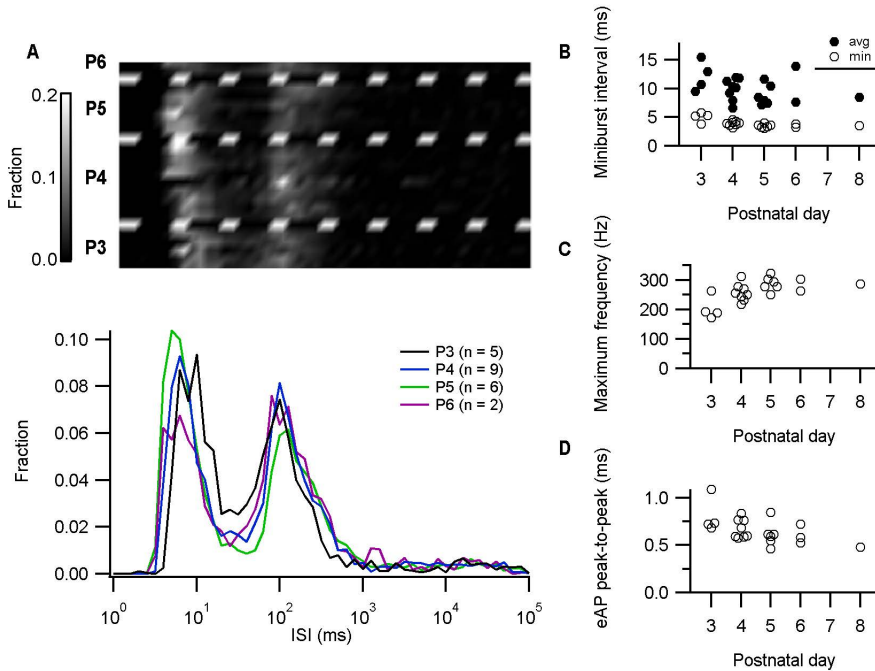


Figure 2.6 Preferred frequencies of spontaneous firing in *in vivo* juxtacellular recordings from the calyx of Held. (A) Upper panel shows probability density plots in grey-scale for individual juxtacellular recordings grouped by pup age. Lower panel displays the average probability density against the interspike interval (ISI) for the different pup ages on a semi-logarithmic plot. (B) The average and minimal miniburst interval (i.e. intervals < 40 ms) against pup age. (C) The maximum instantaneous frequency against pup age. (D) The AP half width, estimated as eAP peak-to-peak interval, against pup age. For B-D: circles represent individual juxtacellularly recorded calyxes.

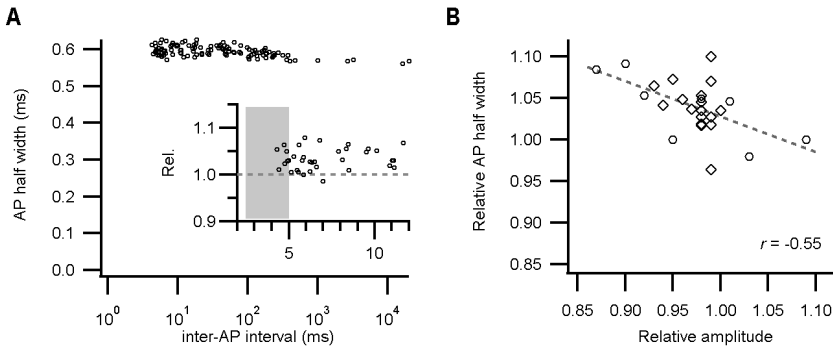


Figure 2.7 AP half width modulation during high-frequency firing is minimal. (A) The AP half width against the inter-AP interval in a whole-cell recording from a P5 calyx. (Inset) The AP half width relative to the preceding AP against the inter-AP interval. (B) The relative size of the AP half width against either the amplitude of juxtacellular eAPs (diamonds) or the rate of rise of whole-cell APs (circles). The line indicates the regression line ($r = -0.55$; $t_{23} = 2.9$; $p = 0.004$).

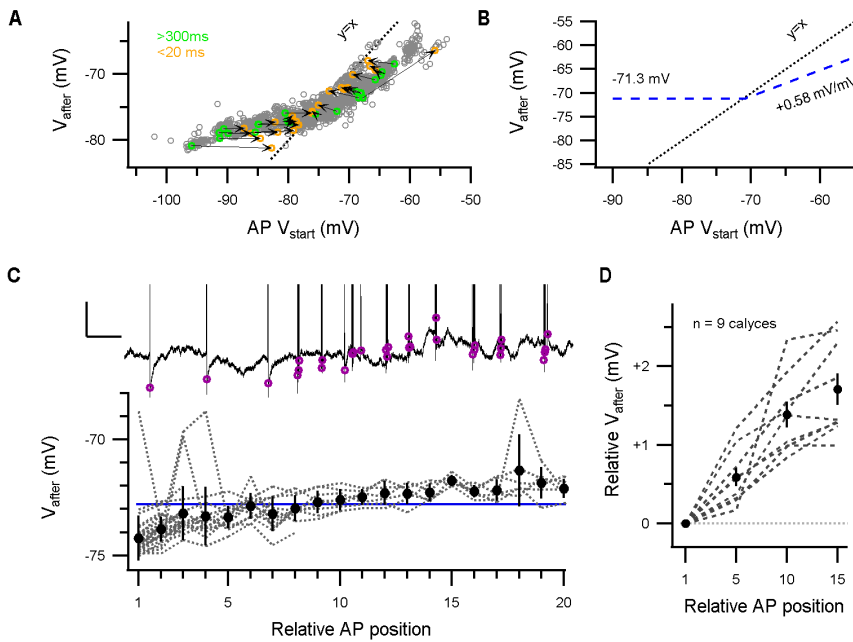


Figure 2.8 V_{after} changes with constant-current injection and during bursting activity. (A) V_{after} against the onset potential of spontaneous APs during long-lasting constant-current injections. Green–orange circle pairs correspond to pairs of APs of which the first AP (green) was not preceded by an AP within 300 ms and the second AP (orange) followed the first one within 20 ms. Dotted line depicts identity line. V_{after} dominates the onset potential of subsequent APs during high-frequency firing. (B) Model graph of the relation between the AP onset potential and V_{after} . For hyperpolarized onset potentials, V_{after} will reach a constant membrane potential (here, -71.3 mV). At depolarized potentials, the afterpotential depolarizes with $+0.58$ mV/mV, possibly due to inactivation of potassium channels like $K_{\text{V}1}$ that counteract the depolarization (Figure 2.9). (C) Upper panel displays an example of an active period where the after-potential (magenta circles) depolarized during the burst. (Calibration bar: 2 mV, 0.2 s.) Lower panel, After-potential against the relative AP position in active periods of a single P6 recording. The blue line indicates the RMP. During activity, the after-potential depolarized, and thereby switched from a HAP to a DAP. (D) The relative changes in after-potential during an active period against the relative AP position across recordings.

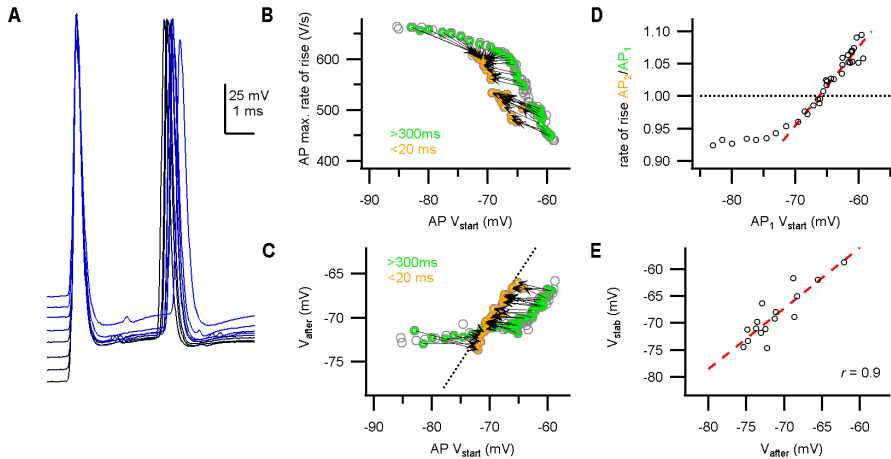


Figure 2.9 The AP stability potential V_{stab} correlated with V_{after} in slice recordings. (A) During constant-current injections, the calyceal axon was stimulated at the midline to elicit an AP doublet with 3-ms interval. APs from a P5 calyx are aligned on the peak of the first AP. Stimulus artifacts are subtracted. (B) AP maximal rate of rise against the onset potential. Doublets are indicated in green–orange circles and connected by an arrow. The arrows reverse direction, suggestive of a stability potential. Additionally, notice the steady-state depression of the AP as a result of the changed onset potentials. (C) Relation between V_{after} and onset potential. V_{after} is relatively constant for onset membrane potentials less than -70 mV. Broken line is the identity line. (D) The relative AP rate of rise of the doublets against the onset potential of the first AP. Red broken line indicates linear fit of data points close to 1. (E) Relation between V_{stab} and V_{after} . Red broken line indicates regression line ($r = 0.9$).

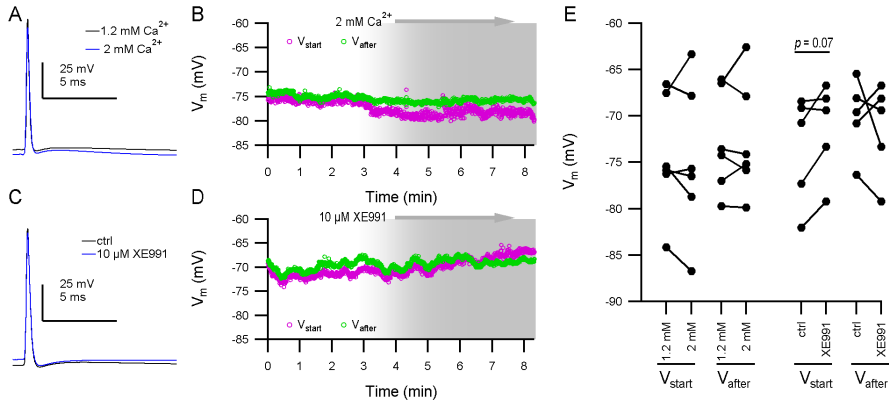


Figure 2.10 The after-potential is independent of calcium concentration or K_v7 channels. (A) Average of 25 APs of a P8 calyx is shown recorded with an extracellular calcium concentration of 1.2 mM (standard concentration, black) or 2 mM (blue). (B) The onset potential (V_{start} , magenta) and V_{after} (green) during an experiment where the extracellular medium was replaced with 2 mM Ca^{2+} extracellular medium. At around $t = 3$ min the new medium entered the bath. Shaded area depicts the expected period where the calyx becomes exposed to the new extracellular medium. Every circle represents a single AP. APs shown in A are from the same recording. (C) Average of 25 APs of a P5 calyx is shown recorded before ('ctrl') and after the addition of 10 μ M XE991. (D) Similar to B, but for K_v7 -blocker XE991. APs shown in B belong to the same experiment. (E) Summary scatter plots for the different pharmacological experiments. Connected circles are from a single recording. No significant effect of higher extracellular calcium concentration was observed on either V_{start} or V_{after} . XE991 did not significantly affect V_{after} , but a trend for a depolarization in the V_{start} was observed ($\Delta V = 2.2 \pm 0.9$, $t_5 = 1.7$, $p = 0.07$), as reported by ref. [165].

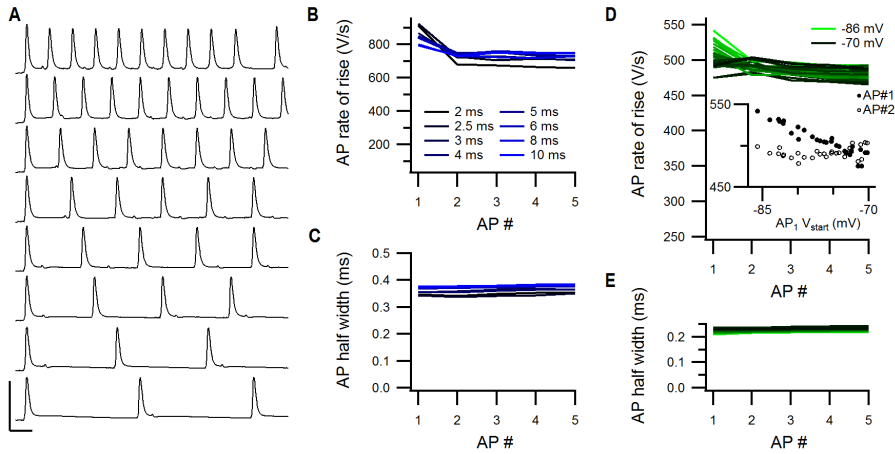


Figure 2.11 High-frequency trains remain stable after the first AP. (A)

Example trains elicited at different intervals by midline electrical stimulation in a P7 slice. AP properties are shown in B and C. Stimulus artifact is subtracted. Calibration bar: 100 mV, 2 ms. (B) AP rate of rise against the AP order number in the train. Only from the first to the second AP a clear change is observed. (C) AP half width against the AP order number in the train. (D) AP rate of rise against the AP order number of a P6 calyx during constant-current injections to bias the onset potential. The onset potential of the first AP is color-coded. The inset shows the AP rate of rise against the onset potential of AP #1. The closed circles are of the first AP in the AP train (AP #1), and the open circles are the second AP in the AP train (AP #2). Whereas the rate of rise of AP #1 was strongly correlated with the biased onset potential ($r = -0.95$), the AP #2 was not ($r = 0.2$). (E) Same as in D, but for the AP half width.

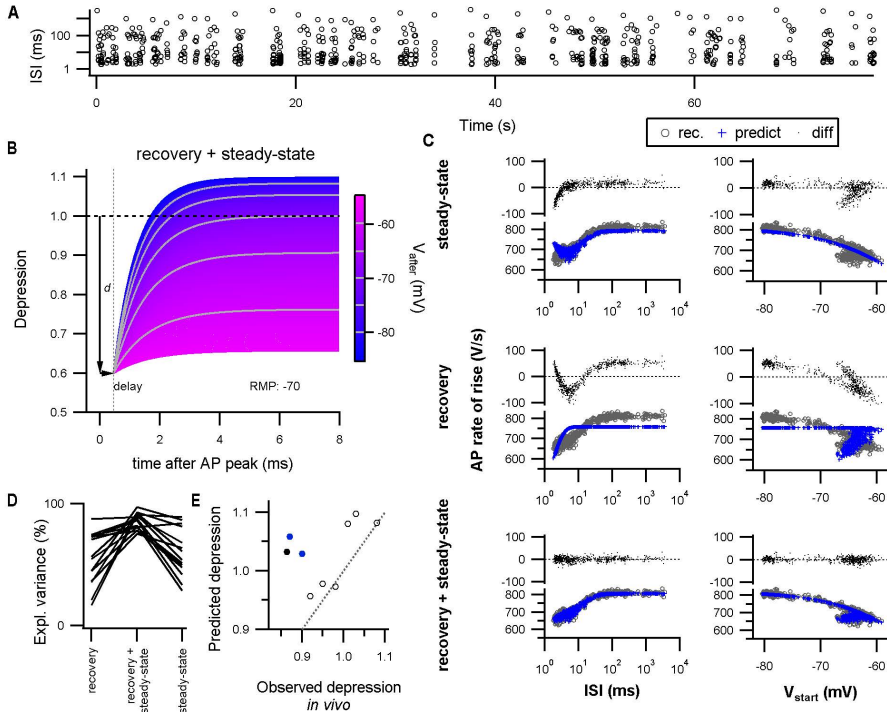


Figure 2.12 Combining *in vivo*-like activity patterns with modeling to analyze the impact of the after-potential on AP depression. (A) Stimulus pattern composed of a range of frequencies with random order. This pattern was used for stimulation of the afferent axon of the calyx of Held to elicit AP firing at a wide range of different frequencies. (B) Expected relative depression following an AP as a function of V_{after} (color). For the plot, it was assumed that there was no residual depression of previous APs and that the RMP was -70 mV. The AP causes a depression (d). Recovery from depression starts after a delay, which was 0.45 ms in this case, as the AP first needs to repolarize. Both the time constant for recovery as well as the steady-state depression depend on V_{after} (“Supplementary Information”). Note that, if the afterpotential is close to RMP, the recovery is complete in 5 ms. Moreover, a HAP will speed up the recovery and could even reverse the relative depression to a relative potentiation, as was indeed observed *in vivo*. (C) The recorded AP rate of rise was fitted by the full AP depression model (recovery plus steady state) or its reduced forms (steady state or recovery alone; “Supplementary Information”). The results for a single recording fitted by the different models are shown. The left panels show the AP rate of rise against the interspike interval (recorded, gray circle; model prediction, blue cross), and the differences between recorded and predicted AP rate of rise are shown on top (black dots). In the Right panels, the relation between the AP rate of rise and the onset potential (V_{start}) of the same dataset is shown. The model that only includes the recovery from depression (explained variance: 45%) shows a bias in the residuals against V_{start} . On the other hand, the model that only includes the steady states (explained variance, 87%) shows a bias in the residuals at the briefest interspike intervals. The combined model describes the data well (explained variance, 97%). (D)

Neural Activity During the Formation of a Giant Auditory Synapse

The explained variance by the different, nested models, showing that both the steady states as well as the recovery from depression significantly contributed to the model.

(E) Based on the average model fit parameters, the interspike intervals recorded *in vivo*, and the onset potentials recorded *in vivo*, the amount of depression was predicted and averaged for intervals (<5 ms). The predicted depression against the observed depression *in vivo* is shown. Dotted line is identity line. Open circles indicate >P4; closed, black circle indicates P3; closed, blue circles indicate P4.

2

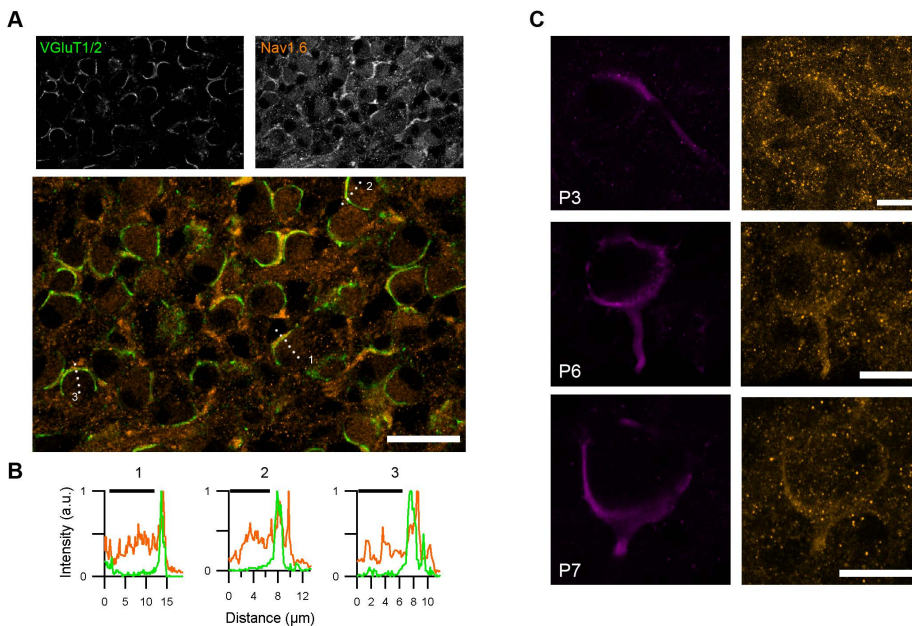


Figure 2.13 Immunolabeling of sodium channel 1.6 ($\text{Na}_v1.6$) in the calyx of Held. (A) Vesicular glutamate transporter 1/2 (VGLUT1/2) (a presynaptic marker) and $\text{Na}_v1.6$ immunolabeling of the MNTB of a P5 rat. Numbers in the lower panel refer to line profiles shown in B. (B) Line profiles of the immunolabeling of presynaptic marker VGLUT1/2 (green) and sodium channel 1.6 (orange). Black bars indicate the postsynaptic neuron. The peak of $\text{Na}_v1.6$ intensity colocalized with VGLUT1/2 or was more distal from the postsynaptic neuron than the VGLUT1/2 peak. (C) Calyceal axons were electroporated *in vivo*, followed by $\text{Na}_v1.6$ labeling. Scale bars: 25 μm (A) and 10 μm (C).

Surgery

All experiments complied with the ethical guidelines for laboratory animals within our institute and with European guidelines, and were approved by the animal ethical committee of the Erasmus MC. The surgical procedures are described in detail in refs. [90, 153].

In vivo electrophysiology and electroporation

Details of the electrophysiological methods have been provided in ref. [153]. In short, whole-cell recordings were obtained with an Axopatch 200B (Molecular Devices Co.) in either voltage-clamp mode at -80 mV, or current-clamp fast mode. Signals were low-pass filtered at 10 kHz (4-pole Bessel), digitized at 25 kHz by an A/D converter (Digidata 1220A, Molecular Devices Co.) and acquired with Clampex 10.2 (Molecular Devices Co.) running on a Windows XP computer. The potassium gluconate-based intrapipette solution contained (in mM): 126 K-gluconate, 20 KCl, 0.5 EGTA, 10 HEPES, 10 Na₂phosphocreatine, 4 Mg-ATP, 0.4 Na₂-GTP with pH 7.2 adjusted with KOH; in some recordings 2 mg/mL biocytin was added to the intrapipette solution. The junction potential of -11 mV was compensated prior to gigaseal formation. All potentials reported in the paper were corrected for the junction potential. Dehydration of the craniotomy was prevented by regularly rinsing and submerging the opening with (in mM): 135 NaCl, 5.4 KCl, 1 MgCl₂, 1.8 CaCl₂, 5 HEPES with pH 7.2 adjusted with NaOH. Stray capacitances were compensated in cell-attached mode, and upon obtaining whole-cell configuration series resistance was measured (Figure 2.5) in voltage-clamp by a 500 ms, 5 mV step from -70 to -75 mV, but the series resistance was not compensated. Every recording session started with a brief, 500 ms current injections to record the intrinsic properties of the calyx. Long, 20s current injections were also performed to assess the change in AP properties by its starting potentials. Spontaneous activity without current injections was also recorded to see the physiological APs during natural firing. In a few recordings (n = 6) voltage-clamp recordings were made at -80 mV without series resistance compensation. These recordings typically showed strong inward currents caused by the invading AP that escaped the voltage clamp.

Due to the combination of a high series resistance and high, distributed pipette capacitance the time constant of the pipette was close to the calyceal

time constants, limiting optimal compensation with the patch-clamp amplifier. AP kinetics *in vivo* were therefore low-pass filtered. To assess the impact of this filtering effect we compared optimally-compensated recordings and undercompensated recordings in slice recordings with low series resistances. Although APs did show more rapid membrane potential changes, there was no change in the relative amount of depression observed at high-frequency firing.

In vivo electroporation was performed as described in ref. [90]. Broken glass pipettes with a tip opening of 15-20 μm were filled with the dye Alexa Fluor 594-dextran (10 % in 0.5 M NaCl), and lowered to a depth of 100-150 μm dorsal of the basilar artery. Electroporation was performed with 0.3 μA , 250 ms pulses at 2 Hz for 5-10 min via a custom-made pipette holder. The dye was allowed to diffuse within the axon for 1-2 h, after which the animal was transcardially perfused as described in ref. [153] for subsequent immunolabeling.

Brainstem slices and slice electrophysiology

Brainstem slices were made from P4-9 neonatal rats as described in ref. [20]. For the slice recordings, the intracellular pipette solution was supplemented with 10-20 μM Alexa Fluor 488 (Molecular Probes) to validate the recorded structure at the end of the recording. Recordings were performed at physiological temperatures (35-36 $^{\circ}\text{C}$, measured in the vicinity of the slice). The extracellular solution contained (mM): 125 NaCl, 2.5 KCl, 1.25 NaH_2PO_4 , 3 myo-inositol, 2 N-pyruvate, 25 glucose, 25 NaHCO_3 , 0.4 L-ascorbic acid, 1 MgSO_4 and 1.2 CaCl_2 . In a few recordings the CaCl_2 concentration was increased to 2 mM, or XE991 (10 μM) was added to the extracellular solution. The extracellular solution was bubbled with carbogen (95% O_2 , 5% CO_2), and was pumped (2-3 mL/min) through an in-line heater (Warner Instruments) into the recording chamber. We waited until the bath temperature stabilized before approaching the calyx. Recordings were made within 7 h post-mortem. Voltage recordings, obtained in CC-fast mode of the Axopatch 200B amplifier, were low-pass filtered at 10 kHz (4-pole Bessel), digitized at 25 or 50 kHz by an A/D converter (Digidata 1322A, Molecular Devices Co.), and acquired with Clampex 8.2 (Molecular Devices Co.) running on Windows XP. Bipolar stimulation electrodes were purchased from MicroProbes for Life Science (PI2ST30.1H10). Stimulation current was maximally 240 μA (threshold usually <100 μA). The junction potential was compensated.

Series resistance was fully compensated for the current-clamp recordings. Stray capacitances were compensated either in voltage clamp or in current clamp mode. Stray capacitance compensation in current clamp mode gave briefer and larger APs, but did not qualitatively alter the findings reported.

Sodium channel immunolabeling

For immunolabeling rat pups were transcidentally perfused as described in ref. [153]. The sodium channel labeling was done as reported in ref. [178]. Images were acquired with a LSM-700 confocal microscope (Zeiss) and for the sodium channel labeling the acquisition settings were optimized for Purkinje cells that were present in the same coronal slice and functioned as a positive control for Na_v1.6 expression [178, 179], before imaging the MNTB. In general, the labeling in the MNTB was stronger than that for Purkinje cells. 3D rendering was done with Volocity (Improvision, Coventry, UK). Images shown in Figure 2.4 were contrasted in Adobe Photoshop 11.0. The other confocal images were contrasted in ImageJ 1.51j. Pseudo-colours were added in ImageJ.

The following antibodies were used in this study: anti-sodium channel 1.6 (#ASC-009, Alomone Labs, 1:1000 or 1:500, rabbit), anti-vesicular glutamate transporter 1 and 2 (#ab5905 and #ab2251, Millipore, 1:2000, guinea pig, guinea pig), and anti-Ankyrin G (clone N106/36; NeuroMab, 1:1000, mouse). Highly cross-absorbed secondary antibodies were used: Alexa Fluor 405, 488, 555, 680 (Molecular Probes), all at 1:200. Control experiments with omission of primary antibody, or 1 h preincubation with control peptide antigen (100 µg/mL, Alomone Labs) reduced Na_v1.6-labeling to background levels. The specificity of the anti-Na_v1.6 antibody has been shown for mice [180].

AP depression model

AP depression was described by a model that included both the steady-state effects of the membrane potential and its effects on the speed of the recovery. The amount of depression is determined by the actual value of the depression coefficient, D , which ranges from 0 to 1. The value of D determines the size of the i th AP (Y_i) relative to the maximal AP rate of rise (Y_{\max}):

$$Y_i = Y_{\max} D \quad \text{eq. 1}$$

At each AP, D decreases by a fraction d :

$$D \rightarrow Dd \quad \text{eq. 2}$$

The depletion factor d can be viewed as the fraction of sodium channels that are not inactivated by the AP. Recovery from depression does not start until after a delay, since the AP has to repolarize first. This delay was set to 1.5 times the average AP half width in each recording. Following this delay, recovery is described by:

$$\frac{dD}{dt} = \frac{D_V - D}{\tau_V} \quad \text{eq. 3}$$

D relaxes to steady-state depression D_V with time constant τ_V . Integration of eq. 3 while assuming that the membrane potential between AP_i and AP_{i+1} is constantly at the onset potential of AP_{i+1} yields the exponential recovery of D between APs:

$$D_t = D_V + (D_{t_0} - D_V) e^{-\frac{(t-t_0)}{\tau_V}} \quad \text{eq. 4}$$

Where t_0 is the time point at which recovery starts following the AP. Both D_V and τ_V were voltage-dependent. The voltage-dependent effects are based on the impact of the membrane potential on the sodium channel conductance, as its recovery from inactivation has a time constant that is voltage-dependent [154], and its steady-state inactivation also depends on the membrane potential. D_V was measured for every calyx by an independent set of experiments where we injected currents to bias the onset potentials of the calyx and after 500 ms stimulated the afferent axon to elicit an AP. The AP rate of rise could then be analyzed as function of onset potential (similar to what is shown in Figure 2.9B) with the following equation:

$$Y_V = Y_{\max} D_V \quad \text{eq. 5}$$

with D_V described by a simple inverse Boltzmann equation:

$$D_V = \frac{1}{1 + e^{(V_{\text{start}} - V_{0.5})/k}} \quad \text{eq. 6}$$

With two free parameters $V_{0.5}$, the half depression potential, and k , the slope factor. Note that for our purpose a polynomial model would suffice as we only want to get an accurate estimate of how V_{start} translates into Y_{\max} . The Boltzmann equation is however expected to be biologically consistent with the inactivation curve of a voltage-gated channel.

The voltage-dependence of τ_v was based on a voltage clamp study of the calyceal sodium channels [159]. Within the studied voltage range the relation between τ_v and the membrane potential in ref. [159] was nearly linear ($r = 1.0$). By linear regression we quantified the relation and multiplied this by a temperature correction factor, which was also obtained from ref. [159]:

$$\tau_v = \frac{0.5}{1.4}(5.75 + 0.00425(V_m + 10)) \quad \text{eq. 7}$$

To correct for the liquid junction potential we added 10 mV to our recorded membrane potential. Note that based on a Hodgkin-Huxley conductance model we would expect the relation between τ_v and V_m to follow a bell-shaped curve, and therefore the linear extrapolation in eq. 7 may underestimate τ_v .

The fit function iteratively calculates the changes in the depression coefficient, D based on the measured onset potentials and intervals. D is initialized at a value of 1. For each subsequent AP, the evolution of D is calculated using eq. 2 and 4. By using eq. 1 and the two free parameters Y_{\max} and d , the measured AP rates of rise were thus fit with the aid of the ‘All-at-once-fitting’ method implemented in Igor Pro 6 (Wavemetrics); this method has the ability to evaluate the iterative function against the data by using the entire dataset instead of single X-Y pairs. The model incorporates two effects of the after-potential: (1) the after-potential sets τ_v and (2) the after-potential determines D_v . By using simpler variants of the model we can assess how these two effects of the after-potential contribute to the observed depression. To analyze the individual contribution of the recovery from depression, we exclude the steady-state effect by fixing D_v to 1 in eq. 4. The contribution of the steady state depression was addressed by excluding the recovery from depression, thus reducing eq. 1 to eq. 5.

In vivo matching of postsynaptic excitability
with spontaneous synaptic inputs
during formation of the rat calyx of Held synapse

Martijn C. Sierksma, Milly S. Tedja, J. Gerard G. Borst

The Journal of Physiology (2017).

Abstract

In the adult, principal neurons of the medial nucleus of the trapezoid body (MNTB) are typically contacted by a single, giant terminal called the calyx of Held, whereas during early development a principal neuron receives inputs from many axons. How these changes in innervation impact the postsynaptic activity has not yet been studied *in vivo*. We therefore recorded spontaneous inputs and intrinsic properties of principal neurons in anesthetized rat pups during the developmental period in which the calyx forms. A characteristic bursting pattern could already be observed at postnatal day (P)2, before the formation of the calyx. At this age, action potentials (APs) were triggered by barrages of summing EPSPs causing plateau depolarizations. In contrast, at P5, a single EPSP reliably triggered APs, resulting in a close match between pre- and postsynaptic firing. Postsynaptic excitability and the size of the largest synaptic events were developmentally matched. The developmental changes in intrinsic properties were estimated by fitting *in vivo* current injections to a Hodgkin-Huxley-type model of the principal neuron. Our simulations indicated that the developmental increases in I_h , low-threshold K^+ -channels, as well as leak currents contributed to the reduction in postsynaptic excitability, but that low-threshold K^+ -channels specifically functioned as a dampening influence in the near-threshold range, thus precluding small inputs from triggering APs. Together, these coincident changes help to propagate bursting activity along the auditory brainstem, and are essential steps towards establishing the relay function of the calyx of Held synapse.

Introduction

The calyx of Held synapse is a giant synapse in the auditory brainstem that relays incoming activity with high accuracy to the principal neuron of the contralateral medial nucleus of the trapezoid body (MNTB; [16]). The MNTB provides well-timed inhibition to its ipsilateral auditory brainstem nuclei, which plays a role in among others sound localization. In new-born rodents the principal neuron is contacted by multiple axons, indicating that innervation is initially divergent, followed by the formation of the (proto)calyx at around P3 [18, 55, 90, 136, 181]. It is well established that a single globular bushy cell can form multiple calyces [17, 89, 92]. Conversely, there is anecdotal evidence that a single

principal neuron can be contacted by more than one calyx [92, 136, 182], and that a principal neuron can receive multiple large inputs during development [137, 138], but otherwise the role of synapse competition and elimination in the development of the calyx of Held synapse is still largely unresolved. Current evidence does indicate that in the adult each principal neuron will typically be innervated by a single calyx of Held [18, 50, 55]. Several factors make the calyx of Held a valuable model system for synapse development in the central nervous system, including the homogeneity of the MNTB, relative ease of identification of the principal neurons, its well-defined function, and its accessibility both *in vitro* and *in vivo*. The calyx of Held thus shares many advantages with the neuromuscular junction as a model system for developmental studies, but comparatively little is known about calyceal synapse development.

Before hearing onset, principal neurons of the MNTB show bursting activity [183], which has a characteristic pattern that originates from the inner hair cells in the cochlea [74, 105, 106]. The exact temporal pattern of this bursting activity is thought to be crucial for the establishment of precise tonotopy [85]. Direct comparison of the pre- and postsynaptic activity indicated that the calyx is already reliably driving its postsynaptic partner after P4 [155]. In contrast, little is known about spontaneous inputs before that period and their impact on principal neurons. Slice studies have shown that principal neurons are hyperexcitable during the first postnatal days [60, 97]. The high membrane resistance, which was measured to be in the $G\Omega$ range, allows small synaptic currents to elicit an action potential (AP). As the calyx develops structurally, the principal neuron's membrane resistance decreases, thereby reducing its excitability [60, 97].

Within this developmental period, many ion channels are upregulated that could be responsible for this reduction in excitability [60, 184, 185], including the low-threshold K^+ -channels K_v1 , hyperpolarization-activated cation channels I_h , and leak channels [186-188]. Around the same time, auditory neurons switch from tonic to phasic firing in both rodents [60] and birds [188, 189], and the low-threshold K^+ -channels may play an important role in this change [190-193]. Together, these slice experiments suggest a developmental switch in firing mode and excitability around the time the calyx of Held develops in rodents.

3

It is not yet known how changes in intrinsic properties of principal neurons relate to the large changes in the spontaneous physiological inputs around the time the calyx of Held forms and how this impacts firing patterns. We therefore made *in vivo* juxtacellular and whole-cell recordings from principal MNTB neurons to measure their spiking activity *in vivo*, their intrinsic properties, the incoming synaptic activity and the postsynaptic responses in P2-6 rat pups. A Hodgkin-Huxley-type model allowed us to investigate the distinct roles of NMDA receptors, low-threshold K⁺-channels, I_h, and the leak conductance in the measured developmental changes in the input-output relations of principal neurons, thus identifying essential steps towards the establishment of the adult relay synapse.

Materials & Methods

Ethical approval

All experimental procedures were in accordance with European legislation and approved by the Dutch Animal Ethics Committee of the Erasmus MC. The investigators declare that the reported experiments complied with the journal's ethical principles and their animal ethics checklist. Wistar dams (Harlan, Horst, The Netherlands) were given *ad libitum* access to food and water, and extra bedding material was provided. The day of birth was taken as postnatal day (P)0.

Animal procedures

Two-to-six-day-old pups of either sex were anaesthetized with 2-3 % isoflurane (Pharmachemie BV, Haarlem) vaporized in medical oxygen (0.4-0.6 l min⁻¹) and placed in supine position. The surgical procedures are described by Rodríguez-Contreras *et al.* [90] with some minor adjustments. Briefly, throughout the surgery the skin temperature was monitored dorsally and kept at 36 °C by a heating pad (FHC Inc., Bowdoin, ME, USA). When the pup became unresponsive to a toe pinch, it was intubated with micro-renathane tubing (OD x ID in mm, P2: 0.64 x 0.30, >P2: 0.84 x 0.36; BrainTree Scientific Inc.) and mechanically ventilated with a MicroVent (7 µl µg⁻¹ + dead volume, 100 min⁻¹; Harvard Apparatus, March, Germany). The larynx, oesophagus and the dorsal tissue were removed to expose the skull in which a small cranial window (1.5 x 1.5 mm) was made to expose the basilar artery and the left and right anterior-inferior

cerebellar artery. The upper cranial meninges overlying the MNTB were gently torn away.

The animal surgery took 45-90 minutes followed by a recovery phase of 30 min and the experimental phase. Within the recovery and experimental phase anaesthesia was kept at a level that adequately kept the animal unresponsive to a toe pinch (0.7-1.3 % isoflurane). Pilot data suggested that surgical levels of anaesthesia suppressed the spontaneous bursting activity, but that the range of anaesthesia levels used during the recordings had no obvious effects on activity. To prevent dehydration, the animal was given intraperitoneal saline injections (30-80 μ l every 2h). The craniotomy was kept moist with Ringer's solution containing (in mM): 135 NaCl, 5.4 KCl, 1 MgCl₂, 1.8 CaCl₂, 5 HEPES with pH 7.2 adjusted with NaOH. After the experimental phase (2-8 h) the animal was deeply anesthetized followed by either decapitation or transcordial perfusion with cold saline followed by cold phosphate-buffered 4 % paraformaldehyde to fix the brain for further histological procedures.

Electrophysiology

Borosilicate capillaries with filament (OD 1.50 mm, ID 0.87 mm, #1403574 Hilgenberg GmbH, Germany) were pulled to long tapered pipettes (ID 1-1.5 μ m) on a P-97 Flaming/Brown micropipette puller (Sutter Instrument Co., CA, USA). Pipettes were filled with intracellular solution containing (in mM): 126 K-gluconate, 20 KCl, 0.5 EGTA, 10 HEPES, 10 Na₂phosphocreatine, 4 Mg-ATP, 0.4 Na₂-GTP with pH 7.2 adjusted with KOH. The pipettes were mounted on a headstage that could be moved within a custom-made setup in three dimensions by micromanipulators (Mini 25 with SM-7, Luigs & Neumann, Germany). The headstage (CV 203BU, Molecular Devices Co., CA, USA) was connected to an Axopatch 200B amplifier (Molecular Devices Co.); signals were low-pass filtered with a 4-pole Bessel filter at 10 kHz, subsequently digitized at 25 kHz by an A/D converter (Digidata 1440A, Molecular Devices Co.), and acquired with Clampex 10.2 (Molecular Devices Co.) running on a Windows XP computer.

When the animal's body temperature was stabilized at 37 °C, we started the experimental phase. The medial region of the brainstem, >200 μ m rostral and >300 μ m lateral from the bifurcation of the anterior-inferior cerebellar

3

artery and the basilar artery, was probed for bursting activity by juxtacellular recordings. Pilot experiments indicated that postsynaptic firing frequency did not depend on isoflurane level, except for a depression at surgical levels. When bursting activity was found, a clean pipette was lowered for the whole-cell recordings. The -11 mV junction potential and stray pipette capacitance were compensated. Upon break-in, the resting membrane potential was noted, and passive properties of the neuron were estimated in voltage-clamp mode based on 30-50 repetitions of a step from -70 to -75 mV. This was repeated between every recording to monitor the series resistance over time. Series resistance was on average $45.0 \pm 1.3 \text{ M}\Omega$ (8-35 % of total resistance; $n = 60$ cells) and remained uncompensated. In current clamp, a series of constant current injections was used to estimate the voltage dependence of the membrane resistance, with the first step hyperpolarizing the cell to at least -100 mV, incrementing to current injections of at least +300 pA. Every step was repeated at least twice. Spontaneous activity recordings of at least 7 min duration were obtained, either in voltage-clamp mode at a holding potential of -80 mV to minimize potassium and chloride currents, or in current-clamp mode, or both if time permitted.

To confirm that we recorded from a principal neuron of the MNTB we used both histological and electrophysiological criteria. For histological verification either biocytin was added to the intracellular solution (2 mg/ml) for further histological procedures, or Evans Blue was injected at the recorded location and, following decapitation, acute slices were made and checked under fluorescence for the injection site. In addition, the presence of a prespike was considered evidence that the recording was from the MNTB. All recordings near a verified recording site were also accepted. Reported recordings met at least one of these criteria.

Immunofluorescence

After perfusion the brain was carefully removed from the skull. Histological procedures were based on the free floating method, as described by Soria van Hove & Borst [194] with minor modifications. Briefly, 25-40 μm coronal sections were cut on a freezing microtome and captured in 0.1 M phosphate-buffered solution. When convenient, the sections were stored overnight at 4 °C. Presynaptic terminals were stained with anti-vesicular glutamate transporter

3. Developmental excitability-input matching in MNTB

(VGlut) 1 and 2 (guinea pig, 1:2000, polyclonal #ab5905 and #ab2251, Millipore) and highly cross-absorbed secondary antibodies produced in goat conjugated to Alexa Fluor-555 against guinea pig (1:200; Molecular Probes). Streptavidin conjugated to Alexa Fluor-488 (1:200, Molecular Probes) was used to stain biocytin. Sytox Blue (1:1000, Molecular Probes) was used to stain both the nucleus and, more weakly, the somatic cytoplasm. Sections were mounted and stored at 4 °C until image acquisition; to prevent evaporation, glass edges were sealed with nail polish.

Image acquisition and processing

A Zeiss confocal microscope (LSM 700, Axio Imager Z2), equipped with four diode lasers at 405, 488, 555, and 639 nm was used to acquire overview and z-stack images of the immunostainings. Z-stacks (1024 x 1024 pixels, voxel size was 310 x 310 x 500 nm) were obtained with a 40x/1.3 NA oil-immersion plan-apochromat objective with optimized pin hole settings, laser power and detector gain settings.

For 3D reconstruction the biocytin-stained structure was automatically detected with the ‘Particle Analyzer (3D)’ plugin of ImageJ with a manually-set threshold. The particle analyzer often returned multiple detected structures of which the experimenter chose the relevant structure to create a mask, which was used to restrict the fluorescent signals to the relevant structure plus its immediate 1 µm vicinity. Enlargement of the mask was performed using ‘Dilate (3D)’ (plugin: 3D Binary Filters, author: Benjamin Schmid). Images were background subtracted after masking. These masked images were imported into Volocity (Improvision, Coventry, UK) to render the z-stacks of the neurons in 3D.

Analysis of electrophysiological recordings

The recordings were imported into Igor Pro 6.34A (Wavemetrics Inc., USA) and analysed by custom-made functions. From the VC-step recordings, series resistance was calculated as the applied voltage step amplitude divided by the peak current amplitude; membrane resistance was obtained by dividing the applied voltage step amplitude by the steady state current amplitude and subtracting the series resistance; membrane capacitance was calculated by the following equation, which takes into account the voltage drop across the series

resistance:

$$C_m = \frac{\int (I_t) - I_{ss} dt}{V_{step}} \left(\frac{I_{ss}}{I_{peak} - I_{ss}} \right)^2 \quad (1)$$

where C_m denotes membrane capacitance; I_t is the recorded current in voltage-clamp, which is integrated from the peak current to a steady-state current after 10 ms; I_{ss} is steady-state current; and V_{step} is the applied voltage step of 5 mV.

A detection algorithm for spontaneous events was developed based on Ankri *et al.* [195]. Excitatory postsynaptic potentials (EPSPs) or currents (EPSCs) were detected based on two criteria: a maximum in the rate of rise (green circles in Figure 3.3E) that was above a manually-set threshold (~ 0.5 V/s) and the existence of an event onset, which was defined as a preceding local maximum in the second derivative (blue circles in Figure 3.3E). This detection method was particularly sensitive to summing EPSPs, but often missed events on the falling phase of an AP or of big events. The event peak of the event was detected as a local maximum in the original recording or, in case of event summation, as the onset of the next event. Prespikes were detected together with the other events and subsequently categorized based on three threshold criteria set by the experimenter: rate of rise, rate of repolarization and amplitude in the original trace. If the onset of an event was detected within a prespike, the onset value of the prespike was used instead as the onset value of the event. EPSPs preceding an AP were subcategorized as preceding the first AP of a miniburst, with the miniburst defined as an AP preceded by an interspike interval of more than 40 ms and succeeded by a second AP within 40 ms (Figure 3.3D). APs were detected by a simple manually-set voltage threshold crossing; AP threshold was defined as the potential at which the second time derivative had its maximum.

Juxtacellular recordings were digitally high-pass filtered at 1 Hz for visual purposes and analysed similarly as the spontaneous recordings; in juxtacellular recordings, prespikes were detected within 20 ms preceding either an eAP or an eEPSP to reduce spurious detection.

The high series resistances in our *in vivo* voltage-clamp recordings resulted in an imperfect voltage-clamp and an underestimation of the real currents [196]. To partially correct for these errors we applied an off-line software-based

deconvolution algorithm that takes capacitive filtering into account [197], which used the membrane capacitance as calculated in eq. (1). To reduce the noise after deconvolution, the voltage-clamp recording was low-pass filtered with a digital binomial filter at a cut-off frequency of 0.6 kHz. This correction had a major impact on the fast peak component (Figure 3.4A and B, blue traces), and EPSC amplitude increased about 5 times on average (range: 2.8 – 18.4; Figure 3.4G). The deconvolved amplitudes of the largest EPSCs were in the same range as the amplitudes of well-clamped EPSCs recorded in slices at the same developmental age [60, 157].

The constant-current injection recordings were corrected off-line for the voltage-drop over the series resistance and elicited APs were detected as before. AP half width was defined as the width halfway the AP threshold and peak. The first APs elicited by the current injections were visually inspected to check their waveform. Steady-state membrane potential values were defined as the median membrane potential from 500-600 ms after the start of current injections; values were rejected if there were multiple APs within this time period or if the median value was >-30 mV.

The Hodgkin-Huxley-like model of a principal MNTB neuron

The Hodgkin-Huxley-like model (HH-model) was based on previous models of the MNTB neuron [187, 198]. Briefly, the model could be described by:

$$-C_m \frac{dV}{dt} = (I_{leak} + I_{Na} + I_{LTK} + I_{HTK} + I_h)_{neuron} + I_{syn} - I_{inj} \quad (2)$$

where C_m is the membrane capacitance; dV/dt represents the change of the membrane potential; I_{leak} is the leak current, I_{Na} is the sodium current; I_{LTK} is the low-threshold potassium current; I_{HTK} is the high-threshold potassium current; I_h is the hyperpolarization-activated current; I_{syn} is the synaptic current obtained from the voltage-clamp recordings; and I_{inj} is the injected current. Except for I_{syn} and I_{inj} , the currents were described by the following equation:

$$I_x = g_{max,x} a_x^{\lambda_x} (1 - \gamma_x + \gamma_x b_x) (V - V_{rev,x}) \quad (3)$$

Where g_{\max} represents the maximal conductance; a is the activation rate; λ is the number of subunits to activate; γ represents the fraction of the total conductance that can inactivate; b is the inactivation rate; and V_{rev} represents the reversal potential for current x . Values for these parameters are given in Table 3.2. The temporal change in subunit a and b was described by the following differential equation:

$$\frac{ds}{dt} = \left(\frac{\alpha_s}{\alpha_s + \beta_s} - s_t \right) (\alpha_s + \beta_s) \quad (4)$$

Where s corresponds to subunit-type h, l, m, n, p or u . For each subunit the voltage-dependency of the rate constants was:

$$\alpha_s = C_\alpha e^{k_\alpha V} \quad \text{and} \quad \beta_s = C_\beta e^{k_\beta V} \quad (5, 6)$$

The constants $C_\alpha, k_\alpha, C_\beta$ and k_β are listed in Table 3.1 and the relation to the currents in Table 3.2. Differential equations were solved with Gear Method/ Backwards Differentiation Formula implemented in Igor Pro 6.34A (function IntegrateODE).

To fit the steady-state potentials of the current injections, the equilibrium value for every subunit was calculated by:

$$s_\infty = \frac{\alpha_s}{\alpha_s + \beta_s} \quad (7)$$

The equilibrium values were used to fit the steady-state potentials with $V_{\text{rev,leak}}, g_{\text{leak}}, g_{\text{LTK}}$ and g_{th} as fitting variables to obtain their maximal conductance as a function of age. g_{Na} and g_{HTK} were excluded from the fits; their estimates were matched with AP properties as described in the Results section (Figure 3.9).

For the synaptic conductance the reversal potential was set at 0 mV and the time course of I_{syn} was based on the *in vivo* recordings after deconvolution using the algorithm described by Traynelis [197]. This could be done for a few stable recordings with low series resistance ($< 35 \text{ M}\Omega$) and with few clamp-escaping APs. Prior to the deconvolution, the few clamp-escaping APs were replaced by resized EPSCs derived from the same trace. Generally, the resized EPSC nicely overlaid the measured EPSC in the period before it was obscured by a clamp-escaping AP. The deconvolved recording was used to calculate the synaptic conductance as:

$$g_{\text{syn}} = \frac{I_{\text{deconvolved}}}{V_h - V_{\text{rev}}} \quad (8)$$

3. Developmental excitability-input matching in MNTB

Table 3.1 Values of the subunit kinetics. Values were based on Macica *et al.* [198], except l and u , which were based on Leao *et al.* [187].

	h	l	m	n	p	u	
C_α	$5.33 \cdot 10^{-4}$	6.947	76.4	0.2719	$7.13 \cdot 10^{-3}$	$9.12 \cdot 10^{-8^*}$	ms^{-1}
k_α	-0.0909	0.03512	0.037	0.04	-0.1942	-0.1	mV^{-1}
C_β	0.787*	0.2248	6.93	0.1974	0.0935	$2.1 \cdot 10^{-3^*}$	ms^{-1}
k_β	0.0691	-0.0319	-0.043	0	0.0058	0	mV^{-1}
$V_{1/2}$	-46	-51	-30	-8	-13	-100	mV

*The original value was multiplied by 0.1 to better match the *in vivo* data.

Table 3.2 Conductance parameters for the Hodgkin-Huxley model. Parameters were based on Macica *et al.* [198], except I_h , which was based on Leao *et al.* [187].

	I_{Leak}	I_{Na}	I_{LTK}	I_{HTK}	I_h	
a	1	m	l	n	u	
b	-	h	-	p	-	
λ	1	3	3	3	1	
γ	0	1	0	0.2	0	
V_{rev}	-72	50	-80	-80	-45	mV

Table 3.3 Age-specific model parameters. Values for g_{leak} , g_{LTK} and g_{Ih} were derived from fitting *in vivo* current-injections to a Hodgkin-Huxley-type model. Values for g_{Na} and g_{HTK} were adjusted to match the *in vivo* action potential properties. C_m was 30 pF for all ages; it was calculated using the first 10 ms from a voltage-step (-70 mV to -75 mV) and adjusted for dendritic capacitances.

	P_2	P_3	P_4	P_5	P_6	
g_{Leak}	2	2.3	2.8	4.5	5.5	nS
g_{Na}	150	180	210	250	300	nS
g_{LTK}	11	14	20	50	70	nS
g_{HTK}	30	50	80	140	300	nS
g_{Ih}	12	25	37	36	31	nS

where V_h is -80 mV and V_{rev} is 0 mV. Finally, the deconvolved recordings were linearly detrended.

The resting membrane potential (RMP) was set at -70 mV in the model by current injection to facilitate the comparison between the different ages. Without the current injection, there was a trend that the RMP of the standard model neurons became slightly more negative with age (-67 mV for the P2 vs. -72 mV for the P6 standard model neuron). We corrected the measured C_m in eq. (1) for the dendrite-related capacitance with a factor of 0.6, yielding about 30 pF.

The model EPSC was composed of an AMPA and an NMDA conductance:

$$I_{EPSC} = (g_{AMPA} + Mg g_{NMDA})(V - V_{rev}) \quad (9)$$

$$Mg = (1 + \frac{4}{7.5} e^{-V/15})^{-1} \quad (10)$$

Where Mg denotes the magnesium block which depended on the membrane potential as described by Steinert *et al.* [199]. Both g_{AMPA} and g_{NMDA} were described by a three state model composed of one opening state and two closing states:

$$g_x = 1.198 \kappa_x \frac{I_{peak}}{V_h - V_{rev}} S_{open} (S_{close,fast} \gamma_x + (1 - \gamma_x) S_{close,slow}) \quad (11)$$

Here, g_x stands for the conductance of x, and x can be either AMPA or NMDA; κ is a scaling factor, which was 1 and 1.9 for AMPA and NMDA, respectively [137, 156]; I_{peak} is the EPSC amplitude as would be recorded in voltage-clamp mode; V_h and V_{rev} are the holding and reversal potential, here 0 and -80 mV for both AMPA and NMDA; S_{open} denotes the open state; $S_{close,fast}$ is the closing state with a fast decay time; γ denotes the relative fraction of fast closing state, set to 0.923 [20] and 0.778 [199] for AMPA and NMDA, respectively; and $S_{close,slow}$ denotes the closing state with the slow decay time. The states followed the following equation:

$$S_{open} = \frac{e^{t/\tau_{rise} + 2}}{1 + e^{t/\tau_{rise} + 2}} \quad \text{and} \quad S_{close,x} = (1 + e^{t/\tau_{decay,x} - 2})^{-1} \quad (12, 13)$$

with t is the time in ms; τ_{rise} is the opening time constant which was 0.15 ms and 0.8 ms; $\tau_{decay,fast}$ was 1.05 ms and 25 ms; and $\tau_{decay,slow}$ was 14.1 ms and 100 ms for AMPA and NMDA, respectively [20, 156, 199]. NMDA currents were delayed by 3.03 ms to be comparable with Steinert *et al.* [199].

In the simulations for which VC recordings were used as input, the NMDA conductance associated with each EPSC was calculated using equation 11. These were summed to get the total NMDA conductance.

Statistical analysis

Values reported are mean and SEM. Statistical significance was calculated by regression with every postnatal day as an independent variable. For frequencies, χ^2 -tests were performed. To assess the HH-model fit, an F-test for comparing nested models was done for every fitting parameter against the simpler model with p -values < 0.1 suggesting an improvement in the fit. The reduction of sums-of-squares is reported as a percentage. A linear regression model was used with the threshold current for evoking an AP as the outcome variable and the conductances g_{LTK} , g_{leak} and g_{Ih} as predictors. The values of the conductances were determined with the HH-model fit, and if a conductance did not make a significant contribution in the HH-model fit, it was set to zero for the linear regression model. The slope values of the conductances in the regression model are reported, and their significance was tested with a post-hoc t -test. The impact of NMDA conductance was tested by a Repeated-Measures ANOVA with the neuron as the nesting variable, and ‘*in vivo* recording’, ‘model with g_{NMDA} ’ and ‘model without g_{NMDA} ’ as predictor variables. Post-hoc paired t -tests were used to assess the significance of the predictor variables. Post-hoc testing was corrected with Bonferroni’s method. Except for the fit improvement, p -values < 0.05 were considered significant.

Results

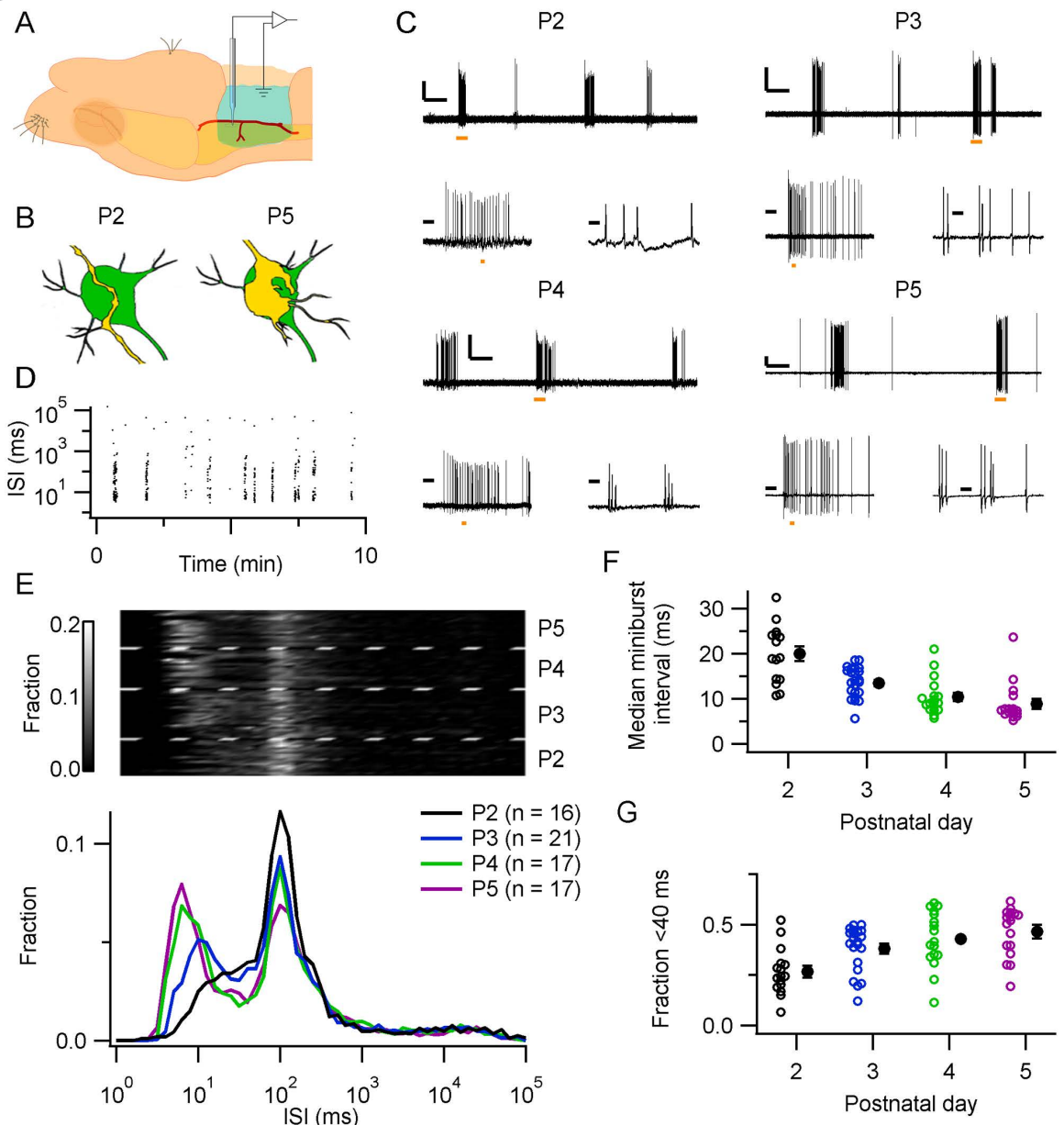
Juxtacellular bursting activity

An important feature of developing auditory nuclei is their bursting activity [111]. As early as P5, a characteristic bursting pattern has been observed at the MNTB [74]. To investigate the developmental changes in this bursting pattern, we made *in vivo* juxtacellular recordings from rat pups aged between P2-5 using a ventral approach (Figure 3.1A). Within this developmental period, the calyx of Held synapse forms, and the innervation of the principal neurons evolves from a divergent projection with conventional boutons at P2 to, typically, a single, very large, axosomatic synapse at P5 (Figure 3.1B) [16, 55, 90, 137]. At P2-5, periods

Neural Activity During the Formation of A Giant Auditory Synapse

of bursting activity could already be detected, and, typically, the recordings showed long periods of no activity (up to tens of seconds) followed by a period of increased activity (burst) that had two preferred firing frequencies at about 10 and 100 Hz, corresponding to interspike intervals of about 100 and 10 ms, respectively (Figure 3.1C-E). We will refer to the ~100 Hz activity as miniburst, and define it as a sequence of action potentials with interspike intervals <40 ms. The interspike interval of 100 ms was remarkably consistent throughout

3



development, in agreement with earlier work [74, 155], whereas the miniburst interval clearly shortened (Figure 3.1D and E; P2: 20.0 ± 1.7 ms, P3: 13.4 ± 0.8 ms, P4: 10.4 ± 0.9 ms, P5: 8.9 ± 1.1 ms, $F_{3,67} = 18.4$, $p = 7 \cdot 10^{-9}$), and the fraction of all intervals that were miniburst intervals increased (Figure 3.1F; P2: $26.6 \pm 2.9\%$, P3: $38.0 \pm 2.5\%$, P4: $42.9 \pm 3.4\%$, P5: $46.5 \pm 2.9\%$, $F_{3,67} = 8.3$, $p = 10^{-4}$). We conclude that a principal neuron can display its characteristic, pre-hearing, bursting activity as early as P2.

To address the relation between pre- and postsynaptic activity, we took advantage of the juxtacellular recordings in which we observed an extracellularly-recorded, clear prespike (Figure 3.2A). Prespikes were observed at P2, P3, P4 and P5 in 2 out of 16, 10 out of 21, 9 out of 17, and 10 out of 17 recordings, respectively, suggesting a developmental increase ($\chi_{23} = 8.6$; $p = 0.03$). The prespike showed, similar to the postsynaptic activity, preferred intervals at around 100 and 10 ms ($n = 21$, cf. Figure 2.6). The miniburst interval of the prespike was shorter than the intervals recorded from its postsynaptic target neuron (8.2 ± 0.5 ms; difference: 2.0 ± 0.8 ms; paired $t_{20} = 2.6$, $p = 0.02$), and did

← **Figure 3.1 Developmental changes in characteristic bursting pattern.**

(A) Illustration of the experimental approach. The MNTB is ventrally approached for electrophysiological recordings, using the origin of the bifurcation of the anterior-inferior cerebellar artery as a landmark. (B) Illustration of the structural development of the axon innervating the principal neuron of the MNTB. Left: a P2 principal neuron (green) is innervated by a passing axon (yellow). Right: at P5, the same neuron is covered by a protocalyx. (C) Four representative juxtacellular recordings obtained at P2-5 showing alternating periods of high activity and silence (upper trace). For each postnatal day, the left lower panel shows a single burst; the right lower panel shows that a burst is composed of minibursts, defined as a period with interspike intervals (ISIs) < 40 ms. Orange bars indicate the periods that are expanded in the other panels. Scale bars for each age: 1 mV; upper panel: 10 s; left lower panel: 0.5 s; right lower panel: 20 ms. (D) Inter-spike interval (ISI) against the time of recording of the P5 example shown in C. (E) Top: ISIs of individual experiments were logarithmically binned and coded in grey scale. Every horizontal line represents the probability density function of the ISIs of a single recording; the recordings were grouped by pup age, separated by the broken lines. Bottom: probability density functions averaged per postnatal day. While the 100 ms interval was unchanged, the miniburst interval shortened during development. (F) Median miniburst interval against postnatal day. (G) Fraction of miniburst intervals against postnatal day. Open circles are single neurons, filled circles are averages with SEM.

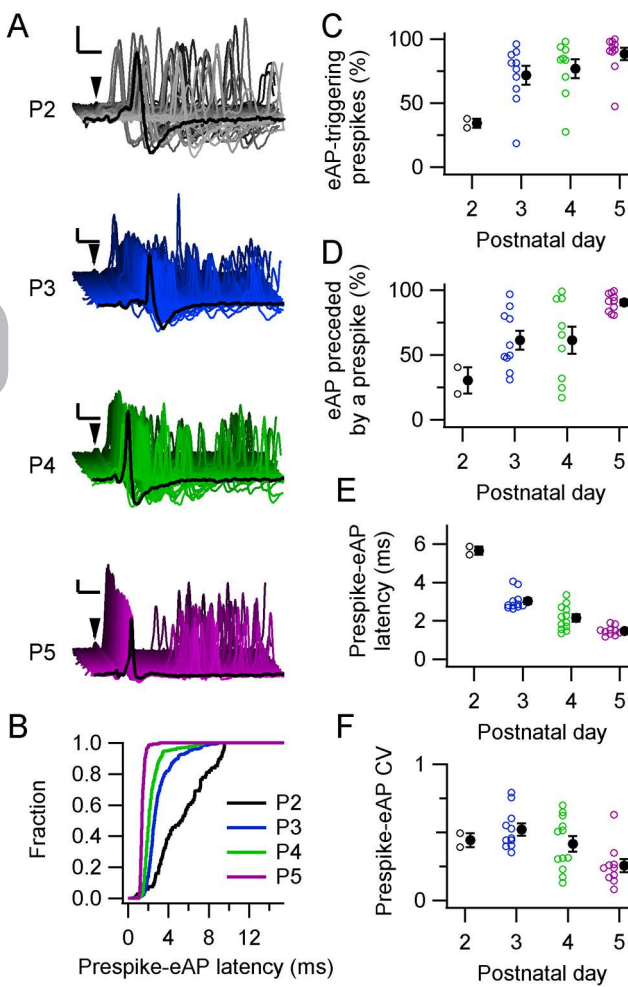


Figure 3.2 Increased dependency of postsynaptic activity on a calyceal input in *in vivo* juxta-cellular recordings from P2-5 rat pups. (A) Waterfall plots of aligned consecutive prespikes (arrowheads) from recordings from P2-5 pups. For each cell all recorded prespikes are shown. The jitter in the delay between prespike and postsynaptic eAP decreased with age. Black trace in front is a representative trace. Calibration bars are 2 ms and 1 mV. (B) Cumulative fraction of the prespike-eAP intervals of the example recordings in A, illustrating that the prespike-interval became shorter and less variable during development. (C) Developmental increase in the fraction of prespikes that triggered a postsynaptic eAP. (D) Developmental increase in the fraction of eAPs that were preceded by a prespike. (E) Developmental decrease in average prespike-eAP latency. (F) Developmental changes in the coefficient of variation (CV) of the prespike-eAP latency. Open circles in C-F are single data points, filled circles are averages with SEM.

not show a clear developmental shortening (P2: 7 ± 1 ms; P3: 10 ± 1 ms; P4: 9 ± 1 ms; P5: 7 ± 1 ms; $r = 0.4$), suggesting that the developmental acceleration of the miniburst is due to a developmental change in either synapse strength or the properties of the target neuron. To assess the impact of prespike-related synapse more comprehensively, we quantified the percentage of prespikes that triggered an extracellularly-recorded AP (eAP), which increased developmentally (Figure 3.2C; P2: $34 \pm 4\%$, P3: $66 \pm 11\%$, P4: $75 \pm 9\%$, P5: $87 \pm 5\%$, $F_{3,20} = 3.8$, $p = 0.02$). Conversely, at P2 most postsynaptic eAPs were not associated with a prespike, while at P5 virtually all eAPs were (Figure 3.2D; P2: $30 \pm 10\%$, P3: $55 \pm 9\%$, P4: $65 \pm 13\%$, P5: $90 \pm 2\%$, $F_{3,20} = 5.6$, $p = 0.006$). Other developmental changes included the shortening of the prespike-eAP interval (Figure 3.2E; P2: 5.65 ± 0.22 ms, P3: 2.83 ± 0.06 ms, P4: 2.11 ± 0.25 ms, P5: 1.48 ± 0.08 ms; $F_{3,21} = 52.0$, $p = 7 \cdot 10^{-10}$) and a

decrease in its coefficient of variation (SD/mean; Figure 3.2F; P2: 0.44 ± 0.12 , P3: 0.54 ± 0.14 , P4: 0.38 ± 0.13 , P5: 0.26 ± 0.13 ; $F_{3,12} = 3.6$, $p = 0.04$), suggesting a strong developmental increase of the calyceal impact on the activity of its principal neuron.

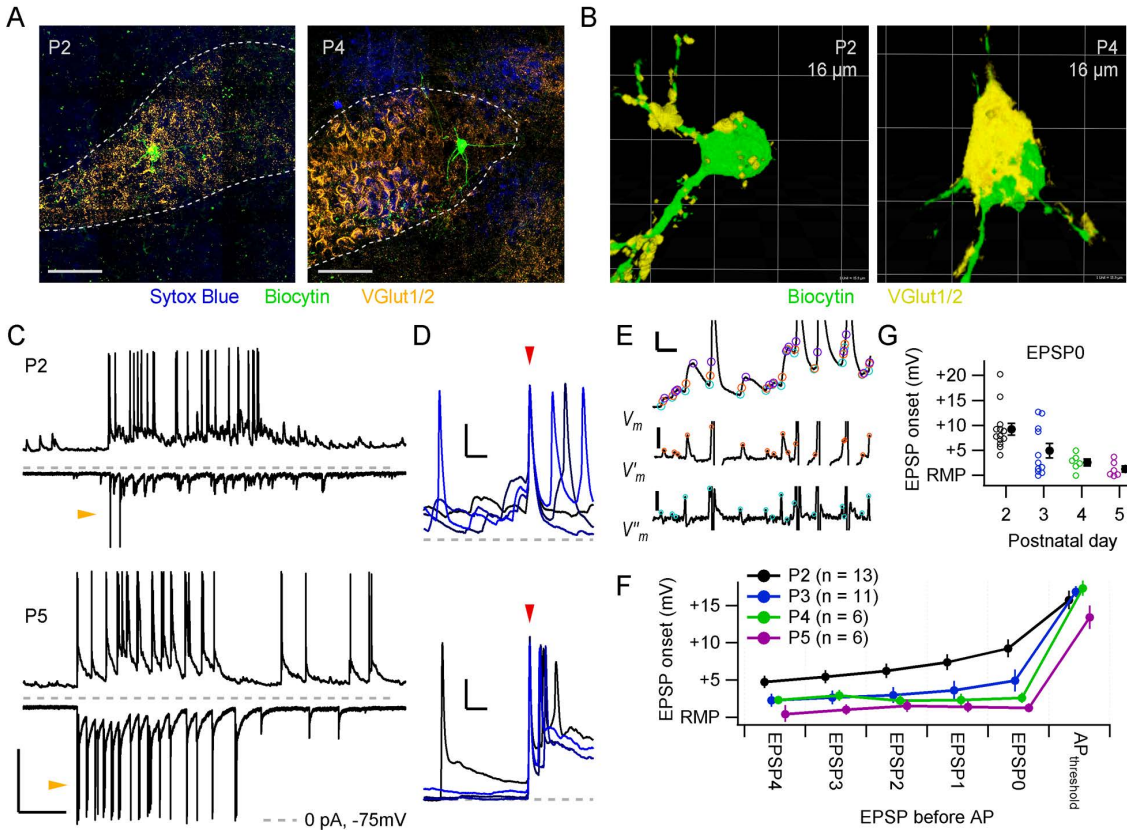
Synaptic barrages trigger postsynaptic APs before a giant input emerges

The juxtacellular recordings suggested that at the youngest ages studied, many or all of the action potentials in principal neurons were triggered by multiple, small synapses. To study more directly how action potentials were triggered at the different postnatal ages, we made *in vivo* whole-cell recordings of principal neurons. A few neurons that had been filled with biocytin via the patch pipette were successfully recovered histologically ($n = 8$ cells from 8 pups). Two examples are shown in Figure 3.3A. Immunocytochemical stainings with VGluT1/2 as a presynaptic marker showed the emergence of an axosomatic synapse between P2 and P4 (Figure 3.3B), in agreement with earlier developmental studies in rat pups [55, 90, 194].

If recording time permitted, principal neurons were recorded both in current and in voltage clamp (Figure 3.3C). In current-clamp recordings, clear periods of increased activity could be observed at all ages, resulting in postsynaptic AP firing at frequencies similar to what we observed in the juxtacellular recordings. Figure 3.3D illustrates that action potentials were generally triggered quite differently in P2 and in P5 neurons. At P2, small excitatory postsynaptic potentials (EPSPs) summated to reach AP threshold, while at older ages a single EPSP could be sufficiently large to trigger an AP. To quantify how APs were triggered, we employed a custom-made detection method (Figure 3.3E) to identify the EPSP that preceded the action potential, as further detailed in the Methods. At P2, the EPSP that triggered the action potential (EPSPo) started from a depolarized potential, while at P5 EPSPo typically started close to the resting membrane potential (RMP), especially when we focused on the first AP of a miniburst (Figure 3.3F and G; P2: $+9.2 \pm 1.2$ mV, P3: $+4.9 \pm 1.5$ mV, P4: $+2.6 \pm 0.7$ mV, P5: $+1.4 \pm 0.7$ mV, $F_{3,31} = 6.7$, $p = 0.001$). Action potential threshold did not change significantly during development (P2: -45.8 ± 1.6 mV, P3: -46.6 ± 1.1 mV, P4: -46.7 ± 1.7 mV, P5: -49.6 ± 2.3 mV, $F_{3,31} = 0.8$, $p = 0.53$) and RMP did not significantly change (P2: -67 ± 2 mV, P3: -70 ± 1 mV, P4: -69 ± 2 mV, P5: -69 ± 1

Neural Activity During the Formation of A Giant Auditory Synapse

3



mV, $F_{3,48} = 1$, $p = 0.33$). Our data thus show that at P2-3, small EPSPs summated to reach AP threshold, while at P5 the largest EPSPs typically triggered postsynaptic APs singlehandedly.

Between P2 and P5 most principal neurons become innervated by a calyx. In the whole-cell recordings we observed the appearance of a large input in both the current-clamp and the voltage-clamp mode (Figure 3.4A and B). The fraction of AP-triggering EPSPs (EPSPo) with a rate of rise above 5 V/s increased during development (Figure 3.4C; P2: 0.19 ± 0.06 , P3: 0.50 ± 0.10 , P4: 0.68 ± 0.09 , P5: 0.82 ± 0.08 , $F_{3,32} = 9.5$, $p = 0.0001$). The frequency of large EPSPs increased between P2 and P5 (Figure 3.4D; P2: 0.13 ± 0.03 Hz, P3: 0.45 ± 0.11 Hz, P4: 0.62 ± 0.12 Hz, P5: 0.75 ± 0.12 , $F_{3,36} = 10.4$, $p = 5 \cdot 10^{-5}$). Similarly, in the voltage-clamp recordings a population of large EPSCs became progressively more distinct from smaller EPSCs (Figure 3.4E), and the frequency of EPSCs with an amplitude above 100 pA strongly increased as well (Figure 3.4F; P2: 0.14 ± 0.03 Hz, P3: 0.60 ± 0.08 Hz, P4: 0.66 ± 0.05 Hz, P5: 0.67 ± 0.09 Hz, $F_{3,43} = 9.3$, $p = 7 \cdot 10^{-5}$). To relate EPSCs

← **Figure 3.3** Action potentials are typically triggered *in vivo* by summation of small EPSPs at P2 and by a single, strong input at P4 or older. (A) Immunofluorescent stainings of the MNTB at P2 (left) and at P4 (right). Dotted line, MNTB borders; blue, nucleotide stain Sytox Blue; green, biocytin; orange, glutamate vesicle marker VGluT1/2. Scale bar is 50 μm . Ventral is to the bottom and medial is to the left. (B) Three-dimensional reconstructions of biocytin-stained neurons with nearby VGluT1/2 staining. (C) Example whole-cell recordings from a principal neuron at P2 (top panel) and P5 (bottom panel) showing a period of increased activity; current-clamp recordings (CC, top traces) show EPSPs and APs; voltage-clamp recordings (VC, bottom traces) show EPSCs and, especially at P5, voltage-clamp escaping action currents (orange arrowheads). Broken lines mark 0 pA for the VC recording and the -75 mV level for the CC recording. Bar is 30 mV, 500 pA and 500 ms. (D) Four example traces (color-coded) aligned on the first AP of a miniburst (red arrowhead) show the prelude to a miniburst at P2 (above) and P5 (below). At P2 multiple EPSPs summated to reach the AP threshold, whereas at P5 no summation was seen. Calibration bars are 10 mV, 10 ms. Grey dashed line marks the resting membrane potential of the recorded neuron. (E) Overview of the detection method based on the rate of rise. In the upper trace the CC recording with EPSPs and truncated APs obtained from a P2 pup is shown; the middle trace is the first time derivative of the CC recording; the lower trace is the second time derivative of the CC recording. Orange circles indicate the maximum rate of rise of the EPSP; light blue circles indicate the EPSP onset; purple circles indicate the EPSP peak. Calibration bars: 5 mV and 10 ms (top); 5 V/s (middle); 8 V/s² (below). (F) Average onset membrane potential of the EPSPs preceding the first AP of the miniburst is plotted against the order number of the EPSP preceding the AP; EPSP₀ is the EPSP reaching the AP threshold, EPSP₁ the EPSP preceding EPSP₀, etc. The membrane potentials are plotted relative to the resting membrane potential (RMP). Data points have been horizontally offset for display purposes. (G) Developmental changes in the average onset membrane potential of the EPSP directly preceding the first AP of the miniburst (EPSP₀). The averages (filled circles with SEM) are also shown in F.

to EPSPs, recordings were made in both voltage-clamp and current-clamp from a total of twenty-three neurons. Although EPSCs and EPSPs of a single neuron were recorded consecutively, some inputs could be identified in both recordings owing to the bimodal distribution of event amplitudes (Figure 3.4A and B) or the presence of a prespike (not shown). To take into account the effect of the series resistance on the amplitude of the EPSCs, we employed off-line deconvolution (Figure 3.4G; see Methods). There was a strong correlation between the deconvolved EPSC amplitude and the rate of rise of the EPSP in the same cell (Figure 3.4H; $r = 0.81$). In summary, our *in vivo* evidence indicated that between P2 and P5 a single large input becomes responsible for AP generation in most principal neurons.

Neural Activity During the Formation of A Giant Auditory Synapse

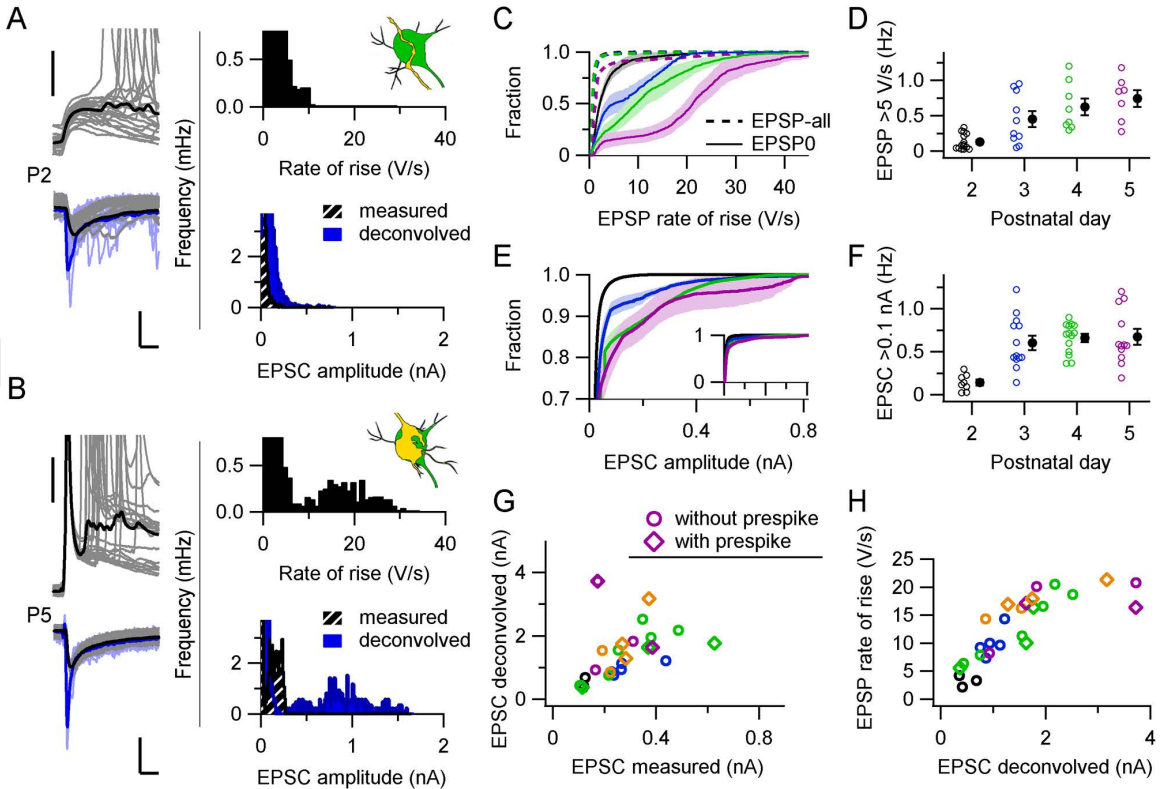


Figure 3.4 Emergence of a large input during development. (A) In a P2 principal neuron twenty EPSPs in CC (upper left) and twenty EPSCs in VC (lower left, grey), and the average big EPSP (black) and EPSC (black) aligned on the onset. VC recordings were deconvolved off-line for capacitive filtering. The same EPSCs after deconvolution (light blue) and the average deconvolved EPSC (blue) are shown. Bars are 20 mV (upper), and 200 pA and 5 ms (lower). Upper right panel, the frequency distribution of EPSP rate of rise; lower right panel, the frequency distribution of EPSC amplitude. (B) Similar as A for a P5 principal neuron, illustrating the appearance of a separate population of large EPSPs and EPSCs. Bars as in A. (C) The averaged cumulative distributions of the maximal rate of rise of all EPSPs (dotted line) and the AP-triggering EPSP (EPSP₀, line) at the different ages (color-coded). A population of large EPSPs (>5 V/s) emerges during development. Colours correspond to the age as in D. (D) The frequency of large EPSPs (>5 V/s) against postnatal day. (E) Truncated averaged cumulative distributions of the EPSC amplitude of different postnatal days (color-coded). Similar to C, large inputs (>100 pA) appeared during development. EPSCs were not deconvolved. Inset shows the entire distributions with the same range of EPSC amplitudes. (F) Developmental increase in the frequency of large EPSCs (>100 pA). (G) EPSC amplitudes before and after deconvolution. The data points are derived from a defined population of EPSCs based on either their rate of rise or the presence of a prespike. The deconvolution retrieved the fast peak of the EPSC, as shown in A and B. Circles are the large EPSCs, diamonds are the prespike-related EPSCs. Colours correspond to age as in D and F, orange is P6. (H) The deconvolved EPSC amplitude against the rate of rise of the EPSP recorded from the same principal neuron. The two measures correlated almost linearly. Colours as in G. Open circles are single data points, filled circles are averages with SEM.

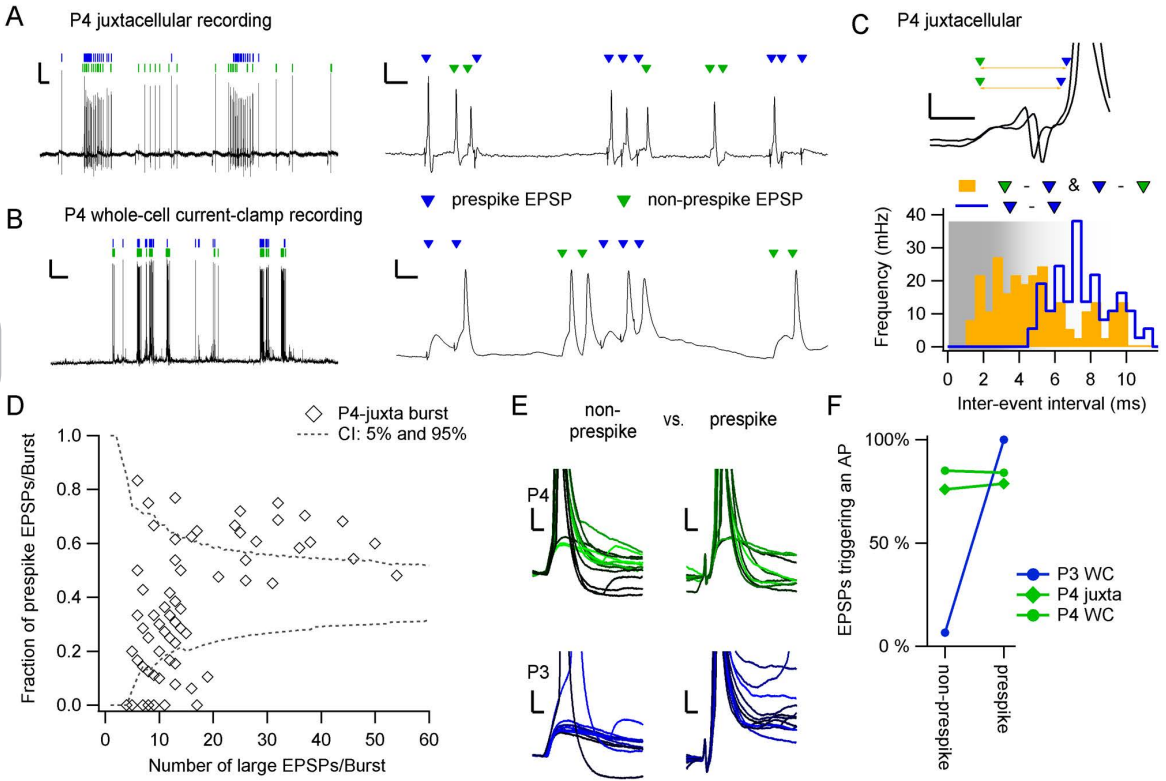
Anecdotal evidence for multiple protocalyces

Serial electron microscopy reconstructions of principal neurons showed that multiple large inputs, defined operationally as inputs with an apposed surface area of at least $25 \mu\text{m}^2$, can form on the same principal neuron during development [136]. Their relative physiological impact on the principal neuron is still largely unknown. In principle, whole-cell recordings do not allow to unambiguously identify the inputs from different axons. However, in a total of three cells electrophysiological evidence for the presence of multiple large inputs was obtained.

In one P₃ and in one P₄ whole-cell recording (2 out of 67), and in one P₄ juxtacellular recording (1 out of 65), two types of big events could be distinguished based on the presence or absence of a prespike (Figure 3.5A and B). Single inputs should obey the refractory period, which was estimated to be 0.9 ms in adult mice [134], but we expect it to be longer in neonatal rats. In the two P₄ recordings we found interevent-intervals below 3 ms, with the smallest interval at 1.4 ms, while the smallest inter-prespike interval in any of our recordings was 3.3 ms (Figure 3.5C). Altogether, it seems likely that for these two P₄ recordings the two events arose from terminals of distinct globular bushy cells.

In the two P₄ recordings the two big events came in at preferred intervals, in agreement with an origin from globular bushy cells, and they co-occurred within a burst, and even in the same miniburst (Figure 3.5A and B). For the juxtacellular recording, a total of 511 prespike-related EPSPs, recorded extracellularly (eEPSP; 41% of large eEPSPs) were detected against 721 non-prespike eEPSPs (59 % of large eEPSPs). To quantify their co-occurrence, the fraction of prespike-related eEPSPs within each burst was calculated (Figure 3.5D). It seemed that, compared to the predictions of a binomial distribution, prespike-related eEPSPs dominated in the bursts with >15 large eEPSPs while being sparse in the bursts with fewer large eEPSPs. Nevertheless, in 15 out of the 18 bursts with 4-6 large eEPSPs, at least one prespike-related eEPSP was present, indicating that the prespike-related EPSP and the non-prespike eEPSP co-occurred regularly. In the P₄ whole-cell recording, every burst contained a prespike-related EPSP, with 39% of large

Neural Activity During the Formation of A Giant Auditory Synapse



EPSPs being prespike-related; in the P₃ whole-cell recording the prespike-related EPSP clearly dominated, since 337 prespike-related EPSPs were detected against 31 large, non-prespike EPSPs (8% of large EPSPs), and these non-prespike large EPSPs were present in only 11 of 25 bursts. In summary, in the three cells with evidence for multiple large inputs, the prespike-related and non-prespike inputs were regularly active together, which suggests a common origin for their activity.

Based on the ultrastructural reconstructions showing multiple large somatic inputs [136], we expected to find prespikes for both large synapses, as the prespike is the electrophysiological hallmark for the presence of a calyx. Moreover, the size of the prespike appears to scale with the surface area of the axon terminal, since we observed in the juxtacellular recordings an increased prespike amplitude during development (not shown). Hence two major axosomatic synapses would be expected to result in two distinct prespike waveforms. However, in none of the recordings we found evidence that the prespikes constituted two different populations, nor did we observe inter-prespike intervals below 3 ms. Nevertheless, for the two P₄ recordings the EPSPs

← **Figure 3.5 Anecdotal evidence for multiple large inputs.** (A) Juxtacellular recording of a P₄ principal neuron with two inputs that often trigger an AP, of which one showed a prespike (blue triangle) and the other did not (green triangle). They were coactive in the same bursts (left) and in the same miniburst (right). Calibration bars indicate 2 mV, 500 ms (left panel) and 10 ms (right panel). (B) Similar to A, but for a whole-cell recording of a P₄ principal neuron. (C) Two examples from the P₄ juxtacellular recording where the non-prespike-related EPSP (green) was followed within 3 ms by a prespike-related EPSP (blue). The yellow line indicates the inter-event interval. Bars indicate 1 mV and 1 ms. Bottom, frequency of the inter-event intervals; orange, intervals between prespike-related and non-prespike-related EPSPs; blue, intervals between prespike-related EPSPs. The shaded area depicts the intervals that might only be obtained from distinct inputs. (D) Fraction of prespike-related EPSPs against the total number of large EPSPs (prespike + non-prespike) within a single burst recorded from the P₄ juxtacellular recording shown in A. Every diamond represents a burst. Dotted line indicates the confidence intervals based on the expected binomial distribution with $p = \text{number of prespike-EPSP/all large EPSPs}$. (E) Comparison of the synaptic strength of both large inputs. From the two whole-cell recordings (P₃ and P₄) examples of the non-prespike EPSP aligned on the maximal rate of rise (left) and of the prespike EPSP aligned on the prespike (right). In the P₄ whole-cell recording (top panel), both kinds of EPSPs were comparable in size and ability to trigger APs. In contrast, in the P₃ whole-cell example (bottom panel) the prespike-related EPSPs were bigger and reliably triggered an AP while the non-prespike EPSP only rarely did. Bars indicate 5 mV and 2 ms. (F) Comparison of the percentage of EPSPs that triggered an AP for non-prespike and prespike-related EPSPs. A single line represents a single recording; the P₃ whole-cell recording is indicated with a blue circle, and was illustrated in E; the P₄ juxtacellular recording is shown as a green diamond, and is illustrated in A and C; the P₄ whole-cell recording is shown as a green circle, and is illustrated in B and E.

seemed of comparable size and shape as they regularly triggered postsynaptic APs at almost equal probability (Figure 3.5D and E). Only in the P₃ whole-cell recording the prespike-related EPSP was clearly bigger and stronger than the non-prespike EPSP (Figure 3.5D and E, blue). Especially in the two P₄ recordings, it remained unclear why a prespike was recorded for only one of the large inputs.

Intrinsic properties of the principal neuron

In the adult situation, the principal neuron responds to a calyceal AP with no more than a single AP. To enable its reliability and precision, the principal neuron needs to change its firing properties during development [16]. The *in vivo* intrinsic properties of principal neurons were investigated by whole-cell constant-current injections (Figure 3.6A). At P₅₋₆, even upon strong, depolarizing current injections, we observed only phasic firing by the principal

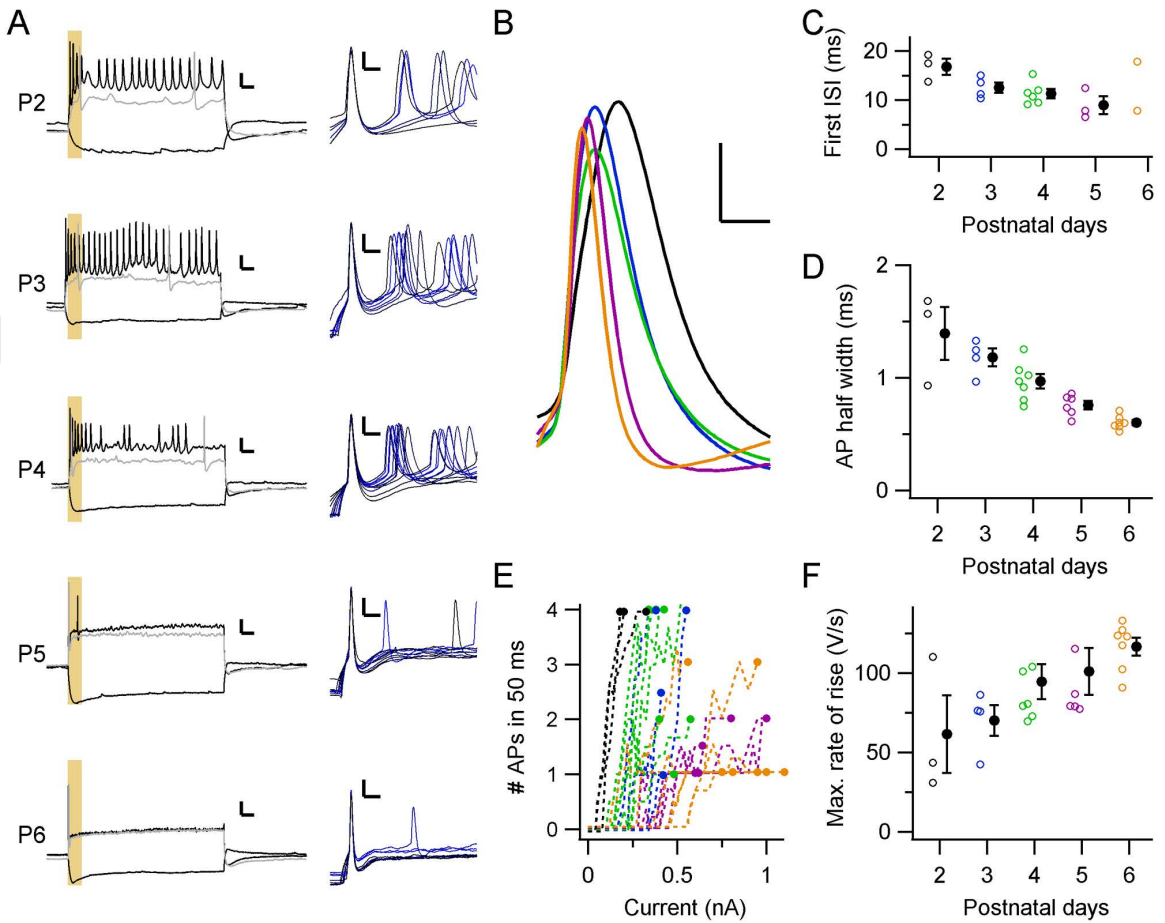


Figure 3.6 Developmental changes in postsynaptic action potentials. (A) Left, Response of principal neurons to constant current injections at different postnatal days. Responses to a hyperpolarizing and two depolarizing current injections of 600 ms are shown. The response of the principal neuron to the smallest current injection that elicited AP firing is shown in grey. The yellow box indicates the first 50 ms of current injections. Right, The APs that were elicited at the start of the current injections are shown aligned on the peak potential. Colour corresponds to injected current amplitude. Bars indicate 20 mV and 50 ms in the left panel and 10 mV and 5 ms in the right panels. (B) The average waveforms of the AP elicited at the start of the current injections in the five neurons shown in A are aligned on their AP threshold, illustrating that the AP kinetics become faster with age. Bars indicate 10 mV and 1 ms. Colours correspond to age as in C. (C) Developmental changes in first interspike interval (ISI). Around P5 the neurons typically fired only a single AP. (D) Developmental changes in AP half width. (E) Relation between average number of APs elicited within the first 50 ms of the current injection (yellow box in A) and strength of current injection. Every line represents an average count of a single recorded neuron; the age is color-coded as in C. (F) Developmental change in maximal rate of rise of the AP. Open circles in C, D and F are single data points, filled circles are averages with SEM.

neurons. In contrast, at P2-3, all neurons fired multiple APs in response to current injections (Figure 3.6A and E). The first interspike interval (ISI) shortened (Figure 3.6B and C; P2: 16.8 ± 1.6 ms, P3: 12.6 ± 1.1 ms, P4: 11.4 ± 0.9 ms, P5: 8.9 ± 1.8 ms; $F_{4,11} = 4.7, p = 0.02$), the AP half width was reduced (Figure 3.6D; P2: 1.40 ± 0.23 ms, P3: 1.18 ± 0.08 ms, P4: 0.97 ± 0.06 ms, P5: 0.76 ± 0.04 ms, P6: 0.60 ± 0.02 ms; $F_{4,22} = 16, p = 3 \cdot 10^{-6}$), and the maximal rate of rise of the first AP increased during development (Figure 3.6F; P2: 62 ± 25 V/s, P3: 70 ± 10 V/s, P4: 95 ± 11 V/s, P5: 101 ± 15 V/s, P6: 117 ± 6 V/s; $F_{4,22} = 2.9, p = 0.045$) [60, 156]; these values may be underestimations because of high series resistances. Although the shape of the evoked first AP was quite similar within a principal neuron (Figure 3.6A), the AP waveform was highly variable during spontaneous activity. The APs showed considerable amplitude depression and broadening within minibursts (Figure 3.3D and Figure 3.6A), to which the synaptic conductances, inactivation of Na⁺ channels and activation of K⁺ channels may contribute. The minimal current needed for AP generation significantly increased with age (Figure 3.6E; P2: 90 ± 20 pA, P3: 300 ± 40 pA, P4: 230 ± 30 pA, P5: 420 ± 30 pA, P6: 430 ± 50 pA, $F_{4,22} = 9.6, p = 0.0001$), indicating a developmental decrease in the intrinsic excitability of the principal neuron.

The passive properties of the principal neuron were estimated from 5 mV hyperpolarizing voltage steps from the holding potential of -70 mV, as detailed in the Methods. Its membrane capacitance remained relatively stable (P2: 47.0 ± 1.2 pF, P3: 48.0 ± 1.3 pF, P4: 49.5 ± 1.4 pF, P5: 49.9 ± 2.5 pF, P6: 47.9 ± 2.8 pF), in contrast to a developmental decline in membrane resistance (Fig. 9E; P2: 279 ± 16 M Ω , P3: 238 ± 17 M Ω , P4: 174 ± 9 M Ω , P5: 172 ± 17 M Ω , P6: 155 ± 27 M Ω , $F_{4,55} = 9.3, p = 8 \cdot 10^{-6}$). In adult mice a membrane resistance of about 80 M Ω has been reported *in vivo* [134], suggesting that the membrane resistance will continue to decline further [200]. We conclude that even though, in agreement with previous reports, we did find that the excitability of the principal neuron decreased during development, surprisingly, the *in vivo* membrane resistance was at most half of the membrane resistance determined in neonatal slices [60, 97].

Matching of excitability and size of synaptic inputs

We next investigated to what extent the size of its largest synaptic inputs was matched with the intrinsic excitability of a principal neuron in the neurons in which both were recorded. First, we calculated the steady-state potentials as the

3

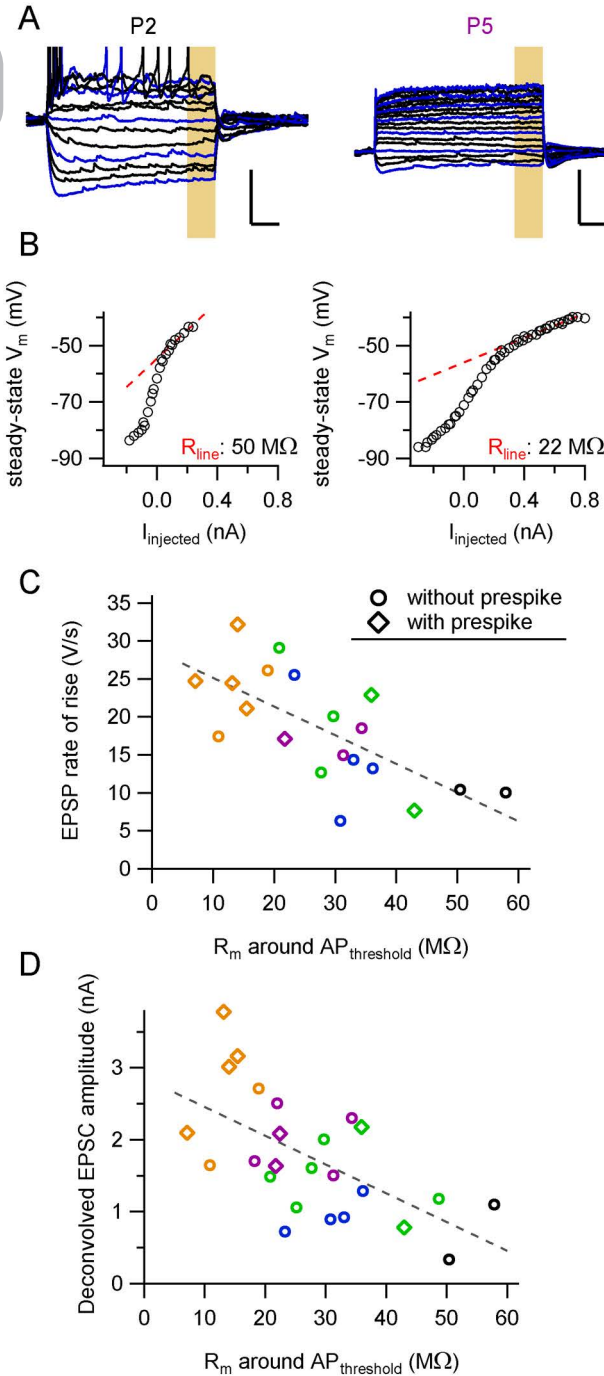


Figure 3.7 Matching of excitability and synaptic inputs of principal neurons. (A) Membrane potential during constant-current injections in a principal neuron from a P2 (left) and a P5 (right) rat pup. Displayed constant-current injection responses start at -120 pA; blue, multiples of 60 pA; black, multiples of 20 pA. Bars indicate 20 mV and 100 ms. (B) Corresponding I-V curves that were derived from the last 100 ms of the constant-current injection (yellow box in A). The steady-state membrane potentials between -50 mV and -45 mV were fitted and the slope of the fitted line (red dotted line) gave the steady-state membrane resistance around AP threshold for both neurons. (C) The average rate of rise of large EPSPs (>5 V/s) against the membrane resistance around AP threshold. (D) The deconvolved amplitude of large EPSCs (>0.5 nA) against the membrane resistance around AP threshold. For C-D: dotted line correspond to a linear fit; Black, blue, green, magenta and orange correspond to P2, P3, P4, P5 and P6, respectively; every point corresponds to a single neuron.

median of the last 100 ms of the constant-current injections and plotted the I-V curve (Figure 3.7A and B). The slope resistance decreased both at depolarized and at hyperpolarized potentials, similar to previous findings [201], probably owing to the activation of hyperpolarization-activated cation channels (g_{lh}) and low-threshold K^+ -channels (g_{LTK}) at hyperpolarized and depolarized potentials, respectively. We fitted the I-V curve between -50 and -45 mV with a straight line to measure the membrane resistance around AP threshold (Figure 3.7B). The membrane resistance around AP threshold significantly correlated inversely to the largest EPSP ($-0.38 \pm 0.09 \mu V s^{-1} \Omega^{-1}$, $t_{18} = -4.0$, $p = 0.001$, $r = -0.68$; Figure 3.7C) and the largest deconvolved EPSC ($-0.04 \pm 0.01 nA/M\Omega$, $t_{23} = -3.7$, $p = 0.001$, $r = -0.61$; Figure 3.7D). Although we cannot exclude the possibility of age as a confounding factor, this suggests that postsynaptic intrinsic excitability and size of synaptic inputs are homeostatically matched.

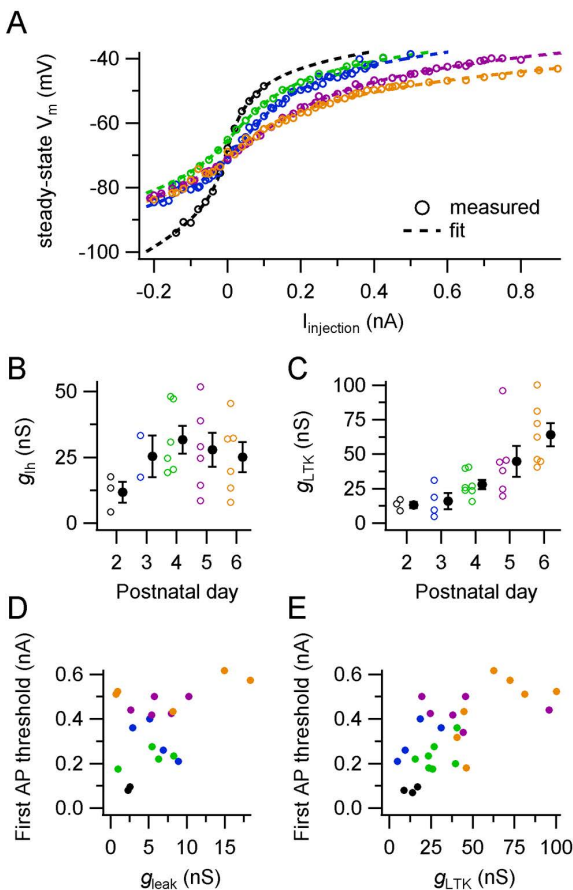


Figure 3.8 Hodgkin-Huxley model fit of voltage-dependent changes in membrane resistance. (A) Relation between steady-state membrane potentials against the injected current of five principal neurons. Broken lines show results of HH-model fit. Individual points show averages from multiple current-injections of a single cell; see B for colour lookup. (B) Developmental changes in fitted g_{lh} . Individual data points represent cells for which g_{lh} made a significant contribution to the fit. (C) Developmental changes in fitted g_{LTK} . (D) Relation between the minimal injected current needed for AP firing and fitted g_{leak} . Only cells in which the leak conductance significantly contributed to the fit are displayed. (E) Relation between the minimal injected current for AP firing and fitted g_{LTK} . For B and C, open circles represent a single neuron, filled circles averages with SEM. For D and E, circles represent single neurons.

A Hodgkin-Huxley-like model captures**the development of principal neurons in vivo**

The observed, large developmental changes in intrinsic properties appeared to involve several different types of ion channels. To understand their contribution to the developmental changes in the way APs were triggered, we constructed a Hodgkin-Huxley-like model (HH-model) for the principal neuron. This model neuron contained five conductances: a leak conductance g_{leak} , g_{Ih} , g_{LTK} , a high-threshold potassium conductance g_{HTK} , and a sodium conductance g_{Na} . Their gating kinetics were based on previous models for the principal neuron of the MNTB ([187, 198]; see Methods), and were kept constant throughout development. Their maximal conductances were estimated for the different ages based on the steady-state potentials of the *in vivo* constant-current injections (Figure 3.7A and B), and subsequently fitted by HH-models to find the minimal HH-model that could account for them (Figure 3.8A). After the passive model, which contained a leak conductance g_{leak} and its reversal potential, was fitted, the improvement of the fit by the addition of g_{LTK} or g_{Ih} was tested for each cell individually. For all recordings, the addition of g_{LTK} significantly improved the fit compared to the passive model (range of explained sums-of-squares: 17-87%); for 22 out of 27 recordings g_{Ih} contributed significantly (9 – 60%) and for one additional recording g_{Ih} was included as it almost reached significance (5% contribution; $p = 0.1$). To test the passive component of the model, the $g_{\text{leak}} + g_{\text{LTK}} + g_{\text{Ih}}$ model was compared against the $g_{\text{LTK}} + g_{\text{Ih}}$ model, and for 20 out of 27 recordings g_{leak} significantly improved the fit (9 – 89%); the fitted leak reversal potentials showed a developmental trend from -62 ± 5 mV at P2 to -87 ± 9 mV at P5, but this trend was not statistically significant ($F_{4,15} = 2.2$, $p = 0.13$). The fitted reversal potentials were compatible with a dominant role for K^+ channels in this leak conductance [186].

It was previously shown that the expression of low-threshold potassium channels in the MNTB increases during development [60, 184]. Our fit results showed an increase of all three conductances during development, but only for g_{LTK} the developmental trend was statistically significant (Figure 3.8B and C; P2: 13 ± 2 nS, P3: 16 ± 6 nS, P4: 28 ± 3 nS, P5: 47 ± 11 nS, P6: 64 ± 8 nS, $F_{4,22} = 6.9$, $p = 0.0009$). Low-threshold potassium channels start to open at depolarized

potentials, thereby increasing the current needed to elicit an AP (I_{APthr}). Indeed, g_{LTK} correlated with the I_{APthr} obtained from the same neuron (Figure 3.8E; 3.4 ± 0.8 pA/nS vs. 0 pA/nS, $t_{23} = 4.5$, Bonferroni-corrected $p = 0.0005$, $r = 0.7$) and similarly g_{leak} significantly raised I_{APthr} (Figure 3.8D; 22 ± 5 pA/nS vs. 0 pA/

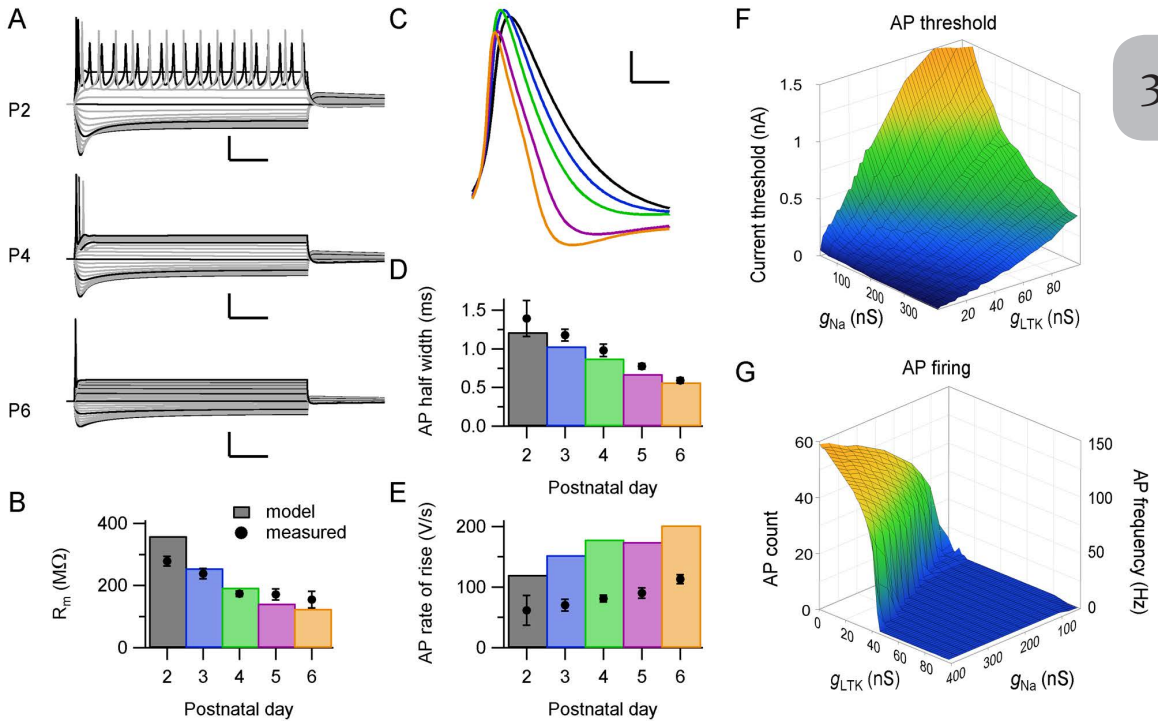


Figure 3.9 The Hodgkin-Huxley model reproduced the *in vivo* intrinsic properties of the principal neuron. (A) Simulations for current injections using the standard model neuron for P2 (top), P4 (middle), and P6 (bottom). The first simulated current injection was at -200 pA; grey steps are incremental current injections of $\Delta 20$ pA; black steps of $\Delta 100$ pA. Calibration bars indicate 25 mV and 100 ms. (B) Bars, the developmental changes in membrane resistance according to the simulations, which were calculated from the steady-state conductances at -70 mV to -75 mV. Circles, average *in vivo* membrane resistance with SEM. (C) Average simulated AP waveforms of the first current-injection elicited APs reveal similar developmental changes as *in vivo* (cf. Figure 3.6B). Calibration bars indicate 10 mV and 2 ms; colours correspond to age as in B. (D) Comparison of measured (filled circles) and simulated (bars) AP half widths shows similar developmental shortening. (E) As D, except maximal rate of rise of the AP. (F) Relation between g_{Na} and g_{LTK} and the minimum current injection needed to elicit an AP. Colours correspond to injected current. (G) Relation between g_{Na} and g_{LTK} and AP frequency or number of evoked APs per 400 ms; g_{leak} , g_{HTK} and g_{Ih} were kept constant at 2.5 nS, 100 nS and 25 nS, respectively. Colours correspond to AP count; the blue plateau indicates one AP.

ns, $t_{23} = 4.6$, Bonferroni-corrected $p = 0.0004$, $r = 0.8$), even when controlling for the effect of g_{LTK} ($F_{2,24} = 21.8$, $p = 9 \cdot 10^{-5}$). We therefore conclude that the developmental increase in g_{LTK} and g_{leak} significantly reduced the excitability of the postsynaptic neuron.

Next, the overall impact of the fitted conductances on the principal cell properties was assessed. We simulated the response of the model neuron to constant-current injections (Figure 3.9A) using parameters based on the average HH-model fits at the different ages (standard model neuron; Table 3.3). The values for g_{Na} and g_{HTK} were increased to replicate the developmental change in AP properties measured *in vivo* (Figure 3.9C-E) [60, 156, 159]. With the resulting set of parameters, the standard model neurons reproduced the developmental switch from continuous to single AP firing (Figure 3.9A), and had a similar membrane resistance as the *in vivo* recordings (Figure 3.9B). Interestingly, g_{LTK} strongly affected the spiking behaviour of the standard model neurons. The increase in g_{LTK} elevated the minimal current needed to elicit an AP (Figure 3.9F) and gave simulated I_{APthr} values similar to the I_{APthr} measured *in vivo* (cf. Figure 3.8F). In response to constant-current injection, the P2 standard model neuron intrinsically fired at miniburst frequencies; g_{LTK} could restrict AP firing to a single AP or could even silence the model neuron if the sodium conductance was sufficiently low (Figure 3.9G). The switch from single AP to tonic firing followed the ratio 1:10 for $g_{\text{LTK}}:g_{\text{Na}}$, although the exact ratio also depended on the other conductances. Comparing the fitted g_{LTK} values for the individual neurons with our simulations, our simulations predicted that the principal neuron would likely switch to phasic firing at P4-5 (Figure 3.9C), consistent with the *in vivo* response of the neurons to constant-current injections. These converging results suggest that our HH-model forms an adequate approximation of the *in vivo* developmental changes in the intrinsic properties of the principal neuron.

To test how accurately we could simulate postsynaptic activity based on the recorded intrinsic properties of the neuron and the recorded incoming activity, we selected the twelve neurons for which the intrinsic properties had been measured and adequate VC- and CC-recordings had been obtained. The aim was to use the recorded EPSCs as input to a model neuron with fitted conductances

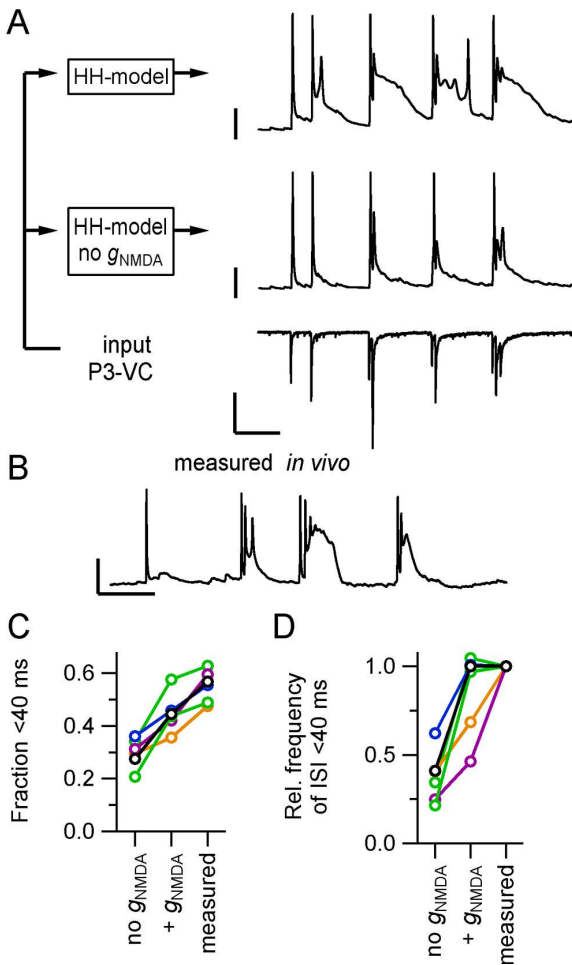


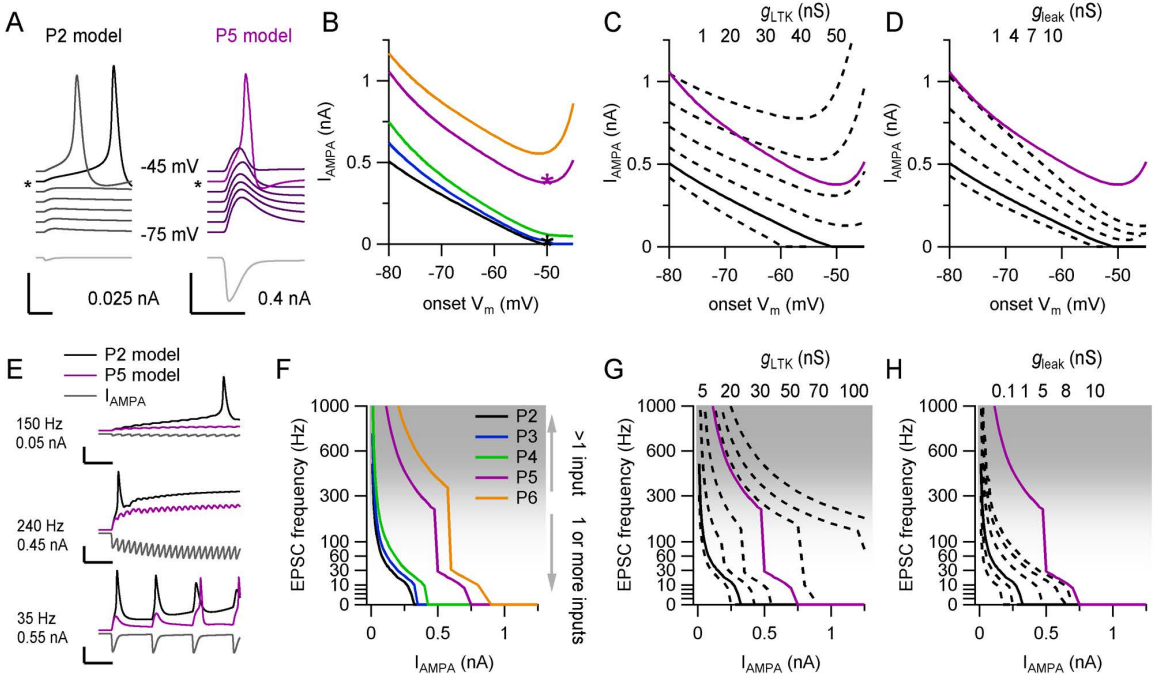
Figure 3.10 Contribution of the NMDA conductance to the minibursts.

(A) Left scheme indicates the modelling conditions with a P3 voltage-clamp recording as input for the Hodgkin-Huxley model (HH-model) either with or without the NMDA conductance with parameters based on the *in vivo* recorded neuron. Right, P3 voltage-clamp recording that was used as input for the model (bottom), modelled current-clamp recording without NMDA conductance (middle), modelled current-clamp recording with NMDA conductance (top). Calibration bars are 1 nA (bottom), 25 mV (middle, top) and 100 ms. (B) Representative trace from the *in vivo* current-clamp recording from the same neuron as in A. Calibration bars are 25 mV and 100 ms. (C) The fraction of interspike intervals <40 ms for 6 neurons (lines) for either the modelled values or the *in vivo* recording. (D) As C, but for the frequency of intervals <40 ms relative to the *in vivo* recording. Colours C and D correspond to age: P2 black, P3 blue, P4 green, P5 magenta, P6 orange; the P3 neuron is shown in A and B.

from the recorded neuron and compare the modelled with the *in vivo* current clamp recording. We first focused on the large EPSCs (>100 pA; *cf.* Figure 3.4), and with the calculated NMDA conductance, the modelled EPSPs' rate of rise approached the *in vivo* EPSPs' rate of rise ($r = 0.9$, model/measured = 0.95 ± 0.07). We then selected from the twelve neurons six VC recordings – two for P4 and one for each of the other postnatal days – for which voltage control was relatively good, as judged by the paucity of clamp-escaping action currents. The full VC recording processed by the model neuron resulted in a modelled current-clamp recording with epochs of high activity with AP firing as seen *in vivo*, except the miniburst intervals were less prevalent (Figure 3.10A, C and D).

Neural Activity During the Formation of A Giant Auditory Synapse

A major part of the synaptic conductance is carried through NMDA receptors, and this conductance was calculated within the model (see Methods). To investigate how the NMDA conductance contributed to AP generation in our *in vivo* recordings, we simulated the same recordings again, except we left out g_{NMDA} . As a consequence, the fraction of APs occurring within minibursts was reduced from 0.45 ± 0.03 to 0.30 ± 0.02 , which was clearly lower than what was measured *in vivo* (0.55 ± 0.02 ; Figure 3.10C; Repeated-Measures $F_{2,10} = 58$, $p = 3 \cdot 10^{-6}$, model no g_{NMDA} vs. model with g_{NMDA} : $t_5 = 4.7$, Bonferroni-corrected $p = 0.01$). In addition, the frequency of miniburst intervals halved in the absence of the NMDA conductance (Figure 3.10D; ratio of model no g_{NMDA} vs. model with g_{NMDA} : 0.45 ± 0.06). Without the NMDA conductance the ‘shoulder’-potential that followed the AP was less pronounced, and it seemed that in our simulations the shoulder-potential was extended compared to the *in vivo* recording (Figure 3.10A and B). Also, the NMDA conductance did not seem to facilitate miniburst firing in our P5 and P6 simulations. In summary, the simulations suggest that the NMDA conductance makes an important contribution to the shoulder-potential that facilitates secondary APs and miniburst firing at the younger ages.



Contribution of developmental increases

in g_{LTK} and g_{leak} to synaptically-triggered APs

A key difference between principal neurons at P2 and P5 was that at P2, APs were typically triggered by summing EPSPs, whereas at P5 APs were typically triggered by a single EPSP, which started close to the resting potential. To investigate the role of the onset membrane potential and the changes in voltage-dependent ion channels to the developmental changes in the minimum EPSP size needed to trigger an AP, we used EPSCs of different amplitude as input to the models representing the different ages. In the P2 standard model neuron even very small EPSCs could already trigger an AP from a depolarized onset potential, whereas in the P5 standard model neuron, much larger EPSCs were needed, and excitability decreased again at very depolarized membrane potentials (Figure 3.11A). In Figure 3.11B we systematically tested what the minimum EPSC size was that was needed to trigger an AP at different onset

← **Figure 3.11 Dissection of the effect of the low-threshold potassium conductance and the leak conductance on postsynaptic firing induced by one or multiple EPSCs.** (A) Left, P2 model output in response to a 25 pA EPSC (grey, bottom panel) at onset membrane potentials ranging between -45 mV (top) and -75 mV (bottom). Right, P5 model output in response to 400 pA EPSC. The asterisk indicates the most negative onset membrane potential at which an AP was detected. Note that in the P5 model the EPSC did not elicit an AP at the -45 mV onset membrane potential. Both calibration bars indicate 20 mV, 300 pA and 10 ms. Colours are added for visual aid. (B) Relation between the EPSC amplitude minimally needed to trigger an AP and the onset potential for different parameter sets, as illustrated in A. The asterisks correspond to the traces indicated with an asterisk in A. (C) Relation between EPSC amplitude and the onset potential at different g_{LTK} -values for the P2 model (broken lines, values given at the top). Solid lines indicate the standard P2 and P5 model for reference. (D), as in C, but for g_{leak} . (E) Three examples of EPSC trains (bottom, grey) with different frequencies and amplitudes and the corresponding output of the P2 model (top, black) and P5 model (top, magenta). Top traces start at -70 mV. Calibration bars indicate 25 mV, 500 pA and 20 ms. (F) Relation between EPSC amplitude minimally needed to trigger an AP and the EPSC frequency for different parameter sets. Shaded area illustrates the frequency range that is unlikely to be attained by a single axon. (G) Relation between the EPSC amplitude minimally needed to trigger an AP and EPSC frequency at different g_{LTK} -values for the P2 model (broken lines, values given at the top side). Solid lines show the standard P2 and P5 model for reference. (H) as in G but for different g_{leak} -values. For C, D, G and H, the conductance values listed on top from left to right correspond to the traces from left to right. For F-H, the resting membrane potential was set at -70 mV.

3

membrane potentials for the standard model neurons (Table 3.3, cf. Figure 3.9). Large EPSCs were needed to trigger an AP at the older ages, even at depolarized onset potentials. In contrast, at the younger ages, small EPSCs could trigger an AP at depolarized potentials. To understand the relative contribution of g_{LTK} and g_{leak} to these developmental changes, we systematically varied the maximal conductance of g_{LTK} and g_{leak} within the P2 standard model neuron to see how they influence the relation between the membrane potential and the minimum EPSC needed to trigger an AP. As g_{LTK} increased, even at depolarized membrane potentials large EPSCs became necessary to trigger an AP, likely due to the activation of g_{LTK} at these potentials (Figure 3.11C). In contrast, whereas an increase in g_{leak} also decreased excitability, at depolarized potentials small EPSCs could still trigger an AP (Figure 3.11D). Because of its slow kinetics, g_{th} had a similar effect as g_{leak} (results not shown). These results suggest that all three conductances could decrease excitability, but that the recruitment of g_{LTK} has the additional effect of strongly limiting the contribution of EPSP summation to AP generation at the older ages.

To test this more directly, we simulated an 0.8 s epoch of bursting activity by generating a train of identical synapse conductances g_{syn} that were based on the model EPSC time course (see Methods). These train simulations confirmed that at high frequencies even small EPSCs could trigger an AP in the P2 standard model neuron, but that for the P5 standard model neuron large EPSCs were needed (Figure 3.11E). This was confirmed in a more systematic test of the minimum EPSC needed to trigger an AP as a function of both EPSC amplitude and frequency within the train for the different age model neurons (Figure 3.11F). While for the P2 model neuron the EPSC frequency and amplitude showed a simple, inverse relation, for the P5 and P6 standard model neuron a vertical plateau in the amplitude-frequency relation appeared; at these settings very high frequencies were needed to substantially lower the EPSC size needed to trigger an AP. To understand the relative impact of g_{LTK} and g_{leak} on these changes, we again systematically altered their conductances within the P2 standard model neuron. The increase in g_{LTK} drastically increased the frequency needed to trigger an AP with a small EPSC, and at increased g_{LTK} , the vertical plateau appeared, suggesting that g_{LTK} differentially changed excitability for smaller

and bigger EPSC amplitudes (Figure 3.11G). In contrast, g_{leak} also affected the minimum frequency needed for an AP, but did so more homogeneously for all amplitudes. The effect of g_{lh} was again comparable to that of g_{leak} (not shown).

At the older ages, EPSPs decayed back to baseline faster than at the younger ages, among others because the increase in g_{leak} and g_{lh} decreased the membrane time constant around the resting membrane potential. Hence, at low frequencies, the AP threshold had to be reached with only minor pre-depolarization (Figure 3.11E, lower panel). The minimum EPSC amplitude that singlehandedly could elicit AP firing corresponds to the vertical plateau— the region where a small decrease in EPSC amplitude demands a disproportionate increase in EPSC frequency to elicit an AP (compare Figure 3.11B with F, C with G). The vertical plateau marks the transition from a situation where a single, large EPSC triggers an AP without the need of substantial pre-depolarization, to a situation where only high-frequency bursting, which causes rapid summation, can activate the sodium conductance before g_{LTK} activates substantially. With increasing g_{LTK} the frequencies needed for small EPSCs to elicit an AP quickly rose, making it unlikely that barrages of small EPSCs during epochs of high activity, as recorded *in vivo*, would be able to “outrun” the activation of g_{LTK} and elicit APs.

With an EPSP rise time of ~ 3 ms within the P5 standard model neuron, at frequencies over 300 Hz the distinction with the single large EPSC regime blurs. Given that, based on our juxtacellular recordings, a single axon has a maximal firing frequency of ~ 300 Hz with maximally 6 APs, it becomes very unlikely that any input will independently generate a postsynaptic AP, unless the synapse is large, which explains the observed, increased dependency of postsynaptic firing on a prespike-related input in our juxtacellular recordings. We conclude that both g_{LTK} and g_{leak} decrease excitability, but that g_{LTK} is particularly effective in suppressing AP generation by EPSP summation, thus biasing the principal neuron to progressively larger inputs.

Discussion

We made *in vivo* recordings from principal neurons of the rat MNTB to study the developmental changes in intrinsic properties and synaptic inputs during the first neonatal week, the period when the calyx of Held synapse forms. The main advantage of our *in vivo* approach was the possibility to study the MNTB development within an intact, spontaneously active system, which allowed us to record the impact of the developing calyceal synapses. Principal neurons showed complex bursting activity that was triggered by spontaneous inputs, consisting of a stable component at around 10 Hz and a faster component that became more prominent and accelerated during development. Postsynaptic firing became increasingly dependent on a prespike-associated input. Whole-cell recordings revealed a developmental change in the way postsynaptic APs were triggered by the spontaneous inputs: at P2, barrages of small EPSPs caused the neuron to fire multiple action potentials elicited from a plateau depolarization, while at P5, APs were typically triggered by a single, large EPSP. At the same time, the intrinsic excitability of the principal neuron changed considerably; these changes included a substantial increase in the conductance of the low-threshold K^+ -channel, g_{LTK} . According to HH-model simulations, this increase of g_{LTK} reduced EPSP summation, thus necessitating large inputs for triggering APs.

Developmental changes in burst firing patterns

Our juxtacellular recordings agree well with our earlier developmental study, for which the youngest age studied was P4 [155]. The present data show an increase in synaptic latencies at the youngest ages and fewer recordings containing prespikes. A complex bursting pattern could already be observed as early as P2. Its 10 Hz component, which has been associated with calcium spike intervals of hair cells [74], remained remarkably stable, whereas the fast component was slower and less pronounced at the youngest ages. At P2, APs were typically triggered by summing EPSPs. The prominent presence of the 10 Hz peak already at that age, in combination with the observation that the EPSPs that triggered the spikes were on average larger than the other EPSPs, indicates that already well before the calyx develops, relatively large inputs at ~100 ms intervals play a key role in triggering action potentials in the principal neurons. The miniburst component did show developmental shortening. Multiple

mechanisms may contribute to this. At these young ages, burst generation in the cochlea is just starting to occur and the maximal instantaneous firing rate in the auditory nerve is still <100 Hz [75, 202]. The maturation of the modified endbulb of Held synapse may precede that of the calyx of Held synapse, but is still far from mature at P2-3 [59]. Interestingly, however, no developmental shortening was observed for the miniburst prespike intervals, and these intervals were shorter than of their postsynaptic counterparts. This indicates that developmental processes within the MNTB can also make a clear contribution to the developmental shortening of miniburst intervals of the principal neurons.

In the two cases in which we distinguished multiple large inputs by the presence or absence of a prespike, their activity was strongly correlated and their co-occurrence extended to single minibursts, suggesting convergence of temporally coactive axons. Little is currently known about the spatial organization of pre-hearing spontaneous activity within the auditory brainstem, but these recordings thus provide anecdotal evidence that neurons wiring together may tend to fire together.

Developmental changes in inputs

In a relatively short period, we observed the emergence of large inputs that could trigger an action potential by themselves. These large inputs often were associated with prespikes, and thus can be expected to occupy a large portion of the postsynaptic somatic surface. An important, unresolved question regarding the development of the calyx of Held synapse is to what extent there is competition between large inputs for somatic space. In P2-6 mice, ultrastructural reconstructions of principal neurons and their axosomatic synapses indicated that 25/119 principal neurons were innervated by multiple large axosomatic terminals [136]. In another study, 7/101 neurons from P7-15 mice showed evidence for multiple large inputs (>440 pA) [138]. In contrast, we found evidence for the presence of multiple large inputs, here defined as inputs >5 V/s or 100 pA (~ 500 pA after deconvolution), in only 3/132 recordings. In each case one input was preceded by a prespike while the other was not. We did not find evidence for the presence of prespikes with different size, which would be evidence for the presence of multiple, large somatic inputs. As disparate as these studies are, the difference seems substantial, and might be explained by a species difference, a

bias against recording from cells with multiple large somatic inputs, the presence of large somatic terminals firing infrequently or having small impact, or large inputs with very similar characteristics. Even though our data are compatible with the view that the presence of multiple protocalyces is a rare phenomenon, without a detailed structure-function analysis of nascent calyces it is currently not possible to resolve the apparent discrepancies with earlier studies. In the next chapter we will return to this issue.

3

Model limitations

We used an HH-model to infer the relative importance of developmental changes in intrinsic properties for the excitability of the principal neurons. A limitation of our model was that we assumed a single compartment, whereas our stainings revealed extensive dendrites and an axon. As the dendrites and axons charge slowly, the capacitive load becomes time dependent. Our capacitance estimates were based on the first 10 ms of a 5 mV-step and were about 50 pF, which still represents an underestimation of the postsynaptic capacitance owing to limited spatial clamp. However, other reported MNTB models used 10-20 pF, which better approximates the somatic capacitance [187, 198], indicating that our capacitance measurements included non-somatic membrane. Although we corrected for the dendritic capacitance (see Methods), the model results are sensitive to the chosen value. Another limitation of our simulations is that the synaptic conductances were obtained from VC recordings at -80 mV, where the NMDA component will be minimal, while it is known to be quite large at neonatal ages in the principal neurons [137, 156]. As the NMDA component is rather slow, it is the NMDA conductance that will be most sensitive to the size of the dendritic capacitance. Lastly, slow voltage-dependent conductances that affect the AP, additional activity-dependent conductances, and short-term synaptic depression were not included in our model [155, 203-205]. Any deviation will alter the outcome of the simulations for long periods of activity. Therefore, the simulations might be fairly reliable for short periods, such as EPSPs or current injections, but will be less reliable when modelling seconds of high synaptic activity, as recorded *in vivo*.

Developmental changes in excitability

We observed a large developmental decrease in the excitability of the principal neurons, which was due to among others a decrease in their resting membrane resistance and an increase in low-threshold K^+ -channels. The developmental decrease in the membrane resistance was in agreement with earlier slice studies in the MNTB [60, 97], in other auditory synapses [59, 188, 206] or in other brain areas [207, 208]. The absolute size of the membrane resistance, however, was only half of the *ex vivo* value. Apart from the absence of spontaneous presynaptic activity *ex vivo*, possible factors explaining this difference include a difference in the composition of the external medium, e.g. a higher neurotransmitter concentration *in vivo*, and the cutting of dendritic branches or the axon during slicing, as suggested by the lower membrane capacitance reported in slices [97].

The membrane resistance was highest close to the resting membrane potential. In the depolarizing direction we found evidence for a developmental increase in the conductance of low-threshold K^+ -channels. Based on the HH-model fits, g_{LTK} increased four-fold between P2 and P6. The reported changes in the HH-model conductances are to be considered as approximate values, since they were measured indirectly and were not pharmacologically confirmed; we also assumed that gating kinetics were constant during development, which may not be correct [209]. There are, however, several arguments that the increase in g_{LTK} is real. Every principal neuron at P2 fired repetitively and at P5-6 most neurons fired only a single AP. Our model reproduced the essential role of g_{LTK} in this change [60, 190, 210]. Moreover, the increase is in general agreement with the postnatal increase in mRNA expression for K_v1 channels in MNTB neurons [60, 184]. A similar developmental increase in low-threshold K^+ -channels has also been observed at other auditory synapses [188, 206]. The alternative possibility that this change was due to a very large increase in g_{HTK} seems highly unlikely, since this would have a major negative impact on the principal neuron's ability to fire APs.

By being located at the initial segment, the K_v1 channels are in an optimal position to control AP generation [190]. Following the increased expression of low-threshold K^+ -channels, the neurons become dependent on a large input, which had to be sufficiently fast to “outrun” the activation of the K_v1 channels. In

this respect they have a similar function as in fast-spiking cortical interneurons [211]. Our simulations also allowed to delineate the different role of leak channels and low-threshold K^+ -channels: both decreased excitability, but low-threshold K^+ -channels were especially effective in preventing EPSP summation, thus effectively restricting AP generation to large inputs.

Despite the increase in K^+ -channels, no clear developmental hyperpolarization of the resting membrane potential was observed, in contrast to the situation at many other synapses [212-215]. Possibly, a concomitant change in the expression of I_h [216] or in other channels or transporters that are active at rest [168, 186] limited the impact of the K^+ channels on the resting membrane potential.

Plateau potentials

During high-frequency bursting, MNTB neurons demonstrated a plateau depolarization *in vivo*. Plateau depolarizations have also been observed during high-frequency calyceal stimulation in slice recordings, and were shown to be NMDA-dependent [217-219] and attenuated by presynaptic activation of adrenergic receptors [218]. Our simulations in which we used the recorded voltage-clamp activity as input to the HH-model were in agreement with an important role for NMDAR activity, even though for definitive confirmation pharmacological blockage would be needed. These plateau potentials are also commonly observed in the developing neocortex, where they may play an important role in network oscillations and synaptic maturation [220]. One possible function of these plateau potentials might be to activate L-type Ca^{2+} channels [221], which are an important source for postsynaptic Ca^{2+} entry [222], and are known to be important for survival of MNTB neurons [123, 223, 224]. Calcium channels have a rather uniform distribution on the postsynaptic soma of principal neurons and can therefore substantially raise nuclear Ca^{2+} concentrations owing to the eccentric location of the nucleus [222], which is often away from the calyx synapse [225]; the nuclear Ca^{2+} increases may play an important role in synaptic development and neuronal survival [226]. The developmental increase in low-threshold potassium channels can limit the impact of plateau potentials [227], and, together with the developmental downregulation of NMDA channels [156, 199, 219], can be expected to restrict the options for large changes in the synaptic makeup of principal neurons.

Relation between innervation and excitability

We did not observe any cells with a very clear mismatch between excitability and size of the inputs. Cells with high excitability had small inputs and cells with low excitability received large inputs. This suggests a temporal, homeostatic matching between protocalyx formation and the reduction of the excitability of principal neurons, and raises the question how this matching is accomplished [209, 228, 229]. Several transcription factors have recently been identified that can regulate K_{V1} expression [230-232]. Interestingly, one of them, the transcription factor *Er81*, is activity-dependent [232], suggesting one way in which the morphological and electrophysiological changes might be coupled. Two transcription factors in *Drosophila*, *Islet* and *Lim3*, together control both *Shaker*, the *Drosophila* homologue of K_{V1} , and several genes related to synaptogenesis, suggesting a second way in which excitability and connectivity might be coupled. Thirdly, the transcription factor *Cux1* controls K_{V1} expression levels, and it has been suggested that the resulting changes in excitability may also influence synaptic innervation [231]. In addition, the contribution of K_{V1} might be fine-tuned by activity-dependent, post-translational modifications, leading to changes in gating kinetics or protein trafficking (reviewed by [191, 233]). Thus, there are several ways in which changes in synaptic inputs and postsynaptic excitability might be coupled [102, 229, 234-237]. Elucidation of the homeostatic mechanisms that ensure that the activity patterns that are generated at the cochlea are propagated to more central structures even though there are major changes in the strength of synaptic connections will require a combination of molecular, anatomical and functional studies.

Acknowledgments: Confocal scanning microscope was accessed via the Optical Imaging Center at Erasmus MC. We thank Kees Donkersloot for technical support, John Soria van Hoeve for surgical training, Rüdiger Geis for helpful discussions, and Elize Haasdijk for support with histology.

In vivo development of multi-innervation of principal cells
of the rat medial nucleus of the trapezoid body

Martijn C. Sierksma, Johan A. Slotman, Adriaan B. Houtsmuller, J. Gerard G. Borst

In preparation

Abstract

4

The calyx of Held synapse is among the best studied synapses of the central nervous system owing to its giant size. During development, the synapse evolves from a classical connection with small boutons to a giant, axosomatic synapse. In accordance with a role for synaptic competition, anecdotal evidence suggests that multiple calyces can form on a principal neuron. However, the impact of the presence of multiple calyces is still unclear, and, more generally, the relation between calyceal shape and strength has not yet been studied *in vivo*. We combined *in vivo* whole-cell recordings of principal neurons of the medial nucleus of the trapezoid body (MNTB) while stimulating their afferent axons, with post-hoc subdiffraction imaging of immuno-labeled terminals. This approach identified multiple inputs of a principal cell. During development the strongest input became stronger while the second strongest did not change, which is not in agreement with a prominent role for giant-synapse competition. Strong inputs associated with a prespike, the hallmark of the presence of a giant terminal, were similar to other strong inputs. With immunolabeling we showed that the active zone protein Piccolo is present in the developing calyx of Held. The size of the terminals labeled for Piccolo and vesicular glutamate transporters (VGluT), and the rat's postnatal age generally predicted the strength of the strongest input *in vivo* well. Only for cells with a large VGluT cluster we recorded a prespike, but we report two exceptions where a large terminal was present without an apparent prespike in the recording. Together, our data are in agreement with a model in which one input grows rapidly and becomes the calyx of Held, followed by a much slower retraction of the other inputs.

Introduction

The synapse is a fundamental building block of the brain with an immense diversity in morphology and strength. Most terminals have a diameter of only about 1 μm , forming a single synaptic contact on a dendrite. In contrast, some synaptic terminals are $>10 \mu\text{m}$, containing >100 release sites [238]. The large size of some of these synapses facilitates the study of their biophysical properties. An example is the calyx of Held synapse in the auditory brainstem, which has become a model synapse to understand synaptic transmission, and

is arguably the best studied synapse of the central nervous system [16]. Its large size spanning ~20 μm makes the calyx one of the few terminals accessible for patch-clamp electrophysiology [19, 20]. Owing to the presence of hundreds of active zones [101, 239, 240], the calyx of Held rapidly depolarizes its postsynaptic neuron in the medial nucleus of the trapezoid body (MNTB) to its action potential threshold, thereby functioning with high fidelity as an inverting relay in the auditory system [16].

It is well established that a single globular bushy cell (GBC) can give rise to more than one calyx of Held [17, 18, 55, 89, 92]. The converse, to what extent principal neurons are innervated by more than one calyx of Held, is currently less clear. This question can be studied both by physiological and by anatomical methods. Both have their limitations, which may be responsible for some of the remaining uncertainties with regard to the question how the calyx of Held forms.

From a large set of electron microscopy (EM) reconstructions of developing principal neurons and nearby axons it was estimated that a single GBC axon contacts >20 principal neurons, and at least five different GBC axons contact a principal neuron [136, 137]. This indicates that the innervation of principal neurons by GBCs is initially divergent. The strength of these synapses undergoes major changes during the first postnatal days [60, 137, 153, 157], and already at around P5, electrophysiological studies both *in vivo* and *in vitro* and EM studies found that one of the connections typically outcompetes the other ones [136, 137, 153]. Based on serial EM reconstruction it was suggested that half of the mouse principal neurons at some developmental stage are contacted by multiple calyceal synapses [60, 136]. However, strong physiological evidence for this is currently still lacking, since *in vivo* recordings of rat principal neurons showed evidence for the presence of multiple strong inputs in only very few cases (Figure 3.5).

One major challenge is to identify all synapses that are functionally connected to the principal neuron. In slice studies there is always the uncertainty associated with possible cutting of inputs during the slice preparation. The advantage with these preparations is the possibility of pair-wise recordings,

4

either electrophysiologically or via imaging methods, of presynaptic and postsynaptic structures which can directly establish functional connectivity [20, 90]. Serial sectioning of tissue combined with EM offers the possibility of fully reconstructing every synapse in a restricted volume [136, 137, 241], and this technique has been used to reconstruct entire calyces [136, 239, 242]. However, it offers only an indirect estimate of the strength of synapses, and combining this technique with electrophysiological recordings is challenging. In contrast, immunolabeling of vesicular glutamate transporters (VGluT) can locate synapses in the MNTB [90, 92, 194] and is easy to combine with electrophysiological recordings. However, the high neuronal density in the MNTB precludes the unambiguous association of the terminal with its postsynaptic target as the VGluT does not signal the release site(s). Piccolo, an active zone protein [243, 244], is abundantly present in young calyces [240]. The combination of VGluT and Piccolo can thus be used as an important indication for the presence of synaptic connectivity in the MNTB. *In vivo* whole-cell recordings can be used to record the inputs that are regularly active [134, 153], but this method does not offer detailed structural information about the synapses. By using *in vivo* electrophysiology and immunolabeling we sought the benefits of both. By using structured illumination microscopy [245] to improve the imaging resolution, we aimed to extend the specificity of the reconstructed synaptic morphology in order to open up the opportunity to relate *in vivo* synaptic strength to high-resolution synapse morphology.

Here, we study the multi-innervation of principal cells within the formation period of the calyx of Held. By electrically stimulating the afferent axons *in vivo* we could separate multiple developing inputs based on current activation threshold, action potential (AP) propagation speed and synaptic strength, while also allowing the recording of spontaneous activity. This significantly increased our ability to distinguish inputs. We show that Piccolo is present in these developing axosomatic terminals, and thus likely identifies a synaptic contact. Cells that we recorded from were then immunolabeled with VGluT and Piccolo and the axosomatic synaptic inputs were identified. These morphological properties were then correlated to *in vivo* synaptic strength and the presence of a prespike.

Materials & Methods

Animals

All procedures conformed to the European legislation and were approved by the local animal ethics committee (EDC, project no. 115-14-11). Wistar dams (WU) were purchased from Charles River and housed within the Erasmus animal facility (EDC). The day of birth or finding the litter was taken as postnatal day (P)0. The dams had ad libitum access to food and water, and additional bedding and shelter material was provided for nest building.

Surgery and in vivo electrophysiology

We used a ventral approach to gain access to the auditory brainstem, as described previously [90, 153]. First, we searched for bursting activity with a glass electrode to find the presumed location of the MNTB. When bursting activity was found, the search pipette was retracted and a bipolar stimulation electrode (MicroProbes for Life Science, PI2ST30.1H10) was placed contralateral from the recorded MNTB, straddling the trapezoid body, as described by Crins *et al.* [155]. In initial experiments the location of the trapezoid body was visualized with optical coherence tomography (OCT). With this technique the axons can be visualized as reflective bands within the craniotomy, and the stimulation electrode was placed based on these images. In later experiments the placement of the stimulation electrode was based on the experience obtained with the OCT imaging. Successful placement was then assessed by measuring the field potential and the associated stimulation current threshold.

Next, whole-cell recordings with biocytin (0.1-0.2 %, w/v) in the pipette solution were made from principal cells; to be confident that the recording was obtained from the same neuron as the one that was recovered with immunolabeling, we only patched one principal neuron per animal (n = 40 rats). Whenever a glia cell or non-principal cell was encountered, the pipette was retracted and a new pipette was used. Membrane potentials were compensated prior to the recordings for a liquid junction potential of -11 mV. Drift in membrane potential was <5 mV and remained uncorrected. Recordings were made with a MultiClamp 700B in current-clamp mode, with the bridge resistance and pipette capacitance compensation on. Bridge resistance was set in the range of 20-70 M Ω and

pipette capacitance compensation was set in the range of 4-6 pF. Owing to the high series resistance the time constants of the stray capacitance (~0.3 ms) and of the cell (at rest ~4 ms) could not be well separated during compensation. We therefore tried to avoid overcompensation, possibly leading to suboptimal compensation settings. Signals were low-pass filtered with a 4-pole Bessel filter at 10 kHz and digitized by a DigiData 1440A (Molecular Devices Co.) at 25 kHz. Acquisition was done with Clampex 10.2 running on a Windows XP computer.

Stimulation intensities were manually adjusted during the experiments. First, we quickly assessed at which stimulation levels new excitatory postsynaptic potentials (EPSPs) were recruited, and at which polarity most inputs could be discerned. Then, stimulation intensity was lowered to the activation threshold of the first input, and step-wise increased over time. In some experiments the stimulation intensity was also stepwise reduced, and then the data were pooled. For every stimulation strength >30 sweeps were collected at 2 Hz. Stimulation current was typically below 0.4 mA to prevent damage to the axons; at high stimulation currents (0.3 mA or higher) antidromic APs with latencies <1 ms were often elicited in the principal neuron.

After a recording from a principal neuron of the MNTB, the animal was deeply anesthetized and perfused with 6-10 mL of cold saline (0.9 % NaCl, w/v), followed by 8-10 mL of 4 % of paraformaldehyde (PFA, w/v) dissolved in 0.12 M phosphate-buffer (PB, pH 7.2-7.4).

Antibodies

The following primary antibodies were used: rabbit polyclonal anti-Piccolo (Synaptic Systems 142003; 1:1000), guinea-pig polyclonal anti-vesicular glutamate transporter 1 (Millipore AB5905; 1:3000) and 2 (Millipore AB2251; 1:3000). Secondary antibodies Alexa Fluor 488 against rabbit and Alexa Fluor 645 against guinea pig were obtained from Jackson (1:200 or 1:400). Streptavidin-Alexa Fluor 594 conjugate (1:000) was obtained from Thermo Fisher Scientific.

Immunolabeling procedure

Immunolabeling procedure is based on the free-floating method. After perfusion the brain was carefully removed from the skull, and post-fixed overnight at 4 °C. Then, it was left overnight in 10 % (w/v) sucrose in 0.1 M

PB, embedded in 10 % (w/v) gelatin and 10 % (w/v) sucrose, and again fixed overnight at 4 °C in 30 % (w/v) sucrose and 10 % (w/v) formaldehyde. The brain was cryoprotected with 30 % (w/v) sucrose solution in 0.1 M PB for >24 hr at 4 °C. Coronal slices (40 µm) were made on a freezing microtome, which were collected in 0.1 M PB. The sections were heated for 3 hr to 80 °C in 10 mM sodium citrate (pH 6 at RT), washed four times for 10 min with 0.9 % (w/v) NaCl in 0.05 M PB (PBS). Then, the sections were pre-absorbed for 1 hr at RT with 10 % (v/v) normal horse serum and 10 % (v/v) Triton X-100 in PBS followed by 36-48 hr incubation at 4 °C with primary antibody solution containing 2 % (v/v) normal horse serum, 0.4 % (v/v) Triton X-100 and the primary antibodies under gentle agitation. The slices were washed four times for 10 min in PBS at RT, and incubated for 2 hr at RT in the secondary antibody solution containing 2 % (v/v) normal horse serum, 0.4 % (v/v) Triton X-100, and the secondary antibodies under gentle agitation. For the biocytin-filled cells the streptavidin conjugate was also added at this step. The slices were washed once for 10 min at RT with PBS, and incubated for 10 min RT in 0.3 µM DAPI (D3571, Invitrogen) in 0.1 M PB. Sections were then washed thrice at RT with 0.1 M PB, mounted on glass coverslips with gelatin-chroomalun, air-dried, and closed with Mowiol solution containing 10 % (w/v) Mowiol 4-88, 25 % (v/v) glycerol in 0.1 M Tris-buffer (pH 8.5). Sections were kept at 4 °C in the dark until further use.

Confocal and structured illumination imaging

Confocal imaging was done on a Zeiss LSM 700 microscope equipped with a plan-apochromat 20x, 0.75 NA and a 63x, 1.4 NA objective, and PMT detectors, or a Zeiss Elyra PS1 microscope which is described below. Images were acquired with optimized settings for laser power, detector gains and pin hole diameters. High-resolution images (2048x2048) were acquired with a pixel size of 0.041 µm laterally and 0.110 µm radially to facilitate the comparison with SIM images. Low-resolution tile images were acquired with a lateral pixel size of 0.274 µm.

Structured-illumination imaging was done on a Zeiss Elyra PS1 system equipped with 488, 561 and 642 nm, 100 mW diode lasers; fluorescence was acquired with a Zeiss plan-apochromat 63x, 1.4 NA objective and an Andor iXon DU 885 EMCCD camera (1002 x 1004 pixels). Gratings were presented at

5 phases and 5 rotations for every depth. Sampling resolution was set to 41 nm laterally and 110 nm radially. The fluorophore signals were acquired sequentially. Reconstructions were made with build-in algorithms using ZEN 2012 SP1 black (v8.1.3.484).

Electrophysiological analysis

EEPSPs were detected as described previously [153] based on an EPSP minimal rate of rise (>0.7 V/s) and an EPSP onset based on the second derivative. A period after the stimulation was defined as the period-of-interest (1.5 to 8 ms post-stimulation), and EPSPs that were present in this period were categorized as 'evoked EPSPs'. Next, we grouped the evoked EPSPs based on stimulus strength, EPSP latency and EPSP rate of rise. We assumed that with increasing stimulation intensities previously-recruited EPSPs would still be activated. For consecutive stimulus intensities Welch's t was calculated for the EPSP latency and rate of rise, and added together. When the summed t -value was above 6 and the increase of the response rate of rise was $>20\%$, we considered the evoked EPSP different. We visually checked whether this difference was due to a new input or just a shift in activation probability of a previously-activated input. For a new input its rate of rise was calculated by subtracting the rates of rise of previously identified inputs when they were of similar latencies (± 0.5 ms). For four recordings we found EPSPs with longer latencies (Figure 4.1C), and for these recordings the Welch's t was calculated but restricted to a latency domain defined by the experimenter. For the example in Figure 4.1C this was 1-3 ms. Lastly, the rate of rise associated with the new input was checked against the spontaneously-occurring EPSP rates of rise, and the defined input was only accepted if a spontaneous EPSP with a similar rate of rise also occurred. In addition to the inputs identified with evoked EPSPs, we identified inputs in the spontaneous EPSPs. By comparing the distribution of EPSP rates of rise of all detected EPSPs in a recording with the evoked EPSPs, we could sometimes identify additional larger inputs (8 large inputs in 8 cells). Within the spontaneous EPSPs, many were of a small size 0.7-2 V/s and inputs were hard to identify. If small EPSPs were not evoked, we visually selecting peaks from the histogram of the EPSP rate of rise (Figure 1C-D) to define these weaker inputs, and added the inputs to the dataset to acknowledge that they are there. However,

the occurrence of weak inputs is likely underestimated due to the lack of good demarcations.

Image analysis

For the confocal images in Figure 4.4C and D local background was reduced by median subtraction with a filter radius of 5 μm . For Figure 4.4E and Figure 4.5, image segmentation was performed as follows. The raw signal of the biocytin-labeling was binarized with a threshold obtained per z-slice with the algorithm ‘Huang’ implemented in ImageJ 1.51r [246]. With a custom-made plugin the structure-of-interest (neuron, calyx) was isolated by grouping contiguous supra-threshold pixels starting from a seed-pixel placed by the experimenter. When a large protrusion from the cell was unconnected, the experimenter would fill a few pixels (<5) to obtain a contiguous connection. The structure-of-interest would then be dilated for 10 pixels to include signals within a distance of 0.4 μm laterally and 1.1 μm radially. The raw images would then be masked for all pixels that were not part of the structure-of-interest. The perisomatic VGlut-labeling was then assigned to one of the three categories by the experimenter based on the somatic area that was contacted by this labeling. This could be the group ‘small’ if no clear cluster was observed; ‘medium’ if the largest cluster covered only a small part of the soma, loosely corresponding to <20%; ‘large’ if the largest cluster clearly covered a significant part of the soma.

All images were pseudo-colored and contrasted in ImageJ v1.5. Color gamma enhancement was performed with Adobe Photoshop 19.1.0. We noticed that the peak intensities of Piccolo and VGlut did not overlap in SIM images. From line profiles it became clear that Piccolo labeling did overlap with lower intensities of VGlut, but not their highest intensities.

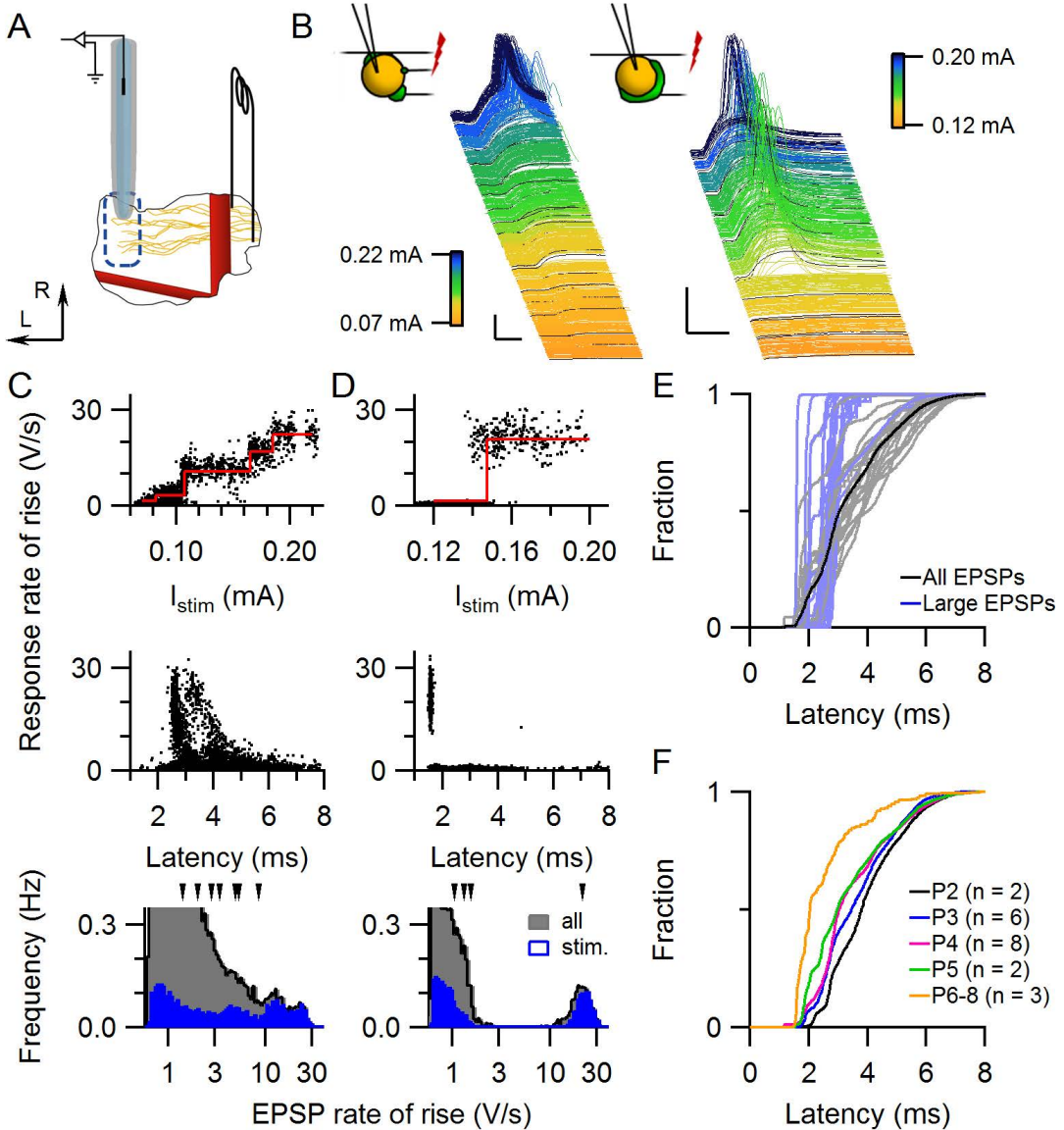
Statistical tests

Linear regression analyses against pup age were performed for the developmental effects. When the developmental effect was significant, the slope of the fit is reported; when not, the average is reported, and subsequently the *F*-statistic with the degrees of freedom, and the *p*-value are reported. Subsequent testing on the same data was Bonferroni-corrected, and is reported as ‘corrected *p*’. Effect sizes of a correlation are reported as Pearson’s *r*. The effect of age on the

Neural Activity During the Formation of A Giant Auditory Synapse

correlation between VGlut cluster and the rate of rise of the strongest input was corrected by including age as an explanatory variable into the regression analysis to first test whether the resulting regression was statistically significant, followed by a post-hoc *t*-test of the slope of the 'age' and 'VGlut cluster'. *P*-values < 0.05 were considered statistically significant.

4



Results

Postsynaptic responses of in vivo-stimulated fibers

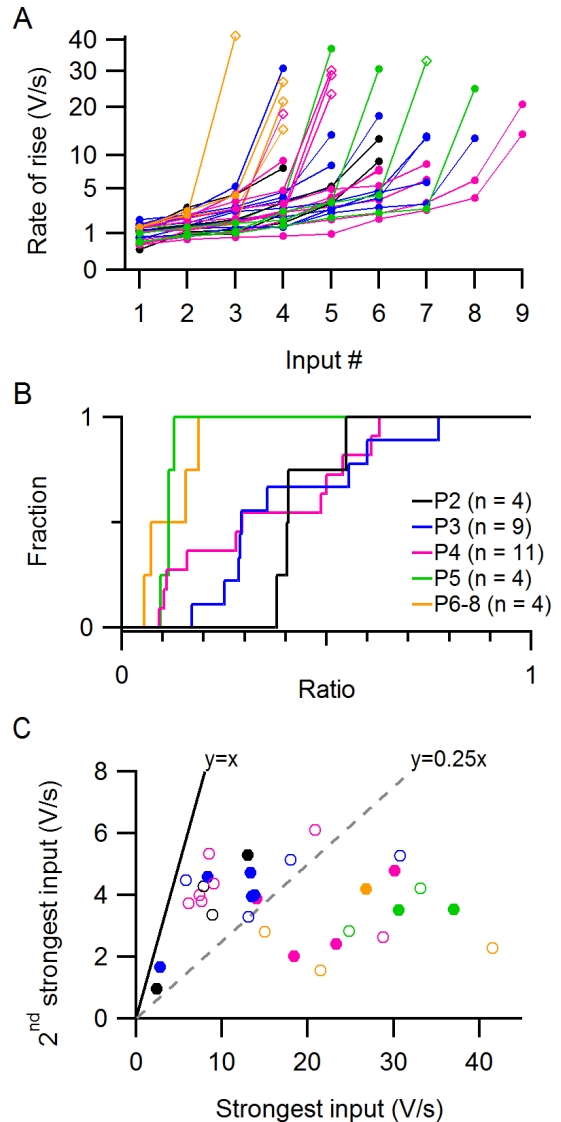
We made *in vivo* whole-cell patch clamp recordings from rat principal neurons in the MNTB around the time the calyx of Held synapse forms [153]. A bipolar stimulation electrode was placed contralaterally from the recording site to activate different axonal inputs based on their activation threshold (see Methods; Figure 4.1A). A field potential could be evoked in the MNTB, which has a stimulation threshold of $83 \pm 19 \mu\text{A}$ (mean \pm SD, $n = 30$ animals, range: 65-140 μA). In a total of 22 cells EPSPs could be evoked and with increasing current stimulation we typically observed either the presence of a large, calyceal-like input, or a more graded increase in EPSP size (Figure 4.1B). In both cases the evoked EPSPs could reach AP threshold ($n = 16$ of 22 cells). To identify the different inputs, we defined jumps in the rates of rise of the evoked responses, as detailed in the Methods, and we will refer to these jumps as inputs. A comparison of the rates of rise of the evoked EPSP with

← **Figure 4.1 Responses to current stimulation of developing calycigenic axons.** (A) Schematic drawing of the experimental approach. A bipolar stimulation electrode straddling the trapezoid body was positioned contralaterally from the recorded MNTB, and whole-cell recordings were made from principal cells of the MNTB. The basilar artery (rostrocaudal, thick red line) and the anterior-inferior cerebellar artery (mediolateral, red line) served as landmarks. Arrows indicate lateral and rostral direction. (B) Waterfall plots of two whole-cell recordings, sorted on stimulation intensity (color-coded). In the P4 example (left) a gradual increase in the evoked EPSP was observed, suggesting the recruitment of multiple inputs, while in the P6 example (right) a single, large EPSP was observed, which elicited a postsynaptic AP. Schematic drawing depicts the assumed synaptic innervation. Scale bars indicate 25 mV and 2 ms. (C) Identification of synaptic inputs. Rates of rise of evoked EPSPs and stimulation intensity (top) or EPSP latency (middle) for the P4 example shown in B. The bottom graph shows the histograms of the rates of rise of evoked and spontaneous EPSPs. Arrow heads on top of the graph indicate the rate of rise of identified inputs. Data points in the top graph were horizontally scatter by $<50 \mu\text{A}$ for visualization. (D) As in C for the P6 example shown in B. (E) Cumulative distribution of latencies of all evoked EPSPs (black) and of large EPSPs ($>10 \text{ V/s}$, blue). Individual cells are shown in light blue and grey. Large EPSPs have a shorter latency than most other EPSPs. (F) The average cumulative distribution of the evoked EPSP latencies grouped by age suggests a developmental increase in propagation speed. Age is colour-coded as shown in the legend. The number of principal cells are reported in the legend.

those of the spontaneously-occurring EPSPs was used as a further check on the accuracy of the identified levels (Figure 4.1C-D). In 8 out of the 22 cells we were unable to activate the cell's strongest input. EPSP subpopulations were found with typical delays of 1-3 and 4-6 ms ($n = 21$ cells; Figure 4.1E), as has been described in slice studies [59, 137, 201]. The large EPSPs always belonged to the subpopulation with shorter delays (1-3 ms; Figure 4.1E). On average the EPSP latencies became smaller during development (Figure 4.1F), suggesting that the different subpopulations might reflect different developmental stages among the calycigenic axons.

4

Figure 4.2 Lack of evidence for competition between strong inputs. (A) For every cell the inputs are incrementally sorted by their average EPSP rate of rise. Diamonds indicate the inputs that were preceded by a prespike. Colors indicate the ages as in B. Note the root scale of ordinate. (B) Cumulative distributions of the ratio of the second strongest and the strongest input for different ages. Legend shows the number of principal cell for each age. (C) The rate of rise of the second strongest input against the strongest. Markers correspond to individual principal cells. Closed markers indicate that both inputs were identified based on spontaneous activity. Line shows identity line and dashed line shows $y=0.25x$. Colors indicate age as in B.



Within this developmental period the principal neuron passes through a stage of exuberant synaptic connectivity [136]. In addition to the 22 cells in which we recorded both evoked and spontaneous EPSPs, in 10 cells we recorded only the spontaneous activity. In total, we identified 180 putative inputs in 32 cells, 5.6 ± 0.3 per cell (mean \pm SEM). By sorting the inputs per cell incrementally based on their mean EPSP rate of rise, a discontinuity between 6-10 V/s is observed, which we used as a threshold to distinguish between weak and strong inputs (Figure 4.2A). To have a measure of synaptic competition we calculated the ratio of the rates of rise of the second strongest and the strongest input (Figure 4.2B). This ratio became smaller during development (-0.07 ± 0.02 /day, $F_{1,30} = 11$, $p = 0.002$). A smaller ratio can signify both an increase of the strongest input rate of rise and a reduction of the second strongest input. We therefore plotted the two against each other (Figure 4.2C). Clearly, the rate of rise of the strongest input increased during development (4.2 ± 1.1 V s⁻¹ day⁻¹, $F_{1,30} = 14$, corrected $p = 0.001$), while the rate of rise of the second strongest did not change (3.7 ± 0.2 V/s, $F_{1,30} = 2.1$, corrected $p = 0.3$). The average rates of rise for inputs identified via stimulation or as spontaneous EPSPs were similar for both the strongest (stim.: 19 ± 3 V/s, $n = 14$; spont.: 16 ± 2 V/s, $n = 18$) and the second strongest input (stim.: 3.9 ± 0.3 V/s, $n = 13$; spont.: 3.6 ± 0.3 V/s, $n = 19$), suggesting that this conclusion did not depend on the identification method. A previous serial EM study identified competing synapses by a ratio of apposed synaptic area (ASA) ≤ 5 [136]. Similarly, we can group the ratio of inputs as competing and non-competing with a ratio of 4 (Figure 4.2C), perfectly separating the rates of rise of P5-8 strongest inputs from the ones of P2. However, the observation that the second strongest input does not change during development is inconsistent the presence of a form of competition between strong synapses in which one connection strengthens at the expense of other connections. We will return to this later, but first we will focus on the properties of strong inputs.

Strong inputs and prespikes

The calyx of Held synapse has been extensively studied in slices [16], but equivalent *in vivo* recordings have not yet been reported. In nine cells we could activate an input associated with an EPSP >10 V/s that could easily be distinguished from the other EPSPs. These inputs could be activated with a

Neural Activity During the Formation of A Giant Auditory Synapse

stimulation current of 0.24 ± 0.05 mA (mean \pm SEM; range 0.12 – 0.40 mA), although the reliability of activation was variable between pups (83 ± 7 % of the stimulations, mean \pm SEM; range 59-100 %). The average latency of the input's EPSP was 2.1 ± 0.1 ms (mean \pm SEM, range 1.6 – 2.5 ms; Figure 4.3C) with little jitter between trials (SD/mean: 2.3 ± 0.4 %, 1.0-3.8 %). Given the distance 500-1000 μ m between the stimulation and recording electrode and a synaptic delay of 0.5 ms, the propagation speed would be on the order of 1 m/s. The AP travel time became less variable with development (jitter vs. age, $r = -0.7$, -0.5 % per day, $F_{1,6} = 6.6$, $p = 0.04$). In addition, a developmental decrease in latency ($r = -0.5$, -0.12 ms/day) suggests an increase in conduction speed. This increase is likely underestimated as we positioned the stimulation electrode as contralaterally as was permitted by the cranial window to be able to separate the stimulus artefact from the responses. These developmental changes will help to enable the precise timing of the calyx of Held in adult, hearing animals.

The calyx of Held-synapse can typically be identified in the postsynaptic recording by the presence of a prespike, a small deflection preceding the large EPSPs [19, 20, 134]. Prespikes can already be detected in the first postnatal week [153, 155]. We therefore checked every strong input for the presence of a prespike (Figure 4.3A). In four of four cells P5-8, six of nine cells of P4-5, and in none of six P2-3 cells the large EPSP was preceded by a prespike (Figure 4.3B). Hence, the presence of the prespike before a large EPSP was more likely at older ages ($r = 0.7$); fit with a logistic function ($SS_{\text{expl}} = 51$ %) yielded a mid-point of 3.8 ± 0.2 days postnatally (mean \pm SD) and a steepness of 0.3 ± 0.3 days, suggesting that within a day most strong inputs switch from not associated to being associated with a prespike.

The strong inputs with and without a prespike were not remarkably different. The EPSPs of strong inputs in the newborn animals had an average rate of rise of 23 ± 2 V/s (mean \pm SEM; range 13-42 V/s), but with a high variability of 24 ± 4 % (mean CV \pm SEM; range 7-38 %). The EPSP amplitude was 18 ± 1 mV (mean \pm SEM; range 12-25 mV), but this is an underestimation as the EPSP of the strong input typically triggered an AP (74 ± 12 %, mean \pm SEM; range 11-100 %) which obscured the EPSP peak. For all but one feature of the strong inputs, differences in the strong inputs were better explained by the postnatal age of the pup

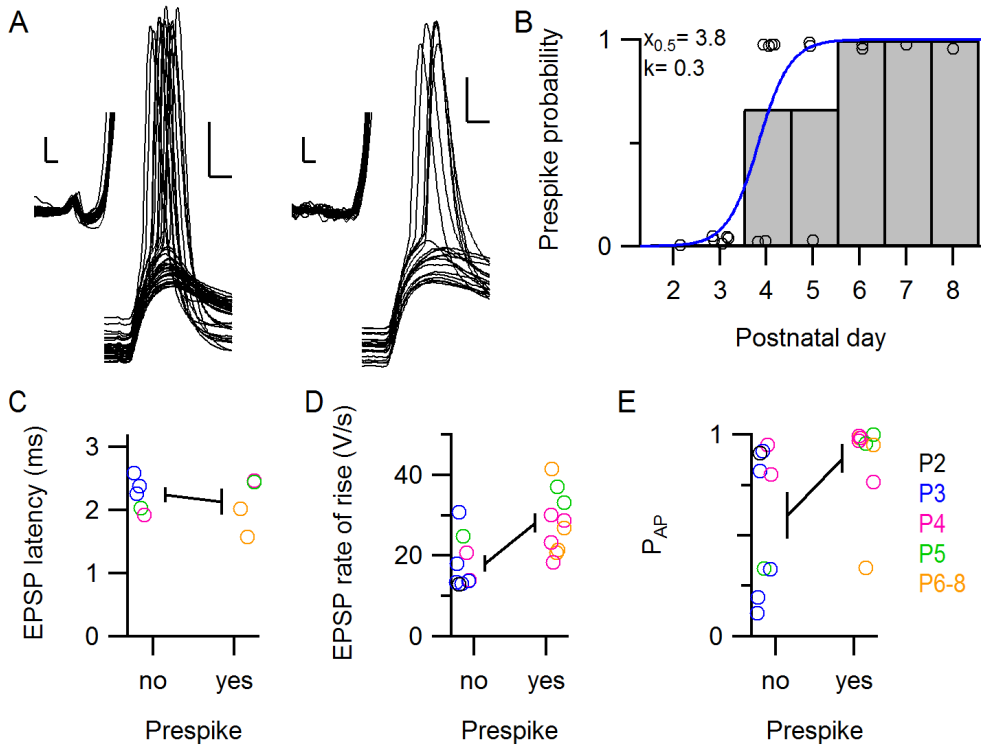


Figure 4.3 Comparison of strong inputs with and without prespikes. (A)

Large EPSPs of a strong input with (left; P6) and of a strong input without (right; P5) a prespike. EPSPs were aligned on their onset. The insets show the same traces with their V_m offsets subtracted. Scale bars indicate 10 mV and 1 ms, and scale bars in the inset indicate 0.5 mV and 0.2 ms. (B) Developmental changes in the presence of a prespike preceding a large EPSP. Circles indicate cells where a large EPSP was recorded. Bars represent age average. Blue line represents the fit of the logistic function with the values reported in the graph. (C-E) Comparison of strong inputs with or without a prespike. In C only evoked large EPSPs were analyzed. Circles indicate individual cells. Line represents the average and SEM.

than by the presence of the prespike, indicating that prespike-related strong inputs shared many properties with the other strong inputs (Figure 4.3C-D). The exception was the reliability of to trigger a postsynaptic action potential ($r = 0.4$ vs 0.1 for age and prespike; Figure 4.3E), but given the small number of observations it remains to be seen whether this is a real difference. While the prespike signals the calyx of Held, it is surprising that strong inputs without a prespike were so comparable to the prespike-associated strong inputs. Do these strong inputs arise from a calyx of Held synapse that does not generate a prespike? We therefore next investigated the structural presence of a calyx of Held as detailed in the next section.

The active zone protein Piccolo in the neonatal auditory brainstem

The synaptic innervation of principal cells undergoes a dramatic change within the first postnatal week in rodents, from small *en passant* boutons to a giant axosomatic terminal. While VGLuT labeling reliably labels the presynaptic terminals throughout the developmental period [90], it does

4

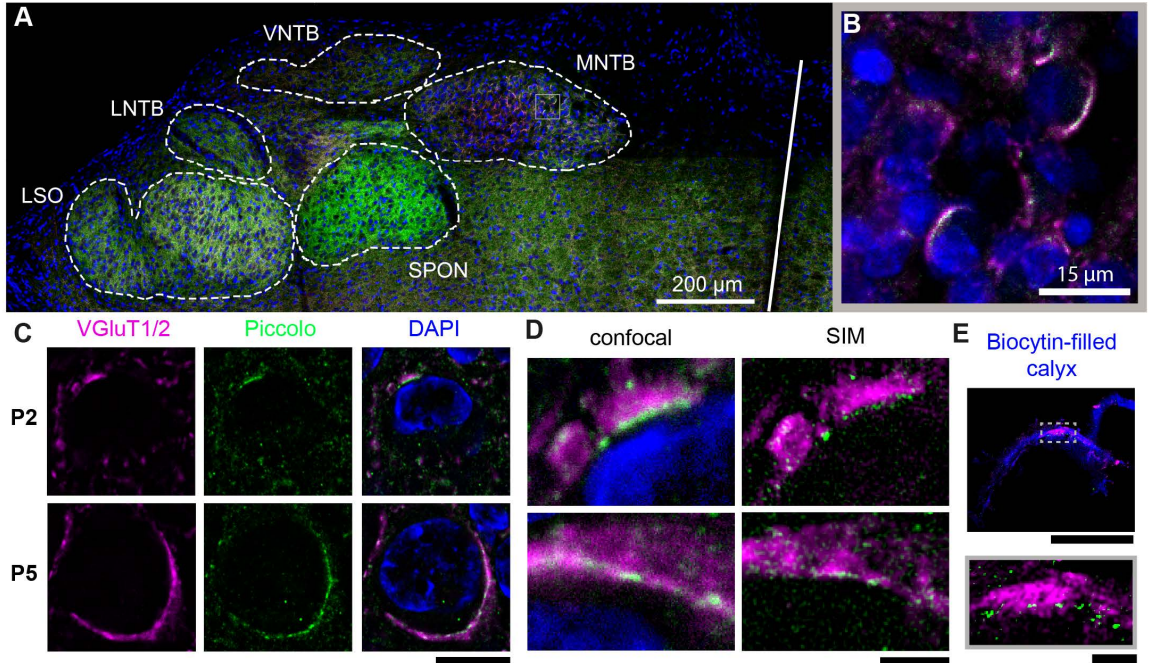


Figure 4.4 Developmental expression of Piccolo in the MNTB.

(A) Fluorescent labeling of Piccolo (green), VGLuT (magenta) and DAPI (blue) in the SOC of a P4 rat. Midline is indicated with a white line. Auditory nuclei are delineated with dashed lines. (B) Higher magnification of the grey box in A showing principal cells of the MNTB with large perisomatic clusters of VGLuT and Piccolo. (C) A P2 and P5 principal cell with fluorescent labeling of VGLuT, Piccolo, and VGLuT + Piccolo + DAPI with confocal microscopy. (D) Comparison of confocal microscopy and structured-illumination microscopy (SIM) of perisomatic clusters of Piccolo and VGLuT of the P2 principal cell shown in C (top), and of the P5 principal cell shown in C (bottom). (E) SIM image of a P5 biocytin-filled calyx (top, blue) with VGLuT and Piccolo, and revealed active zone-like structures in the Piccolo labeling (bottom). Non-calyceal labeling was masked. Scale bars indicate 200 μm in A, 15 μm in B, 10 μm in C, 2 μm in D, and 10 and 1 μm in E. Images in C and D were background-subtracted. Abbreviations: LSO, lateral superior olive; MNTB, medial nucleus of the trapezoid body; P, postnatal; SIM, structured-illumination microscopy; SOC, superior olivary complex; SPON, superior periolivary nucleus; VGLuT, vesicular glutamate transporter 1 and 2; VNTB, ventral nucleus of the trapezoid body.

not indicate release sites. We therefore tested whether Piccolo could be used to visualize the release face of terminals within this developmental period. Already at P₃₋₄ Piccolo labeling was found throughout the superior olivary complex (SOC) in all auditory nuclei ($n = 8$ rats; Figure 4.4A). Although the labeling was not particularly strong in the MNTB, it clearly co-labeled large perisomatic structures with VGluT (Figure 4.4B). Even at P₂ the Piccolo labeling could delineate an edge of the larger VGluT-clusters (Figure 4.4C, $n = 2$ of 5 P₂ animals). Piccolo puncta were also found outside the somatic regions of the MNTB, and occasionally a Piccolo punctum was found in the soma of the principal cells (Figure 4.4C). Generally, the Piccolo edges appeared to be composed of individual spots which were close to diffraction-limit (Figure 4.4C-D). We turned to structured-illumination microscopy [245], which revealed that Piccolo clusters in the confocal microscopy were indeed composed of multiple spots (Figure 4.4D). These spots were also found in biocytin-filled calyces, indicating that Piccolo is present in the active zones of the calyx of Held at P₅ ($n = 11$ of 12 calyces; Figure 4.4E). Piccolo thus identifies the release face of synapses and thereby helps to identify the target of VGluT-positive structures, especially for the axosomatic terminals for which the shape of the soma can be inferred (Figure 4.4C-D). However, terminals on dendrites could not be related to the correct postsynaptic neuron in the absence of a good postsynaptic marker.

Structure-function relation of the neonatal calyx of Held synapse

From the 32 recorded cells we recovered 20 cells with immunolabeling. In these 20 cells we compared the presence of prespikes and strong inputs with the somatic VGluT clusters. The VGluT clusters were divided in three groups: small puncta, medium-size clusters covering less than 20% of the somatic area, and large clusters covering more than 20% (Figure 4.5A). This threshold corresponds to lower values reported for calyceal endings in neonatal mice [137], and is half or even less than half of the coverage found for older calyces [101, 239]. Every recovered cell was assigned to one of these categories. As expected, large VGluT clusters were more often observed at the older ages (Figure 4.5B). Moreover, the VGluT category assignment correlated with the rate of rise of the strongest input ($r = 0.7$; Figure 4.5C). This correlation remained significant when we statistically correct for age (cluster difference: 5.9 ± 1.8 V/s, $t_{17} = 3.3$, corrected

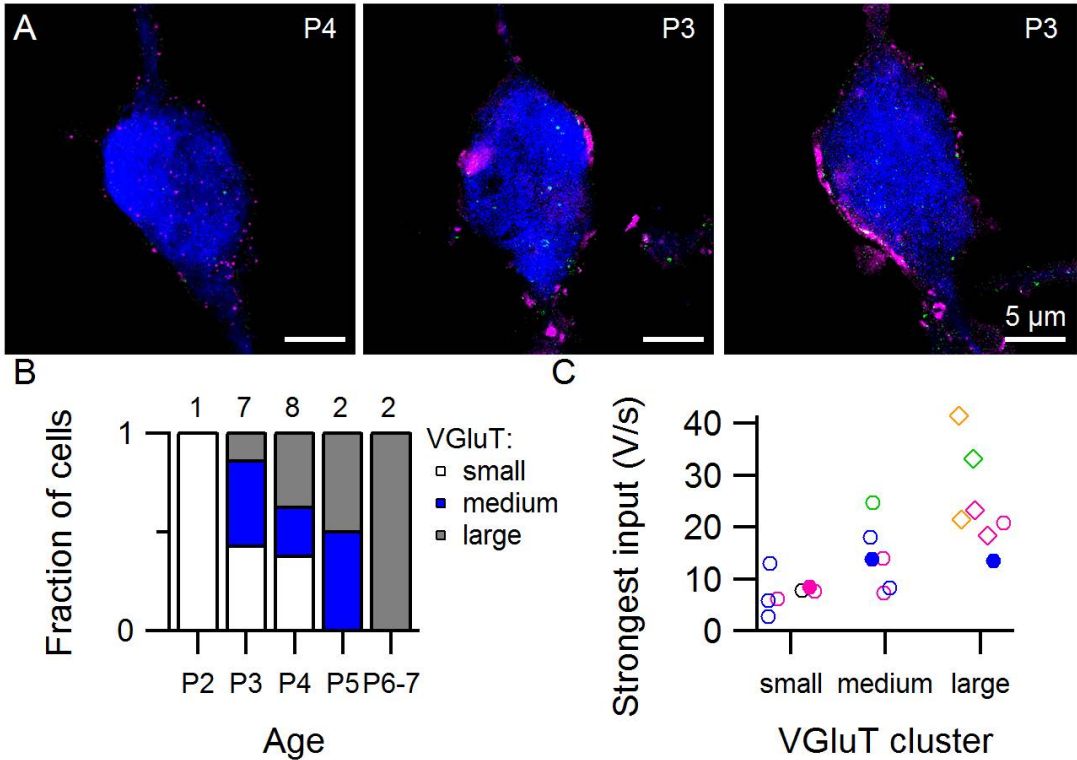


Figure 4.5 Synaptic morphology correlates with *in vivo* responses. (A) Three principal somata immunolabeled for biocytin (blue), VGluT (magenta) and Piccolo (green). From left to right the examples represent the category with ‘small’ clusters, ‘medium’ clusters and a ‘large’ cluster, respectively. Surrounding labeling is masked for visualization. (B) Relative frequency of cells belonging to VGluT categories during development. Numbers on top indicate numbers of cells per group. (C) Structure-function correlation of the strongest input and the VGluT category of the cell. Colors indicate age as in previous figures. Diamonds indicate the cells with a prespike, and closed markers correspond to the examples illustrated in A.

$p = 0.005$; age effect: $4.2 \pm 1.5 \text{ V s}^{-1} \text{ day}^{-1}$, $t_{17} = 2.8$, corrected $p = 0.01$). There is a developmental increase in the rate of rise of the strongest input over and above the increase in VGluT cluster type. The VGluT category was a good indicator of synaptic strength of the strongest input, but additional factors must also play an important role, since inputs with a rate of rise of $\sim 13 \text{ V/s}$ could be found within all three VGluT categories (Figure 4.5C).

The presence of a prespike clearly depends on the size of the synapse, since prespikes were never observed for small or medium VGluT clusters ($n = 0$ of 13 cells; Figure 4.5C). Only terminals with large VGluT clusters gave rise to

a prespike ($n = 5$ of 7 cells), but we also observed two cells in P₃₋₄ animals with a large terminal and they lacked a measurable prespike. Both terminals clearly covered a significant area on the postsynaptic neuron and therefore undoubtedly belonged to the ‘large’ category (see right panel of Figure 4.5A for the P₃ example). As the two synapses were also the youngest in the large VGluT category (P₃ and P₄ against 2 P₄, 1 P₅, 1 P₆ and 1 P₇), the lack of a prespike might be related to the immaturity of the presynaptic terminal. These anecdotal observations show that the absence of a prespike does not mean the absence of a large terminal.

Discussion

In this study we combined *in vivo* electrophysiology with immunolabeling of the developing calyx of Held synapse. With electrical stimulation we were able to identify multiple inputs of a single principal neuron. Typically, increasing stimulation levels showed either a graded increase or a single, large jump in the response rate of rise. The strongest inputs showed overall a shorter latency. Within a cell, the strongest input was typically more than twice as strong as the other ones, and this difference increased during development, with little change in the second strongest input. We found that the presence of a prespike becomes more likely during development, but that otherwise strong inputs with and without a prespike are similar. We showed that in the first postnatal week Piccolo is present in the SOC and in the neonatal calyceal terminals, which aided in identifying the postsynaptic target of a terminal. VGluT/Piccolo clusters were found perisomatically and the size of the VGluT cluster correlated with the strength of the strongest input *in vivo*. Neurons with a prespike had a large VGluT-cluster, but the reverse was not necessarily true.

Limitations

To identify inputs we used their minimal activation threshold, their latency and the distribution of spontaneous EPSP sizes. On average, we identified 5.6 inputs per cell. For comparison, prior to synaptic elimination 5-12 axons connect to a principal neuron in EM studies [137]. The maximal stimulation current that could be used to activate afferent axons was limited by the threshold for direct postsynaptic activation, as this obscured any synaptic inputs. This

could still happen even though we used bipolar stimulation electrodes, placed contralaterally from the recorded neuron. Preferably, the stimulation electrode is placed at the midline where all calycigenic axons converge ventrally. However, to avoid postsynaptic activation we placed the stimulation electrode more laterally. This location may have led to preferential activation of the axon bundles that run ventrally from the other MNTB [55]. Based on the comparison of spontaneous and evoked activity, in 8 out of 22 cells we were unable to activate the cell's strongest input. As we were able to distinguish with the stimulation 80 synapses (both large and small) in these 22 cells, at least 1 in 10 axons (8 out of 80), but probably more on the order of one in three axons (8 out of 22) was not activated. Spontaneous activity partially negated this problem, but may have introduced a bias towards the most active synapses. To what extent synaptic inputs of the principal neuron are active in every spontaneous activity burst is unknown, but anecdotal evidence showed extensive co-occurrence of two distinct, large inputs during spontaneous bursts [153]. Altogether, we believe to have identified most synaptic inputs except for some smaller inputs.

Our method of characterizing EPSP populations in the spontaneous EPSPs has some limitations. We used the presence of a clear peak in the histogram to indicate the presence of an input. However, these peaks were generally distinguishable only for the larger EPSPs. Any input giving rise to an EPSP smaller than 2 V/s will merge in the histogram with the large bulk of small EPSPs. Nonetheless, the rates of rise of the strongest and second strongest input were very similar with either method.

Efforts to further subdivide the population of large EPSPs were unsuccessful. We tested whether the strong inputs could be further subdivided based on the presence of inter-event intervals that were shorter than the refractory period or the silent period within minibursts [153], but this also did not lead to the identification of additional connections.

Prespikes

We obtained anecdotal evidence that large terminals do not necessarily generate a measurable prespike. In this study we recorded from a P₃ and a P₄ principal cell that showed morphological evidence of a substantial axosomatic terminal, but had no measurable prespike in the whole-cell current-clamp recording. We cannot exclude that a small prespike would have been measurable in these cells in a voltage clamp recording, as this would avoid the filtering by the resting membrane time constant of the postsynaptic cell. In a previous study we observed three cells with two strong inputs, in each case one with and one without a prespike [153]. We do not exclude the possibility that one of the inputs may have been dendritic.

The prespike is a hallmark for the mature calyx of Held synapse. In *in vivo* juxtacellular (loose-patch) recordings, the characteristic complex waveform, which includes both a prespike and the postsynaptic response, has been used as evidence that the location of the recording site was in the MNTB [74, 133, 134, 153, 155, 183, 247]; in these recordings the prespike is thought to reflect the extracellular potential generated by the calyceal membrane currents during the presynaptic AP [134]. In postsynaptic whole-cell recordings these currents can be picked up as well [20]. They consist of capacitive currents, which will scale with the first derivative of the membrane potential and the calyceal area, and resistive currents, which depend on density and distribution of calyceal ion channels. The presence of the prespike thus reflects the somatic location, proximity and large apposition surface area (ASA) of the calyx, the large capacitive currents associated with the rapid calyceal AP, and the lack of large phase differences of presynaptic membrane currents along the release face.

We observed a rapid developmental switch in the association of strong inputs with the presence of a prespike. This switch might thus be explained by an increase in ASA [136, 137] and by an increase in the size or isochronism of appositional membrane currents. The size of the presynaptic capacitive currents will increase as a result of the developmental acceleration of the calyceal AP ([156] and CHAPTER 2). Whereas after the second postnatal week the sodium channels in the calyx of Held will be concentrated at the heminode [159, 162],

they are probably still present at the release face shortly after calyx formation (CHAPTER 2), which may have profound effects on the expected size of the postsynaptically recorded prespike. Finally, the relative size of the admittance of the postsynaptic membrane facing the synaptic cleft compared to that of other nearby membranes and of the synaptic cleft itself is also important. Changes in the size, isochronism, or coupling of presynaptic membrane currents during this developmental period should thus underlie the rapid developmental emergence of the prespike. Our current data do not allow a strong conclusion with regard to the underlying mechanism underlying the switch, even though our observation that some large terminals did not elicit a measurable prespike and our observation that large inputs with and without a prespike had similar properties argues against a simple change in size or isochronism as the main underlying factor.

Developmental innervation of the MNTB

The prevalence of multiple calyces on a single principal neuron has been a subject of debate. In slice recordings multiple large inputs have been observed [60, 137, 138]. EM reconstructions gave structural evidence for the presence of multiple large terminals [136, 137], as well as a study with BrainBow-type mice imaging entire MNTBs [249]. Half of the principal neurons were contacted at some time point during development by multiple large terminals [136], and a small group of MNTB neurons (~10 %) may be persistently innervated by multiple calyces [136, 249]. This is surprising as in the manifold *in vivo* studies of the MNTB none has reported on this subpopulation (summarized in Table 4.1).

How can one identify multiple calyces in electrophysiological recordings? The most apparent possibility is the presence of two types of prespikes in the same principal cell. As already discussed, this was not observed. A second possibility is when a prespike or a strong input does not obey the refractory period of globular bushy cells [153, 247]. This method can be used by stimulation via two electrodes [247], or by using the spontaneous activity *in vivo* [153]. As discussed, this method did not reveal a second strong input. A third possibility is that *in vivo* the sound-evoked responses of a principal neuron are more likely related to two than a single globular bushy cell. With this method different complex waveforms have

been distinguished in a single recording [247]. To our knowledge, this method has not yet been applied to identify multiple calyceal synapses. One caveat is that none of these experiments were designed to identify multiple calyces, and therefore the subpopulation of principal cells might have been ignored or perhaps excluded as abnormal. Still, given the large body of published work on *in vivo* electrophysiology of the rodent MNTB (>25 papers), it seems unlikely that so many studies overlooked, ignored or missed 10% of the principal neurons. Although the number of cells in this paper is low, within this developmental period many principal cells are supposed to be contacted by multiple calyces [136], and we estimate that 3-10 of these cells should have been contacted by multiple calyces, whereas we did not observe convincing evidence for this in our recordings.

How, then, to resolve this discrepancy? There may be a species difference between rats and mice, as the presence of multiple large synapses seem to be more likely in mice (Table 4.1), but none of the *in vivo* studies with adult mice reported any evidence for the presence of multiple strong inputs. A recent study identified in mice calyceal-like terminals in the MNTB that originated from the glycinergic VNTB [250] which likely underlie the strong inhibitory inputs to the principal neuron observed after hearing onset [251, 252]. The morphological development of these terminals has not been studied. A third possibility is a dissociation between terminal size and postsynaptic impact, where a large terminal generates a small EPSP. Structurally, Rodríguez-Contreras *et al.* [90] found that the terminals formed quicker than that they became filled with vesicles. Then, based on the work presented in this chapter, these large terminals would give rise to an EPSP of 2-6 V/s which does not independently trigger *in vivo* a postsynaptic AP. However, we found a clear correlation between the size of the VGluT cluster and synaptic strength, and even as the accumulation of VGluT in the terminal is protracted over multiple days [90], this would not explain why multiple calyceal innervation is neither observed at later ages [92] nor found in our within-cell analysis. For now, our results suggest that if multiple large calyces are formed on individual principal cells during development, then they are rare or very weak.

One last possibility is that 'silent' calyces exists. We call them silent as they are not revealed in our recordings of spontaneous activity. Silent calyces have to be labeled by VGluT as they do contain synaptic vesicles [136, 137], but perhaps only sparsely as they are not identified in our labeling. However, they might be activated with current stimulation in slices, and hence identified in these studies [137, 138, 253]. Silent calyces might be identifiable by genetic techniques, such as GFP reconstitution across synaptic partners [254], but it is uncertain to what extent less active synapses would be labeled, and would also need additional technical development to allow the deployment with the electrophysiological approach taken here. Probably a more straightforward approach would be to combine *in vivo* recordings with ultrastructural reconstruction of the recorded principal neurons and all its inputs.

Synaptic competition for mono-innervation

During the formation of the calyx of Held the strongest input increased in strength, while the second strongest input was stable. A similar increase in strength during their development has been observed for other synapses. Before the mono-innervation was established for the neuromuscular junction (NMJ), a single input became >4 fold stronger than the other inputs [255]. This was due to both an increase in strength of the strongest input and a decrease in the other(s) [255]. For the climbing fiber (CF) synapse of the cerebellar Purkinje cell (PC), a fourfold strengthening of the strongest input was observed [256] while other inputs remained constant [257]. Subsequently, one of the immature CFs is allowed to translocate from the soma to the apical dendrite [258, 259], which ends the competition [260]. We found that the ratio of the second strongest input and the strongest input reduced between P2 to P5-8. A ratio of 4 separated the principal neurons at the beginning of calyx formation (P2) from principal cells at later ages where the calyx is formed. This is consistent with a model where initially similar inputs compete for the principal neuron with a single winner input increasing in strength.

The type of competition might be very different between these synapses; the NMJ competes at and for a small patch of the muscle membrane [261, 262], while CFs compete at the soma for the apical dendrite [259]. This means that the expansion of one NMJ necessarily involves the shrinkage of another as

is reflected in the change of NMJ strength. Similarly, multiple calyces might compete for the limited somatic area [136, 137], but the observation that the second strongest input remained stable does not agree with an NMJ-type of competition, where the increase of the largest input occurs at the expense of others. It has been suggested for the calyx of Held that once it forms, it stays [92], similar to the CF synapse. From EM studies of the calyx development, a very different picture emerged [136, 137] which suggested a development with dynamics more like the NMJ. However, persistent multi-innervation of skeletal muscles or Purkinje cells are rare phenomena (NMJ: [263]; PC: [260]). For these two synapses live imaging of the competition *in vivo* has answered many questions concerning the progress of their synapse formation [260, 263, 264]. Future research may reveal the *in vivo* dynamics of calyx formation and suggests whether its formation is more like the CF, more like the NMJ, or wholly different altogether..

Acknowledgments: We are very grateful for the help of Elize Haasdijk and Celina Glimmerveen, who performed the immunolabeling. We thank Marcel van der Heijden, Peter Bremen and Aaron Wong for advice on the analyses.

Table 4.1 Evidence for and against the presence of multiple calyceal innervation. I mainly focused on the published work involving *in vivo* electrophysiology of the MNTB. In addition, there is a large body of literature on slice electrophysiology of the MNTB which was not included. We are not aware of any references to multiple calyces in these studies besides the ones listed in the table.

	Reference	species	strain	age	Type of experiment	Multiple calyces
[138]	Bergsman et al. 2004	mouse	multiple	P7-12	Slice ephys	7 in 101
[92]	Rodríguez-Contreras et al. 2006	rat	Wistar	P4-18	Slice tracing	1 in 86
[137]	Hoffpauir et al. 2006	mouse	FVB/NJ	P0-4	Slice ephys	4 in 29
[137]	Hoffpauir et al. 2006	mouse	FVB/NJ	P0-4	EM	2 in 19
[136]	Holcomb et al. 2013	mouse	FVB/NJ	P2-9	EM	31 in 164
	Thesis Matho and Livet	mouse	Thy1-Brainbow1.oL / CAGGS-CreERTM	P10-60	confocal	10 % (in >1000)
[252]	Xiao et al. 2013	mouse	BMPRIa/1b DKO	P1-16	Slice ephys	nr
[252]	Xiao et al. 2013	mouse	BMPRIa/1b DKO	P8	EM	2 in 4
[153]	Sierksma et al. 2017	rat	Wistar	P2-5	<i>In vivo</i> ephys	3 in 132
[133]	Guinan and Li 1990	cat	-	adult	<i>In vivo</i> ephys	0 in n.r.
[265]	Sommer et al. 1993	rat	Sprague-Dawley	adult	<i>In vivo</i> ephys	0 in 6
[266]	Tsuchitani 1997	cat	-	adult	<i>In vivo</i> ephys	0 in 40
[267]	Smith et al. 1998	cat	-	y. adults	<i>In vivo</i> ephys	0 in 37
[268]	Kopp-Scheinpflug et al. 2003	gerbil	-	3-6 mo	<i>In vivo</i> ephys	0 in 146
[269]	Kopp-Scheinpflug et al. 2003	mouse	<i>kcnai</i> -null	3-4 we	<i>In vivo</i> ephys	0 in 47
[270]	Green and Sanes (2005)	gerbil	-	P15-19, adults	<i>In vivo</i> ephys	0 in 331
[271]	Tolnai et al. 2008a	rat	multiple	adult	<i>In vivo</i> ephys	0 in 64
[272]	Tolnai et al. 2008b	gerbil	-	2-4 mo	<i>In vivo</i> ephys	0 in 149

4. Multi-innervation at the MNTB

	Reference	species	strain	age	Type of experiment	Multiple calyces
[247]	McLaughlin et al. 2008	cat	-	adult	In vivo ephys	0 in 49
[273]	Kadner and Berrebi (2008)	rat	Sprague-Dawley	adult	In vivo ephys	0 in 19
[274]	Kopp-Scheinflug et al. 2008a	gerbil, mouse, rat	C ₃ HeB/FeJ, Long Evans	adult	In vivo ephys	0 in 186
[275]	Kopp-Scheinflug et al. 2008b	gerbil	-	3-6 mo	In vivo ephys	0 in 33
[276]	Steinert et al. 2008	mouse	C ₃ HeB/FeJ	P17-70	In vivo ephys	0 in n.r.
[277]	Tolnai et al. 2009	gerbil	-	adult	In vivo ephys	0 in 122
[134]	Lorteije et al. 2009	mouse	C57BL/6	4-5 we	In vivo ephys	0 in 24
[183]	Sonntag et al. 2009	mouse	CBA/J and C57BL/6J	P8-28	In vivo ephys	0 in 289
[278]	Englitz et al. 2009	gerbil	-	2-4 mo	In vivo ephys	0 in 177
[74]	Tritsch et al. 2010	rat	Wistar	P4-8	In vivo ephys	0 in 34
[279]	Lorteije et al. 2011	mouse	C57BL/6	4-5 we	In vivo ephys	0 in 18
[155]	Crins et al. 2011	rat	Wistar	P4-29	In vivo ephys	0 in 37
[280]	Sonntag et al. 2011	mouse	CBA/J and C57BL/6J	P8-14, P23, P28	In vivo ephys	0 in 42
[281]	Wang et al. 2013	mouse	C57BL/6	5-9 we	In vivo ephys	0 in 21
[282]	Di Guilmi et al. (2014)	mouse	mixed	4-7 we	In vivo ephys	0 in 29
[283]	Koka et al. (2014)	cat	-	Adult	In vivo ephys	0 in 103
[284]	Wang et al. 2015	mouse	Mutants on C57BL/6	4-9 we	In vivo ephys	0 in 107
[284]	Wang et al. 2015	mouse	mutants on C57BL/6	4-12 we	Confocal	0 in 100
[285]	Blosa et al. 2015	mouse	mutants on C57BL/6	3-5 we	In vivo ephys	0 in 55
[286]	Gao and Berrebi (2016)	rat	Sprague-Dawley	2-3 mo	In vivo ephys	0 in 54
[287]	Stange-Marten et al. 2017	gerbil, mouse	CBA/Ca	2-5 we	In vivo ephys	0 in 27

General Discussion

CHAPTER 5

Martijn C. Sierksma

The primary focus of this thesis is the electrophysiological development of the rat medial nucleus of the trapezoid body (MNTB) *in vivo*. In the GENERAL INTRODUCTION I discussed the possible relevance of neural activity in the development of brain circuitry and the limited knowledge we have for the role of neural activity in the auditory brainstem.

In CHAPTER 2 I described the presynaptic activity of the calyceal terminals within the period of calyceal formation. Neural spiking occurred at very high frequencies with minimal spike depression, and this suggested a mechanism that conserves action potential (AP) shape during extreme conditions. This mechanism very likely relates to the sodium channel's fast recovery from inactivation and the membrane potential attained after the AP.

In CHAPTER 3 we focused on the postsynaptic development and found a clear correlation between the size of the largest excitatory input and the postsynaptic excitability. As the calyx of Held-synapse becomes a relay synapse we compared the postsynaptic activity with the presynaptic activity. While the calyceal terminals were already firing at high frequencies, postsynaptic activity did not reliably follow the presynaptic AP until postnatal day (P)5. These developmental changes were related to a transition in how the AP threshold was reached; that was by summation of smaller excitatory postsynaptic potentials (EPSPs) at P2 versus a single, large EPSP at P5. By modeling the different properties of the principal neuron, we found that the low-threshold potassium channels were pivotal in this switch as the developmental increase in low-threshold potassium channels restricts firing to large, fast-depolarizing EPSPs.

In CHAPTER 4 the main topic was the multi-innervation of single principal cells of the MNTB. Within the formation period of the calyx of Held, the strongest input of principal cells was strengthened while the second strongest input was neither strengthened nor weakened. Within a day (P3-4) strong inputs became associated with a prespike. Prespike-associated strong inputs were, however, not very different from other strong inputs. Piccolo was already present in calyces at P5. Together with vesicular glutamate transporters (VGluT), Piccolo might be a presynaptic marker for the developing calyx of Held synapses. For a subset of cells I recorded from *in vivo*, the strength of the strongest input was related to the presence of large axosomatic terminals. A clear correlation was found

with the strongest input of single principal cells and their individual terminals. Moreover, the prespike-associated inputs were only recorded from cells with a large terminal. For the converse, two exceptions were reported of principal cells with a large terminal, but no input with a prespike.

In this chapter I compare the main findings in this thesis with the existing literature, which generally took an *ex vivo* approach. I discuss some requisite properties of neurons and terminals to firing at very high frequencies with a special emphasis on the after-potential of the calyx of Held. I revisit the role of developmental activity in circuitry refinement and compare the auditory system to other well-studied systems. I will suggest common motifs in the development of very distinct synapses, and speculate on the role of neural activity and the role of cooperation instead of competition of axonal projections in the formation of topological circuits. But first, I will consider some methodological limitations of the previous three chapters.

Technical considerations

Use of anesthesia

In our experimental design, the rat pup was anesthetized with isoflurane suspended in medical oxygen. Although it seems inevitable that a main effect of anesthesia will be on neural processes, we have not extensively investigated the impact of anesthesia on the principal cells, calyces, its upstream centers, nor on developmental processes. We did reduce the isoflurane concentration after surgery to a level that still kept the animal nonreflexive to a paw pinch (SOP for surgery) during the experimental recordings (or higher when reported otherwise). In general, this led to a 50 % reduction of the isoflurane concentration after surgery (0.7-1.2 % isoflurane in 3-4 L/min of medical oxygen). Others have studied the impact of isoflurane in slice preparations. Wu *et al.* [288] found that isoflurane reduced neurotransmitter release with an IC₅₀ of 0.35 mM (equivalent to 1.5 %) by a small reduction of the action potential amplitude of the calyx of Held [289]. Isoflurane also inhibits potassium channels, and in particular K_{v3}, but at 0.35 mM this effect is very small [290]. Isoflurane might activate two-pore potassium channels [291]. The experiments of Wu *et al.* [288] were performed at room temperature and this might change the anesthetic

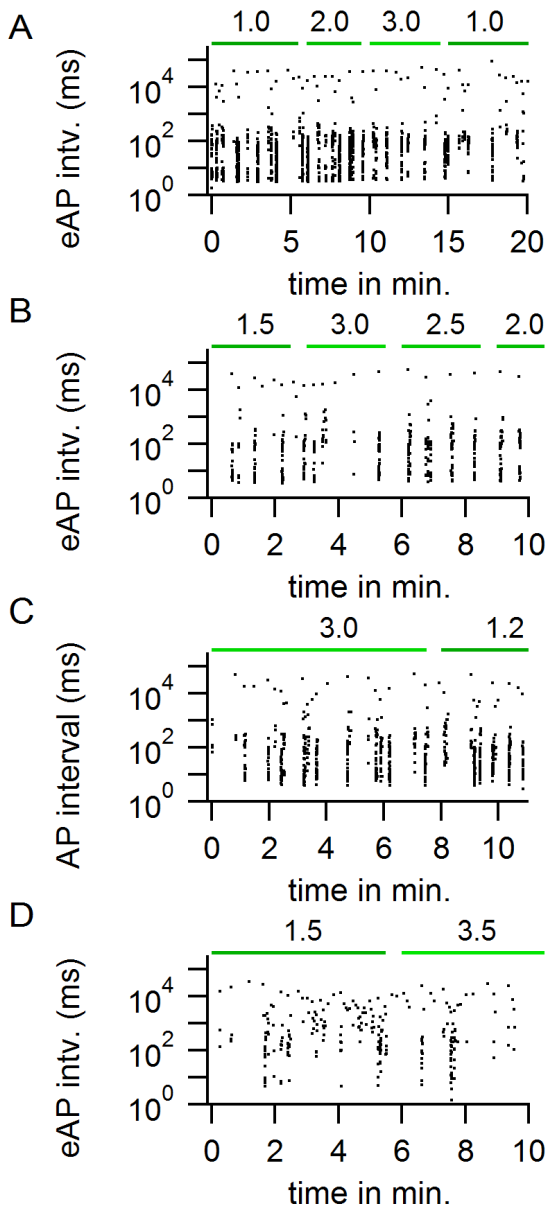


Figure 5.1 Neural activity in the MNTB in the presence of different levels of isoflurane. (A) AP intervals over time in a juxtacellular recording of a P8 calyx, (B) a P5 calyx, (C) in a whole-cell recording of a P3 principal cell, and (D) a juxtacellular recording of a P4 principal cell. The numbers at the top of the graph indicate the isoflurane concentration in percentages of the ventilation mixture during the period indicated by the green bars.

5

effects [288]. In general, isoflurane reduces glutamatergic neurotransmission [292-295]. In our pilot experiments we did not observe any obvious changes in the firing patterns of calyces or principal cells when we varied the isoflurane concentrations in the pup's ventilation mix (Figure 5.1). Based on our experience the effects of isoflurane on the pup behavior at the start of the surgery are visible within a minute. We therefore believe that the anesthesia had a minimal impact on neurotransmission at the level of calyx of Held synapse.

More uncertain is the impact of long-term exposure of isoflurane. During the 1-2 hours surgery the animal was kept at 2.5-2.0 % isoflurane, followed by 30-60 min period of recovery at 1.5 % isoflurane. Then, experiments were started and anesthesia was set to a level (0.7-1.5 %) that suppressed the animal's reflexes. In Figure 5.1 it seems that a brief period of higher anesthesia does not change the firing patterns, but we do not know what the impact is of the pre-experimental isoflurane levels. The post-surgery recovering period was included to negate these build-up effects, but this was not directly tested. Nevertheless, the activity generated by the cochlea seems to be transmitted to the MNTB, has similar properties as in cochlear slice preparations [74] and as *in vivo* experiments of older rodents using either ketamine-xylazine [183] or isoflurane as anesthesia [155]. We therefore believe that the anesthesia had only a small effect on synaptic transmission at the level of the MNTB. These effects might accumulate at later stages of the auditory system, possibly leading to significant effects on neocortical neurotransmission [296]. However, between the cochlea and the MNTB transmission occurs via giant synapses that are able to reliably trigger a postsynaptic AP even when their strength would be slightly reduced by anesthesia. Nonetheless, our observations of the effects of anesthesia are limited and some subtle effects may have been missed.

In vivo electrophysiology

The advent of patch-clamp electrophysiology in the eighties [297] established whole-cell recordings as a classical method in neuroscience, resulting in a significant expansion of our understanding of single-cell electrical activity and the underlying conductances. Although the technique was primarily developed for *in vitro* approaches, it became quickly applied to cells in living organisms as well [298-301], and has even been automated [302]. Nevertheless, this technique has methodological challenges and limitations when applied *in vivo*. The main limitations arise from the high series resistance and high, distributed stray capacitance compared to *in vitro* applications, leading to a low-pass filtering of the recordings. This filtering most clearly affects fast electrical fluctuations such as the AP and large postsynaptic currents and potentials, which have been the main focus in the previous chapters.

APs can be very fast in the auditory system, on the order of hundreds of μs . To properly record these fast voltage changes the electrical circuit needs to be able to track these changes without loading the cell with currents [303]. However, filtering of the voltage changes by the recording pipette does occur [297]. The pipette introduces two elements to the recording configuration: (1) an access resistance and (2) distributed pipette capacitance. The combined impact of the access resistance with the capacitance can be approximated as an RC filter with a time constant in the order of 0.1-1 ms in *in vivo* recordings (30 M Ω and 5 pF gives 0.15 ms). With current injections the observed time constant depends on the access resistance and the combination of the stray capacitance with the cell's capacitance, giving a time constant of about ~ 1 ms. Patch-clamp amplifiers can

5

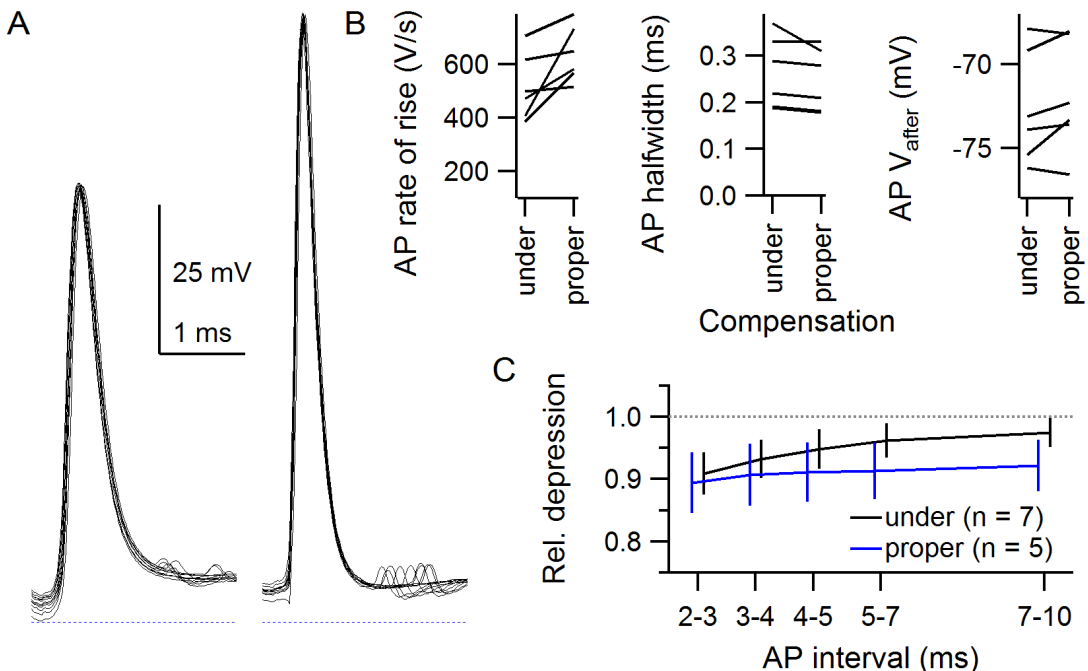


Figure 5.2 The impact of capacitance neutralization on the calyceal AP.

(A) Elicited APs of a P6 calyx in a slice preparation with the compensation circuit optimized based on the voltage-clamp settings (suboptimal; left) or optimized in current-clamp mode (optimal, right). $R_s = 32$ M Ω . Dotted line is -75 mV. (B) Comparison of AP properties when compensation is suboptimal (under) or optimal (proper). (C) The relative depression against AP intervals. Lines around the average represent SD. Notice that the depression with optimal compensation is still minimal.

actively counteract the pipette's filtering by positively feeding back the current needed to charge the pipette (see their manuals), thereby reducing (with a slight delay) the filtering, but this can inadvertently lead to non-physiological voltage dynamics if the compensation circuit is improperly set [304]. Moreover, to set the amplifier's circuitry for capacitance neutralization, the experimenter usually needs to visually distinguish between the charging of stray capacitance and the charging of the cell membrane which becomes difficult if the stray time constants are not an order of magnitude smaller than the time constant of the cell. For the principal cell, its time constant at rest is in the order of 2-5 milliseconds. Hence, proper compensation is not trivial when making whole-cell recordings *in vivo*.

With the AxoPatch 200B amplifier, we compensated the pipette's stray capacitance in voltage-clamp mode without any further compensation and then switched to the fast current-clamp mode. This underestimates the total stray capacitance, leading to a suboptimal compensation of our recordings. As the access resistance was not very different between recordings (Figure 2.5) we considered the impact of the filtering to be similar across recordings. Secondly, we tried to assess the impact of suboptimal compensation in slice recordings. Calyceal APs were elicited in slices by midline stimulation when the compensation circuitry was set either suboptimally or optimally. As illustrated in Figure 5.2A, the additional capacitive load slows down the AP, thereby reducing its maximal rate of rise (rel. change: 0.81 ± 0.07 , $n = 6$, one-sided $t_5 = 2.7$, $p = 0.02$), its maximal repolarization (0.75 ± 0.08 , $n = 6$, one-sided $t_5 = 3.2$, $p = 0.01$) and its amplitude (0.86 ± 0.05 , $n = 6$, one-sided $t_5 = 2.7$, $p = 0.02$). For the AP half width we find a trend for a slight broadening (1.06 ± 0.03 , $n = 6$, one-sided $t_5 = 1.9$, $p = 0.06$). For the after-potential there is no significant change (difference: 0.6 ± 0.4 mV, $n = 6$, two-sided $t_5 = 1.6$, $p = 0.18$) and if there is, it is less than 2 mV (Figure 5.2B). This indicates that suboptimal compensation will significantly slow the *in vivo* recorded AP. Then, how reliable is the relative depression that we measured in CHAPTER 2? For this, I compared the recordings where I stimulated with *in vivo*-like patterns. Despite the high filtering under suboptimal compensation, the amount of depression was similar between conditions (2-3 ms intervals: 0.91 ± 0.01 vs. 0.89 ± 0.02 , two-sided $t_{10} = 0.6$, $p = 0.5$). I therefore

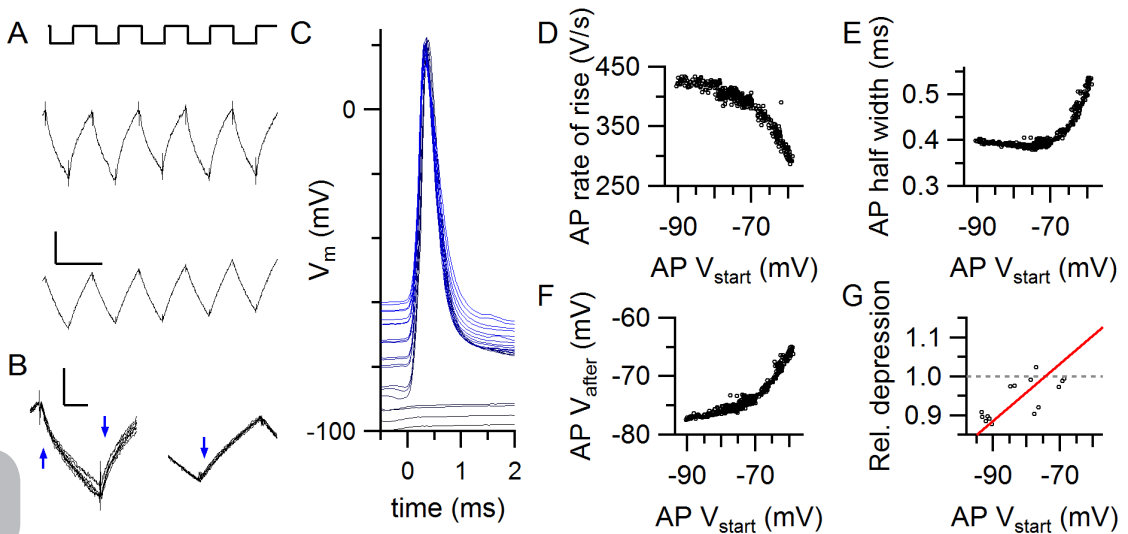


Figure 5.3 *In vivo* compensation with the Multiclamp 700B does not qualitatively alter the calyceal AP. (A) To optimize the capacitance neutralization we injected square-pulse currents at 100 Hz (top trace) to elicit a voltage change of 5-10 mV. The middle trace was recorded *in vivo* from a P5 principal neuron ($R_s = 36 \text{ M}\Omega$, $R_m = 140 \text{ M}\Omega$, $C_p = 3.8 \text{ pF}$, $C_m = 32 \text{ pF}$) after optimization of the capacitance neutralization circuitry. The lower trace was recorded *in vivo* from a P7 calyx ($R_s = 16 \text{ M}\Omega$, $R_m = 320 \text{ M}\Omega$, $C_p = 3.7 \text{ pF}$, $C_m = 22 \text{ pF}$). Scale bars indicate 2 mV and 10 ms. (B) Left and right traces are overlays of the responses shown in A. Note that in the left trace there is a residual slow time constant (blue arrows) caused by the pipette that cannot be compensated with the Multiclamp 700B amplifier. This component is very small in the right example. Scale bars indicates 2 mV and 2 ms. (C) Single APs of the calyx of Held, also shown in A and B, evoked by midline stimulation *in vivo* with constant current injections to bias the onset potential. The start of the current injections was 300 ms before the stimulation. (D-F) Changes in AP properties related to the onset potential (V_{start}) of the same calyx of Held in A-C. (G) Doublets of APs were also elicited to measure the stability potential. Only 15 doublets were elicited before the recording quality degraded. Still, a trend for a stability potential was observed ($r = 0.7$).

conclude that optimal compensation mainly scales the recorded AP close to the real calyceal AP without changing the dynamics. As the depression was taken as a relative measure, this scaling does not substantially affect the outcome.

Lastly, the quality of the voltage recording depend on the type of amplifier used. Ideally, the amplifier should act as an ideal voltmeter, and not draw any current from the cell; such amplifiers are called true voltage followers. The Axopatch 200B, the amplifier we used in CHAPTER 2 and 3, is not a true voltage

follower and therefore might distort the calyceal AP [304]. Therefore, we used the Multiclamp 700B, a voltage follower, in the experiments in CHAPTER 4. Nonetheless, with this amplifier the high series resistance and distributed stray capacitance remained a problem. The compensation circuitry of this amplifier was only able to compensate with a fast time constant and did not compensate the slower components observed *in vivo* (Figure 5.3A-B). We recorded 1 calyx *in vivo* under near-ideal conditions with the MultiClamp 700B amplifier ($R_s = 16 \text{ M}\Omega$, $C_p = 3.7 \text{ pF}$, Figure 5.3C). With this single recording we could replicate the steady-state depression of APs determined by the onset potential (V_{start}), the non-linear relation of V_{start} with the AP half width, and the relation between V_{after} and V_{start} (Figure 5.3D-F). To get the stability potential, we elicited doublets with a 3 ms interval, but this experiment could not be finished due to a sudden increase in R_s . Nonetheless, a trend for a stability potential was observed (mean \pm SEM, $-74 \pm 3 \text{ mV}$), and the data are compatible with the idea that V_{stab} matched the V_{after} of -75 mV (Figure 5.3G). Our main findings of CHAPTER 2 therefore are likely replicated with the Multiclamp 700B, indicating that our conclusions are unlikely to be spurious.

Propagation of neural activity

During development of the auditory nervous system bursting activity composed of high-frequency minibursts can be observed at various stations [74, 155, 183]. We found that the calyceal terminals have sodium channels that rapidly recover from inactivation and that they attain a specific membrane potential following an AP. We propose that both are specializations that contribute to the ability of the calyx to be able to propagate high-frequency firing.

During high-frequent firing sodium channels need to open, inactivate or deactivate, and recover from inactivation within a brief period to be ready for the next AP. The most limiting process is the time needed for sodium channels to recovery from inactivation [159]. If this process is too slow, it leads to accumulation of sodium channels in their inactivated state during high-frequency firing. For the calyx of Held, the recovery from inactivation is very rapid, although it does depend on the membrane potential [159]. Auxiliary sodium channel subunits might reduce inactivation by altering the sodium

5 channel's kinetics [312-317] or by bypassing the inactivation mode via a putative pore-block mode [160]. Na_v1.6's ability to use β-subunit interaction to bypass the inactivated state increases sodium channel availability after an AP [318, 319], making Na_v1.6 more suitable for high-frequency firing [320]. The giant auditory synapses are morphologically and functionally specialized to follow firing frequencies [26, 117, 156, 321, 322], and instantaneous firing frequencies up to 500 Hz are transiently present when sound is presented to cats [133] or mice [134]. We found that Na_v1.6 was already present in the newly-formed calyces, and its presence coincided with the ability to already fire at high frequencies (CHAPTER 2). Na_v1.6 is also present in the spiral ganglion neuron, the globular bushy cell and the principal neuron of the MNTB [118, 159, 323], where it likely enables faithful and precisely-timed action potential propagation for binaural coincident detection in the auditory brainstem nuclei [25]. In addition, high firing frequencies are sustained by a structural specialization, called the heminode, where at the transition of myelination to the terminal sodium channels are clustered in an activity-dependent manner [162]. This clustering shortens the terminal's AP [159] and increases reliability of AP invasion [161]. I did not observe heminodes in this developmental period (CHAPTER 2), possibly indicating that the calyx can attain high instantaneous frequencies without this special structure. The sodium channels are thus important determinants for high-frequency firing.

In CHAPTER 2 I described another important property for high-frequency firing: the after-potential. Its role is to set the onset potential of the next AP and as the membrane potential is the main determinant of the calyceal AP waveform, it stabilizes the AP shape during firing. Only at very high frequencies we observed a contribution of sodium channel inactivation. An activity-independent after-potential is not a necessary feature for high-frequency firing in the way that sodium channel's recovery from inactivation is. If the after-potential would be different after every AP, it would neither affect the calcium current and neurotransmitter release [176], nor within limits affect the firing frequency. However, it would change the shape of the AP that starts at the after-potential and this will impact neurotransmission [175]. It is well described that the postsynaptic EPSC of the calyx of Held synapse quickly depresses

during high-frequency firing [20, 156, 324], and this might make the stability of the presynaptic AP look insignificant compared to the large depression in the postsynaptic EPSC. However, the depression is much less apparent *in vivo* due to spontaneous firing and a lower release probability [134, 325], and therefore the subtle changes in AP shape might indeed impact neurotransmission. Lastly, axon excitability also influences the speed of AP propagation [326], and a depolarized starting potential decelerates AP propagation and vice versa. An activity-independent after-potential therefore also stabilizes AP propagation speed (see Figure 2.9A) which might be an important feature for coincident detection of binaural sounds [25, 327]. I therefore predict that the activity-independent after-potential is not just a property of the terminal, but a general property of an axon that is involved in the precisely-timed relay of high firing frequencies.

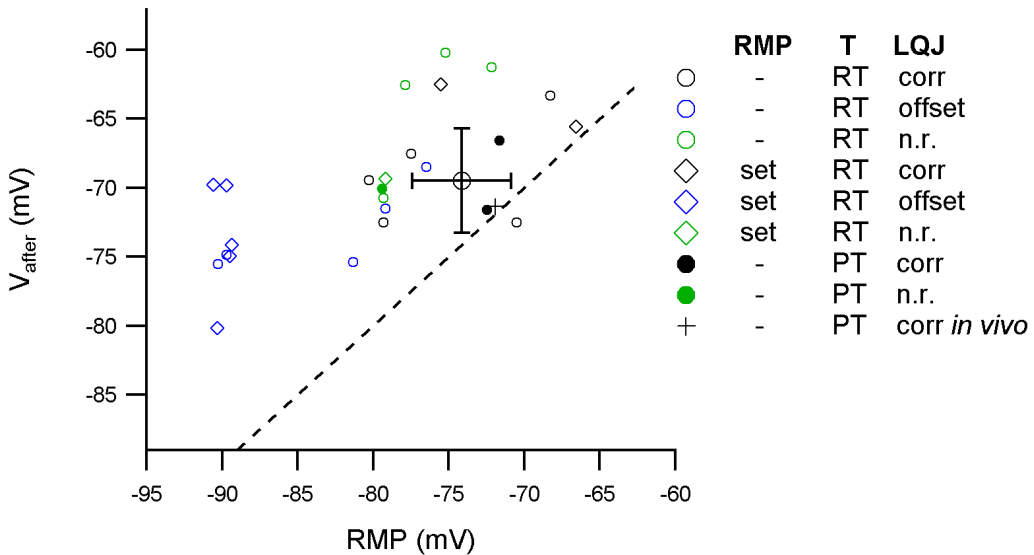


Figure 5.4 Graphical summary of literature review on the resting membrane potential (RMP) and the after-potential (V_{after}) of the calyx of Held. Every symbol corresponds to a recording from a calyceal AP reported in a peer-reviewed paper (listed in Table 5.1). The authors not always reported the exact values. In these cases I tried to measure the RMP and/or V_{after} from an illustrated calyceal AP. Symbols indicate: (1) whether RMP was set or not, (2) whether experiments were performed at room temperature (RT, 20–26 °C) or physiological temperatures (PT, 30–37 °C), and (3) whether the liquid junction potential was corrected (corr), not corrected in the paper (offset, values have been offset in the graph by -10 mV for both axes) or correction not reported (n.r.). The average RMP and V_{after} is shown with their respective SD. The average was calculated for the recordings for which RMP was not set and LQJ was corrected. Some of the data points have been slightly shifted by <1 mV for visual purposes. Dashed line indicates identity line.

Neural Activity During the Formation of a Giant Auditory Synapse

	Reference	DAP/HAP	RMP	LJP	T
[19]	Forsythe (1994)	<i>n.r.</i>	-73 ± 5 mV	<i>n.r.</i>	RT
[20]	Borst <i>et al.</i> (1995)	DAP (3-12 mV)	-80 mV	-11 mV, adj.	RT
[405]	Helmchen <i>et al.</i> (1997)	DAP	-75 and -80 mV	-11 mV, adj.	RT
[222]	Bollmann <i>et al.</i> (1998)	DAP	<i>n.r.</i>	-11 mV, adj.	RT
[157]	Chuhma & Ohmori (1998)	HAP (2-4 mV)	-70.5 mV	-10 mV, adj.	RT
[406]	Wang <i>et al.</i> (1998)	DAP	<i>n.r.</i>	<i>n.r.</i>	RT
[317]	Schneggenburger <i>et al.</i> (1999)	<i>n.r.</i>	-80 mV	<i>n.r.</i>	RT
[156]	Taschenberger <i>et al.</i> (2000)	DAP	-80 mV	not	RT
5 [407]	Chuhma <i>et al.</i> (2001)	<i>n.r.</i>	-58 to -67 mV	<i>n.r.</i>	RT
[408]	Chuhma & Ohmori (2002)	<i>n.r.</i>	Set to -70 mV	-10 mV, adj.	RT
[218]	Leão & Von Gersdorff (2002)	DAP	Set to -65 mV	not	RT
[101]	Taschenberger <i>et al.</i> (2002)	DAP	<i>n.r.</i>	not	RT
[190]	Dodson <i>et al.</i> (2003)	DAP (-62.5 ± 1.6 mV)	-75 mV	-7 mV, adj	RT
[409]	Kushmerick <i>et al.</i> (2004)	DAP	Set to -80 mV	not	RT
[159]	Leão <i>et al.</i> (2005)	DAP	Set to -80 mV	<i>n.r.</i>	RT
[410]	Kushmerick <i>et al.</i> (2006)	DAP	Set to -80 mV	<i>n.r.</i>	PT
[122]	Erazo-Fischer <i>et al.</i> (2007)	DAP	-80 mV	<i>n.r.</i>	RT
[170]	Kim <i>et al.</i> (2007)	DAP (-60 mV)	Set to -80 mV	-11 mV, not	RT
[411]	Nakamura & Takashi (2007)	DAP and HAP	-68.3 ± 1.4 mV	-11 mV, adj	RT
[166]	Huang & Trussell (2008)	<i>n.r.</i>	-77 mV	adj.	RT
[412]	Nakamura <i>et al.</i> (2008)	Small HAP	-71 mV	<i>n.r.</i>	RT
[413]	Paradiso & Wu (2009)	DAP 10-20 mV	-78 mV	<i>n.r.</i>	RT
[152]	Kim <i>et al.</i> (2010)	DAP 7 mV	Set to -80 mV	-11 mV, not	RT
[165]	Huang & Trussell (2011)	<i>n.r.</i>	-75.4 ± 0.9 mV	adj.	PT
[325]	Lin <i>et al.</i> (2011)	DAP	-80 mV	<10 mV, not	RT
[168]	Kim <i>et al.</i> (2012)	DAP	-72 mV	-11 mV	PT
[414]	Huang & Trussell (2014)	<i>n. r.</i>	-73.2 ± 1.6 mV	adj.	PT
[176]	Clarke <i>et al.</i> (2016)	DAP 10-20 mV	-80 mV	-11 mV, not	RT
[162]	Xu <i>et al.</i> (2016)	DAP 6-11 mV	-70 mV	-11 mV, not	RT

← **Table 5.1 Summary of the literature on the after-potential of the calyx of Held.** Data in the table is shown in Figure 5.4, and more information can be found there.

It was already described for the crayfish neuromuscular axon that the direction of the after-potential could be inverted by changing the AP onset potential, and that during high-frequency firing only the first AP could be altered by offsetting the resting membrane potential [144]. This remarkable stability in AP waveform was exactly what we found *in vivo*, but the after-potential of the calyx of Held *in vivo* was not the large depolarizing after-potential that is described in slices [20, 152, 156, 159]. Borst *et al.* [20] already reported that the after-potential amplitude changed with the AP onset potential, and Dodson *et al.* [171] and Kim *et al.* [152] reported a convergence at -62.5 mV and -70 mV, respectively. For the other papers, I made an overview of their RMP and the reported after-potential in order to calculate their putative V_{after} (Figure 5.4). Strikingly, in a subset of experiments the RMP was set to a hyperpolarized membrane potential by current injections; these membrane potentials become even more negative following correction for the liquid junction potential. If we exclude these experiments, we find that RMP is -78 ± 6.1 mV ($n = 20$, mean \pm SD) and V_{after} is -70 ± 6 mV ($n = 23$, mean \pm SD). At physiological temperatures the resting membrane potential depolarizes 8 mV [168], and therefore these findings agree with our observation that the V_{after} is close to RMP *in vivo*.

The similarity of V_{after} and RMP is surprising as the underlying currents setting both are likely to be very different. One difference between V_{after} and RMP is their sensitivity to biasing currents. While the resting membrane resistance is in the order of 200 M Ω , the calculated slope resistance at V_{after} is 1-10 M Ω . The channels activating after the AP basically voltage clamp the membrane potential at a specific potential which happens to be close to RMP. The conductances that set RMP are mediated by $K_{v7.5}$ [165], I_h -channels [169], Na^+/K^+ -ATPase [170], and a persistent opening of sodium channels [166]. The resurgent current has been suggested to underlie the depolarizing after-potential [152]. With their model we found that the resurgent current would be only 0.5-0.6% of the total sodium channels which gives a current of ~ 500 pA (total: ~ 0.7 μS ; resurgent: ~ 4 nS). To clamp the membrane potential, we also need a current that counteracts the

5 depolarizing resurgent current. For this, the low-threshold, and possibly high-threshold, potassium channels are known to be open during the after-potential [171]. To get a V_{after} of -70 mV the total potassium conductance that is needed to balance out the resurgent current would be ~50 nS. This is insufficient to explain the clamping of the membrane potential and indeed, in the model the clamping effect was not observed. The conductances need to be an order of magnitude larger to clamp the membrane potential in a way we observed in CHAPTER 2. Therefore, our current model of the after-potential is missing an accurate description of its channel composition. We suggest that chloride channels might be involved, specifically Anoctamin 1 (also known as Tmem16a) as it is calcium-activated and abundantly present in the calyx [328]. In many nerve terminals, including the young calyx [322], $[\text{Cl}^-]$ is relatively high [323]. Hence, the chloride reversal potential is depolarized compared to the calyceal RMP. Moreover, in *Necturus* taste cells, calcium-dependent chloride channels contribute to the somatic afterdepolarization [324]. It remains remarkable that the RMP and V_{after} are closely related in the calyx of Held and further study of the underlying mechanism, including a possible role of calcium-dependent chloride currents would be interesting.

A specific after-potential is a shared feature of many axonal structures. Besides the calyx of Held a specific after-potential and/or its known conductances are present in the endbulbs of Held [325], cerebellar basket terminals [146, 326], cerebellar Purkinje terminals [327, 328], cerebellar mossy fiber boutons [329], hippocampal mossy fiber boutons [142, 149], neuromuscular axons [143, 144, 330, 331], and cortical layer 5 axons [332]. Note that the somatic after-potential is distinct from the axonal after-potential; for instance for cortical neurons a combination of a dendritic calcium spike and a sodium spike from the first node of Ranvier underlies the AP afterdepolarization [333]. Therefore, a distinct after-potential seems to be a highly conserved property of axons.

These synapses diverge in their functions. On the one hand we have the relay-type synapses that excel in temporally-precise high-frequency activity, including the giant auditory synapses, the cerebellar mossy fiber synapse and the neuromuscular synapse. The cerebellar mossy fiber bouton follows high-frequency activity [141, 329], and remains stable during extreme firing

frequencies [329]. It is therefore noteworthy that the cerebellar mossy fiber bouton has a specific after-potential which has not been explicitly described [141, 329] and that these boutons seem to have a form of AP depression that mirrors the AP starting potential (Figure 4A in [329] and Figure 3C in [334]). A similar finding was found for the endbulb of Held (Figure 6A in [325]), and an inhibitory Purkinje terminal (Figure 5A in [327], Figure 3B in [328]), although the Purkinje terminals did fail to fire at high frequencies [327], which is surprising as the Purkinje cell does fire *in vivo* at these frequencies [335, 336]. The cerebellar basket terminal, also inhibitory, is exceptional as its large after-potential reverses between -50 and -40 mV [146] while it is at the same time able to follow 100 Hz AP firing [327]. Its after-potential was relatively ineffective in altering the calcium currents [146] as was also found for the calyx of Held [176]. On the other hand we have the cortical and hippocampal synapses which are integration-type synapses as they trigger an AP by synaptic integration. Slight changes in AP waveform significantly change the postsynaptic EPSP [177, 332]. For the hippocampal mossy fiber synapse high-frequency activity strongly facilitates the EPSP to reach the postsynaptic AP threshold [337], indicating that its function strongly depends on its firing frequency [142, 177]. Both cortical and hippocampal axons seem to have a specific after-potential that is close to -70 mV [142, 338]. In light of the very diverse functions of these synapses, do these after-potentials have a function beyond stabilizing high-frequency neurotransmission?

Dynamically adjusting the after-potential might tentatively be a novel form of synaptic plasticity. The stabilization effect of the after-potential at the calyx of Held arises by its approximation of the stability potential, but what would be the consequence of dissociating the after-potential from the stability potential? Currently, there is no data yet on the stability potentials of these terminals. We predict for the cerebellar mossy fiber terminal that the same mechanisms for AP stability are present, that is fast channel kinetics and a specific after-potential. For the other terminals a stability potential might exist, although for the hippocampal mossy fiber synapse it might not be close to the after-potential as their APs are known to change [142]. A hyperpolarization beyond its specific after-potential might accelerate the recovery from inactivation of voltage-gated potassium channels and thereby approaching a stability potential,

albeit possibly at nonphysiological levels. Conversely, a recent paper found that a change of the specific after-potential to more positive values increased AP depression [339]. Our prediction that the stability potential and after-potential of the hippocampal mossy fiber synapse are dissociated, also suggest that the dissociation might change synaptic transmission via the AP waveform. Then, changes in the after-potential might be a novel way to alter synaptic strength in all these terminals. A putative candidate might be the trafficking of K_v1 [340-343] or other voltage-dependent or calcium-dependent channels. For now, we have no evidence that this type of plasticity exists.

5

Further investigation on the role of the after-potential in neurotransmission needs a method to manipulate the after-potential. Acute changes of the after-potential of the calyx of Held has been achieved in slices [152, 171], although not with a temporal precision that is needed to investigate the impact of the after-potential on neurotransmission. Perhaps with the use of well-timed activation of channelrhodopsins the after-potential might be manipulated, opening new avenues to study the role of the after-potential.

High-frequency firing also depends on potassium channels that restrict the duration of the AP. Two types of potassium conductances are generally distinguished for the MNTB: high-threshold and low-threshold potassium conductances [192, 344]. These two types are distinguished based on the membrane potential at which they become activated (-30 mV and -70 mV, respectively) and their differential sensitivity to dendrotoxin and tetraethylammonium (TEA). These two types of conductances seem to correspond loosely to potassium channel subunit-family K_v3 and K_v1 , respectively, but more types of conductances can be distinguished using toxins or knock-out strategies [191]. As we have neither investigated the exact potassium current nor the K_v subunit expression, we named the conductances functionally. Within this developmental period low-threshold potassium channels are strongly upregulated in the principal neurons [60, 185] and both low-threshold and high-threshold potassium channels in the globular bushy cells [345]. This upregulation not only accelerates the AP [346], it also eliminates aberrant AP generation in the calyx [171] and the principal neuron [190, 192, 201]. Moreover, the current flowing through high-threshold potassium channels can

be significantly enhanced during >400 Hz firing frequencies [172], which makes AP firing at the highest frequencies possible. We observed the same functional development *in vivo*: a developmental increase in the rate of repolarization, leading to a clear developmental narrowing of the calyceal AP (Figure 2.5) and the AP of the principal neuron (Figure 3.6). The high-frequency minibursts originate from the spiral ganglion neuron's responses to the glutamate release of the IHC [74, 202]. This activity is then transmitted via the modified endbulb of Held to the globular bushy cells that give rise to the calyx of Held. As we observed high-frequency activity at P₃ (CHAPTER 2), the intermediate axons, neuron and synapses were likely capable of high-frequency firing at this developmental stage, while the principal neuron was still developing (CHAPTER 3). This suggests a developmental gradient in the auditory brainstem from the auditory nerve to the brainstem nuclei, all going through a similar development to sustain precisely-timed high-frequency activity.

Neural activity in development

Neural activity is a general phenomenon in developing neural circuits. The contribution of electrical activity can be distinguished as permissive or instructive [78]. A permissive contribution indicates that neural activity, while necessary for the developmental processes, does not determine the exact connectivity. As an example, neural activity might have a trophic role on the developing projection; without activity the projection is degenerated, while with activity it is allowed to continue to develop. An instructive contribution indicates that neural activity does inform the exact connectivity. Here, the classical example is the Hebbian principle 'fire together, wire together' [347, 348], indicating that the co-occurrence of presynaptic and postsynaptic firing will eventually lead to a stronger synaptic connection. Although it is hard to distinguish the two types of contributions in development, it is important to keep in mind that these contributions of activity are mechanistically very different. In the next paragraphs I will compare the calyx of Held to three strong synapses whose development has been extensively studied: the neuromuscular junction, the retinogeniculate synapse and the climbing fiber-Purkinje synapse.

5

In this thesis we focused on neural activity in the auditory system. We found that neural activity reliably propagates in the MNTB as we did not observe principal neurons which did not fire during synaptically-active bursts. In this developmental period a giant synapse is formed and relay-type synaptic characteristics are obtained ([18, 55, 60, 97, 136, 137, 349] and this thesis). These changes also underlie a circuitry refinement at the MNTB as a principal neuron faithfully follows the activity of a single, large synaptic input. The fact that we did not observe the activity of multiple large synapses connected to a single principal cell after P₄ indicates that the principal cell's responses become virtually identical to its presynaptic partner, a globular bushy cell, upon calyx formation. For the auditory brainstem the inputs can be characterized by their response to tone frequencies, and their spatial organization follows a tonotopical gradient [61]. As apoptosis of principal cells is minimal during subsequent development [92] (and assuming no cell migration after calyx formation), the topological mapping of the cochlear nucleus in the MNTB is functionally established after P₄, and thereby MNTB's tonotopy. What follows is a developmental period of structural refinement, including the pruning of collaterals [90], the invaginations of the calyx of Held [55, 91], as well as the maturation of the calyx of Held synapse [16] and possibly the principal neuron [95]. However, these processes will not alter the auditory identity of the principal cell, which is inherited from the innervating GBC. Therefore, we conclude that tonotopy of the MNTB is very likely established at P₅.

Circuitry refinement occurs first functionally, then structurally. In the GENERAL INTRODUCTION we already introduced the two forms of refinement, where a structural refinement can be observed by pruning of structures, and a functional refinement when the responses of a neuron becomes increasingly determined by a selective type of input. We observed that *in vivo* the principal neuron becomes increasingly unresponsive to small inputs, while concertedly a single input increases in strength, as was found in slice studies [60, 97, 157]. Structural refinement continues until hearing onset [90]. Similar temporal dissociation of the two types of refinement have been observed for other developing projections. For the MNTB-LSO projection a sharpening of the postsynaptic responses was observed prior to structural refinement [350].

For the neuromuscular junction (NMJ) embryonic multi-innervation of a muscle fiber is followed by a long period of refinement, ending with mono-innervation in the first postnatal weeks [262, 351, 352]. Before mono-innervation a single axon increased in synaptic strength, which was then followed by a retraction of the outcompeted axon [255, 261, 352]. However, the structural refinement is highly dynamic: in a few cases the largest input was taken over by a smaller input over multiple days [264], or a retracting ‘loser’ axon rapidly reestablishes connectivity if the ‘winner’ axon is lesioned [263]. Hence, NMJ development is not necessarily a simple expansion of the strongest synapse.

A slightly different developmental profile can be found for the projection from the retina to the lateral geniculate nucleus (LGN). Seven to 40 retinal ganglion cells (RGCs) from both eyes converge on a lateral geniculate nucleus (LGN) relay cell at birth. A period of refinement follows, during which axons segregate into eye-specific areas [353, 354]. Functionally, 1-3 strong RGC synapses per LGN cell emerge [355-358], while some weak inputs remain present [357]. This functional refinement arises via the formation and elimination of small boutons [359]. Finally, another refinement period of axonal branches takes place after eye opening [359].

Lastly, we consider the development of the climbing fiber(CF)-cerebellar Purkinje synapse. Most Purkinje cells become mono-innervated in the first week postnatally after being contacted by >5 immature CFs [256, 259, 360, 361]. The CFs initially contact the soma of the cell, where one synapse is selectively strengthened and allowed to expand to the Purkinje apical dendrite [258, 259]. A later period of nonselective elimination of the somatic CF synapses establishes the mono-innervation [258, 259]. Structurally, the largest somatic CF does not always translocate to the dendrite [260], suggesting synaptic competition at the level of the soma. Ablation of the translocating ‘winner’ CF led to a take-over by another CF, but without ablation take-over of a translocating CF was not observed [260].

Despite their disparate origins of activity, the refinement processes are all accompanied with spontaneous activity *in vivo* (auditory: [74], this thesis; NMJ: [255, 362]; visual: [363, 364]; Purkinje: [336, 365, 366]), which might reflect a fundamental need for neural activity in synaptic refinement [78, 367].

Spatiotemporal properties of activity

5

The spatiotemporal properties of the neural activity in a developing network have been studied most extensively in the visual system. Isolated retinas show spontaneous activity that propagates from neighboring RGCs in wave-like manner [368-371], and these waves were observed *in vivo* at the superior colliculus [372]. Due to wave-like organization of the activity, the proximity of RGCs is implicitly encoded in the time difference and synchronization of their activity and this could be used to organize retinotopic maps at their targets [371, 373]. While starting highly synchronized, the activity in the retina developmentally desynchronizes [370, 374]. The desynchronization of activity correlates with circuitry refinement. (Note that increased synchronization of postsynaptic activity with impaired/delayed synaptic elimination is self-explanatory, but increased synchronization of presynaptic neurons with impaired/delayed synaptic elimination can indicate an instructive role of presynaptic activity in synaptic elimination). Early desynchronization led to less retinotopic refinement ([375, 376], but see [377, 378], and a reanalysis in [374]). Synchronized activity of small patches of RGCs was enough to rescue retinotopic refinement, but it did not rescue eye-specific segregation [379]. In contrast, optogenetically synchronizing the monocular activity of many RGCs disrupted retinotopy, while the asynchrony of binocular RGC activity strengthened eye-specific segregation [380]. Therefore, the temporal desynchronization of RGC activity might inform sequentially eye-specific segregation, retinotopy and RGC-type-dependent circuitries [373].

Other developing networks have a similar developmental progression in their neural activity. The isolated spinal cord preparation has spontaneous calcium waves [381], giving rise to synchronized activity mediated via gap junctions [382]. Besides the involvement of activity in neuronal differentiation and axon pathfinding [383], these waves likely pace synapse elimination of NMJ [261]. Different types of synchronized activity are present [384, 385], namely short-duration bursts leading to muscle twitching [386] and long-duration bursts comparable to complex motor events [362]. These different bursts might pattern the developing network for different motor behaviors. Interestingly, early desynchronization of spinal activity accelerated NMJ elimination [387], while

delayed NMJ elimination coincided with prolonged synchronized activity [388]. As in the visual system, this indicates an essential role for desynchronization of activity in the process of synapse elimination [262, 382, 389]. Whether this activity instructs the topology of neuromuscular innervation is unclear, but neural activity is definitely essential for the developing circuitry [390].

In the developing cerebellum, Purkinje cell activity is composed of simple spikes and complex spikes [336], of which the latter is accompanied with calcium influx [365]. *In vivo* calcium imaging revealed a shift from synchronized to desynchronized activity of Purkinje cells and CFs in the first postnatal week [365]. Again, extending synchronized activity of the CFs led to persistent multi-innervation [391]. Somatic and dendritic multi-innervation also persisted in a mouse model that expresses a chloride channel in Purkinje cells [392]. Similarly, in Purkinje cells that miss $\text{Ca}_v2.1$ channels dendritic multi-innervation by CFs occurred [393] accompanied with increased synchronization of Purkinje cell activity [365]. Whether these models show persistent synchronization of CF activity has not yet been investigated. Therefore, desynchronization of presynaptic activity might inform CF elimination, but there is an additional role for the Purkinje cell in this process. Together, these different systems suggest an important switch from synchronized to desynchronized activity in the formation of the network.

At the MNTB, we observed barrages of EPSPs reflecting highly synchronized activity of multiple GBCs. Although spatial synchronization has not been directly observed, our observation that large barrages of EPSPs constituted the principal neuron's activity (CHAPTER 3) suggests that multiple converging axons were simultaneously active. In addition, in two of the three examples of multi-innervation by large synapses their activity was extensively synchronized (CHAPTER 3). As these axons likely contact multiple principal cells [92, 136, 137], activity of multiple principal cells will be synchronized. Moreover, the developmental decrease in the principal cell's excitability and the observation that the principal cell faithfully follows a single, strong input after P5, likely results in less synchronized activity at the population level as each principal neuron will start to relay the activity of single GBC input instead of multiple inputs.

5

The synchronization of the activity of multiple inputs of the principal cell might originate from how activity is generated in the cochlea. Neighbouring inner hair cells can be synchronized by supporting cells of the Kölliker's organ and cholinergic synapses ([75, 103, 105] but see the review of [111] for alternative views). In the first postnatal weeks this activity is composed of high-frequency activity in prolonged bursts ([74, 155] and this thesis), and at the end of the second postnatal week auditory firing becomes random and continuous [155, 183]. How auditory activity is spatially synchronized and whether this reflects tonotopy might be more directly investigated by genetically-encoded calcium sensors to read out the activity (ARO abstracts: PD 5, Babola et al. 2017; PS 810, Lombroso et al. 2016).

The activity of IHCs can be influenced via a cholinergic projection originating in the brainstem [23]. These cholinergic projections are present at birth [394], with the postsynaptic responses of apical IHCs peaking at P8 [395], causing inhibition of IHC activity [105, 107, 395]. In a mouse model that lacks the $\alpha 9$ -subunit of the acetylcholine receptor [396] the inner hair cells are thought to be unresponsive to the cholinergic projection [85]. The absence of cholinergic modulation caused in the auditory projections an increase in number of APs firing in briefer bursts and a more diffuse tonotopy of the LSO [85]. What is missing is how this has changed the synchronization of IHCs. In parallel to the other system, we speculate that the degraded tonotopy of the LSO could be the result of a prolonged/increased synchronization of IHC activity. Furthermore, if neural activity of the auditory system is based on waves of cochlear activity, we predict that after P4 MNTB's activity is tonotopically organized. Synchronized activity continues after calyx formation until P8-9 [155]. This might reflect a role for synchronized activity to pattern the auditory circuitry that develop after the MNTB, including the lateral lemniscus, MSO and LSO, and perhaps even up to the auditory cortex.

Synchronized activity causes plateau potentials/calcium waves.

What is the effect of synchronized activity and desynchronized activity on the postsynaptic neuron, and how does this lead to circuitry refinement? Waves of synchronized activity cause postsynaptic plateau potentials and mediate calcium influx. We define a plateau potential as a sustained depolarization following the postsynaptic AP at membrane potential around or even above AP threshold. A novel observation in our studies was the presence of large plateau potentials coinciding with the APs of the principal cell (CHAPTER 3). Based on our *in silico* model NMDA receptors might mediate these plateau potentials, as was found in slice studies of P7 and older mice [217, 219]. During the plateau potentials the magnesium block of NMDA receptors is incompletely expelled [199, 217]. This will lead to a substantial calcium influx mediated partially via NMDA receptors, but mainly via voltage-gated calcium channels [222]. The secondary spikes on top of the plateau potential are well-timed during the burst activity to reactivate NMDA receptors and voltage-gated calcium channels, thereby sustaining high intracellular calcium levels. To investigate the role of calcium in development, genetic elimination of $Ca_v1.3$ [122-124] or $Ca_v1.2$ [223] could reveal its role, but major apoptosis impeded further investigation of synaptic differentiation and elimination in these models. My own pilot experiments to image a calcium sensor *in vivo* failed due to brain movements corresponding to breathing and heartbeat. This impeded a direct investigation of the *in vivo* calcium dynamics. During development, the plateau potentials become temporally restricted and eliminated by the upregulation of high- and low-threshold potassium channels ([191] and CHAPTER 3). As the expression of low-threshold potassium channels strongly correlates with the presence of a large EPSP (CHAPTER 3), the plateau potentials mainly arise in the period of synaptic differentiation of the calyx of Held synapse.

Plateau potentials are also present during synaptic differentiation in other developing systems. Synchronized RGC activity leads to a barrage of EPSPs at the LGN relay cell [397] followed by a plateau potential [221, 356, 358, 398]. This plateau potential is mainly mediated via voltage-gated calcium channels, with an additional role for NMDA receptors [221, 356, 358, 398]. The occurrence of plateau potentials was developmentally diminished and coincided with synaptic

differentiation [356]. The voltage-gated calcium channels were found to regulate synaptic long-term depression and potentiation *in vitro* [399]. In a mouse model lacking a subunit of the L-type voltage-gated calcium channel plateau potentials were absent, synaptic differentiation and elimination were impeded, and eye-specific segregation was less precise [221]. Whether these developmental effects are caused by the plateau potential independently or by altered calcium influx remains to be investigated.

Revisiting the development of the CF-Purkinje synapse, the role of the postsynaptic neuron becomes more apparent in the context of plateau potentials. Plateau potentials were observed *in vivo*, together with large calcium influx [366], and this calcium influx was not mediated via NMDA receptors [257, 366]. The plateau potentials were caused by synchronized activity of synapses, and in a PC-specific $Ca_v2.1$ knockout mouse model that has plateau potentials [366], multi-innervation persisted [366, 393]. Similarly, in another mouse model with persistent multi-innervation, calcium influx was reduced [400]. Slice studies have dissected a possible role for calcium influx. Pairing CF-PC activity strengthened the strongest CF and reduced the weaker CFs [257, 401]. This segregation effect might be explained by the location of calcium influx as voltage-gated calcium channels translocate to the dendrite with the CF [402].

Altogether, it is tempting to suggest that synchronized activity causes plateau potentials/calcium influx that triggers Hebbian-like strengthening of synapses, and by desynchronization a negative Hebbian-like mechanism weakens the synapses that are not sufficiently strong, leading to their elimination. This would lead to circuitry refinement that can allow topological rearrangement of the network given three conditions: (1) Preliminary synapse formation should be either very diffuse or establish a crude topological map; (2) the strength of synchronization should be topologically equal to avoid a bias in the network to strongest synchronized projections; (3) postsynaptic mechanisms should not be topologically different. Alternatively, there might be a topological matching of postsynaptic mechanisms with presynaptic gradients in synchronization. Even if this hypothesis holds true, it does not aim to explain subcellular (re)distribution at all these synapses (soma vs. dendrite, proximal vs. distal) and does not encompass the developmental dependency on other (inhibitory) synapses,

neuromodulators and trophic factors [367, 390]. It might, nonetheless, present a fundamental building mechanism for developing topologically-arranged circuitries. This thesis described the synchronization of the activity of multiple inputs, the presence of plateau potentials and the strengthening of a single input. The next step would be to demonstrate that Hebbian-like plasticity occurs at the calyx of Held synapse and unravel the molecular mechanisms that are involved in these processes.

More ‘a team effort’ than competition?

Synapse development has long been viewed as a competitive process. To my knowledge the idea of competition was first introduced by Hubel and Wiesel to explain the shift in ocular dominance columns towards the experienced eye and away from the deprived eye [403]. *In vivo* imaging of synapse development showed highly dynamic changes [258, 260, 263, 264] for which the use of the terms ‘winner’ and ‘loser’ by the authors implies a competition. Moreover, the spatial restriction of the mentioned synapses is consistent with competition: the calyx of Held for somatic area, the NMJ for a restricted muscle area, and the climbing fiber for the PC dendrite. In this process the strengthening of one synapse might necessarily involve a weakening of others, consistent with the idea that for ‘one to grow, the others must go’. Hence, the idea of synaptic competition is indeed compelling, but might there be another view?

For the developing climbing fiber, Kawamura *et al.* [366] pointed out that “*weak CFs are not simply ‘losers’ but can contribute to the generation of [burst firing] by firing in cluster with strong CF inputs and thus can promote the selection of a single ‘winner’ CF*”. In an *in vivo* imaging study where the retraction of a ‘loser’ axon was visualized, the authors speculated that the same axon might have formed a winning synapse somewhere else [264], which might suggest that more remote processes influence the outcome besides the competition. In addition to the absence of a trade-off between the strength of the strongest and the second strongest input (CHAPTER 4), the need for EPSP summation at P2-3 to trigger an AP (CHAPTER 3), which initiates putative molecular mechanisms for synapse development, suggests quite the opposite of competition; a need for cooperative development where the absence of a single projection impedes the development

of its comrade projections. In the case of monocular projections, it might be beneficial to redistribute all resources away from an eye that is not functional via a competitive process. However, competition might be less favorable to preserve tonotopy as it could lead to loss of essential projections.

The idea of cooperation versus competition can be empirically tested. If cooperation is important, improving the development of one projection should promote the development of his comrade projections. However, the competition doctrine would demand a reduced development of the surrounding projections due to the developmental advantage of this one projection. The inverse would also be true, the handicap of one projection should degrade surrounding projections that depend on this projection, while competition suggests that it would benefit the development of the other projections. To investigate this, we will need to examine the development of surrounding projections in the presence of a subset of altered projections. With the progress in genetic tools that stochastically change a subset of neurons, it will be possible to test this hypothesis in the near future.

Future directions

In this thesis I have mainly focused on the *in vivo* electrophysiological properties of developing calyx of Held synapses. The main findings seem in agreement with what has been described for other synapses and this argues that the developing calyx of Held synapse might be a useful research model to investigate synapse development.

Regarding the development of the calyx of Held, outstanding questions remain. How dynamic is the formation of the calyx of Held? Can a calyx of Held be replaced by another, similar to the NMJ, or does it stay once formed, similar to the climbing fiber? *In vivo* imaging of the calyceal collaterals has been successful [90], but imaging the formation of the calyx of Held has proven to be a challenge. Genetic labeling strategies via postnatal viral injections are too late to be useful to visualize calyx formation [182]. *In utero* electroporation might overcome this problem, but has a rather low success rate [404]. Without the identification of a GBC-specific promotor that is expressed prenatally, it will be difficult to move forward.

Another important step to be taken is to unravel the spatiotemporal properties of the developmental activity in the auditory brainstem. To record the activity researchers generally use either calcium indicators or multi-electrode arrays. However, the vascularization of the MNTB makes it not only hard to image the area, it also limits the use of multi-electrode arrays, as it is easy to damage a blood vessel. Both methods might in principal work with more optimization. Another way forward might be to record single cells from multiple auditory areas simultaneously. Based on their co-activity and location indirect inferences can be made on the spatiotemporal properties of the auditory activity. Thirdly, controlling the activity of a select group of IHCs or SGNs while recording from the MNTB might also inform us on the convergence and elimination of multiple projections.

One major limitations in the existing literature of auditory development is the dependency of cell survival on neural activity. Overcoming the developmental apoptosis as a result of the perturbations might reveal the role of neural activity in synapse development. I suggest two ways forward. The first possibility is to develop tools to alter only a small subset of neurons under the assumption that the trophic support is not affected by these treatments. The second possibility is to identify the genetic program that makes the cells independent of trophic support, and turn on this genetic program prior to the perturbation to eliminate the induced cell death. Both ideas need substantial development of tools before they can be employed. When these methods are in place, it will be interesting to revisit previous mouse models to see how the perturbation then changes auditory brainstem development.

When we know in detail how activity is organized and how the calyx of Held is formed, the specific roles of a wide-range of proteins in these processes can be addressed. A temporally fine-grained study at all major developmental milestones will unravel at what time points and in which processes the protein is involved and how this protein contributes to the establishment of the calyx of Held. Here, a focus on cell adhesion molecules might reveal which cell-adhesion proteins are involved in transsynaptic signaling and which factor might signal the calycigenic axon to cover the postsynaptic soma. Next, the role of second messengers might be of particular interest as they combine information

from chemical cues in the environment as well as the neural activity present. Although entirely ignored within this thesis, there is likely to be a prominent role for MNTB glia cells in synapse development. As no master transcription factor or other protein has been identified to regulate giant synapse formation, it might be the more subtle levels in proteins, protein-protein interactions and protein modifications that cue the synapse to become a giant.

Conclusions

5 One important step in the development of the brain is the formation of connections between cells by a synapse. The calyx of Held synapse is a special synapse with properties that are important for its role in the auditory brainstem, but its development might involve processes that are general to synapse development. In this thesis we have shown that neural activity is present during its formation, and have described in some detail how the activity is organized at the level of single principal neurons.

Shortly after the formation of the calyx of Held, the axon terminal already obtained features that enable adult-like high-frequency firing. Based on the first *in vivo* whole-cell recordings of the calyx of Held, we advanced a role of the calyceal after-potential in high-frequency activity, similar to what was suggested for the crayfish neuromuscular terminal [144]. We speculate that the after-potential might have a broader significance in neurotransmission than was previously assumed.

With postsynaptic whole-cell recordings we followed the formation of the calyx of Held synapse and the complementary development of the principal cell. For the first time a within-cell comparison was made of postsynaptic excitability and synaptic strength, revealing an evident correlation between synaptic development and postsynaptic properties, suggesting homeostatic plasticity of which the molecular mechanism remains to be investigated. Plateau potentials were found within this period. By correlation to other work, these plateau potentials sustain elevations in intracellular calcium level which might be important for the increase in synaptic strength.

Finally, the synaptic convergence on a principal cell was investigated during the period of calyx formation. The first *in vivo* characterization of the calyx

of Held synapse by means of midline stimulation of the afferent axon was given. With midline stimulation we also identified different converging inputs of a single principal cell, revealing that while the second strongest input was not changing, the strongest input became significantly stronger between P2 and P5-8. During development strong inputs became associated with a prespike, identifying them as calyces of Held, but they were surprisingly similar to strong inputs without a prespike recorded from other principal cells. Lastly, with midline stimulation we did not identify multiple strong inputs converging on a single principal cell, indicating that synaptic competition for calyx formation might progress differently than was expected.

The results described in this thesis indicate that in many ways the development of the calyx of Held synapse mirrors the development of other synapses. Thus, given the advantages of the calyx of Held synapse, this synapse constitutes a unique research model to probe the fundamental processes that govern synapse development in the mammalian central nervous system.

Summary / Samenvatting

CHAPTER 6

Martijn C. Sierksma

Neural Activity During the Formation of a Giant Auditory Synapse

The formation of synapses is a critical step in the development of the brain. During this developmental stage neural activity propagates across the brain from synapse to synapse. This activity is thought to instruct the precise, topological connectivity found in the sensory central nervous system. In the GENERAL INTRODUCTION some possible hypotheses for establishing topological connectivity in the brain are put forward. In this thesis I demonstrated that during the period when a giant auditory synapse is formed, the calyx of Held synapse, including both the calyx itself and its postsynaptic target, the principal neuron of the medial nucleus of the trapezoid body, displays bursts of neural firing.

6 With our unique *in vivo* approach I describe in CHAPTER 2 the patterns of neural activity at the calyx of Held in neonatal rats. Despite the young age of the pup and the early stage of calyx development, very brief intervals between action potentials (APs) were observed with only minor changes in the shape of the calyceal AP. One of the processes that keeps the AP shape invariant was related to the absolute membrane potential attained following the AP, the after-potential. I propose that there might be an essential role for the after-potential to stabilize the AP shape in high frequency firing.

In CHAPTER 3 I focus on the developmental changes in the calyx of Held synapse and the postsynaptic neuron. In a few days a relay synapse emerges that reliably drives postsynaptic activity. The other synaptic inputs become less relevant for postsynaptic firing, because of changes in the intrinsic properties of the postsynaptic neuron. I demonstrate a clear correlation between the postsynaptic excitability and the emergence of the relay synapse, possibly indicating a homeostatic matching of the size of the inputs and the size of the input resistance. In the days prior to the appearance of the relay synapse, the activity of many converging synapses caused a continuous depolarization. By means of modeling I suggest that this depolarization only helps to trigger postsynaptic APs in the period before the relay synapse emerges, as an increase in low-threshold potassium channels precluded the triggering of postsynaptic APs by slowly-rising, prolonged depolarizations at the later developmental stages.

From the many terminals that connect to a principal neuron in neonatal rats, typically a single calyx of Held remains in the adult. During this period I expected that multiple calyces would initially form on a principal cell followed by the selection of a single ‘winner’ calyx of Held, as indicated by some other studies. In CHAPTER 4 I describe in detail that we do not observe electrophysiological evidence for multiple calyceal innervations *in vivo*. Weak inputs were present throughout this period. While the strongest input became stronger, the second strongest input retained its strength. Our attempt to retrieve the morphology of the terminals that are formed on the recorded neuron did not reveal a clear mismatch between our electrophysiological recordings and the terminal. I propose some possible explanations for the apparent discrepancy between previous studies and my findings. In the end, either multiple calyces are rarely formed on single rat principal cells or they are very weak for their giant size.

In the GENERAL DISCUSSION I address some possible confounding factors in my research. I return to the propagation of neural activity in the auditory brainstem and the mechanisms that are essential for firing with high frequencies. I elaborate on the role of the after-potential to expand on the idea that the after-potential has a role in stabilizing neural activity that extends beyond the calyx of Held. I also speculate on its possible influence on synaptic neurotransmission which could be an intriguing, new type of plasticity. Next, the neural activity during the formation of the calyx of Held synapse is compared to what is known about the formation of other well-studied synapses. I highlight the similarities in their development with emphasis on a temporal dissociation of synaptic strengthening and synaptic elimination, and the role of synchronized and desynchronized activity. I briefly discuss the hypothesis that a form of cooperation other than synaptic competition might be crucial to the development of the sensory nervous system and continue to suggest what the major next steps will be to understand the formation of the calyx of Held. This thesis will hopefully contribute towards making the calyx of Held synapse a leading research model to investigate the role of neural activity in synapse formation.

Het aanleggen van synapsen vormt een essentiële stap in de ontwikkeling van het brein. Tijdens deze fase van de ontwikkeling vuren neuronen actiepotentialen (APs). Deze neurale activiteit beïnvloedt mogelijk de vorming van synapsen en daarmee de topologie van het sensorische zenuwstelsel. In de ALGEMENE INTRODUCTIE bespreek ik mogelijke mechanismen waarmee topologische netwerken kunnen worden aangelegd. In dit proefschrift toon ik aan dat tijdens de vorming van een auditieve reuzensynaps, de calyx van Held-synaps, zowel de calyx als zijn postsynaptische partner, het principale neuron van de mediale nucleus van het corpus trapezoideum, periodes met sterk verhoogde activiteit vertoont.

6

In HOOFDSTUK 2 beschrijf ik dat door middel van onze unieke benadering we in staat zijn om in pasgeboren ratten de specifieke patronen in de neurale activiteit van calyces van Held te meten. Ondanks de leeftijd van de rat en het vroege ontwikkelingsstadium van de synaps waren de intervallen tussen de APs al zeer kort. Dit had, verrassend genoeg, weinig consequenties voor de vorm van de APs. Een belangrijke bevinding was dat de ongevoeligheid van de vorm van de AP voor de hoge vuurfrequentie samen hing met de absolute membraanpotentialen die op de AP volgen, de napotentiaal. Hiermee is voor het eerst een functie aangetoond voor de napotentiaal bij hoge vuurfrequenties in zoogdieren. Misschien is de napotentiaal zelfs wel kenmerkend voor axonale eindigingen die met een hoge frequentie vuren.

In HOOFDSTUK 3 beschrijf ik de veranderingen in de calyx van Held-synaps en het postsynaptische neuron. In enkele dagen na de geboorte verandert één synaps in een betrouwbare relais-synaps ('relay synapse' in het engels). Als de calyx een AP vuurt, dan vuurt het postsynaptische neuron ook een AP. Deze synaps verschijnt tijdens de ontwikkeling uit de vele andere synapsen die bij het principale neuron horen. Terwijl vele synapsen aanvankelijk een belangrijke bijdrage leveren aan het vuurgedrag van het principale neuron, verdwijnt hun invloed tijdens de ontwikkeling, als gevolg van veranderingen in de prikkelbaarheid van het postsynaptische neuron. Ik toon aan dat de prikkelbaarheid van het postsynaptische neuron correleert met de sterkte van de relais-synaps, wat mogelijk een aanwijzing is voor homeostatische plasticiteit. In de paar dagen waarin de relais-synaps verschijnt is er sprake van

plateaupotentiaalen die veroorzaakt wordt door de activiteit van vele synapsen. Door middel van computermodellen toon ik aan dat de periode waarin plateaupotentiaalen bijdragen aan het vuurgedrag van het postsynaptische neuron beperkt is tot het moment waarop de relais-synaps is gevormd. Dit komt voornamelijk door een toename in kaliumkanalen die openen tussen de rustpotentiaal en de drempelpotentiaal van het neuron.

De relais-synaps verschijnt uit een populatie van synapsen die aanvankelijk zeer vergelijkbaar zijn. Op basis van eerdere anatomische studies verwachtte ik dat meerdere calyces zich zouden vormen op een enkele principale neuron, waarvan vervolgens één calyx zou overblijven. Echter, in HOOFDSTUK 4 beschrijf ik dat we in onze metingen geen bewijs vinden voor multi-calyceale innervatie. In plaats daarvan vinden we dat het principale neuron niet meer dan één sterke synaps heeft. Tijdens de ontwikkeling zien we dat de sterkste synaptische input sterker wordt, zonder daarbij een duidelijk verandering te zien in de op-één-na-sterkste input. Ik beschrijf dat de kracht van de sterkste synaps nauw samenhangt met de aanwezigheid van bepaalde synaptische eiwitten rond het cellichaam van het neuron. Ik stel enkele mogelijkheden voor om de ogenschijnlijke discrepantie tussen de anatomische studies en onze bevindingen te verklaren en ik concludeer dat óf de neuronen die gemeten zijn niet meerdere calyces van Held hebben of dat maar één calyx per neuron sterk wordt terwijl de andere calyces zwak blijven.

In de ALGEMENE DISCUSSIE bespreek ik enkele factoren waarvoor we niet kunnen corrigeren in onze experimenten. We kijken opnieuw naar de functie van de napotentiaal om het idee te versterken dat de napotentiaal een bepalende rol heeft in het ondersteunen van activiteit met korte AP-intervallen. Daarbij speculeer ik over een mogelijk effect van de napotentiaal op synaptische neurotransmissie en dit zou een nog niet eerder beschreven vorm van synaptische plasticiteit kunnen zijn. Vervolgens vergelijk ik de neurale activiteit tijdens de vorming van de calyx van Held-synaps met wat bekend is over andere synapsen. De overeenkomsten in ontwikkeling worden besproken en ik leg daarbij de nadruk op een temporele scheiding van het sterker worden van één synaps en het verwijderen van de andere synapsen, en op de synchronisatie van de synaptische en postsynaptische activiteit. In tegenstelling tot de veel

Neural Activity During the Formation of a Giant Auditory Synapse

besproken competitie tussen synapsen, bespreek ik de mogelijkheid dat een vorm van samenwerking tussen de vele synaptische inputs de basis vormt voor het aanleggen van topologische neurale netwerken. Ik benoem de belangrijkste vervolgstappen in het onderzoek naar de vorming van de calyx van Held-synaps. Alles bij elkaar genomen zet het werk in dit proefschrift de eerste stappen om de calyx van Held-synaps op de kaart te zetten als een onderzoeksmodel voor de rol van neurale activiteit in synapsvorming in het zich ontwikkelende centrale zenuwstelsel.

List of references

REFERENCES

Neural Activity During the Formation of a Giant Auditory Synapse

- 1 Hamburger, V. (1988). Ontogeny of neuroembryology. *The Journal of Neuroscience* 8, 3535-40, <http://www.jneurosci.org/content/jneuro/8/10/3535.full.pdf>.
- 2 López-Muñoz, F. & Alamo, C. (2009). Historical evolution of the neurotransmission concept. *Journal of Neural Transmission* 116, 515-33, <http://dx.doi.org/10.1007/s00702-009-0213-1>.
- 3 Bennett, M. R. *History of the Synapse*. 1st edn, (CRC Press, 2001), <http://dx.doi.org/10.4324/9780203302545>.
- 4 Ramón y Cajal, S. Neuron theory or reticular theory? Objective evidence of the anatomical unity of nerve cells. (Con. Sup. Investig. Cient., Inst. Cajal, Madrid, 1954).
- 5 Jones, E. G. (1999). Golgi, Cajal and the Neuron Doctrine. *Journal of the History of the Neurosciences* 8, 170-78, <http://www.tandfonline.com/doi/abs/10.1076/jhin.8.2.170.1838>.
- 6 Shepherd, G. M. (1972). The neuron doctrine: a revision of functional concepts. *The Yale Journal of Biology and Medicine* 45, 584-99, <http://www.ncbi.nlm.nih.gov/pmc/articles/PMC2591810/>.
- 7 Sherrington, C. S. *The central nervous system*. Vol. 3 (1897).
- 8 Langley, J. N. (1901). Observations on the physiological action of extracts of the supra-renal bodies. *The Journal of Physiology* 27, 237-56, <http://dx.doi.org/10.1113/jphysiol.1901.sp000869>.
- 9 Loewi, O. (1921). Über humorale übertragbarkeit der herznervenwirkung. *Pflügers Archiv European Journal of Physiology* 189, 239-42, <http://dx.doi.org/10.1007/bf01738910>.
- 10 Dale, H. H. (1906). On some physiological actions of ergot. *The Journal of physiology* 34, 163-206, <http://dx.doi.org/10.1113/jphysiol.1906.sp001148>.
- 11 Bennett, M. R. (2000). The concept of transmitter receptors: 100 years on. *Neuropharmacology* 39, 523-46, [http://dx.doi.org/10.1016/S0028-3908\(99\)00137-9](http://dx.doi.org/10.1016/S0028-3908(99)00137-9).
- 12 Hodgkin, A. L. & Huxley, A. F. (1952). A quantitative description of membrane current and its application to conductance and excitation in nerve. *Journal of Physiology* 117, 500-44, <http://jp.physoc.org/content/117/4/500.long>.
- 13 Katz, B. & Miledi, R. (1965). The effect of calcium on acetylcholine release from motor nerve terminals. *Proceedings of the Royal Society B* 161, 496-503, <http://dx.doi.org/10.1098/rspb.1965.0017>.
- 14 Katz, B. & Miledi, R. (1965). Release of acetylcholine from a nerve terminal by electric pulses of variable strength and duration. *Nature* 207, 1097-8, <http://dx.doi.org/10.1038/2071097a0>.
- 15 Katz, B. & Miledi, R. (1967). Tetrodotoxin and neuromuscular transmission. *Proceedings of the Royal Society B* 167, 8-22, <http://dx.doi.org/10.1098/rspb.1967.0010>.
- 16 Borst, J. G. G. & Soria van Hoeve, J. (2012). The calyx of Held synapse: from model synapse to auditory relay. *Annual Review of Physiology* 74, 199-224, <http://dx.doi.org/10.1146/annurev-physiol-020911-153236>.

- 17 Held, H. (1893). Die centrale Gehörleitung. *Archiv für Anatomie und Physiologie, Anatomie Abtheil*, 201-48.
- 18 Morest, D. K. (1968). The growth of synaptic endings in the mammalian brain: a study of the calyces of the trapezoid body. *Zeitschrift für Anatomie und Entwicklungsgeschichte* 127, 201-20, <http://dx.doi.org/10.1007/BF00526129>.
- 19 Forsythe, I. D. (1994). Direct patch recording from identified presynaptic terminals mediating glutamatergic EPSCs in the rat CNS, in vitro. *J Physiol* 479, 381-87, <http://dx.doi.org/10.1113/jphysiol.1994.sp020303>.
- 20 Borst, J. G. G., Helmchen, F. & Sakmann, B. (1995). Pre- and postsynaptic whole-cell recordings in the medial nucleus of the trapezoid body of the rat. *J Physiol* 489, 825-40, <http://dx.doi.org/10.1113/jphysiol.1995.sp021095>.
- 21 Borst, J. G. G. & Sakmann, B. (1996). Calcium influx and transmitter release in a fast CNS synapse. *Nature* 383, 431-4, <http://www.nature.com/nature/journal/v383/n6599/pdf/383431a0.pdf>.
- 22 Borst, J. G. G. & Rusu, S. I. in *Synaptic mechanisms in the auditory system* Springer Handbook of Auditory Research (eds L.O. Trussell, A. N. Popper, & R. R. Fay) Ch. 5, 95-134 (Springer, 2011).
- 23 Thompson, A. M. & Schofield, B. R. (2000). Afferent projections of the superior olivary complex. *Microsc Res Tech* 51, 330-54, [http://dx.doi.org/10.1002/1097-0029\(200011\)51:4<330::AID-JEMT4>3.0.CO;2-X](http://dx.doi.org/10.1002/1097-0029(200011)51:4<330::AID-JEMT4>3.0.CO;2-X).
- 24 Guinan, J. J., Jr., Guinan, S. S. & Norris, B. E. (1972). Single auditory units in the superior olive complex I: Responses to sounds and classifications based on physiological properties. *Int J Neurosci* 4, 101-20, <http://dx.doi.org/10.3109/00207457209147165>.
- 25 Grothe, B., Pecka, M. & McAlpine, D. (2010). Mechanisms of sound localization in mammals. *Physiol Rev* 90, 983-1012, <http://dx.doi.org/10.1152/physrev.00026.2009>.
- 26 Yu, W. M. & Goodrich, L. V. (2014). Morphological and physiological development of auditory synapses. *Hear Res* 311, 3-16, <http://dx.doi.org/10.1016/j.heares.2014.01.007>.
- 27 Solnica-Krezel, L. (2005). Conserved Patterns of Cell Movements during Vertebrate Gastrulation. *Current Biology* 15, R213-R28, <http://www.sciencedirect.com/science/article/pii/S0960982205002770>.
- 28 Solnica-Krezel, L. & Sepich, D. S. (2012). Gastrulation: Making and Shaping Germ Layers. *Annual Review of Cell and Developmental Biology* 28, 687-717, <http://www.annualreviews.org/doi/abs/10.1146/annurev-cellbio-092910-154043>.
- 29 Hall, B. K. (2008). The neural crest and neural crest cells: discovery and significance for theories of embryonic organization. *Journal of Biosciences* 33, 781-93, <http://dx.doi.org/10.1007/s12038-008-0098-4>.
- 30 Smith, J. L. & Schoenwolf, G. C. (1997). Neurulation: coming to closure. *Trends in Neurosciences* 20, 510-17, [http://dx.doi.org/10.1016/S0166-2236\(97\)01121-1](http://dx.doi.org/10.1016/S0166-2236(97)01121-1).
- 31 Lumsden, A. & Krumlauf, R. (1996). Patterning the vertebrate neuraxis. *Science* 274, 1109, <http://dx.doi.org/10.1126/science.274.5290.1109>.

Neural Activity During the Formation of a Giant Auditory Synapse

- 32 Wurst, W. & Bally-Cuif, L. (2001). Neural plate patterning: upstream and downstream of the isthmic organizer. *Nature Reviews Neuroscience* 2, 99-108.
- 33 Farago, A. F., Awatramani, R. B. & Dymecki, S. M. (2006). Assembly of the Brainstem Cochlear Nuclear Complex Is Revealed by Intersectional and Subtractive Genetic Fate Maps. *Neuron* 50, 205-18, <http://www.sciencedirect.com/science/article/pii/S089662730600211X>.
- 34 Wullimann, M. F., Mueller, T., Distel, M. et al. (2011). The Long Adventurous Journey of Rhombic Lip Cells in Jawed Vertebrates: A Comparative Developmental Analysis. *Frontiers in Neuroanatomy* 5, <http://journal.frontiersin.org/article/10.3389/fnana.2011.00027>.
- 35 Appler, J. M. & Goodrich, L. V. (2011). Connecting the ear to the brain: Molecular mechanisms of auditory circuit assembly. *Progress in Neurobiology* 93, 488-508, <http://www.sciencedirect.com/science/article/pii/S0301008211000050>.
- 36 Noramly, S. & Grainger, R. M. (2002). Determination of the embryonic inner ear. *Journal of Neurobiology* 53, 100-28, <http://dx.doi.org/10.1002/neu.10131>.
- 37 Anderson, D., Groves, A., Lo, L. et al. (1997). Cell Lineage Determination and the Control of Neural Identity in the Neural Crest. *Cold Spring Harbor symposia on quantitative biology* 62, 493-504, <http://dx.doi.org/10.1101/SQB.1997.062.01.056>.
- 38 Radosevic, M., Fargas, L. & Alsina, B. (2014). The Role of *her4* in Inner Ear Development and Its Relationship with Proneural Genes and Notch Signalling. *PLOS ONE* 9, e109860, <http://dx.doi.org/10.1371/journal.pone.0109860>.
- 39 Jeon, S.-J., Fujioka, M., Kim, S.-C. & Edge, A. S. B. (2011). Notch Signaling Alters Sensory or Neuronal Cell Fate Specification of Inner Ear Stem Cells. *The Journal of Neuroscience* 31, 8351-58, <http://dx.doi.org/10.1523/JNEUROSCI.6366-10.2011>.
- 40 Raft, S., Koundakjian, E. J., Quinones, H. et al. (2007). Cross-regulation of *Ngn1* and *Math1* coordinates the production of neurons and sensory hair cells during inner ear development. *Development* 134, 4405-15. <http://dx.doi.org/10.1242/dev.009118>.
- 41 Raft, S., Nowotschin, S., Liao, J. & Morrow, B. E. (2004). Suppression of neural fate and control of inner ear morphogenesis by *Tbx1*. *Development* 131, 1801-12, <http://dx.doi.org/10.1242/dev.01067>.
- 42 Riccomagno, M. M., Martinu, L., Mulheisen, M., Wu, D. K. & Epstein, D. J. (2002). Specification of the mammalian cochlea is dependent on Sonic hedgehog. *Genes & Development* 16, 2365-78, <http://dx.doi.org/10.1101/gad.1013302>.
- 43 Ma, Q., Chen, Z., Barrantes, I. d. B., Luis de la Pompa, J. & Anderson, D. J. (1998). *neurogenin1* Is Essential for the Determination of Neuronal Precursors for Proximal Cranial Sensory Ganglia. *Neuron* 20, 469-82, [http://dx.doi.org/10.1016/S0896-6273\(00\)80988-5](http://dx.doi.org/10.1016/S0896-6273(00)80988-5).
- 44 Rubel, E. W. & Fritzsch, B. (2002). Auditory system development: primary auditory neurons and their targets. *Annu Rev Neurosci* 25, 51-101, <http://dx.doi.org/10.1146/annurev.neuro.25.112701.142849>.

- 45 Nichols, D. H. & Bruce, L. L. (2006). Migratory routes and fates of cells transcribing the Wnt-1 gene in the murine hindbrain. *Developmental Dynamics* 235, 285-300. <http://dx.doi.org/10.1002/dvdy.20611>.
- 46 Copp, A. J. (2005). Neurulation in the cranial region – normal and abnormal. *Journal of Anatomy* 207, 623-35, <http://dx.doi.org/10.1111/j.1469-7580.2005.00476.x>.
- 47 Copp, A. J., Greene, N. D. E. & Murdoch, J. N. (2003). The genetic basis of mammalian neurulation. *Nat Rev Genet* 4, 784-93, <http://dx.doi.org/10.1038/nrg1181>.
- 48 Altman, J. & Bayer, S. A. (1980). Development of the brain stem in the rat. III. Thymidine-radiographic study of the time of origin of neurons of the vestibular and auditory nuclei of the upper medulla. *J Comp Neurol* 194, 877-904, <http://www3.interscience.wiley.com/cgi-bin/fulltext/109686447/PDFSTART>.
- 49 Marrs, G. S., Morgan, W. J., Howell, D. M., Spirou, G. A. & Mathers, P. H. (2013). Embryonic origins of the mouse superior olivary complex. *Dev Neurobiol* 73, 384-98, <http://dx.doi.org/10.1002/dneu.22069>.
- 50 Nakamura, P. A. & Cramer, K. S. (2011). Formation and maturation of the calyx of Held. *Hear Res* 276, 70-78, <http://dx.doi.org/10.1016/j.heares.2010.11.004>.
- 51 Karis, A., Pata, I., van Doorninck, J. H. et al. (2001). Transcription factor GATA-3 alters pathway selection of olivocochlear neurons and affects morphogenesis of the ear. *Journal of Comparative Neurology* 429, 615-30, [http://dx.doi.org/10.1002/1096-9861\(20010122\)429:4<615::AID-CNE8>3.0.CO;2-F](http://dx.doi.org/10.1002/1096-9861(20010122)429:4<615::AID-CNE8>3.0.CO;2-F).
- 52 Koundakjian, E. J., Appler, J. L. & Goodrich, L. V. (2007). Auditory Neurons Make Stereotyped Wiring Decisions before Maturation of Their Targets. *The Journal of Neuroscience* 27, 14078-88, <http://dx.doi.org/10.1523/JNEUROSCI.3765-07.2007>.
- 53 Lu, C. C., Appler, J. M., Houseman, E. A. & Goodrich, L. V. (2011). Developmental Profiling of Spiral Ganglion Neurons Reveals Insights into Auditory Circuit Assembly. *The Journal of Neuroscience* 31, 10903-18, <http://dx.doi.org/10.1523/JNEUROSCI.2358-11.2011>.
- 54 Bruce, L. L., Kingsley, J., Nichols, D. H. & Fritsch, B. (1997). The development of vestibulocochlear efferents and cochlear afferents in mice. *International Journal of Developmental Neuroscience* 15, 671-92, <http://www.sciencedirect.com/science/article/pii/S0736574896001207>.
- 55 Kandler, K. & Friauf, E. (1993). Pre- and postnatal development of efferent connections of the cochlear nucleus in the rat. *Journal of Comparative Neurology* 328, 161-84, <http://dx.doi.org/10.1002/cne.903280202>.
- 56 Niblock, M. M., Brunso-Bechtold, J. K. & Henkel, C. K. (1995). Fiber outgrowth and pathfinding in the developing auditory brainstem. *Brain Res Dev Brain Res* 85, 288-92, [http://dx.doi.org/10.1016/0165-3806\(95\)00002-U](http://dx.doi.org/10.1016/0165-3806(95)00002-U).
- 57 Marcotti, W., Johnson, S. L., Holley, M. C. & Kros, C. J. (2003). Developmental changes in the expression of potassium currents of embryonic, neonatal and mature mouse inner hair cells. *J Physiol* 548, 383-400, <http://jp.physoc.org/content/548/2/383.full>.

Neural Activity During the Formation of a Giant Auditory Synapse

- 58 Johnson, S. L., Marcotti, W. & Kros, C. J. (2005). Increase in efficiency and reduction in Ca²⁺ dependence of exocytosis during development of mouse inner hair cells. *The Journal of physiology* 563, 177-91, <http://dx.doi.org/10.1113/jphysiol.2004.074740>.
- 59 Marrs, G. S. & Spirou, G. A. (2012). Embryonic assembly of auditory circuits: spiral ganglion and brainstem. *J Physiol* 590, 2391-408, <http://dx.doi.org/10.1113/jphysiol.2011.226886>.
- 60 Hoffpauir, B. K., Kolson, D. R., Mathers, P. H. & Spirou, G. A. (2010). Maturation of synaptic partners: functional phenotype and synaptic organization tuned in synchrony. *J Physiol* 588, 4365-85, <http://dx.doi.org/10.1113/jphysiol.2010.198564>.
- 61 Kandler, K., Clause, A. & Noh, J. (2009). Tonotopic reorganization of developing auditory brainstem circuits. *Nat Neurosci* 12, 711-7, <http://dx.doi.org/10.1038/nn.2332>.
- 62 Holt, C. E. (1984). Does timing of axon outgrowth influence initial retinotectal topography in *Xenopus*? *The Journal of Neuroscience* 4, 1130-52, <http://dx.doi.org/10.1523/JNEUROSCI.04-04-01130.1984>.
- 63 Holt, C. E. & Harris, W. A. (1993). Position, guidance, and mapping in the developing visual system. *Journal of Neurobiology* 24, 1400-22, <http://dx.doi.org/10.1002/neu.480241011>.
- 64 Fritzschn, B. (2003). Development of inner ear afferent connections: forming primary neurons and connecting them to the developing sensory epithelia. *Brain Research Bulletin* 60, 423-33, <http://www.sciencedirect.com/science/article/pii/S0361923003000480>.
- 65 Sperry, R. W. (1963). Chemoaffinity in the orderly growth of nerve fiber patterns and connections. *Proceedings of the National Academy of Sciences* 50, 703-10, <http://www.pnas.org/content/50/4/703.short>.
- 66 Mosca, T. J., Hong, W., Dani, V. S., Favaloro, V. & Luo, L. (2012). Trans-synaptic Teneurin signalling in neuromuscular synapse organization and target choice. *Nature* 484, 237-41, <http://dx.doi.org/10.1038/nature10923>.
- 67 Hong, W., Mosca, T. J. & Luo, L. (2012). Teneurins instruct synaptic partner matching in an olfactory map. *Nature* 484, 201-07, <http://dx.doi.org/10.1038/nature10926>.
- 68 Fritzschn, B., Fariñas, I. & Reichardt, L. F. (1997). Lack of neurotrophin 3 causes losses of both classes of spiral ganglion neurons in the cochlea in a region-specific fashion. *J Neurosci* 17, 6213-25, <http://www.jneurosci.org/content/17/16/6213.long>.
- 69 Schimmang, T., Tan, J., Müller, M. et al. (2003). Lack of Bdnf and TrkB signalling in the postnatal cochlea leads to a spatial reshaping of innervation along the tonotopic axis and hearing loss. *Development* 130, 4741-50, <http://dx.doi.org/10.1242/dev.00676>.
- 70 Fariñas, I., Jones, K. R., Tessarollo, L. et al. (2001). Spatial Shaping of Cochlear Innervation by Temporally Regulated Neurotrophin Expression. *The Journal of Neuroscience* 21, 6170-80, <http://www.jneurosci.org/content/21/16/6170>.
- 71 Coppola, V., Kucera, J., Palko, M. E. et al. (2001). Dissection of NT3 functions in vivo by gene replacement strategy. *Development* 128, 4315-27, <http://dev.biologists.org/content/128/21/4315>.

- 72 Song, H.-j., Ming, G.-l. & Poo, M.-m. (1997). cAMP-induced switching in turning direction of nerve growth cones. *Nature* 388, 275-79, <http://www.nature.com/nature/journal/v388/n6639/full/388275a0.html>.
- 73 McCaig, C., Sangster, L. & Stewart, R. (2000). Neurotrophins enhance electric field-directed growth cone guidance and directed nerve branching. *Developmental Dynamics* 217, 299-308, [http://dx.doi.org/10.1002/\(SICI\)1097-0177\(200003\)217:3<299::AID-DVDY8>3.0.CO;2-G](http://dx.doi.org/10.1002/(SICI)1097-0177(200003)217:3<299::AID-DVDY8>3.0.CO;2-G).
- 74 Tritsch, N. X., Rodríguez-Contreras, A., Crins, T. T. H. et al. (2010). Calcium action potentials in hair cells pattern auditory neuron activity before hearing onset. *Nat Neurosci* 13, 1050-2, <http://dx.doi.org/10.1038/nn.2604>.
- 75 Tritsch, N. X., Yi, E., Gale, J. E., Glowatzki, E. & Bergles, D. E. (2007). The origin of spontaneous activity in the developing auditory system. *Nature* 450, 50-5, <http://dx.doi.org/10.1038/nature06233>.
- 76 Hubel, D. H. & Wiesel, T. N. (1963). Shape and arrangement of columns in cat's striate cortex. *The Journal of physiology* 165, 559-68, <http://dx.doi.org/10.1113/jphysiol.1963.sp007079>.
- 77 Hubel, D. H. & Wiesel, T. N. (1970). The period of susceptibility to the physiological effects of unilateral eye closure in kittens. *The Journal of physiology* 206, 419-36, <http://dx.doi.org/10.1113/jphysiol.1970.sp009022>.
- 78 Katz, L. C. & Shatz, C. J. (1996). Synaptic activity and the construction of cortical circuits. *Science* 274, 1133-8, <http://dx.doi.org/10.1126/science.274.5290.1133>.
- 79 Chapman, B., Jacobson, M. D., Reiter, H. O. & Stryker, M. P. (1986). Ocular dominance shift in kitten visual cortex caused by imbalance in retinal electrical activity. *Nature* 324, 154-56, <http://dx.doi.org/10.1038/324154a0>.
- 80 Feller, M. B. & Scanziani, M. (2005). A precritical period for plasticity in visual cortex. *Current Opinion in Neurobiology* 15, 94-100, <http://www.sciencedirect.com/science/article/pii/S0959438805000139>.
- 81 Hensch, T. K. (2005). Critical period mechanisms in developing visual cortex. *Current Topics in Developmental Biology* 69, 215-37, [http://dx.doi.org/10.1016/S0070-2153\(05\)69008-4](http://dx.doi.org/10.1016/S0070-2153(05)69008-4).
- 82 Van der Loos, H. & Woolsey, T. A. (1973). Somatosensory Cortex: Structural Alterations following Early Injury to Sense Organs. *Science* 179, 395-98, <http://dx.doi.org/10.1126/science.179.4071.395>.
- 83 Sanes, D. H. & Siverls, V. (1991). Development and specificity of inhibitory terminal arborizations in the central nervous system. *J Neurobiol* 22, 837-54, <http://www3.interscience.wiley.com/cgi-bin/fulltext/109699527/PDFSTART>.
- 84 Kapfer, C., Seidl, A. H., Schweizer, H. & Grothe, B. (2002). Experience-dependent refinement of inhibitory inputs to auditory coincidence-detector neurons. *Nat Neurosci* 5, 247-53, <http://dx.doi.org/10.1038/nn810>.

Neural Activity During the Formation of a Giant Auditory Synapse

- 85 Clause, A., Kim, G., Sonntag, M. et al. (2014). The precise temporal pattern of prehearing spontaneous activity is necessary for tonotopic map refinement. *Neuron* 82, 822-35, <http://dx.doi.org/10.1016/j.neuron.2014.04.001>.
- 86 Seidl, A. H. & Grothe, B. (2005). Development of sound localization mechanisms in the mongolian gerbil is shaped by early acoustic experience. *J Neurophysiol* 94, 1028-36, <http://jn.physiology.org/cgi/content/full/94/2/1028>.
- 87 Sanes, D. & Constantine-Paton, M. (1983). Altered activity patterns during development reduce neural tuning. *Science* 221, 1183-85, <http://dx.doi.org/10.1126/science.6612332>
- 88 Leake, P. A., Snyder, R. L. & Hradek, G. T. (2002). Postnatal refinement of auditory nerve projections to the cochlear nucleus in cats. *J Comp Neurol* 448, 6-27, <http://dx.doi.org/10.1002/cne.10176>.
- 89 Kuwabara, N., DiCaprio, R. A. & Zook, J. M. (1991). Afferents to the medial nucleus of the trapezoid body and their collateral projections. *Journal of Comparative Neurology* 314, 684-706, <http://dx.doi.org/10.1002/cne.903140405>.
- 90 Rodríguez-Contreras, A., van Hoesve, J. S., Habets, R. L. P., Locher, H. & Borst, J. G. G. (2008). Dynamic development of the calyx of Held synapse. *Proc Natl Acad Sci U S A* 105, 5603-8, <http://dx.doi.org/10.1073/pnas.0801395105>.
- 91 Ford, M. C., Grothe, B. & Klug, A. (2009). Fenestration of the calyx of Held occurs sequentially along the tonotopic axis, is influenced by afferent activity, and facilitates glutamate clearance. *J Comp Neurol* 514, 92-106, <http://dx.doi.org/10.1002/cne.21998>.
- 92 Rodríguez-Contreras, A., de Lange, R. P. J., Lucassen, P. J. & Borst, J. G. G. (2006). Branching of calyceal afferents during postnatal development in the rat auditory brainstem. *J Comp Neurol* 496, 214-28, <http://dx.doi.org/10.1002/cne.20918>.
- 93 Youssoufian, M., Couchman, K., Shivdasani, M. N., Paolini, A. G. & Walmsley, B. (2008). Maturation of auditory brainstem projections and calyces in the congenitally deaf (dn/dn) mouse. *J Comp Neurol* 506, 442-51, <http://dx.doi.org/10.1002/cne.21566>.
- 94 Wright, S., Hwang, Y. & Oertel, D. (2014). Synaptic transmission between end bulbs of Held and bushy cells in the cochlear nucleus of mice with a mutation in Otoferrin. *Journal of Neurophysiology* 112, 3173-88, <http://dx.doi.org/10.1152/jn.00522.2014>.
- 95 Leao, R. N., Sun, H., Svahn, K. et al. (2006). Topographic organization in the auditory brainstem of juvenile mice is disrupted in congenital deafness. *J Physiol* 571, 563-78, <http://jp.physoc.org/content/571/3/563.full>.
- 96 Wu, S. H. & Oertel, D. (1987). Maturation of synapses and electrical properties of cells in the cochlear nuclei. *Hear Res* 30, 99-110, [http://dx.doi.org/10.1016/0378-5955\(87\)90187-0](http://dx.doi.org/10.1016/0378-5955(87)90187-0).
- 97 Rusu, S. I. & Borst, J. G. G. (2011). Developmental changes in intrinsic excitability of principal neurons in the rat medial nucleus of the trapezoid body. *Dev Neurobiol* 71, 284-95, <http://dx.doi.org/10.1002/dneu.20856>.

- 98 Grande, G., Negandhi, J., Harrison, R. V. & Wang, L. Y. (2014). Remodelling at the calyx of Held-MNTB synapse in mice developing with unilateral conductive hearing loss. *J Physiol* 592, 1581-600, <http://dx.doi.org/10.1113/jphysiol.2013.268839>.
- 99 Ryugo, D. K., Wu, M. M. & Pongstaporn, T. (1996). Activity-related features of synapse morphology: a study of endbulbs of held. *J Comp Neurol* 365, 141-58, [http://dx.doi.org/10.1002/\(SICI\)1096-9861\(19960129\)365:1<141::AID-CNE11>3.0.CO;2-T](http://dx.doi.org/10.1002/(SICI)1096-9861(19960129)365:1<141::AID-CNE11>3.0.CO;2-T).
- 100 Nicol, M. J. & Walmsley, B. (2002). Ultrastructural basis of synaptic transmission between endbulbs of Held and bushy cells in the rat cochlear nucleus. *J Physiol* 539, 713-23, <http://dx.doi.org/10.1113/jphysiol.2001.012972>.
- 101 Taschenberger, H., Leão, R. M., Rowland, K. C., Spirou, G. A. & von Gersdorff, H. (2002). Optimizing synaptic architecture and efficiency for high-frequency transmission. *Neuron* 36, 1127-43, [http://dx.doi.org/10.1016/S0896-6273\(02\)01137-6](http://dx.doi.org/10.1016/S0896-6273(02)01137-6).
- 102 Turrigiano, G. G. & Nelson, S. B. (2004). Homeostatic plasticity in the developing nervous system. *Nat Rev Neurosci* 5, 97-107, <http://dx.doi.org/10.1038/nrn1327>.
- 103 Wang, Han C., Lin, C.-C., Cheung, R. et al. (2015). Spontaneous Activity of Cochlear Hair Cells Triggered by Fluid Secretion Mechanism in Adjacent Support Cells. *Cell* 163, 1348-59, <http://dx.doi.org/10.1016/j.cell.2015.10.070>.
- 104 Kros, C. J., Ruppersberg, J. P. & Rüsch, A. (1998). Expression of a potassium current in inner hair cells during development of hearing in mice. *Nature* 394, 281-4, <http://www.nature.com/nature/journal/v394/n6690/full/394281a0.html>.
- 105 Sendin, G., Bourien, J., Rassendren, F., Puel, J. L. & Nouvian, R. (2014). Spatiotemporal pattern of action potential firing in developing inner hair cells of the mouse cochlea. *Proc Natl Acad Sci U S A* 111, 1999-2004, <http://dx.doi.org/10.1073/pnas.1319615111>.
- 106 Johnson, S. L., Eckrich, T., Kuhn, S. et al. (2011). Position-dependent patterning of spontaneous action potentials in immature cochlear inner hair cells. *Nat Neurosci* 14, 711-7, <http://dx.doi.org/10.1038/nn.2803>.
- 107 Glowatzki, E. & Fuchs, P. A. (2000). Cholinergic Synaptic Inhibition of Inner Hair Cells in the Neonatal Mammalian Cochlea. *Science* 288, 2366-68, <http://science.sciencemag.org/content/sci/288/5475/2366.full.pdf>.
- 108 Hoffpauir, B. K., Marrs, G. S., Mathers, P. H. & Spirou, G. A. (2009). Does the brain connect before the periphery can direct? A comparison of three sensory systems in mice. *Brain Research* 1277, 115-29, <http://dx.doi.org/10.1016/j.brainres.2009.02.050>.
- 109 Lelli, A., Asai, Y., Forge, A., Holt, J. R. & Géléoc, G. S. G. (2009). Tonal Gradient in the Developmental Acquisition of Sensory Transduction in Outer Hair Cells of the Mouse Cochlea. *Journal of Neurophysiology* 101, 2961-73, <https://dx.doi.org/10.1152/jn.00136.2009>.
- 110 Fettiplace, R. & Kim, K. X. (2014). The Physiology of Mechanoelectrical Transduction Channels in Hearing. *Physiological Reviews* 94, 951-86, <https://dx.doi.org/10.1152/physrev.00038.2013>.

Neural Activity During the Formation of a Giant Auditory Synapse

- 111 Wang, H. C. & Bergles, D. E. (2015). Spontaneous activity in the developing auditory system. *Cell Tissue Res* 361, 65-75, <http://dx.doi.org/10.1007/s00441-014-2007-5>.
- 112 Sanes, D. H. & Takács, C. (1993). Activity-dependent refinement of inhibitory connections. *European Journal of Neuroscience* 5, 570-4, <http://dx.doi.org/10.1111/j.1460-9568.1993.tb00522.x>.
- 113 Mostafapour, S. P., Cochran, S. L., Del Puerto, N. M. & Rubel, E. W. (2000). Patterns of cell death in mouse anteroventral cochlear nucleus neurons after unilateral cochlea removal. *The Journal of Comparative Neurology* 426, 561-71, [http://dx.doi.org/10.1002/1096-9861\(20001030\)426:4<561::AID-CNE5>3.0.CO;2-G](http://dx.doi.org/10.1002/1096-9861(20001030)426:4<561::AID-CNE5>3.0.CO;2-G).
- 114 Leake, P. A., Hradek, G. T., Chair, L. & Snyder, R. L. (2006). Neonatal deafness results in degraded topographic specificity of auditory nerve projections to the cochlear nucleus in cats. *The Journal of Comparative Neurology* 497, 13-31, <http://dx.doi.org/10.1002/cne.20968>.
- 115 Leao, R. N., Oleskevich, S., Sun, H. et al. (2004). Differences in glycinergic mIPSCs in the auditory brain stem of normal and congenitally deaf neonatal mice. *J Neurophysiol* 91, 1006-12, <http://jn.physiology.org/cgi/content/full/91/2/1006>.
- 116 Oleskevich, S., Youssoufian, M. & Walmsley, B. (2004). Presynaptic plasticity at two giant auditory synapses in normal and deaf mice. *J Physiol* 560, 709-19, <http://jp.physoc.org/content/560/3/709.long>.
- 117 Oleskevich, S. & Walmsley, B. (2002). Synaptic transmission in the auditory brainstem of normal and congenitally deaf mice. *J Physiol* 540, 447-55, <http://dx.doi.org/10.1113/jphysiol.2001.013821>.
- 118 Leão, R. N., Naves, M. M., Leão, K. E. & Walmsley, B. (2006). Altered sodium currents in auditory neurons of congenitally deaf mice. *Eur J Neurosci* 24, 1137-46, <http://dx.doi.org/10.1111/j.1460-9568.2006.04982.x>.
- 119 Cao, X.-J., McGinley, M. J. & Oertel, D. (2008). Connections and synaptic function in the posteroventral cochlear nucleus of deaf jerker mice. *The Journal of Comparative Neurology* 510, 297-308, <http://dx.doi.org/10.1002/cne.21788>.
- 120 Couchman, K., Garrett, A., Deardorff, A. S. et al. (2011). Lateral superior olive function in congenital deafness. *Hearing Research* 277, 163-75, <https://dx.doi.org/10.1016/j.heares.2011.01.012>.
- 121 Sanes, D. H., Markowitz, S., Bernstein, J. & Wardlow, J. (1992). The influence of inhibitory afferents on the development of postsynaptic dendritic arbors. *J Comp Neurol* 321, 637-44, <http://dx.doi.org/10.1002/cne.903210410>.
- 122 Erazo-Fischer, E., Striessnig, J. & Taschenberger, H. (2007). The role of physiological afferent nerve activity during in vivo maturation of the calyx of Held synapse. *J Neurosci* 27, 1725-37, <http://www.jneurosci.org/cgi/content/full/27/7/1725>.
- 123 Hirtz, J. J., Boesen, M., Braun, N. et al. (2011). Cav1.3 calcium channels are required for normal development of the auditory brainstem. *J Neurosci* 31, 8280-94, <http://dx.doi.org/10.1523/JNEUROSCI.5098-10.2011>.

- 124 Hirtz, J. J., Braun, N., Griesemer, D. et al. (2012). Synaptic Refinement of an Inhibitory Topographic Map in the Auditory Brainstem Requires Functional CaV_{1.3} Calcium Channels. *The Journal of Neuroscience* 32, 14602-16, <https://dx.doi.org/10.1523/jneurosci.0765-12.2012>.
- 125 Noh, J., Seal, R. P., Garver, J. A., Edwards, R. H. & Kandler, K. (2010). Glutamate co-release at GABA/glycinergic synapses is crucial for the refinement of an inhibitory map. *Nat Neurosci* 13, 232-38, <http://dx.doi.org/10.1038/nn.2478>.
- 126 Seal, R. P., Akil, O., Yi, E. et al. (2008). Sensorineural Deafness and Seizures in Mice Lacking Vesicular Glutamate Transporter 3. *Neuron* 57, 263-75, <http://www.sciencedirect.com/science/article/pii/S0896627307010227>.
- 127 Toyoshima, M., Sakurai, K., Shimazaki, K. et al. (2009). Deficiency of neural recognition molecule NB-2 affects the development of glutamatergic auditory pathways from the ventral cochlear nucleus to the superior olivary complex in mouse. *Dev Biol* 336, 192-200, <http://dx.doi.org/10.1016/j.ydbio.2009.09.043>.
- 128 Hashisaki, G. T. & Rubel, E. W. (1989). Effects of unilateral cochlea removal on anteroventral cochlear nucleus neurons in developing gerbils. *Journal of Comparative Neurology* 283, 465-73, <http://dx.doi.org/10.1002/cne.902830402>.
- 129 Harris, J. A., Hardie, N. A., Bermingham-McDonogh, O. & Rubel, E. W. (2005). Gene expression differences over a critical period of afferent-dependent neuron survival in the mouse auditory brainstem. *The Journal of Comparative Neurology* 493, 460-74, <http://dx.doi.org/10.1002/cne.20776>.
- 130 McKay, S. M. & Oleskevich, S. (2007). The role of spontaneous activity in development of the endbulb of Held synapse. *Hearing Research* 230, 53-63, <https://dx.doi.org/10.1016/j.heares.2007.05.006>.
- 131 Sun, J.-Y. & Wu, L.-G. (2001). Fast kinetics of exocytosis revealed by simultaneous measurements of presynaptic capacitance and postsynaptic currents at a central synapse. *Neuron* 30, 171-82, [http://dx.doi.org/10.1016/S0896-6273\(01\)00271-9](http://dx.doi.org/10.1016/S0896-6273(01)00271-9).
- 132 Kay, A. R., Alfonso, A., Alford, S. et al. (1999). Imaging synaptic activity in intact brain and slices with FM1-43 in *C. elegans*, lamprey, and rat. *Neuron* 24, 809-17, [http://dx.doi.org/10.1016/S0896-6273\(00\)81029-6](http://dx.doi.org/10.1016/S0896-6273(00)81029-6).
- 133 Guinan, J. J., Jr. & Li, R. Y.-S. (1990). Signal processing in brainstem auditory neurons which receive giant endings (calyces of Held) in the medial nucleus of the trapezoid body of the cat. *Hear Res* 49, 321-34, [http://dx.doi.org/10.1016/0378-5955\(90\)90111-2](http://dx.doi.org/10.1016/0378-5955(90)90111-2).
- 134 Lorteije, J. A. M., Rusu, S. I., Kushmerick, C. & Borst, J. G. G. (2009). Reliability and precision of the mouse calyx of Held synapse. *J Neurosci* 29, 13770-84, <http://dx.doi.org/10.1523/JNEUROSCI.3285-09.2009>.
- 135 Morest, D. K. (1968). The collateral system of the medial nucleus of the trapezoid body of the cat, its neuronal architecture and relation to the olivo-cochlear bundle. *Brain Research* 9, 288-311, [http://dx.doi.org/10.1016/0006-8993\(68\)90235-7](http://dx.doi.org/10.1016/0006-8993(68)90235-7).

Neural Activity During the Formation of a Giant Auditory Synapse

- 136 Holcomb, P. S., Hoffpauir, B. K., Hoyson, M. C. et al. (2013). Synaptic inputs compete during rapid formation of the calyx of Held: a new model system for neural development. *J Neurosci* 33, 12954-69, <http://dx.doi.org/10.1523/JNEUROSCI.1087-13.2013>.
- 137 Hoffpauir, B. K., Grimes, J. L., Mathers, P. H. & Spirou, G. A. (2006). Synaptogenesis of the calyx of Held: rapid onset of function and one-to-one morphological innervation. *J Neurosci* 26, 5511-23, <http://dx.doi.org/10.1523/JNEUROSCI.5525-05.2006>.
- 138 Bergsman, J. B., De Camilli, P. & McCormick, D. A. (2004). Multiple large inputs to principal cells in the mouse medial nucleus of the trapezoid body. *J Neurophysiol* 92, 545-52, <http://dx.doi.org/10.1152/jn.00927.2003>.
- 139 Debanne, D., Campanac, E., Bialowas, A., Carlier, E. & Alcaraz, G. (2011). Axon physiology. *Physiol Rev* 91, 555-602, <http://dx.doi.org/10.1152/physrev.00048.2009>
- 140 Bucher, D. & Goillard, J. M. (2011). Beyond faithful conduction: short-term dynamics, neuromodulation, and long-term regulation of spike propagation in the axon. *Prog Neurobiol* 94, 307-46, <http://dx.doi.org/10.1016/j.pneurobio.2011.06.001>.
- 141 Rancz, E. A., Ishikawa, T., Duguid, I. et al. (2007). High-fidelity transmission of sensory information by single cerebellar mossy fibre boutons. *Nature* 450, 1245-8, <http://dx.doi.org/10.1038/nature05995>.
- 142 Geiger, J. R. & Jonas, P. (2000). Dynamic control of presynaptic Ca₂₊ inflow by fast-inactivating K⁺ channels in hippocampal mossy fiber boutons. *Neuron* 28, 927-39, [http://dx.doi.org/10.1016/S0896-6273\(00\)00164-1](http://dx.doi.org/10.1016/S0896-6273(00)00164-1).
- 143 Barrett, E. F. & Barrett, J. N. (1982). Intracellular recording from vertebrate myelinated axons: mechanism of the depolarizing afterpotential. *Journal of Physiology* 323, 117-44, <http://dx.doi.org/10.1113/jphysiol.1982.sp014064>.
- 144 Lin, J. W. (2008). Electrophysiological events recorded at presynaptic terminals of the crayfish neuromuscular junction with a voltage indicator. *J Physiol* 586, 4935-50, <http://dx.doi.org/10.1113/jphysiol.2008.158089>.
- 145 Powell, K., Mathy, A., Duguid, I. & Häusser, M. (2015). Synaptic representation of locomotion in single cerebellar granule cells. *Elife* 4, <http://dx.doi.org/10.7554/eLife.07290>.
- 146 Begum, R., Bakiri, Y., Volynski, K. E. & Kullmann, D. M. (2016). Action potential broadening in a presynaptic channelopathy. *Nat Commun* 7, 12102, <http://dx.doi.org/10.1038/ncomms12102>.
- 147 Llinás, R., Steinberg, I. Z. & Walton, K. (1981). Presynaptic calcium currents in squid giant synapse. *Biophys J* 33, 289-321, [http://dx.doi.org/10.1016/S0006-3495\(81\)84898-9](http://dx.doi.org/10.1016/S0006-3495(81)84898-9).
- 148 Poage, R. E. & Zengel, J. E. (2002). Repolarization of the presynaptic action potential and short-term synaptic plasticity in the chick ciliary ganglion. *Synapse* 46, 189-98, <http://dx.doi.org/10.1002/syn.10135>.

- 149 Hoppa, M. B., Gouzer, G., Armbruster, M. & Ryan, T. A. (2014). Control and plasticity of the presynaptic action potential waveform at small CNS nerve terminals. *Neuron* 84, 778-89, <http://dx.doi.org/10.1016/j.neuron.2014.09.038>.
- 150 Ford, K. J. & Davis, G. W. (2014). Archaelhodopsin voltage imaging: synaptic calcium and BK channels stabilize action potential repolarization at the *Drosophila* neuromuscular junction. *J Neurosci* 34, 14517-25, <http://dx.doi.org/10.1523/JNEUROSCI.2203-14.2014>.
- 151 Hu, H. & Jonas, P. (2014). A supercritical density of Na⁺ channels ensures fast signaling in GABAergic interneuron axons. *Nat Neurosci* 17, 686-93, <http://dx.doi.org/10.1038/nn.3678>.
- 152 Kim, J. H., Kushmerick, C. & von Gersdorff, H. (2010). Presynaptic resurgent Na⁺ currents sculpt the action potential waveform and increase firing reliability at a CNS nerve terminal. *J Neurosci* 30, 15479-90, <http://dx.doi.org/10.1523/JNEUROSCI.3982-10.2010>.
- 153 Sierksma, M. C., Tedja, M. S. & Borst, J. G. (2017). In vivo matching of postsynaptic excitability with spontaneous synaptic inputs during formation of the rat calyx of Held synapse. *J Physiol* 595, 207-31, <http://dx.doi.org/10.1113/JP272780>.
- 154 Lewis, A. H. & Raman, I. M. (2014). Resurgent current of voltage-gated Na⁺ channels. *J Physiol* 592, 4825-38, <http://dx.doi.org/10.1113/jphysiol.2014.277582>.
- 155 Crins, T. T. H., Rusu, S. I., Rodríguez-Contreras, A. & Borst, J. G. G. (2011). Developmental changes in short-term plasticity at the rat calyx of Held synapse. *J Neurosci* 31, 11706-17, <http://dx.doi.org/10.1523/JNEUROSCI.1995-11.2011>.
- 156 Taschenberger, H. & von Gersdorff, H. (2000). Fine-tuning an auditory synapse for speed and fidelity: developmental changes in presynaptic waveform, EPSC kinetics, and synaptic plasticity. *J Neurosci* 20, 9162-73, <http://www.jneurosci.org/cgi/content/full/20/24/9162>.
- 157 Chuhma, N. & Ohmori, H. (1998). Postnatal development of phase-locked high-fidelity synaptic transmission in the medial nucleus of the trapezoid body of the rat. *J Neurosci* 18, 512-20, <http://www.jneurosci.org/cgi/content/full/18/1/512>.
- 158 Bean, B. P. (2007). The action potential in mammalian central neurons. *Nat Rev Neurosci* 8, 451-65, <http://dx.doi.org/10.1038/nrn2148>.
- 159 Leão, R. M., Kushmerick, C., Pinaud, R. et al. (2005). Presynaptic Na⁺ channels: locus, development, and recovery from inactivation at a high-fidelity synapse. *J Neurosci* 25, 3724-38, <http://dx.doi.org/10.1523/JNEUROSCI.3983-04.2005>.
- 160 Lewis, A. H. & Raman, I. M. (2014). Resurgent current of voltage-gated Na⁺ channels. *Journal of Physiology* 592, 4825-38, <http://dx.doi.org/10.1113/jphysiol.2014.277582>.
- 161 Berret, E., Kim, S. E., Lee, S. Y., Kushmerick, C. & Kim, J. H. (2016). Functional and structural properties of ion channels at the nerve terminal depends on compact myelin. *J Physiol* 594, 5593-609, <http://dx.doi.org/10.1113/JP272205>.

Neural Activity During the Formation of a Giant Auditory Synapse

- 162 Xu, J., Berret, E. & Kim, J. H. (2016). Activity-dependent formation and location of voltage-gated sodium channel clusters at a CNS nerve terminal during postnatal development. *Journal of Neurophysiology*, <http://dx.doi.org/10.1152/jn.00617.2016>.
- 163 Zhou, W. & Goldin, A. L. (2004). Use-dependent potentiation of the Nav1.6 sodium channel. *Biophys J* 87, 3862-72, <http://dx.doi.org/10.1529/biophysj.104.045963>.
- 164 Kaplan, M. R., Cho, M. H., Ullian, E. M. et al. (2001). Differential control of clustering of the sodium channels Nav1.2 and Nav1.6 at developing CNS nodes of Ranvier. *Neuron* 30, 105-19, [http://dx.doi.org/10.1016/S0896-6273\(01\)00266-5](http://dx.doi.org/10.1016/S0896-6273(01)00266-5).
- 165 Huang, H. & Trussell, L. O. (2011). KCNQ5 channels control resting properties and release probability of a synapse. *Nat Neurosci* 14, 840-7, <http://dx.doi.org/10.1038/nn.2830>.
- 166 Huang, H. & Trussell, L. O. (2008). Control of presynaptic function by a persistent Na⁺ current. *Neuron* 60, 975-9, <http://dx.doi.org/10.1016/j.neuron.2008.10.052>.
- 167 Ishikawa, T., Nakamura, Y., Saitoh, N. et al. (2003). Distinct roles of Kv1 and Kv3 potassium channels at the calyx of Held presynaptic terminal. *J Neurosci* 23, 10445-53, <http://www.jneurosci.org/cgi/content/full/23/32/10445>.
- 168 Kim, J. H. & von Gersdorff, H. (2012). Suppression of spikes during posttetanic hyperpolarization in auditory neurons: the role of temperature, Ih currents, and the Na⁺-K⁺-ATPase pump. *J Neurophysiol* 108, 1924-32, <http://dx.doi.org/10.1152/jn.00103.2012>.
- 169 Cuttle, M. F., Rusznák, Z., Wong, A. Y., Owens, S. & Forsythe, I. D. (2001). Modulation of a presynaptic hyperpolarization-activated cationic current (I_h) at an excitatory synaptic terminal in the rat auditory brainstem. *J Physiol* 534, 733-44, <http://dx.doi.org/10.1111/j.1469-7793.2001.00733.x>.
- 170 Kim, J. H., Sizov, I., Dobretsov, M. & von Gersdorff, H. (2007). Presynaptic Ca²⁺ buffers control the strength of a fast post-tetanic hyperpolarization mediated by the α₃ Na⁺/K⁺-ATPase. *Nat Neurosci* 10, 196-205, <http://dx.doi.org/10.1038/nn1839>.
- 171 Dodson, P. D., Billups, B., Rusznák, Z. et al. (2003). Presynaptic rat Kv1.2 channels suppress synaptic terminal hyperexcitability following action potential invasion. *J Physiol* 550, 27-33, <http://jp.physoc.org/content/550/1/27.long>.
- 172 Yang, Y. M., Wang, W., Fedchyshyn, M. J. et al. (2014). Enhancing the fidelity of neurotransmission by activity-dependent facilitation of presynaptic potassium currents. *Nat Commun* 5, 4564, <http://dx.doi.org/10.1038/ncomms5564>.
- 173 Alle, H., Roth, A. & Geiger, J. R. P. (2009). Energy-efficient action potentials in hippocampal mossy fibers. *Science* 325, 1405-8, <http://dx.doi.org/10.1126/science.1174331>.
- 174 Soleng, A. F., Baginskas, A., Andersen, P. & Raastad, M. (2004). Activity-dependent excitability changes in hippocampal CA₃ cell Schaffer axons. *J Physiol* 560, 491-503, <http://dx.doi.org/10.1113/jphysiol.2004.071225>.
- 175 Borst, J. G. G. & Sakmann, B. (1999). Effect of changes in action potential shape on calcium currents and transmitter release in a calyx-type synapse of the rat auditory brainstem. *Philos Trans R Soc Lond B Biol Sci* 354, 347-55, <http://rstb.royalsocietypublishing.org/content/354/1381/347.long>.

- 176 Clarke, S. G., Scarnati, M. S. & Paradiso, K. G. (2016). Neurotransmitter release can be stabilized by a mechanism that prevents voltage changes near the end of action potentials from affecting calcium currents. *Journal of Neuroscience* 36, 11559–72, <http://dx.doi.org/10.1523/JNEUROSCI.0066-16.2016>.
- 177 Bischofberger, J., Engel, D., Frotscher, M. & Jonas, P. (2006). Timing and efficacy of transmitter release at mossy fiber synapses in the hippocampal network. *Pflügers Arch* 453, 361–72, <http://dx.doi.org/10.1007/s00424-006-0093-2>.
- 178 de Ruiter, M. M., De Zeeuw, C. I. & Hansel, C. (2006). Voltage-gated sodium channels in cerebellar Purkinje cells of mormyrid fish. *J Neurophysiol* 96, 378–90, <http://dx.doi.org/10.1152/jn.00906.2005>.
- 179 Jenkins, S. M. & Bennett, V. (2001). Ankyrin-G coordinates assembly of the spectrin-based membrane skeleton, voltage-gated sodium channels, and L1 CAMs at Purkinje neuron initial segments. *Journal of Cell Biology* 155, 739–46, <http://dx.doi.org/10.1083/jcb.200109026>.
- 180 Black, J. A., Renganathan, M. & Waxman, S. G. (2002). Sodium channel Nav1.6 is expressed along nonmyelinated axons and it contributes to conduction. *Molecular Brain Research* 105, 19–28, [http://dx.doi.org/10.1016/S0169-328X\(02\)00385-6](http://dx.doi.org/10.1016/S0169-328X(02)00385-6).
- 181 Kil, J., Kageyama, G. H., Semple, M. N. & Kitzes, L. M. (1995). Development of ventral cochlear nucleus projections to the superior olivary complex in gerbil. *J Comp Neurol* 353, 317–40, <http://dx.doi.org/10.1002/cne.903530302>.
- 182 Wimmer, V. C., Nevian, T. & Kuner, T. (2004). Targeted in vivo expression of proteins in the calyx of Held. *Pflügers Arch* 449, 319–33, <http://dx.doi.org/10.1007/s00424-004-1327-9>.
- 183 Sonntag, M., Englitz, B., Kopp-Scheinflug, C. & Rübsamen, R. (2009). Early postnatal development of spontaneous and acoustically evoked discharge activity of principal cells of the medial nucleus of the trapezoid body: an in vivo study in mice. *J Neurosci* 29, 9510–20, <http://dx.doi.org/10.1523/JNEUROSCI.1377-09.2009>.
- 184 Kolson, D. R., Wan, J., Wu, J. et al. (2016). Temporal patterns of gene expression during calyx of Held development. *Dev Neurobiol* 76, 166–89, <http://dx.doi.org/10.1002/dneu.22306>.
- 185 Ehmann, H., Hartwich, H., Salzig, C. et al. (2013). Time-dependent gene expression analysis of the developing superior olivary complex. *J Biol Chem* 288, 25865–79, <http://dx.doi.org/10.1074/jbc.M113.490508>.
- 186 Berntson, A. K. & Walmsley, B. (2008). Characterization of a potassium-based leak conductance in the medial nucleus of the trapezoid body. *Hear Res* 244, 98–106, <http://dx.doi.org/10.1016/j.heares.2008.08.003>.
- 187 Leao, R. N., Svahn, K., Berntson, A. & Walmsley, B. (2005). Hyperpolarization-activated (I_h) currents in auditory brainstem neurons of normal and congenitally deaf mice. *Eur J Neurosci* 22, 147–57, <http://dx.doi.org/10.1111/j.1460-9568.2005.04185.x>.
- 188 Gao, H. & Lu, Y. (2008). Early development of intrinsic and synaptic properties of chicken nucleus laminaris neurons. *Neuroscience* 153, 131–43, <http://dx.doi.org/10.1016/j.neuroscience.2008.01.059>.

Neural Activity During the Formation of a Giant Auditory Synapse

- 189 Kuenzel, T., Wirth, M. J., Luksch, H., Wagner, H. & Mey, J. (2009). Increase of Kv3.1b expression in avian auditory brainstem neurons correlates with synaptogenesis in vivo and in vitro. *Brain Res* 1302, 64-75, <http://dx.doi.org/10.1016/j.brainres.2009.09.046>.
- 190 Dodson, P. D., Barker, M. C. & Forsythe, I. D. (2002). Two heteromeric Kv1 potassium channels differentially regulate action potential firing. *J Neurosci* 22, 6953-61, <http://www.jneurosci.org/cgi/content/full/22/16/6953>.
- 191 Johnston, J., Forsythe, I. D. & Kopp-Scheinpflug, C. (2010). Going native: voltage-gated potassium channels controlling neuronal excitability. *J Physiol* 588, 3187-200, <http://dx.doi.org/10.1113/jphysiol.2010.191973>.
- 192 Brew, H. M. & Forsythe, I. D. (1995). Two voltage-dependent K⁺ conductances with complementary functions in postsynaptic integration at a central auditory synapse. *J Neurosci* 15, 8011-22, <http://www.jneurosci.org/content/15/12/8011.long>.
- 193 Peusner, K. D., Gamkrelidze, G. & Giaume, C. (1998). Potassium currents and excitability in second-order auditory and vestibular neurons. *J Neurosci Res* 53, 511-20, [http://dx.doi.org/10.1002/\(SICI\)1097-4547\(19980901\)53:5<511::AID-JNR1>3.0.CO;2-C](http://dx.doi.org/10.1002/(SICI)1097-4547(19980901)53:5<511::AID-JNR1>3.0.CO;2-C).
- 194 Soria Van Hove, J. & Borst, J. G. G. (2010). Delayed appearance of the scaffolding proteins PSD-95 and Homer-1 at the developing rat calyx of Held synapse. *J Comp Neurol* 518, 4581-90, <http://dx.doi.org/10.1002/cne.22479>.
- 195 Ankri, N., Legendre, P., Faber, D. S. & Korn, H. (1994). Automatic detection of spontaneous synaptic responses in central neurons. *J Neurosci Methods* 52, 87-100, [http://dx.doi.org/10.1016/0165-0270\(94\)90060-4](http://dx.doi.org/10.1016/0165-0270(94)90060-4).
- 196 Williams, S. R. & Mitchell, S. J. (2008). Direct measurement of somatic voltage clamp errors in central neurons. *Nature Neuroscience* 11, 790-8, <http://dx.doi.org/10.1038/nn.2137>.
- 197 Traynelis, S. F. (1998). Software-based correction of single compartment series resistance errors. *Journal of Neuroscience Methods* 86, 25-34, [http://dx.doi.org/10.1016/S0165-0270\(98\)00140-X](http://dx.doi.org/10.1016/S0165-0270(98)00140-X).
- 198 Macica, C. M., von Hehn, C. A. A., Wang, L.-Y. et al. (2003). Modulation of the Kv3.1b potassium channel isoform adjusts the fidelity of the firing pattern of auditory neurons. *J Neurosci* 23, 1133-41, <http://www.jneurosci.org/cgi/content/full/23/4/1133>.
- 199 Steinert, J. R., Postlethwaite, M., Jordan, M. D. et al. (2010). NMDAR-mediated EPSCs are maintained and accelerate in time course during maturation of mouse and rat auditory brainstem in vitro. *J Physiol* 588, 447-63, <http://jp.physoc.org/content/588/3/447.long>.
- 200 Scott, L. L., Mathews, P. J. & Golding, N. L. (2005). Posthearing developmental refinement of temporal processing in principal neurons of the medial superior olive. *J Neurosci* 25, 7887-95, <http://dx.doi.org/10.1523/JNEUROSCI.1016-05.2005>.
- 201 Banks, M. I. & Smith, P. H. (1992). Intracellular recordings from neurobiotin-labeled cells in brain slices of the rat medial nucleus of the trapezoid body. *Journal of Neuroscience* 12, 2819-37, <http://www.jneurosci.org/cgi/reprint/12/7/2819>.

- 202 Tritsch, N. X. & Bergles, D. E. (2010). Developmental regulation of spontaneous activity in the mammalian cochlea. *J Neurosci* 30, 1539-50, <http://www.jneurosci.org/cgi/content/full/30/4/1539>.
- 203 Taschenberger, H., Scheuss, V. & Neher, E. (2005). Release kinetics, quantal parameters and their modulation during short-term depression at a developing synapse in the rat CNS. *J Physiol* 568, 513-37, <http://jp.physoc.org/content/568/2/513.long>.
- 204 Yang, B., Desai, R. & Kaczmarek, L. K. (2007). Slack and Slick KNa channels regulate the accuracy of timing of auditory neurons. *J Neurosci* 27, 2617-27, <http://dx.doi.org/10.1523/JNEUROSCI.5308-06.2007>.
- 205 Hardman, R. M. & Forsythe, I. D. (2009). Ether-à-go-go-related gene K⁺ channels contribute to threshold excitability of mouse auditory brainstem neurons. *J Physiol* 587, 2487-97, <http://jp.physoc.org/content/587/11/2487.long>.
- 206 Kuba, H., Koyano, K. & Ohmori, H. (2002). Development of membrane conductance improves coincidence detection in the nucleus laminaris of the chicken. *J Physiol* 540, 529-42, <http://dx.doi.org/10.1113/jphysiol.2001.013365>.
- 207 Shah, R. D. & Crair, M. C. (2008). Mechanisms of response homeostasis during retinocollicular map formation. *J Physiol* 586, 4363-9, <http://dx.doi.org/10.1113/jphysiol.2008.157222>.
- 208 Spitzer, N. C., Kingston, P. A., Manning, T. J. & Conklin, M. W. (2002). Outside and in: development of neuronal excitability. *Curr Opin Neurobiol* 12, 315-23, [http://dx.doi.org/10.1016/S0959-4388\(02\)00330-6](http://dx.doi.org/10.1016/S0959-4388(02)00330-6).
- 209 Moody, W. J. & Bosma, M. M. (2005). Ion channel development, spontaneous activity, and activity-dependent development in nerve and muscle cells. *Physiol Rev* 85, 883-941, <http://dx.doi.org/10.1152/physrev.00017.2004>.
- 210 Brew, H. M., Hallows, J. L. & Tempel, B. L. (2003). Hyperexcitability and reduced low threshold potassium currents in auditory neurons of mice lacking the channel subunit Kv1.1. *J Physiol* 548, 1-20, <http://dx.doi.org/10.1113/jphysiol.2002.035568>.
- 211 Goldberg, E. M., Clark, B. D., Zaghera, E. et al. (2008). K⁺ channels at the axon initial segment dampen near-threshold excitability of neocortical fast-spiking GABAergic interneurons. *Neuron* 58, 387-400, <http://dx.doi.org/10.1016/j.neuron.2008.03.003>.
- 212 Ramoa, A. S. & McCormick, D. A. (1994). Developmental changes in electrophysiological properties of LGNd neurons during reorganization of retinogeniculate connections. *J Neurosci* 14, 2089-97, <http://www.jneurosci.org/cgi/reprint/14/4/2089>.
- 213 Belleau, M. L. & Warren, R. A. (2000). Postnatal development of electrophysiological properties of nucleus accumbens neurons. *J Neurophysiol* 84, 2204-16, <http://jn.physiology.org/content/84/5/2204.long>.
- 214 Zhou, F.-M. & Hablitz, J. J. (1996). Postnatal development of membrane properties of layer I neurons in rat neocortex. *J Neurosci* 16, 1131-9, <http://www.jneurosci.org/content/16/3/1131.long>.

Neural Activity During the Formation of a Giant Auditory Synapse

- 215 Warren, R. A. & Jones, E. G. (1997). Maturation of neuronal form and function in a mouse thalamo-cortical circuit. *J Neurosci* 17, 277-95, <http://www.jneurosci.org/content/17/1/277.long>.
- 216 Rothman, J. S. & Manis, P. B. (2003). The roles potassium currents play in regulating the electrical activity of ventral cochlear nucleus neurons. *J Neurophysiol* 89, 3097-113, <http://dx.doi.org/10.1152/jn.00127.2002>.
- 217 Joshi, I., Yang, Y.-M. & Wang, L.-Y. (2007). Coincident activation of metabotropic glutamate receptors and NMDA receptors (NMDARs) downregulates perisynaptic/extrasynaptic NMDARs and enhances high-fidelity neurotransmission at the developing calyx of Held synapse. *J Neurosci* 27, 9989-99, <http://www.jneurosci.org/cgi/content/full/27/37/9989>.
- 218 Leão, R. M. & von Gersdorff, H. (2002). Noradrenaline increases high-frequency firing at the calyx of Held synapse during development by inhibiting glutamate release. *J Neurophysiol* 87, 2297-306, <http://jn.physiology.org/cgi/content/full/87/5/2297>.
- 219 Futai, K., Okada, M., Matsuyama, K. & Takahashi, T. (2001). High-fidelity transmission acquired via a developmental decrease in NMDA receptor expression at an auditory synapse. *J Neurosci* 21, 3342-9, <http://www.jneurosci.org/cgi/content/full/21/10/3342>.
- 220 Allene, C. & Cossart, R. (2010). Early NMDA receptor-driven waves of activity in the developing neocortex: physiological or pathological network oscillations? *J Physiol* 588, 83-91, <http://dx.doi.org/10.1113/jphysiol.2009.178798>.
- 221 Dilger, E. K., Krahe, T. E., Morhardt, D. R. et al. (2015). Absence of plateau potentials in dLGN cells leads to a breakdown in retinogeniculate refinement. *J Neurosci* 35, 3652-62, <http://dx.doi.org/10.1523/JNEUROSCI.2343-14.2015>.
- 222 Bollmann, J. H., Helmchen, F., Borst, J. G. G. & Sakmann, B. (1998). Postsynaptic Ca₂₊ influx mediated by three different pathways during synaptic transmission at a calyx-type synapse. *Journal of Neuroscience* 18, 10409-19, <http://www.jneurosci.org/content/18/24/10409.long>.
- 223 Ebbers, L., Satheesh, S. V., Janz, K. et al. (2015). L-type calcium channel Cav1.2 is required for maintenance of auditory brainstem nuclei. *J Biol Chem* 290, 23692-710, <http://dx.doi.org/10.1074/jbc.M115.672675>.
- 224 Satheesh, S. V., Kunert, K., Rüttiger, L. et al. (2012). Retrocochlear function of the peripheral deafness gene *Cacna1d*. *Hum Mol Genet* 21, 3896-909, <http://dx.doi.org/10.1093/hmg/dds217>.
- 225 Holcomb, P. S., Deerinck, T. J., Ellisman, M. H. & Spirou, G. A. (2013). Construction of a polarized neuron. *J Physiol* 591, 3145-50, <http://dx.doi.org/10.1113/jphysiol.2012.248542>.
- 226 West, A. E. & Greenberg, M. E. (2011). Neuronal activity-regulated gene transcription in synapse development and cognitive function. *Cold Spring Harb Perspect Biol* 3, <http://dx.doi.org/10.1101/cshperspect.a005744>.

- 227 Sanchez, J. T., Seidl, A. H., Rubel, E. W. & Barria, A. (2012). Control of neuronal excitability by NMDA-type glutamate receptors in early developing binaural auditory neurons. *J Physiol* 590, 4801-18, <http://dx.doi.org/10.1113/jphysiol.2012.228734>.
- 228 Walmsley, B., Berntson, A., Leao, R. N. & Fyffe, R. E. W. (2006). Activity-dependent regulation of synaptic strength and neuronal excitability in central auditory pathways. *J Physiol* 572, 313-21, <http://jp.physoc.org/content/572/2/313.full>.
- 229 Davis, G. W. (2013). Homeostatic signaling and the stabilization of neural function. *Neuron* 80, 718-28, <http://dx.doi.org/10.1016/j.neuron.2013.09.044>.
- 230 Wolfram, V., Southall, T. D., Günay, C. et al. (2014). The transcription factors islet and Lim3 combinatorially regulate ion channel gene expression. *J Neurosci* 34, 2538-43, <http://dx.doi.org/10.1523/JNEUROSCI.4511-13.2014>.
- 231 Rodríguez-Tornos, F. M., Briz, C. G., Weiss, L. A. et al. (2016). Cux1 Enables Interhemispheric Connections of Layer II/III Neurons by Regulating Kv1-Dependent Firing. *Neuron* 89, 494-506, <http://dx.doi.org/10.1016/j.neuron.2015.12.020>.
- 232 Dehorter, N., Ciceri, G., Bartolini, G. et al. (2015). Tuning of fast-spiking interneuron properties by an activity-dependent transcriptional switch. *Science* 349, 1216-20, <http://dx.doi.org/10.1126/science.aab3415>.
- 233 Kaczmarek, L. K., Bhattacharjee, A., Desai, R. et al. (2005). Regulation of the timing of MNTB neurons by short-term and long-term modulation of potassium channels. *Hear Res* 206, 133-45, <http://dx.doi.org/10.1016/j.heares.2004.11.023>.
- 234 Wolfram, V. & Baines, R. A. (2013). Blurring the boundaries: developmental and activity-dependent determinants of neural circuits. *Trends Neurosci* 36, 610-9, <http://dx.doi.org/10.1016/j.tins.2013.06.006>.
- 235 Kratsios, P., Pinan-Lucarré, B., Kerk, S. Y. et al. (2015). Transcriptional coordination of synaptogenesis and neurotransmitter signaling. *Curr Biol* 25, 1282-95, <http://dx.doi.org/10.1016/j.cub.2015.03.028>.
- 236 Santiago, C. & Bashaw, G. J. (2014). Transcription factors and effectors that regulate neuronal morphology. *Development* 141, 4667-80, <http://dx.doi.org/10.1242/dev.110817>.
- 237 Yin, J. & Yuan, Q. (2015). Structural homeostasis in the nervous system: a balancing act for wiring plasticity and stability. *Front Cell Neurosci* 8, 439, <http://dx.doi.org/10.3389/fncel.2014.00439>.
- 238 Atwood, H. L. & Karunanithi, S. (2002). Diversification of synaptic strength: presynaptic elements. *Nat Rev Neurosci* 3, 497-516, <http://dx.doi.org/10.1038/nrn876>.
- 239 Sätzler, K., Söhl, L. F., Bollmann, J. H. et al. (2002). Three-dimensional reconstruction of a calyx of Held and its postsynaptic principal neuron in the medial nucleus of the trapezoid body. *J Neurosci* 22, 10567-79, <http://www.jneurosci.org/cgi/content/full/22/24/10567>.

Neural Activity During the Formation of a Giant Auditory Synapse

- 240 Dondzillo, A., Sätzler, K., Horstmann, H. et al. (2010). Targeted three-dimensional immunohistochemistry reveals localization of presynaptic proteins Bassoon and Piccolo in the rat calyx of Held before and after the onset of hearing. *J Comp Neurol* 518, 1008-29, <http://dx.doi.org/10.1002/cne.22260>.
- 241 Denk, W. & Horstmann, H. (2004). Serial Block-Face Scanning Electron Microscopy to Reconstruct Three-Dimensional Tissue Nanostructure. *PLOS Biology* 2, e329, <https://dx.doi.org/10.1371/journal.pbio.0020329>.
- 242 Qiu, X., Zhu, Q. & Sun, J. (2015). Quantitative analysis of vesicle recycling at the calyx of Held synapse. *Proceedings of the National Academy of Sciences* 112, 4779-84, <http://www.pnas.org/content/112/15/4779.abstract>.
- 243 Südhof, Thomas C. (2012). The Presynaptic Active Zone. *Neuron* 75, 11-25, <http://dx.doi.org/10.1016/j.neuron.2012.06.012>.
- 244 Gundelfinger, E. D., Reissner, C. & Garner, C. C. (2016). Role of Bassoon and Piccolo in Assembly and Molecular Organization of the Active Zone. *Frontiers in Synaptic Neuroscience* 7, <https://www.frontiersin.org/article/10.3389/fnsyn.2015.00019>.
- 245 Gustafsson, M. G. L. (2005). Nonlinear structured-illumination microscopy: Wide-field fluorescence imaging with theoretically unlimited resolution. *Proceedings of the National Academy of Sciences of the United States of America* 102, 13081-86, <https://dx.doi.org/10.1073/pnas.0406877102>.
- 246 Huang, L.-K. & Wang, M.-J. J. (1995). Image thresholding by minimizing the measures of fuzziness. *Pattern recognition* 28, 41-51, [http://dx.doi.org/10.1016/0031-3203\(94\)E0043-K](http://dx.doi.org/10.1016/0031-3203(94)E0043-K).
- 247 Mc Laughlin, M., van der Heijden, M. & Joris, P. X. (2008). How secure is in vivo synaptic transmission at the calyx of Held? *J Neurosci* 28, 10206-19, <http://dx.doi.org/10.1523/JNEUROSCI.2735-08.2008>.
- 248 Sierksma, M. C. & Borst, J. G. G. (2017). Resistance to action potential depression of a rat axon terminal in vivo. *Proceedings of the National Academy of Sciences* 114, 4249-54, <https://dx.doi.org/10.1073/pnas.1619433114>.
- 249 Matho, K. S. H. Structure and dynamism in a central neural circuit in adulthood and postnatal development. PhD thesis, Université Pierre et Marie Curie, (2013).
- 250 Albrecht, O., Dondzillo, A., Mayer, F., Thompson, J. A. & Klug, A. (2014). Inhibitory projections from the ventral nucleus of the trapezoid body to the medial nucleus of the trapezoid body in the mouse. *Frontiers in Neural Circuits* 8, <https://www.frontiersin.org/article/10.3389/fncir.2014.00083>.
- 251 Awatramani, G. B., Turecek, R. & Trussell, L. O. (2004). Inhibitory control at a synaptic relay. *J Neurosci* 24, 2643-7, <http://www.jneurosci.org/cgi/content/full/24/11/2643>.
- 252 Awatramani, G. B., Turecek, R. & Trussell, L. O. (2005). Staggered development of GABAergic and glycinergic transmission in the MNTB. *J Neurophysiol* 93, 819-28, <http://dx.doi.org/10.1152/jn.00798.2004>.

- 253 Xiao, L., Michalski, N., Kronander, E. et al. (2013). BMP signaling specifies the development of a large and fast CNS synapse. *Nat Neurosci* 16, 856-64, <http://dx.doi.org/10.1038/nn.3414>.
- 254 Macpherson, L. J., Zaharieva, E. E., Kearney, P. J. et al. (2015). Dynamic labelling of neural connections in multiple colours by trans-synaptic fluorescence complementation. *Nature Communications* 6, 10024, <http://dx.doi.org/10.1038/ncomms10024>.
- 255 Colman, H., Nabekura, J. & Lichtman, J. W. (1997). Alterations in Synaptic Strength Preceding Axon Withdrawal. *Science* 275, 356-61, <https://dx.doi.org/10.1126/science.275.5298.356>.
- 256 Hashimoto, K. & Kano, M. (2003). Functional Differentiation of Multiple Climbing Fiber Inputs during Synapse Elimination in the Developing Cerebellum. *Neuron* 38, 785-96, [http://dx.doi.org/10.1016/S0896-6273\(03\)00298-8](http://dx.doi.org/10.1016/S0896-6273(03)00298-8).
- 257 Bosman, L. W. J., Takechi, H., Hartmann, J., Eilers, J. & Konnerth, A. (2008). Homosynaptic Long-Term Synaptic Potentiation of the “Winner” Climbing Fiber Synapse in Developing Purkinje Cells. *The Journal of Neuroscience* 28, 798-807, <https://dx.doi.org/10.1523/jneurosci.4074-07.2008>.
- 258 Hashimoto, K., Ichikawa, R., Kitamura, K., Watanabe, M. & Kano, M. (2009). Translocation of a “winner” climbing fiber to the Purkinje cell dendrite and subsequent elimination of “losers” from the soma in developing cerebellum. *Neuron* 63, 106-18, <http://dx.doi.org/10.1016/j.neuron.2009.06.008>.
- 259 Watanabe, M. & Kano, M. (2011). Climbing fiber synapse elimination in cerebellar Purkinje cells. *Eur J Neurosci* 34, 1697-710, <http://dx.doi.org/10.1111/j.1460-9568.2011.07894.x>.
- 260 Carrillo, J., Nishiyama, N. & Nishiyama, H. (2013). Dendritic Translocation Establishes the Winner in Cerebellar Climbing Fiber Synapse Elimination. *The Journal of Neuroscience* 33, 7641-53, <https://dx.doi.org/10.1523/jneurosci.4561-12.2013>.
- 261 Sanes, J. R. & Lichtman, J. W. (1999). Development of the vertebrate neuromuscular junction. *Annu Rev Neurosci* 22, 389-442, <http://dx.doi.org/10.1146/annurev.neuro.22.1.389>.
- 262 Darabid, H., Perez-Gonzalez, A. P. & Robitaille, R. (2014). Neuromuscular synaptogenesis: coordinating partners with multiple functions. *Nature Reviews Neuroscience* 15, 703, <http://dx.doi.org/10.1038/nrn3821>.
- 263 Turney, S. G. & Lichtman, J. W. (2012). Reversing the Outcome of Synapse Elimination at Developing Neuromuscular Junctions In Vivo: Evidence for Synaptic Competition and Its Mechanism. *PLOS Biology* 10, e1001352, <https://doi.org/10.1371/journal.pbio.1001352>.
- 264 Walsh, M. K. & Lichtman, J. W. (2003). In vivo time-lapse imaging of synaptic takeover associated with naturally occurring synapse elimination. *Neuron* 37, 67-73, [http://dx.doi.org/10.1016/S0896-6273\(02\)01142-X](http://dx.doi.org/10.1016/S0896-6273(02)01142-X).

Neural Activity During the Formation of a Giant Auditory Synapse

- 265 Sommer, I., Lingenhöhl, K. & Friauf, E. (1993). Principal cells of the rat medial nucleus of the trapezoid body: an intracellular *in vivo* study of their physiology and morphology. *Experimental Brain Research* 95, 223-39, <http://dx.doi.org/10.1007/BF00229781>.
- 266 Tsuchitani, C. (1997). Input from the medial nucleus of trapezoid body to an interaural level detector. *Hear Res* 105, 211-24, [http://dx.doi.org/10.1016/S0378-5955\(96\)00212-2](http://dx.doi.org/10.1016/S0378-5955(96)00212-2).
- 267 Smith, P. H., Joris, P. X. & Yin, T. C. T. (1998). Anatomy and physiology of principal cells of the medial nucleus of the trapezoid body (MNTB) of the cat. *J Neurophysiol* 79, 3127-42, <http://jn.physiology.org/content/79/6/3127.full>.
- 268 Kopp-Scheinpflug, C., Lippe, W. R., Dorrscheidt, G. J. & Rübsamen, R. (2003). The medial nucleus of the trapezoid body in the gerbil is more than a relay: comparison of pre- and postsynaptic activity. *J Assoc Res Otolaryngol* 4, 1-23, <http://www.springerlink.com/content/garedxg4h6trukvv>.
- 269 Kopp-Scheinpflug, C., Fuchs, K., Lippe, W. R., Tempel, B. L. & Rübsamen, R. (2003). Decreased temporal precision of auditory signaling in *Kcna1*-null mice: an electrophysiological study *in vivo*. *J Neurosci* 23, 9199-207, <http://www.jneurosci.org/cgi/content/full/23/27/9199>.
- 270 Green, J. S. & Sanes, D. H. (2005). Early appearance of inhibitory input to the MNTB supports binaural processing during development. *J Neurophysiol* 94, 3826-35, <http://jn.physiology.org/cgi/content/full/94/6/3826>.
- 271 Tolnai, S., Hernandez, O., Englitz, B., Rübsamen, R. & Malmierca, M. S. (2008). The medial nucleus of the trapezoid body in rat: spectral and temporal properties vary with anatomical location of the units. *European Journal of Neuroscience* 27, 2587-98, <https://dx.doi.org/10.1111/j.1460-9568.2008.06228.x>.
- 272 Tolnai, S., Englitz, B., Kopp-Scheinpflug, C. et al. (2008). Dynamic coupling of excitatory and inhibitory responses in the medial nucleus of the trapezoid body. *Eur J Neurosci* 27, 3191-204, <http://onlinelibrary.wiley.com/doi/10.1111/j.1460-9568.2008.06292.x/full>.
- 273 Kadner, A. & Berrebi, A. S. (2008). Encoding of temporal features of auditory stimuli in the medial nucleus of the trapezoid body and superior paraolivary nucleus of the rat. *Neuroscience* 151, 868-87, <http://dx.doi.org/10.1016/j.neuroscience.2007.11.008>.
- 274 Kopp-Scheinpflug, C., Tolnai, S., Malmierca, M. S. & Rübsamen, R. (2008). The medial nucleus of the trapezoid body: comparative physiology. *Neuroscience* 154, 160-70, <http://dx.doi.org/10.1016/j.neuroscience.2008.01.088>.
- 275 Kopp-Scheinpflug, C., Dehmel, S., Tolnai, S. et al. (2008). Glycine-mediated changes of onset reliability at a mammalian central synapse. *Neuroscience* 157, 432-45, <http://dx.doi.org/10.1016/j.neuroscience.2008.08.068>.
- 276 Steinert, J. R., Kopp-Scheinpflug, C., Baker, C. et al. (2008). Nitric oxide is a volume transmitter regulating postsynaptic excitability at a glutamatergic synapse. *Neuron* 60, 642-56, <http://dx.doi.org/10.1016/j.neuron.2008.08.025>.

- 277 Tolnai, S., Englitz, B., Scholbach, J., Jost, J. & Rübsamen, R. (2009). Spike transmission delay at the calyx of Held in vivo: rate dependence, phenomenological modeling, and relevance for sound localization. *J Neurophysiol* 102, 1206-17, <http://dx.doi.org/10.1152/jn.00275.2009>
- 278 Englitz, B., Tolnai, S., Typlt, M., Jost, J. & Rübsamen, R. (2009). Reliability of synaptic transmission at the synapses of Held in vivo under acoustic stimulation. *PLoS One* 4, e7014, <http://dx.doi.org/10.1371/journal.pone.0007014>.
- 279 Lorteije, J. A. M. & Borst, J. G. G. (2011). Contribution of the mouse calyx of Held synapse to tone adaptation. *Eur J Neurosci* 33, 251-8, <http://dx.doi.org/10.1111/j.1460-9568.2010.07507.x>.
- 280 Sonntag, M., Englitz, B., Typlt, M. & Rübsamen, R. (2011). The calyx of Held develops adult-like dynamics and reliability by hearing onset in the mouse in vivo. *J Neurosci* 31, 6699-709, <http://dx.doi.org/10.1523/JNEUROSCI.0575-11.2011>.
- 281 Wang, T., Rusu, S. I., Hruskova, B., Turecek, R. & Borst, J. G. G. (2013). Modulation of synaptic depression of the calyx of Held synapse by GABAB receptors and spontaneous activity. *J Physiol* 591, 4877-94, <http://dx.doi.org/10.1113/jphysiol.2013.256875>.
- 282 Di Guilmi, M. N., Wang, T., Inchauspe, C. G. et al. (2014). Synaptic gain-of-function effects of mutant Cav2.1 channels in a mouse model of familial hemiplegic migraine are due to increased basal [Ca²⁺]_i. *Journal of Neuroscience* 34, 7047-58, <http://dx.doi.org/10.1523/JNEUROSCI.2526-13.2014>.
- 283 Koka, K. & Tollin, D. J. (2014). Linear coding of complex sound spectra by discharge rate in neurons of the medial nucleus of the trapezoid body (MNTB) and its inputs. *Frontiers in Neural Circuits* 8, <https://dx.doi.org/10.3389/fncir.2014.00144>.
- 284 Wang, T., de Kok, L., Willemsen, R., Elgersma, Y. & Borst, J. G. G. (2015). In vivo synaptic transmission and morphology in mouse models of Tuberous sclerosis, Fragile X syndrome, Neurofibromatosis type 1, and Costello syndrome. *Front Cell Neurosci* 9, 234, <http://dx.doi.org/10.3389/fncel.2015.00234>.
- 285 Blosa, M., Sonntag, M., Jäger, C. et al. (2015). The extracellular matrix molecule brevican is an integral component of the machinery mediating fast synaptic transmission at the calyx of Held. *J Physiol* 593, 4341-60, <http://dx.doi.org/10.1113/JP270849>.
- 286 Gao, F. & Berrebi, A. S. (2016). Forward masking in the medial nucleus of the trapezoid body of the rat. *Brain Structure and Function* 221, 2303-17, <https://dx.doi.org/10.1007/s00429-015-1044-5>.
- 287 Stange-Marten, A., Nabel, A. L., Sinclair, J. L. et al. (2017). Input timing for spatial processing is precisely tuned via constant synaptic delays and myelination patterns in the auditory brainstem. *Proceedings of the National Academy of Sciences* 114, E4851-E58, <https://dx.doi.org/10.1073/pnas.1702290114>.
- 288 Wu, X.-S., Sun, J.-Y., Evers, A. S., Crowder, M. & Wu, L.-G. (2004). Isoflurane inhibits transmitter release and the presynaptic action potential. *Anesthesiology* 100, 663-70, <http://anesthesiology.pubs.asahq.org/article.aspx?articleid=1943095>.

Neural Activity During the Formation of a Giant Auditory Synapse

- 289 Mazze, Richard I., Rice, Susan A. & Baden, Jeffrey M. (1985). Halothane, Isoflurane, and Enflurane MAC in Pregnant and Nonpregnant Female and Male Mice and Rats. *Anesthesiology* 62, 339-41, <http://anesthesiology.pubs.asahq.org/article.aspx?articleid=1955433>.
- 290 Friederich, P., Benzenberg, D., Trellakis, S. & Urban, Bernd W. (2001). Interaction of Volatile Anesthetics with Human Kv Channels in Relation to Clinical Concentrations. *Anesthesiology* 95, 954-58, <http://anesthesiology.pubs.asahq.org/article.aspx?articleid=1944433>.
- 291 Patel, A. J., Honoré, E., Lesage, F. et al. (1999). Inhalational anesthetics activate two-pore-domain background K⁺ channels. *Nature Neuroscience* 2, 422, <https://dx.doi.org/10.1038/8084>.
- 292 Westphalen, R. I. & Hemmings Jr., H. C. (2006). Volatile Anesthetic Effects on Glutamate versus GABA Release from Isolated Rat Cortical Nerve Terminals: Basal Release. *Journal of Pharmacology and Experimental Therapeutics* 316, 208-15, <https://dx.doi.org/10.1124/jpet.105.090647>.
- 293 Baumgart, J. P., Zhou, Z.-Y., Hara, M. et al. (2015). Isoflurane inhibits synaptic vesicle exocytosis through reduced Ca²⁺ influx, not Ca²⁺-exocytosis coupling. *Proceedings of the National Academy of Sciences* 112, 11959-64, <https://dx.doi.org/10.1073/pnas.1500525112>.
- 294 Zimin, Pavel I., Woods, Christian B., Quintana, A. et al. (2016). Glutamatergic Neurotransmission Links Sensitivity to Volatile Anesthetics with Mitochondrial Function. *Current Biology* 26, 2194-201, <http://www.sciencedirect.com/science/article/pii/S0960982216306595>.
- 295 Pocock, G. & Richards, C. D. (1993). Excitatory and inhibitory synaptic mechanisms in anaesthesia. *British Journal of Anaesthesia* 71, 134-47, <https://dx.doi.org/10.1093/bja/71.1.134>.
- 296 Sitdikova, G., Zakharov, A., Janackova, S. et al. (2014). Isoflurane suppresses early cortical activity. *Annals of Clinical and Translational Neurology* 1, 15-26, <http://dx.doi.org/10.1002/acn3.16>.
- 297 Hamill, O. P., Marty, A., Neher, E., Sakmann, B. & Sigworth, F. J. (1981). Improved patch-clamp techniques for high-resolution current recording from cells and cell-free membrane patches. *Pflügers Archiv* 391, 85-100, <http://dx.doi.org/10.1007/BF00656997>.
- 298 Margrie, T. W., Brecht, M. & Sakmann, B. (2002). In vivo, low-resistance, whole-cell recordings from neurons in the anaesthetized and awake mammalian brain. *Pflügers Arch* 444, 491-8, http://www.ncbi.nlm.nih.gov/entrez/query.fcgi?cmd=Retrieve&db=PubMed&dopt=Citation&list_uids=12136268.
- 299 Margrie, T. W., Meyer, A. H., Caputi, A. et al. (2003). Targeted whole-cell recordings in the mammalian brain in vivo. *Neuron* 39, 911-8, <http://dx.doi.org/10.1007/s00424-002-0831-z>.
- 300 Kitamura, K., Judkewitz, B., Kano, M., Denk, W. & Häusser, M. (2008). Targeted patch-clamp recordings and single-cell electroporation of unlabeled neurons in vivo. *Nat Methods* 5, 61-7, <http://www.nature.com/nmeth/journal/v5/n1/full/nmeth1150.html>.

- 301 Pei, X., Volgushev, M., Vidyasagar, T. R. & Creutzfeldt, O. D. (1991). Whole cell recording and conductance measurements in cat visual cortex in-vivo. *NeuroReport* 2, 485-88, <http://dx.doi.org/10.1097/00001756-199108000-00019>.
- 302 Kodandaramaiah, S. B., Franzesi, G. T., Chow, B. Y., Boyden, E. S. & Forest, C. R. (2012). Automated whole-cell patch-clamp electrophysiology of neurons in vivo. *Nature Methods* 9, 585, <https://dx.doi.org/10.1038/nmeth.1993>.
- 303 Magistretti, J., Mantegazza, M., de Curtis, M. & Wanke, E. (1998). Modalities of Distortion of Physiological Voltage Signals by Patch-Clamp Amplifiers: A Modeling Study. *Biophysical Journal* 74, 831-42, [https://doi.org/10.1016/S0006-3495\(98\)74007-X](https://doi.org/10.1016/S0006-3495(98)74007-X).
- 304 Magistretti, J., Mantegazza, M., Guatteo, E. & Wanke, E. (1996). Action potentials recorded with patch-clamp amplifiers: are they genuine? *Trends in Neurosciences* 19, 530-4, [http://dx.doi.org/10.1016/S0166-2236\(96\)40004-2](http://dx.doi.org/10.1016/S0166-2236(96)40004-2).
- 305 Smith, R. D. & Goldin, A. L. (1998). Functional Analysis of the Rat I Sodium Channel in *Xenopus* Oocytes. *Journal of Neuroscience* 18, 811-20. <http://dx.doi.org/10.1523/JNEUROSCI.18-03-00811.1998>.
- 306 Smith, M. R., Smith, R. D., Plummer, N. W., Meisler, M. H. & Goldin, A. L. (1998). Functional Analysis of the Mouse Scn8a Sodium Channel. *The Journal of Neuroscience* 18, 6093-102. <http://dx.doi.org/10.1523/JNEUROSCI.18-16-06093.1998>.
- 307 Morgan, K., Stevens, E. B., Shah, B. et al. (2000). β_3 : An additional auxiliary subunit of the voltage-sensitive sodium channel that modulates channel gating with distinct kinetics. *Proceedings of the National Academy of Sciences* 97, 2308-13, <http://www.pnas.org/content/97/5/2308.abstract>.
- 308 Yu, F. H., Westenbroek, R. E., Silos-Santiago, I. et al. (2003). Sodium Channel β_4 , a New Disulfide-Linked Auxiliary Subunit with Similarity to β_2 . *The Journal of Neuroscience* 23, 7577-85, <http://dx.doi.org/10.1523/JNEUROSCI.23-20-07577.2003>.
- 309 Shah, B. S., Stevens, E. B., Gonzalez, M. I. et al. (2000). β_3 , a novel auxiliary subunit for the voltage-gated sodium channel, is expressed preferentially in sensory neurons and is upregulated in the chronic constriction injury model of neuropathic pain. *European Journal of Neuroscience* 12, 3985-90, <http://dx.doi.org/10.1046/j.1460-9568.2000.00294.x>.
- 310 Isom, L., De Jongh, K., Patton, D. et al. (1992). Primary structure and functional expression of the beta 1 subunit of the rat brain sodium channel. *Science* 256, 839-42, <http://dx.doi.org/science.256.5058.839>.
- 311 Zhou, W. & Goldin, A. L. (2004). Use-Dependent Potentiation of the Nav1.6 Sodium Channel. *Biophysical Journal* 87, 3862-72, <http://dx.doi.org/10.1529/biophysj.104.045963>.
- 312 Rush, A. M., Dib-Hajj, S. D. & Waxman, S. G. (2005). Electrophysiological properties of two axonal sodium channels, Nav1.2 and Nav1.6, expressed in mouse spinal sensory neurones. *The Journal of Physiology* 564, 803-15, <http://dx.doi.org/10.1113/jphysiol.2005.083089>.

Neural Activity During the Formation of a Giant Auditory Synapse

- 313 Raman, I. M., Sprunger, L. K., Meisler, M. H. & Bean, B. P. (1997). Altered Subthreshold Sodium Currents and Disrupted Firing Patterns in Purkinje Neurons of Scn8a Mutant Mice. *Neuron* 19, 881-91, [http://dx.doi.org/10.1016/S0896-6273\(00\)80969-1](http://dx.doi.org/10.1016/S0896-6273(00)80969-1).
- 314 Wu, S. H. & Kelly, J. B. (1993). Response of neurons in the lateral superior olive and medial nucleus of the trapezoid body to repetitive stimulation: intracellular and extracellular recordings from mouse brain slice. *Hear Res* 68, 189-201, [http://dx.doi.org/10.1016/0378-5955\(93\)90123-1](http://dx.doi.org/10.1016/0378-5955(93)90123-1).
- 315 Schneggenburger, R., Sakaba, T. & Neher, E. (2002). Vesicle pools and short-term synaptic depression: lessons from a large synapse. *Trends Neurosci* 25, 206-12, [http://dx.doi.org/10.1016/S0166-2236\(02\)02139-2](http://dx.doi.org/10.1016/S0166-2236(02)02139-2).
- 316 Kim, K. X. & Rutherford, M. A. (2016). Maturation of NaV and KV Channel topographies in the auditory nerve spike initiator before and after developmental onset of hearing function. *J Neurosci* 36, 2111-8, <http://dx.doi.org/10.1523/JNEUROSCI.3437-15.2016>
- 317 Schneggenburger, R., Meyer, A. C. & Neher, E. (1999). Released fraction and total size of a pool of immediately available transmitter quanta at a calyx synapse. *Neuron* 23, 399-409, [http://dx.doi.org/10.1016/S0896-6273\(00\)80789-8](http://dx.doi.org/10.1016/S0896-6273(00)80789-8).
- 318 Borst, J. G. G. (2010). The low synaptic release probability in vivo. *Trends Neurosci* 33, 259-66, <http://dx.doi.org/10.1016/j.tins.2010.03.003>.
- 319 Debanne, D. (2004). Information processing in the axon. *Nat Rev Neurosci* 5, 304-16, <http://dx.doi.org/10.1038/nrn1397>.
- 320 Ford, M. C., Alexandrova, O., Cossell, L. et al. (2015). Tuning of Ranvier node and internode properties in myelinated axons to adjust action potential timing. *Nat Commun* 6, 8073, <http://dx.doi.org/10.1038/ncomms9073>.
- 321 Cho, S. J., Jeon, J. H., Chun, D. I., Yeo, S. W. & Kim, I.-B. (2014). Anoctamin 1 expression in the mouse auditory brainstem. *Cell and tissue research* 357, 563-69, <https://dx.doi.org/10.1007/s00441-014-1897-6>.
- 322 Price, G. D. & Trussell, L. O. (2006). Estimate of the chloride concentration in a central glutamatergic terminal: a gramicidin perforated-patch study on the calyx of Held. *J Neurosci* 26, 11432-6, <http://www.jneurosci.org/cgi/content/full/26/44/11432>.
- 323 Levy, R. A. (1977). The role of GABA in primary afferent depolarization. *Progress in Neurobiology* 9, 211-67, [https://dx.doi.org/10.1016/0301-0082\(77\)90002-8](https://dx.doi.org/10.1016/0301-0082(77)90002-8).
- 324 McBride Jr., D. W. & Roper, S. D. (1991). Ca²⁺-dependent chloride conductance in Necturus taste cells. *The Journal of Membrane Biology* 124, 85-93, <https://dx.doi.org/10.1007/BF01871367>.
- 325 Lin, K.-H., Oleskevich, S. & Taschenberger, H. (2011). Presynaptic Ca²⁺ influx and vesicle exocytosis at the mouse endbulb of Held: a comparison of two auditory nerve terminals. *The Journal of Physiology* 589, 4301-20, <http://dx.doi.org/10.1113/jphysiol.2011.209189>.

- 326 Southan, A. P. & Robertson, B. (2000). Electrophysiological Characterization of Voltage-Gated K⁺ Currents in Cerebellar Basket and Purkinje Cells: Kv₁ and Kv₃ Channel Subfamilies Are Present in Basket Cell Nerve Terminals. *The Journal of Neuroscience* 20, 114-22, <http://www.jneurosci.org/content/jneuro/20/1/114>.
- 327 Kawaguchi, S. Y. & Sakaba, T. (2015). Control of inhibitory synaptic outputs by low excitability of axon terminals revealed by direct recording. *Neuron* 85, 1273-88, <http://dx.doi.org/10.1016/j.neuron.2015.02.013>.
- 328 Díaz-Rojas, F., Sakaba, T. & Kawaguchi, S.-y. (2015). Ca₂₊ current facilitation determines short-term facilitation at inhibitory synapses between cerebellar Purkinje cells. *The Journal of Physiology* 593, 4889-904, <http://dx.doi.org/10.1113/JP270704>.
- 329 Ritzau-Jost, A., Delvendahl, I., Rings, A. et al. (2014). Ultrafast action potentials mediate kilohertz signaling at a central synapse. *Neuron* 84, 152-63, <http://dx.doi.org/10.1016/j.neuron.2014.08.036>.
- 330 Morita, K., David, G., Barrett, J. N. & Barrett, E. F. (1993). Posttetanic hyperpolarization produced by electrogenic Na⁺-K⁺ pump in lizard axons impaled near their motor terminals. *Journal of Neurophysiology* 70, 1874-84, <http://dx.doi.org/10.1152/jn.1993.70.5.1874>.
- 331 Augustine, G. J. (1990). Regulation of transmitter release at the squid giant synapse by presynaptic delayed rectifier potassium current. *Journal of Physiology* 431, 343-64, <http://dx.doi.org/10.1113/jphysiol.1990.sp018333>.
- 332 Kole, M. H. P., Letzkus, J. J. & Stuart, G. J. (2007). Axon initial segment Kv₁ channels control axonal action potential waveform and synaptic efficacy. *Neuron* 55, 633-47, <http://dx.doi.org/10.1016/j.neuron.2007.07.031>.
- 333 Kole, Maarten H. P. (2011). First Node of Ranvier Facilitates High-Frequency Burst Encoding. *Neuron* 71, 671-82, <https://doi.org/10.1016/j.neuron.2011.06.024>.
- 334 Thomsen, L. B., Jörntell, H. & Midtgaard, J. (2010). Presynaptic calcium signalling in cerebellar mossy fibres. *Frontiers in Neural Circuits* 4, <https://dx.doi.org/10.3389/neuro.04.001.2010>.
- 335 Zhou, H., Lin, Z., Voges, K. et al. (2014). Cerebellar modules operate at different frequencies. *eLife* 3, e02536, <https://doi.org/10.7554/eLife.02536>.
- 336 Arancillo, M., White, J. J., Lin, T., Stay, T. L. & Sillitoe, R. V. (2015). In vivo analysis of Purkinje cell firing properties during postnatal mouse development. *J Neurophysiol* 113, 578-91, <http://dx.doi.org/10.1152/jn.00586.2014>.
- 337 Delvendahl, I., Weyhermüller, A., Ritzau-Jost, A. & Hallermann, S. (2013). Hippocampal and cerebellar mossy fibre boutons – same name, different function. *The Journal of Physiology* 591, 3179-88, <http://dx.doi.org/10.1113/jphysiol.2012.248294>.
- 338 Kole, M. H. P., Ilschner, S. U., Kampa, B. M. et al. (2008). Action potential generation requires a high sodium channel density in the axon initial segment. *Nature Neuroscience* 11, 178-86, <http://dx.doi.org/10.1038/nn2040>.

Neural Activity During the Formation of a Giant Auditory Synapse

- 339 Ohura, S. & Kamiya, H. (2018). Short-Term Depression of Axonal Spikes at the Mouse Hippocampal Mossy Fibers and Sodium Channel-Dependent Modulation. *eNeuro* 5, <https://dx.doi.org/10.1523/eneuro.0415-17.2018>.
- 340 Williams, M. R., Fuchs, J. R., Green, J. T. & Morielli, A. D. (2012). Cellular Mechanisms and Behavioral Consequences of Kv1.2 Regulation in the Rat Cerebellum. *The Journal of Neuroscience* 32, 9228-37, <https://dx.doi.org/10.1523/jneurosci.6504-11.2012>.
- 341 Nesti, E., Everill, B. & Morielli, A. D. (2004). Endocytosis as a Mechanism for Tyrosine Kinase-dependent Suppression of a Voltage-gated Potassium Channel. *Molecular Biology of the Cell* 15, 4073-88, <https://dx.doi.org/10.1091/mbc.E03-11-0788>.
- 342 Connors, E. C., Ballif, B. A. & Morielli, A. D. (2008). Homeostatic Regulation of Kv1.2 Potassium Channel Trafficking by Cyclic AMP. *Journal of Biological Chemistry* 283, 3445-53, <https://dx.doi.org/10.1074/jbc.M708875200>.
- 343 Stirling, L., Williams, M. R. & Morielli, A. D. (2009). Dual Roles for RHOA/RHO-Kinase In the Regulated Trafficking of a Voltage-sensitive Potassium Channel. *Molecular Biology of the Cell* 20, 2991-3002, <https://dx.doi.org/10.1091/mbc.E08-10-1074>.
- 344 Wang, L.-Y., Gan, L., Forsythe, I. D. & Kaczmarek, L. K. (1998). Contribution of the Kv3.1 potassium channel to high-frequency firing in mouse auditory neurones. *J Physiol* 509, 183-94, <http://jp.physoc.org/content/509/1/183.full>.
- 345 Körber, C., Dondzillo, A., Eisenhardt, G. et al. (2014). Gene expression profile during functional maturation of a central mammalian synapse. *Eur J Neurosci* 40, 2867-77, <http://dx.doi.org/10.1111/ejn.12661>.
- 346 Dodson, P. D. & Forsythe, I. D. (2004). Presynaptic K⁺ channels: electrifying regulators of synaptic terminal excitability. *Trends Neurosci* 27, 210-7, <http://dx.doi.org/10.1016/j.tins.2004.02.012>.
- 347 Löwel, S. & Singer, W. (1992). Selection of intrinsic horizontal connections in the visual cortex by correlated neuronal activity. *Science* 255, 209-12, <https://www.jstor.org/stable/2876252>.
- 348 Hebb, D. *The Organization of Behavior*. (Wiley, New York, 1949), [http://dx.doi.org/10.1016/S0361-9230\(99\)00182-3](http://dx.doi.org/10.1016/S0361-9230(99)00182-3).
- 349 Kandler, K. & Friauf, E. (1995). Development of glycinergic and glutamatergic synaptic transmission in the auditory brainstem of perinatal rats. *J Neurosci* 15, 6890-904, <http://www.jneurosci.org/content/15/10/6890.long>.
- 350 Kim, G. & Kandler, K. (2003). Elimination and strengthening of glycinergic/GABAergic connections during tonotopic map formation. *Nature Neuroscience* 6, 282, <http://dx.doi.org/10.1038/nn1015>.
- 351 Redfern, P. A. (1970). Neuromuscular transmission in new-born rats. *The Journal of Physiology* 209, 701-09, <http://dx.doi.org/10.1113/jphysiol.1970.sp009187>.
- 352 Lichtman, J. W. & Colman, H. (2000). Synapse Elimination and Indelible Memory. *Neuron* 25, 269-78, [https://doi.org/10.1016/S0896-6273\(00\)80893-4](https://doi.org/10.1016/S0896-6273(00)80893-4).

- 353 Guido, W. (2008). Refinement of the retinogeniculate pathway. *J Physiol* 586, 4357-62, <http://dx.doi.org/10.1113/jphysiol.2008.157115>.
- 354 Huberman, A. D., Feller, M. B. & Chapman, B. (2008). Mechanisms underlying development of visual maps and receptive fields. *Annu Rev Neurosci* 31, 479-509, <http://dx.doi.org/10.1146/annurev.neuro.31.060407.125533>.
- 355 Chen, C. & Regehr, W. G. (2000). Developmental remodeling of the retinogeniculate synapse. *Neuron* 28, 955-66, [http://dx.doi.org/10.1016/S0896-6273\(00\)00166-5](http://dx.doi.org/10.1016/S0896-6273(00)00166-5).
- 356 Lo, F. S., Ziburkus, J. & Guido, W. (2002). Synaptic mechanisms regulating the activation of a Ca²⁺-mediated plateau potential in developing relay cells of the LGN. *J Neurophysiol* 87, 1175-85, <http://jn.physiology.org/content/87/3/1175.long>.
- 357 Litvina, E. Y. & Chen, C. (2017). Functional Convergence at the Retinogeniculate Synapse. *Neuron* 96, 330-38.e5, <http://dx.doi.org/10.1016/j.neuron.2017.09.037>.
- 358 Jaubert-Miazza, L., Green, E., Lo, F.-S. et al. (2005). Structural and functional composition of the developing retinogeniculate pathway in the mouse. *Visual Neuroscience* 22, 661-76, <https://dx.doi.org/10.1017/S0952523805225154>.
- 359 Hong, Y. K., Park, S., Litvina, E. Y. et al. (2014). Refinement of the retinogeniculate synapse by bouton clustering. *Neuron* 84, 332-9, <http://dx.doi.org/10.1016/j.neuron.2014.08.059>.
- 360 Crepel, F., Mariani, J. & Delhaye-Bouchaud, N. (1976). Evidence for a multiple innervation of Purkinje cells by climbing fibers in the immature rat cerebellum. *Journal of Neurobiology* 7, 567-78, <http://dx.doi.org/10.1002/neu.480070609>.
- 361 Delhaye-Bouchaud, N., Crepel, F. & Mariani, J. (1975). Demonstration of temporary multi-innervation of the cerebellar Purkinje cells by the ascending fibers during development in the rat. *Comptes rendus hebdomadaires des seances de l'Academie des sciences. Serie D: Sciences naturelles* 281, 909-12, <https://www.ncbi.nlm.nih.gov/pubmed/811398>.
- 362 Inácio, A. R., Nasretdinov, A., Lebedeva, J. & Khazipov, R. (2016). Sensory feedback synchronizes motor and sensory neuronal networks in the neonatal rat spinal cord. *Nature Communications* 7, 13060, <https://dx.doi.org/10.1038/ncomms13060>.
- 363 Galli, L. & Maffei, L. (1988). Spontaneous impulse activity of rat retinal ganglion cells in prenatal life. *Science* 242, 90-1, <http://dx.doi.org/10.1126/science.3175637>.
- 364 Weliky, M. & Katz, L. C. (1999). Correlational Structure of Spontaneous Neuronal Activity in the Developing Lateral Geniculate Nucleus in Vivo. *Science* 285, 599-604, <https://dx.doi.org/10.1126/science.285.5427.599>.
- 365 Good, J.-M., Mahoney, M., Miyazaki, T. et al. (2017). Maturation of Cerebellar Purkinje Cell Population Activity during Postnatal Refinement of Climbing Fiber Network. *Cell Reports* 21, 2066-73, <http://dx.doi.org/10.1016/j.celrep.2017.10.101>.
- 366 Kawamura, Y., Nakayama, H., Hashimoto, K. et al. (2013). Spike timing-dependent selective strengthening of single climbing fibre inputs to Purkinje cells during cerebellar development. *Nature Communications* 4, 2732, <http://dx.doi.org/10.1038/ncomms3732>.

Neural Activity During the Formation of a Giant Auditory Synapse

- 367 Leighton, A. H. & Lohmann, C. (2016). The Wiring of Developing Sensory Circuits—From Patterned Spontaneous Activity to Synaptic Plasticity Mechanisms. *Frontiers in Neural Circuits* 10, <https://dx.doi.org/10.3389/fncir.2016.00071>.
- 368 Feller, M. B., Wellis, D. P., Stellwagen, D., Werblin, F. S. & Shatz, C. J. (1996). Requirement for Cholinergic Synaptic Transmission in the Propagation of Spontaneous Retinal Waves. *Science* 272, 1182-87, <https://dx.doi.org/10.1126/science.272.5265.1182>.
- 369 Meister, M., Wong, R., Baylor, D. & Shatz, C. (1991). Synchronous bursts of action potentials in ganglion cells of the developing mammalian retina. *Science* 252, 939-43, <https://dx.doi.org/10.1126/science.2035024>.
- 370 Wong, R. O. L., Meister, M. & Shatz, C. J. (1993). Transient period of correlated bursting activity during development of the mammalian retina. *Neuron* 11, 923-38, [https://dx.doi.org/10.1016/0896-6273\(93\)90122-8](https://dx.doi.org/10.1016/0896-6273(93)90122-8).
- 371 Wong, R. O. L. (1999). Retinal waves and visual system development. *Annual Review of Neuroscience* 22, 29-47, <https://dx.doi.org/10.1146/annurev.neuro.22.1.29>.
- 372 Ackman, J. B., Burbridge, T. J. & Crair, M. C. (2012). Retinal waves coordinate patterned activity throughout the developing visual system. *Nature* 490, 219-25, <http://dx.doi.org/10.1038/nature11529>.
- 373 Torborg, C. L. & Feller, M. B. (2005). Spontaneous patterned retinal activity and the refinement of retinal projections. *Progress in Neurobiology* 76, 213-35, <https://dx.doi.org/10.1016/j.pneurobio.2005.09.002>.
- 374 Cutts, C. S. & Eglon, S. J. (2014). Detecting Pairwise Correlations in Spike Trains: An Objective Comparison of Methods and Application to the Study of Retinal Waves. *The Journal of Neuroscience* 34, 14288-303, <https://dx.doi.org/10.1523/jneurosci.2767-14.2014>.
- 375 McLaughlin, T., Torborg, C. L., Feller, M. B. & O'Leary, D. D. (2003). Retinotopic map refinement requires spontaneous retinal waves during a brief critical period of development. *Neuron* 40, 1147-60, [https://dx.doi.org/10.1016/S0896-6273\(03\)00790-6](https://dx.doi.org/10.1016/S0896-6273(03)00790-6).
- 376 Blankenship, A. G., Hamby, A. M., Firl, A. et al. (2011). The Role of Neuronal Connexins 36 and 45 in Shaping Spontaneous Firing Patterns in the Developing Retina. *The Journal of Neuroscience* 31, 9998-10008, <https://dx.doi.org/10.1523/jneurosci.5640-10.2011>.
- 377 Huberman, A. D., Wang, G.-Y., Liets, L. C. et al. (2003). Eye-specific retinogeniculate segregation independent of normal neuronal activity. *Science* 300, 994-98, <https://www.jstor.org/stable/3833939>.
- 378 Torborg, C. L., Hansen, K. A. & Feller, M. B. (2005). High frequency, synchronized bursting drives eye-specific segregation of retinogeniculate projections. *Nature neuroscience* 8, 72, <https://dx.doi.org/10.1038/nn1376>.
- 379 Xu, H.-P., Furman, M., Mineur, Y. S. et al. (2011). An instructive role for patterned spontaneous retinal activity in mouse visual map development. *Neuron* 70, 1115-27, <http://dx.doi.org/10.1016/j.neuron.2011.04.028>.

- 380 Zhang, J., Ackman, J. B., Xu, H.-P. & Crair, M. C. (2011). Visual map development depends on the temporal pattern of binocular activity in mice. *Nature Neuroscience* 15, 298, <http://dx.doi.org/10.1038/nn.3007>.
- 381 O'Donovan, M. J., Bonnot, A., Wenner, P. & Mentis, G. Z. (2005). Calcium imaging of network function in the developing spinal cord. *Cell Calcium* 37, 443-50, <https://dx.doi.org/10.1016/j.ceca.2005.01.012>.
- 382 Personius, K. E. & Balice-Gordon, R. J. (2001). Loss of Correlated Motor Neuron Activity during Synaptic Competition at Developing Neuromuscular Synapses. *Neuron* 31, 395-408, [https://dx.doi.org/10.1016/S0896-6273\(01\)00369-5](https://dx.doi.org/10.1016/S0896-6273(01)00369-5).
- 383 Borodinsky, L. N., Belgacem, Y. H. & Swapna, I. (2012). Electrical activity as a developmental regulator in the formation of spinal cord circuits. *Current Opinion in Neurobiology* 22, 624-30, <https://dx.doi.org/10.1016/j.conb.2012.02.004>.
- 384 Warp, E., Agarwal, G., Wyart, C. et al. (2012). Emergence of Patterned Activity in the Developing Zebrafish Spinal Cord. *Current Biology* 22, 93-102, <https://dx.doi.org/10.1016/j.cub.2011.12.002>.
- 385 Wenner, P. (2012). Motor Development: Activity Matters After All. *Current Biology* 22, R47-R48, <https://dx.doi.org/10.1016/j.cub.2011.12.008>.
- 386 Bos, R., Brocard, F. & Vinay, L. (2011). Primary Afferent Terminals Acting as Excitatory Interneurons Contribute to Spontaneous Motor Activities in the Immature Spinal Cord. *The Journal of Neuroscience* 31, 10184-88, <https://dx.doi.org/10.1523/jneurosci.0068-11.2011>.
- 387 Personius, K. E., Chang, Q., Mentis, G. Z., O'Donovan, M. J. & Balice-Gordon, R. J. (2007). Reduced gap junctional coupling leads to uncorrelated motor neuron firing and precocious neuromuscular synapse elimination. *Proceedings of the National Academy of Sciences* 104, 11808-13, <https://dx.doi.org/10.1073/pnas.0703357104>.
- 388 Personius, K. E., Karnes, J. L. & Parker, S. D. (2008). NMDA Receptor Blockade Maintains Correlated Motor Neuron Firing and Delays Synapse Competition at Developing Neuromuscular Junctions. *The Journal of Neuroscience* 28, 8983-92, <https://dx.doi.org/10.1523/jneurosci.5226-07.2008>.
- 389 Favero, M., Busetto, G. & Cangiano, A. (2012). Spike timing plays a key role in synapse elimination at the neuromuscular junction. *Proceedings of the National Academy of Sciences* 109, E1667-E75, <https://dx.doi.org/10.1073/pnas.1201147109>.
- 390 Kirkby, L. A., Sack, G. S., Firl, A. & Feller, M. B. (2013). A role for correlated spontaneous activity in the assembly of neural circuits. *Neuron* 80, 1129-44, <http://dx.doi.org/10.1016/j.neuron.2013.10.030>.
- 391 Andjus, P. R., Zhu, L., Cesa, R., Carulli, D. & Strata, P. (2003). A change in the pattern of activity affects the developmental regression of the purkinje cell polyinnervation by climbing fibers in the rat cerebellum. *Neuroscience* 121, 563-72, [https://dx.doi.org/10.1016/S0306-4522\(03\)00556-6](https://dx.doi.org/10.1016/S0306-4522(03)00556-6).
- 392 Lorenzetto, E., Caselli, L., Feng, G. et al. (2009). Genetic perturbation of postsynaptic activity regulates synapse elimination in developing cerebellum. *Proc Natl Acad Sci USA* 106, 16475-80, <http://dx.doi.org/10.1073/pnas.0907298106>.

Neural Activity During the Formation of a Giant Auditory Synapse

- 393 Hashimoto, K., Tsujita, M., Miyazaki, T. et al. (2011). Postsynaptic P/Q-type Ca²⁺ channel in Purkinje cell mediates synaptic competition and elimination in developing cerebellum. *Proc Natl Acad Sci U S A* 108, 9987-92, <http://dx.doi.org/10.1073/pnas.1101488108>
- 394 Simmons, D. D. (2002). Development of the inner ear efferent system across vertebrate species. *Journal of Neurobiology* 53, 228-50, <http://dx.doi.org/10.1002/neu.10130>.
- 395 Katz, E., Elgoyhen, A. B., Gómez-Casati, M. E. et al. (2004). Developmental Regulation of Nicotinic Synapses on Cochlear Inner Hair Cells. *The Journal of Neuroscience* 24, 7814-20, <https://dx.doi.org/10.1523/jneurosci.2102-04.2004>.
- 396 Vetter, D. E., Liberman, M. C., Mann, J. et al. (1999). Role of alpha9 nicotinic ACh receptor subunits in the development and function of cochlear efferent innervation. *Neuron* 23, 93-103, [http://dx.doi.org/10.1016/S0896-6273\(00\)80756-4](http://dx.doi.org/10.1016/S0896-6273(00)80756-4).
- 397 Mooney, R., Penn, A. A., Gallego, R. & Shatz, C. J. (1996). Thalamic Relay of Spontaneous Retinal Activity Prior to Vision. *Neuron* 17, 863-74, [https://dx.doi.org/10.1016/S0896-6273\(00\)80218-4](https://dx.doi.org/10.1016/S0896-6273(00)80218-4).
- 398 Dilger, E. K., Shin, H. S. & Guido, W. (2011). Requirements for synaptically evoked plateau potentials in relay cells of the dorsal lateral geniculate nucleus of the mouse. *J Physiol* 589, 919-37, <http://dx.doi.org/10.1113/jphysiol.2010.202499>.
- 399 Žiburkus, J., Dilger, E. K., Lo, F.-S. & Guido, W. (2009). LTD and LTP at the Developing Retinogeniculate Synapse. *Journal of Neurophysiology* 102, 3082-90, <https://dx.doi.org/10.1152/jn.90618.2008>.
- 400 Kawata, S., Miyazaki, T., Yamazaki, M. et al. (2014). Global Scaling Down of Excitatory Postsynaptic Responses in Cerebellar Purkinje Cells Impairs Developmental Synapse Elimination. *Cell Reports* 8, 1119-29, <https://dx.doi.org/10.1016/j.celrep.2014.07.014>.
- 401 Ohtsuki, G. & Hirano, T. (2008). Bidirectional plasticity at developing climbing fiber-Purkinje neuron synapses. *European Journal of Neuroscience* 28, 2393-400, <https://dx.doi.org/10.1111/j.1460-9568.2008.06539.x>.
- 402 Bosman, L. W. J. & Konnerth, A. (2009). Activity-dependent plasticity of developing climbing fiber-Purkinje cell synapses. *Neuroscience* 162, 612-23, <https://dx.doi.org/10.1016/j.neuroscience.2009.01.032>.
- 403 Wiesel, T. N. & Hubel, D. H. (1963). Single-cell responses in striate cortex of kittens deprived of vision in one eye. *Journal of Neurophysiology* 26, 1003-17, <http://jn.physiology.org/content/jn/26/6/1003.full.pdf>.
- 404 David, L. S., Aitoubah, J., Lesperance, L. S. & Wang, L. Y. (2014). Gene delivery in mouse auditory brainstem and hindbrain using in utero electroporation. *Mol Brain* 7, 51, <http://dx.doi.org/10.1186/s13041-014-0051-4>.
- 405 Helmchen, F., Borst, J. G. G. & Sakmann, B. (1997). Calcium dynamics associated with a single action potential in a CNS presynaptic terminal. *Biophys J* 72, 1458-71, [http://dx.doi.org/10.1016/S0006-3495\(97\)78792-7](http://dx.doi.org/10.1016/S0006-3495(97)78792-7).

- 406 Wang, L.-Y. & Kaczmarek, L. K. (1998). High-frequency firing helps replenish the readily releasable pool of synaptic vesicles. *Nature* 394, 384-88, <http://www.nature.com/nature/journal/v394/n6691/full/394384a0.html>.
- 407 Chuhma, N. & Ohmori, H. (2001). Differential development of Ca²⁺ dynamics in presynaptic terminal and postsynaptic neuron of the rat auditory synapse. *Brain Res* 904, 341-4, [http://dx.doi.org/10.1016/S0006-8993\(01\)02506-9](http://dx.doi.org/10.1016/S0006-8993(01)02506-9).
- 408 Chuhma, N. & Ohmori, H. (2002). Role of Ca²⁺ in the synchronization of transmitter release at calyceal synapses in the auditory system of rat. *J Neurophysiol* 87, 222-28, <http://jn.physiology.org/content/87/1/222.long>.
- 409 Kushmerick, C., Price, G. D., Taschenberger, H. et al. (2004). Retroinhibition of presynaptic Ca²⁺ currents by endocannabinoids released via postsynaptic mGluR activation at a calyx synapse. *J Neurosci* 24, 5955-65, <http://www.jneurosci.org/cgi/content/full/24/26/5955>.
- 410 Kushmerick, C., Renden, R. & von Gersdorff, H. (2006). Physiological temperatures reduce the rate of vesicle pool depletion and short-term depression via an acceleration of vesicle recruitment. *J Neurosci* 26, 1366-77, <http://dx.doi.org/10.1523/JNEUROSCI.3889-05.2006>.
- 411 Nakamura, Y. & Takahashi, T. (2007). Developmental changes in potassium currents at the rat calyx of Held presynaptic terminal. *J Physiol* 581, 1101-12, <http://dx.doi.org/10.1113/jphysiol.2007.128702>.
- 412 Nakamura, T., Yamashita, T., Saitoh, N. & Takahashi, T. (2008). Developmental changes in calcium/calmodulin-dependent inactivation of calcium currents at the rat calyx of Held. *J Physiol* 586, 2253-61, <http://jp.physoc.org/content/586/9/2253.long>.
- 413 Paradiso, K. & Wu, L. G. (2009). Small voltage changes at nerve terminals travel up axons to affect action potential initiation. *Nat Neurosci* 12, 541-3, <http://dx.doi.org/10.1038/nn.2301>.
- 414 Huang, H. & Trussell, Laurence O. (2014). Presynaptic HCN Channels Regulate Vesicular Glutamate Transport. *Neuron* 84, 340-46, <https://dx.doi.org/10.1016/j.neuron.2014.08.046>.

Addendum

ADDENDUM

Martijn C. Sierksma

PhD portfolio

Publications

Sierksma and Borst (2017). Resistance to action potential depression of a rat axon terminal *in vivo*. PNAS, 114 (16): 4249-4254. DOI: 10.1073/pnas.1619433114

Sierksma, Tedja and Borst (2017). *In vivo* matching of postsynaptic excitability with spontaneous synaptic inputs during formation of the rat calyx of Held synapse. JPhysiol, 595: 207-231. DOI: 10.1113/jp272780

Sierksma[†], Kroon[†] and Meredith (2013). Investigating mechanisms underlying neurodevelopmental phenotypes of autistic and intellectual disability disorders: a perspective. Front Syst Neurosci 7:75. DOI: 10.3389/fnsys.2013.00075

[†]contributed equally

Poster presentations

SfN annual meeting (2016). Sierksma MC, Borst JGG. Resistance to spike depression of a rat central axon terminal during *in vivo* high-frequency firing.

Dutch Neuroscience Meeting (2016). Sierksma MC, Borst JGG. Resistance to spike depression of an axon terminal *in vivo*.

ONWAR retraite (2015). Sierksma MC, Tedja MS, Borst JGG. The role of synaptic summation in triggering action potentials in the developing calyx of Held-target *in vivo*.

Endo-Neuro-Psycho Meeting (2012). Sierksma MC, Kramvis I, Meredith RM. GABAergic transmission in the developing hippocampus of Fmr1 knock-out mice. *Best poster prize*.

Teaching

- **VO Hearing disabilities** (third year BSc Medicine): 2015, 2016, 2017
- **VO Ultrasound Imaging** (first year BSc Medicine): 2015, 2016
- **VO Smooth muscle** (first year BSc Medicine): 2014, 2015, 2016
- **VO Heart potential** (first year BSc Medicine): 2016
- **VO Toxin assignment** (first year MSc Neuroscience): 2015, 2016

- **Experimental Neurophysiology: Theory and Practice** (ONWAR): 2016
- **Demo slice whole-cell electrophysiology** (intro MSc Neuroscience): 2016
- **Master thesis** – Anne van der Poel: 2014-2015

VO is a practical session on the specified topic.

Education during PhD

OIC – Microscopic Image Analysis (winter 2017)

Erasmus Optophysiology group (2016-2017)

Integrity in Science (2016)

Erasmus Neurophysiology Group (2014-2015, 3 presentations)

AMIE – Translational imaging course ‘from mouse to man’ (2015)

Art. 9 course (2014)

Monday morning meetings (5 presentations)

Group discussions (~10 presentations)

A

Prior education

Exchange Honours MSc Neurosciences Amsterdam/Rotterdam (2011-2013)

at the VU University in Amsterdam and Erasmus MC in Rotterdam, *cum laude*

BSc Biology (2007-2011) at Leiden University

Atheneum Nature and Health (2001-2007) at CSG De Lage Waard in

Papendrecht

Organization

Brain Awareness Rotterdam 2017: open day at the department

The departmental PhD-meetings

Annual departmental outing 2015

Science and Faith – course for lay public (2012, 2013, 2014)

Curriculum Vitae

Martijn Christiaan Sierksma werd geboren op 17 december 1988 te Gorinchem. Hij rondde in 2007 zijn VWO Atheneum af aan de middelbare school Christelijke Scholengemeenschap De Lage Waard te Papendrecht en vervolgde zijn opleiding aan de Universiteit Leiden. Tijdens zijn Bachelor Biologie ontwikkelde de promovendus zijn interesse in cellulaire biologie en fysiologie. In 2011 behaalde hij zijn BSc-grad en vervolgde zijn studie bij de onderzoeksmaster Neurowetenschappen aan de Vrije Universiteit van Amsterdam waar hij vervolgens werd toegelaten tot de ereuitwisselingsmaster van Amsterdam en Rotterdam (Exchange Honours Master Amsterdam-Rotterdam). Tijdens zijn opleiding volgde de promovendus een stage in de groep van dr. Rhiannon M. Meredith waar hij onderzoek deed naar mogelijke ontwikkelingsverstoringen in de hippocampus van een muismodel voor het Fragiel X syndroom en een tweede stage in de groep van prof. Ole Paulsen in Cambridge, Verenigd Koninkrijk waarbij een nieuw ontwikkelingsproces beschreven werd in de somatosensorische hersenschors. In het najaar van 2013 behaalde de promovendus zijn mastergraad met lof en begon zijn promotiewerk beschreven in deze thesis onder leiding van prof. J. Gerard G. Borst.

Sinds 23 juni 2014 is de promovendus getrouwd met Evelyn Martine Sierksma en zij wonen in Den Haag.

De promovendus is in 2018 begonnen met een nieuw project bij dr. Xavier Nicol aan L'Institut de la Vision te Parijs, waar onderzocht wordt hoe de vezels van nabijgelegen retinale ganglionaire cellen elkaars ontwikkeling beïnvloeden.

Dankwoord

Allereerst wil ik graag iedereen bedanken die een essentiële bijdrage hebben geleverd aan het werk in dit proefschrift.

Ik ben erg dankbaar voor de begeleiding van prof. Gerard Borst. Bedankt voor je geduld en de vrijheid om fouten te maken. Je haarscherpe opmerkingen hebben me altijd uitgedaagd om mijn werk en mijn denken te verbeteren.

Voor alle gesprekken als het werk moeizaam ging of als ik aan afleiding toe was, bedank ik Marcel van der Heijden. Ik heb je frisse blik op biologie erg gewaardeerd en je uitgebreide uitleg van de biofysica van het slakkenhuis was een fantastische afleiding als ik niet aan het werk wilde.

Rue Geis, John Soria van Hoeve, Milly Tedja, Andy Plauška en Tiantian Wang. Bedankt voor jullie hulp bij het leren van de operatie en suggesties hoe de operatie verbeterd kon worden.

Ik ben Rue ook heel dankbaar voor alle discussies over *in vivo* electrofysiologie.

Voor alle hulp bij technische problemen met de apparatuur en de gemakkelijke gesprekken over natuurkunde, biologie en computers bedank ik Kees Donkersloot. Zonder jou zou ik heel veel tijd verloren hebben aan het herstellen van allerlei technische apparatuur.

Voor alle histologie werk ben ik Elize Haasdijk en Erika Goedknecht zeer denkbaar. Bedankt voor jullie geduld met al mijn vragen en voor jullie tijd en energie om een fantastische histologielab draaiende te houden. Daarbij wil ik ook graag Fereshta Zakeri en Celina Glimmerveen bedanken voor jullie bijdrage aan de immunofluorescentiekleuringen.

Met betrekking tot data-analyse ben ik Marcel van der Heijden, Aaron Wong en Peter Bremen erg dankbaar. Jullie kritische blik op mijn werk heeft mijn werk op een hoger niveau gebracht.

Als laatste bedank ik Johan Slotman voor alle hulp met superresolutie-microscopie en de beeldanalyse.

Alle experimenten zijn uitgevoerd in de groep van Gerard Borst en Marcel van der Heijden. Graag bedank ik Gerard Borst, Marcel van der Heijden, Kees

Neural Activity During the Formation of a Giant Auditory Synapse

Donkersloot, Rue Geis, Eder de Moraes en Anita de Oliveira Silva, Tiantian Wang, Andrius Plauška, John Soria van Hoeve, Milly Tedja, Laura de Kok, Alexandra Cunha, Anne van der Poel, Aaron Wong, Yarmo Mackenbach, Tobio Aarts, Ghais Houtak, Linda Gaillard, Nigel Cooper, Fereshta Zakeri, Peter Bremen, Anna Vavakou en Maurits van den Berg voor jullie collegialiteit en het creëren van een fantastische werkomgeving. Bedankt voor alle gesprekken, lunches, koffie en afleiding.

Voor alle hulp met moleculair werk wil ik graag Edwin Mientjes en Geeske van Woerden bedanken. Ondanks dat mijn pogingen in moleculaire biologie niet heel succesvol zijn geweest, het heeft zeker niet gelegen aan al jullie hulp. Heel erg bedankt voor jullie tijd en uitleg.

Verder ben ik heel dankbaar voor iedereen van de afdeling Neurowetenschappen voor een gezellige en uitdagende plek om te werken. Ook al kan ik niet iedereen noemen, wil ik toch enkele mensen uitlichten:

Saša Peter, ik heb je passie voor electrofysiologie erg gewaardeerd. Bedankt voor je aanstekelijke en onverwoestbare positieve houding.

Dick Jaarsma, bedankt voor alle gesprekken over kleuringen en wetenschap in het algemeen.

Diana Rotaru, Jolet van der Bree en Vincenzo Romano, het was erg leuk om met jullie het afdelingsuitje te organiseren.

Sander Lindeman en Shashini Munshi, wat kan ik zeggen. Het waren een paar fantastische PhD-bijeenkomsten.

Voor een fantastische organisatie van een Open Dag voor de Brain Awareness Week bedank ik Aaron Wong, Carmen Schaeffer, Francois Blot, Marlou Kooiker, Sander Lindeman, Simona Gornati, Shashini Munshi en Yarmo Mackenbach. Een onvergetelijke ervaring waar ik met veel plezier op terug kijk. Bedankt voor die tijd.

De afdeling zou in chaos vervallen, ware het niet voor Loes Nijs-de Langen en Elise Buitenhuis-Linssen (en Elize Haasdijk, maar ik heb je al bedankt). Bedankt voor jullie hulp met allerlei zaken aangaande de organisatiestructuur van het Erasmus MC en de administratie die daarbij hoort.

Lieve Evelyn, bedankt voor al je steun en je begrip als ik weer tot laat aan het werk was. Zonder jouw steun, je begrip en je luisterend oor zou ik niet gered hebben.

Pa en ma, jullie onafgebroken vertrouwen en steun door de jaren heen hebben me gedragen tot waar ik nu ben. Jullie zijn een groot voorbeeld voor me en ik draag dit boek aan jullie op. *Mijn dankbaarheid meet zich niet aan hoe het had kunnen zijn, maar aan de weg die ik onder jullie hoede afgelegd heb.* Bedankt voor alles.

